This is to certify that the
dissertation entitled

ADVANCING THERMOELECTRIC RESEARCH WITH NEW
MEASUREMENT SYSTEMS AND THERMOELECTRIC MODELING
FOR AC ELECTRICAL MEASUREMENTS

presented by

Adam Darwin Downey

has been accepted towards fulfillment
of the requirements for the

Ph. D. degree in Electrical & Computer Engineering

Tim Hogan
Major Professor's Signature

4/25/06
Date

ADVANCING THERMOELECTRIC RESEARCH WITH NEW MEASUREMENT SYSTEMS AND THERMOELECTRIC MODELING FOR AC ELECTRICAL MEASUREMENTS

By

Adam Darwin Downey

A DISSERTATION

Submitted to
Michigan State University
in partial fulfillment of the requirements
for the degree of

DOCTOR OF PHILOSOPHY

Department of Electrical and Computer Engineering

2006

ADVANCING
SYSTEMS

Bulk therm

MSU for use in h

exhibit figures of m

develop power gen

development of th

evaluate the comp

conductivity, and

In this resea

simultaneous mea

thermopower. B

measurements ar

system called the

and the second s

measurements (3

reference materi

investigation of

synthesis param

ABSTRACT

ADVANCING THERMOELECTRIC RESEARCH WITH NEW MEASUREMENT SYSTEMS AND THERMOELECTRIC MODELING FOR AC ELECTRICAL MEASUREMENTS

By

Adam Darwin Downey

Bulk thermoelectric materials are created and studied at Michigan State University (MSU) for use in high temperature power generation devices. These new materials exhibit figures of merit, ZT, which approach values of 2 near 800K, and are being used to develop power generators that convert heat flow to electricity. To help with the development of the thermoelectric materials, new measurement systems are needed to evaluate the components of the figure of merit (electrical conductivity, thermal conductivity, and thermopower).

In this research work, two measurement systems are developed for the simultaneous measurements of electrical conductivity, thermal conductivity, and thermopower. Both systems use a new "drifting in temperature" technique where measurements are made as the overall sample temperature slowly drifts in time. The first system called the "Drift System", is for low temperature measurements (100K to 300K) and the second system, "Ultra High Temp System", is for high temperature measurements (300K to 900K). The accuracy of these systems was verified using reference materials. The Ultra High Temp System has become a very useful tool in the investigation of new thermoelectric materials as doping concentrations and material synthesis parameters are changed.

In additio

modules and sin

new AC model f

comparing the in

modeling of the

transmission lin

model could be

single thermoel

thermal wave de

module's inputs,

but not with the

Finally, th

merit measurem

merit on more th

amounts of data

thermal process

In addition to this research, the AC impedance characteristics of thermoelectric modules and single pellets were investigated. This research led to the development of a new AC model for thermoelectric modules using AC electrical measurements by comparing the impedance behavior of thermoelectric modules to a simple RC circuit. The modeling of thermoelectric materials was then expanded upon by the application of transmission line theory to describe the thermal dynamic behavior in a module. This new model could be applied to commercially available modules as well as unicouples, and single thermoelectric pellets. Infrared imaging was used to verify the existence of a thermal wave developing along the module legs due to an AC electrical signal at the module's inputs. This thermal wave can be modeled with the transmission line theory, but not with the simple RC one-port model.

Finally, this research discusses a new ZT measurement system for rapid figure of merit measurements of new materials. This system is capable of measuring the figure of merit on more than 30 samples per week at room temperature. For the first time, large amounts of data can be collected for statistical analysis on doping concentrations and thermal processing to determine the optimal sample preparation conditions.

I would li

factor in my ent

experience to be

attitudes, ethics,

appreciated. I w

whom I have wo

I would li

Reinhard, and D

presentation and

I would li

family, and frien

Financial s

0867 MURI prog

ACKNOWLEDGMENTS

I would like to thank my advisor Dr. Timothy P. Hogan. He has been a major factor in my enthusiasm for research and my desire to pursue a Ph.D. It has been a great experience to be a part of his research team and be surrounded by people with such great attitudes, ethics, and working manner. Dr. Hogan's guidance in this thesis is very much appreciated. I would also like to thank all of the Hogan's Heroes and all the people with whom I have worked with in the thermoelectric project.

I would like to thank Dr. Mercouri Kanatzidis, Dr. Tim Grotjohn, Dr. Donnie Reinhard, and Dr. Gregory Wierzba for taking the time to review my thesis, attending my presentation and contributing to some helpful discussions.

I would like to especially thank my wife, Cori, my parents, my parents-in-law, family, and friends for all of their support throughout the years.

Financial support from the Office of Naval Research (Contract No. N00014-02-1-0867 MURI program) is gratefully acknowledged.

TABLE OF CONTENTS

LIST OF TABLES

LIST OF FIGURES

Images in this

Images in this dissertation are presented in color.

1.1 Introduct

Michiga

materials and r

materials. Th

(Electrical and

but also with t

thermoelectric

Research (ON

materials, obta

thermoelectric

thermoelectric

300K respect

- to be

  have

- to id

  devic

- to he

- and t

  powe

As a member o

to characterize

measurement s

Chapter 1: Introduction to Thermoelectrics Research

1.1 Introduction

Michigan State University (MSU) explores thermoelectric research to identify new materials and measurement techniques and explore applications for these thermoelectric materials. This research is a collaborative effort not only between departments at MSU (Electrical and Computer Engineering, Mechanical Engineering, Chemistry, and Physics) but also with the University of Michigan and Iowa State University. The goal of this thermoelectric research, which has been guided by the funding from the Office of Naval Research (ONR), is to advance the scientific community's knowledge of thermoelectric materials, obtain a better understanding of how to manufacture the most efficient thermoelectric material for high temperature applications, and to create a 1kW thermoelectric power generation device for hot and cold side temperatures at 850K and 300K, respectively, with the highest efficiency. My role in this research includes:

- to be a part of the team that tests and characterizes thermoelectric materials that have been made at MSU
- to identify new materials with good prospects of being used in thermoelectric devices
- to help better understand what makes a good thermoelectric material
- and to determine how to use these materials to create a functional device for power generation.

As a member of this measurement team I have not only used existing equipment at MSU to characterize thermoelectric materials, but have developed a new transport measurement system capable of measuring transport properties of materials over the

temperature r...
dependant the...
have also inv...
new measurem...
dependent be...
electrical con...
merit of a giv...
provides a cap...
previously av...
measuring the...
described circ...
scientific com...
techniques fo...
measurement...

The un...
system for h...
thermoelectr...
obtained for...
thermoelectr...
investigate t...

Findi...
measuring t...
similar sam...

temperature range of 25°C to 1000°C. Typical measurements include temperature dependant thermopower, electrical conductivity, and thermal conductivity. In addition, I have also investigated impedance spectroscopy on thermoelectric materials to develop a new measurement technique along with two theoretical models to describe the frequency dependent behavior of thermoelectric materials. The three physical properties of electrical conductivity, thermopower, and thermal conductivity determine the figure of merit of a given sample. The transport measurement system described in this thesis provides a capability to reach measurement temperature as high as 1000°C which was not previously available in this laboratory. The development of a system capable of measuring the frequency dependant behavior of thermoelectric materials along with the described circuit based models for understanding these behaviors is unique to the scientific community to the best of our knowledge. This has provided new investigative techniques for measuring the figure of merit for faster, more reliable, and more accurate measurements.

The uniqueness of the research into developing a new transport measurement system for high temperatures is that high temperature properties of quaternary cubic thermoelectric material, along with other materials developed at MSU, have been obtained for the first time. Since these measurements will give the first insight into thermoelectric properties at higher temperatures, the system is an important tool used to investigate these new materials.

Finding the figure of merit for thermoelectric materials at MSU typically involves measuring thermoelectric power and electrical conductivity at high temperatures while a similar sample is measured for thermal conductivity elsewhere. The uniqueness of the research into

is that the fig

directly. The

impedance be

could be perf

an important

1.2 Thesis O

Introdu

and fundamen

knowledge, w

new thermoel

characterizing

research done

(Drift System

System), and

materials. Im

models that d

materials (RC

investigations

measurements

The experimen

performed on

research into investigating the frequency dependant behavior of thermoelectric materials is that the figure of merit for these materials over a temperature range can be found directly. The models developed for this research help to explain the frequency dependant impedance behavior and can also be used to explain how a faster figure of merit test could be performed on multiple samples. This system along with the relevant models is an important tool in characterizing thermoelectric materials.

1.2 Thesis Outline

Introduced in the first part of the thesis is a brief overview of the history, theories and fundamentals applied to thermoelectrics. These sections will outline the background knowledge, which will be needed for the proceeding chapters. Descriptions of old and new thermoelectric materials will be discussed along with various techniques of characterizing thermoelectric materials and devices. The next sections describe the new research done at MSU, which includes a new system for low temperature measurements (Drift System), a new system for high temperature measurements (Ultra High Temp System), and finally the investigations of impedance spectroscopy on thermoelectric materials. Impedance spectroscopy measurements will lead to the development of two models that describe the AC frequency dependant behavior of the thermoelectric materials (RC One-Port Model and Thermal Transmission Line Model). Based on investigations of the impedance, a final system is created for rapid figure of merit measurements at room temperature of multiple samples simultaneously (ZT Machine). The experimental results will be presented for all systems along with detailed analysis performed on the frequency dependant impedance measurements.

2.1 Introduc

Therm

been a topic

air condition

alternate way

generate enor

which could

thermoelectri

global impact

consumption.

atmosphere.

Thermo

temperature g

electrical ener

module) for c

used thermoco

the tip and ba

However, unl

thermoelectric

watch from bo

wasted heat fr

Chapter 2: Thermoelectric Fundamentals

2.1 Introduction

Thermoelectrics (converting thermal energy to electrical energy and vice versa) has been a topic of research for many years. In everyday life, people are using refrigerators, air conditioners, fans, and heat sinks to keep objects cool. Thermoelectrics provide alternate ways to cool objects that may be more practical or effective. People also generate enormous amounts of wasted heat energy from automobiles and industrial plants which could be transformed back into useful electrical energy with the help of thermoelectric generators. Converting waste heat back into useful power can have major global impacts. For example, making trucks more fuel-efficient may reduce gas consumption. Using less gas can lead to lower automobile emissions, which impacts the atmosphere.

Thermoelectric (TE) modules are devices the can convert thermal energy from a temperature gradient to electrical energy for power generation or vice versa (providing electrical energy to the thermoelectric module to create a temperature gradient across the module) for cooling applications. Power generation devices work similarly to commonly used thermocouples, which produce a voltage that depends upon the temperature between the tip and base of the thermocouple and the materials used in that thermocouple. However, unlike a typical thermocouple used for temperature measurements, thermoelectric modules for power generation can generate enough electricity to power a watch from body heat, power onboard electronics of a satellite in deep space, convert wasted heat from an automobile to power electronic systems and make the overall vehicle performance r

deep waters w

With n

operated in ar

another impor

temperature c

applications s

Therm

electrical ener

There are thre

and Thomson

merit, ZT, wh

coefficient), e

is the absolut

figure of mer

and will be d

below.

This se

discuss anoth

research, the

thermal conc

performance more efficient, and provide electricity from nuclear heat of a submarine in deep waters without any moving parts or added noise.

With no moving parts, TE modules are rugged, reliable, and quiet. They can be operated in any orientation and in zero gravity environments. For cooling applications, another important feature is the ease with which a TE module can be precisely temperature controlled, an important advantage for scientific, military, and aerospace applications such as infrared detectors and laser diodes.

Thermoelectric research is the study of the conversion between thermal and electrical energy [1,2]. Thermoelectric technology has been around since the 1800s. There are three main effects that appear in thermoelectrics: Seebeck effect, Peltier effect, and Thomson effect. Thermoelectric material properties are governed by the figure of merit, ZT, which is governed by the thermopower, α (also know as the absolute Seebeck coefficient), electrical conductivity, σ, and thermal conductivity, κ, of a sample, while T is the absolute temperature [3]. Z has units of 1/K making ZT a unitless quantity. The figure of merit, ZT, is extremely important for describing the thermoelectric performance and will be discussed extensively throughout this paper. The equation for ZT is shown below.

$$ZT = \frac{\alpha^2 \cdot \sigma}{\kappa} \cdot T \quad \text{(unitless)} \qquad (2.1)$$

This section will describe the three main effects for thermoelectrics. It will also discuss another important equation that is used quite extensively in thermoelectric research, the Wiedemann-Franz Law. This law identifies the relationship between thermal conductivity and electrical conductivity for TE materials. Finally, thermocouples and ther

discusse

2.2 Pelti

Afte

is absorbe

different c

is caused b

temperatur

The Peltier c

materials (A a

The Peltier c

temperature c

The Peltier he

and thermoelectric module configurations (layout), properties, and applications are also discussed.

2.2 Peltier Effect

After the discovery of the Seebeck effect, Jean Peltier discovered in 1834 that heat is absorbed or liberated when an electric current passes through an interface between two different conductors. A diagram of this effect is shown in Figure 2-1. The Peltier effect is caused by the fact that a heat current in a homogeneous conductor, even at a constant temperature, accompanies an electric current.

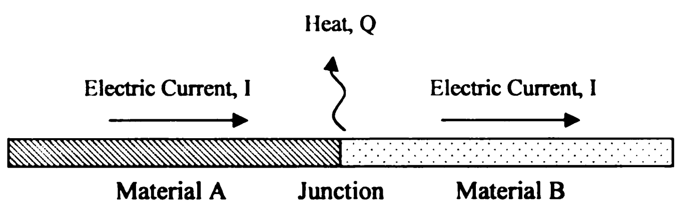

Figure 2-1: Peltier effect diagram

The Peltier coefficient, Π_{AB}, is directly related to the change in heat between two materials (A and B), per electric current, I, as shown here.

$$\Pi_{AB} = \frac{dQ}{dt \cdot I} \quad \text{(V)} \tag{2.2}$$

The Peltier coefficient can also be related to the Seebeck coefficient times the temperature of the junction.

$$\Pi_{AB} = \alpha_{AB} \cdot T \quad \text{(V)} \tag{2.3}$$

The Peltier heat, P_Q, is related to the electric current by the Peltier coefficient as,

$$P_Q = \frac{dQ}{dt} = \Pi_{AB} \cdot I \quad \text{(W)} \tag{2.4}$$

Peltier also d

so is the direc

23 Thomson

In 1854

reversible trar

where the dire

to the warme

previously e

A diagram o

The Th

or

Peltier also discovered that the effect is reversible. If the direction of current is reversed, so is the direction of heat exchange at the boundaries of materials A and B. [4]

2.3 Thomson Effect

In 1854 a phenomenon discovered by William Thomson (Lord Kelvin) found that a reversible transverse heat flow occurs into or out of a conductor of a particular metal where the direction depends upon whether an electric current flows from the colder side to the warmer or from the warmer to the colder side of a metal. Any temperature gradient previously existing in the conductor is thus modified if an electric current is applied [5]. A diagram of this is shown in Figure 2-2.

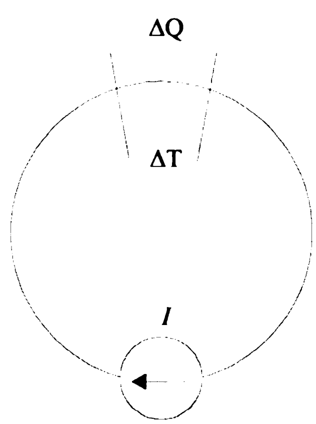

Figure 2-2: Thomson effect diagram

The Thomson effect, γ, is related to the Seebeck effect,

$$\gamma = \frac{d\alpha}{dT} \cdot T \quad \text{(V/K)} \tag{2.5}$$

or

The Thoms

2.4 Wieden

Therm

phonons and

thermal con

When a sam

lattice will v

conductivity

contribution.

contribution

contribution.

thermal cond

component o

properties.

For me

electrical con

thermal and e

$$\alpha(T) = \int_0^T \frac{\gamma(T')}{T'} \cdot dT' \quad \text{(V/K)} \tag{2.6}$$

The Thomson coefficient relates the Thomson heat, Γ_Q, and electrical current through,

$$\Gamma_Q = \frac{dQ}{dT} = -\gamma \cdot I \cdot \Delta T \quad \text{(W)} \tag{2.7}$$

2.4 Wiedemann-Franz Law

Thermal conductivity is the ability for a material to conduct heat. Both the phonons and the charge carriers can conduct heat through the material such that the total thermal conductivity will include electronic and lattice contributions as shown here.

$$\kappa_{total} = \kappa_{lattice} + \kappa_{electronic} \quad (\text{Wm}^{-1}\text{K}^{-1}) \tag{2.8}$$

When a sample is placed in a low temperature environment, the atoms in the crystal lattice will vibrate at a lower intensity which can make the contribution of thermal conductivity from the lattice very small or even negligible compared to the electronic contribution. At sufficiently high temperatures, the lattice will vibrate so much that the contribution of thermal conductivity from the lattice dominates the electronic contribution. Between these two extremes, both mechanisms will contribute to the total thermal conductivity. With thermoelectric materials, it is often possible to reduce one component of the thermal conductivity without appreciably affecting the other material properties.

For metals, the thermal conductivity is high, and those metals, which are the best electrical conductors, are also the best thermal conductors. At a given temperature, the thermal and electrical conductivities of metals are proportional, but raising the temperature

conductivity

where

The va

300K

where κ is t

applies for

The

thermal co

a sample v

diffusivity

from both

Te) mate

1850 S c

semicon

can be c

be deco

temperature increases the thermal conductivity while decreasing the electrical conductivity. This behavior is quantified in the Wiedemann-Franz Law shown below.

$$\frac{\kappa}{\sigma} = L \cdot T \quad (\mathrm{W\Omega K^{-1}}) \tag{2.9}$$

where

κ = thermal conductivity (W/m·K)
σ = electrical conductivity (S/m)
L = Lorenz number = 2.45x10^{-8} WΩK^{-2}
T = temperature (K)

The value of this Lorenz number was found using quantum mechanics such that at 300K

$$L = \frac{\kappa}{\sigma \cdot T} = \frac{\pi^2 \cdot k^2}{3 \cdot e^2} = 2.45 \times 10^{-8} \quad (\mathrm{W\Omega K^{-2}}) \tag{2.10}$$

where κ is the Boltzmann constant (1.3807x10^{-23} J/K). This constant of proportionality applies for temperatures above the Debye temperature, θ_D.

The Wiedemann-Franz Law is useful for estimating the temperature dependent thermal conductivity of measured TE samples. For example, the thermal conductivity on a sample with a certain crystal structure can be found experimentally using the flash diffusivity-specific heat method. This thermal conductivity will include contributions from both the crystal lattice and the electrons. A published sample of LAST (Pb-Sb-Ag-Te) material had a thermal conductivity of 2.3 Wm^{-1}K^{-1} and electrical conductivity of 1850 S/cm at room temperature [6]. For LAST materials (degenerately doped semiconductors), at some arbitrary temperature with mixed scattering, the Lorenz number can be calculated as 2.28x10-8 WΩK^{-2} [7]. The lattice and electronic contributions may be decoupled to give the electronic contribution from Wiedemann-Franz as

$\kappa_{electronic}$

$\kappa_{lattice} = \kappa$

is measured

concentratic

contribution

calculated ar

2.5 Thermo

Therm

research and

conductors

that has bee

standardize

in Table 2-

Figure 2-

$\kappa_{electronic} = L \cdot \sigma \cdot T = 1.27$ Wm^{-1}K^{-1}. Now the lattice contribution can be found as $\kappa_{lattice} = \kappa_{total} - \kappa_{electronic} = 2.3 - 1.27 = 1.03$ Wm^{-1}K^{-1}. When another TE sample is measured with similar composition and crystal lattice (but possibly doped at another concentration), the electrical conductivity of the material will change. Assuming the contribution from the lattice remains the same, the electronic contribution can again be calculated and used in estimating the total thermal conductivity of the sample.

2.5 Thermocouples

Thermocouples are fundamental to thermoelectrics and are commonly used in research and measurements. A thermocouple is made of any two dissimilar electrical conductors such as copper and constantan. A type-E (chromel-constantan) thermocouple that has been spark welded together is shown in Figure 2-3. There are eight NIST standardized thermocouple types [8], which have been well characterized and are shown in Table 2-1.

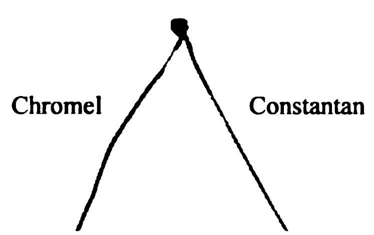

Figure 2-3: Type-E thermocouple spark-welded together using 25.4μm in diameter wire.

Tab

Type
N
T
J
E
K
B
R
S

However, m

thermocoup

in which it w

fields, etc.).

configuratio

The en

V_{AB} is devel

Table 2-1: Thermocouple types and their corresponding Seebeck voltage

Type	Materials	Thermopower (μV/K) at 25°C	Temperature Range (°C)
N	Nicrosil - Nisil	26.5	500 to 1000
T	Copper-Constantan	41	0 to 350
J	Iron - Constantan	51.5	0 to 750
E	Chromel - Constantan	61	0 to 900
K	Chromel - Alumel	40.5	0 to 1250
B	Platinum 6% Rhodium – Platinum 30% Rhodium	0	800 to 1700
R	Platinum – Platinum 13% Rhodium	6	0 to 1450
S	Platinum – Platinum 10% Rhodium	6	0 to 1450

However, many other thermocouple combinations are available. Each type of thermocouple has different features such as its voltage output sensitivity, the environment in which it will work (vacuum or no vacuum, oxidizing or inert atmospheres, magnetic fields, etc.), and the temperature range that it is appropriate for. Figure 2-4 shows a configuration for a single ended thermocouple made of two different materials (A and B).

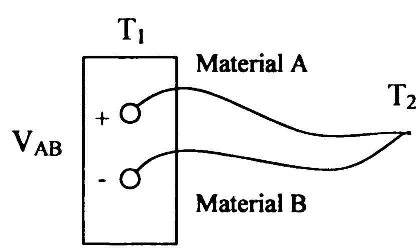

Figure 2-4: Single ended thermocouple

The ends of both thermocouples are thermally ground to T_1 and T_2. The voltage, V_{AB}, is developed based on the thermopowers of each material where,

$$V_{AB} = \int_{T_1}^{T_2} \alpha_A \cdot dT + \int_{T_2}^{T_1} \alpha_B \cdot dT = \int_{T_1}^{T_2} (\alpha_A - \alpha_B) \cdot dT = \int_{T_1}^{T_2} \alpha_{AB} \cdot dT \qquad (2.11)$$

Here. α_{AB} is

Seebeck of

single-ende

end of the t

used to find

as long as b

between the

V

Fi

In this case

wires are b

This can b

From here

the therm

T, which

junction

Here, α_{AB} is used to represent the Seebeck of the thermocouple. See Table 2-1 for the Seebeck of standard thermocouples at room temperature. To get an absolute temperature, single-ended thermocouples can be used as long as the temperature at the measurement end of the thermocouples is well known. A calibrated diode or platinum resistor can be used to find this temperature. Extension wires can be used without any extra calculations as long as both wires have the same thermopower and the same temperature gradient between the ends of the wires. An example of this is shown in Figure 2-5.

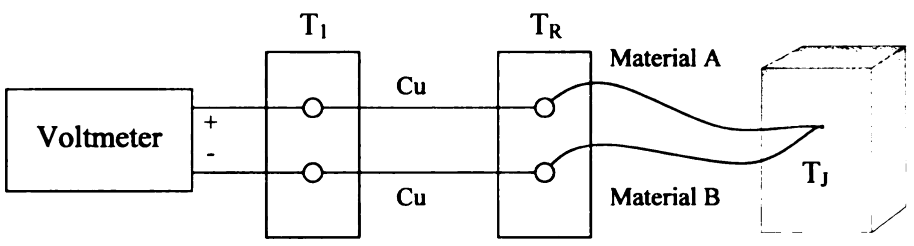

Figure 2-5: Typical thermocouple setup for temperature measurements

In this case, T_R is a reference junction where the temperature is known and the extension wires are both copper. T_1 does not need to be known to find the junction temperature T_J. This can be shown as follows,

$$\begin{aligned} V_{\text{meter}} &= \int_{T_1}^{T_R} \alpha_{Cu} \cdot dT + \int_{T_R}^{T_J} \alpha_A \cdot dT + \int_{T_J}^{T_R} \alpha_B \cdot dT + \int_{T_R}^{T_1} \alpha_{Cu} \cdot dT \\ &= \int_{T_R}^{T_J} (\alpha_A - \alpha_B) \cdot dT = \int_{T_R}^{T_J} \alpha_{AB} \cdot dT \end{aligned} \tag{2.12}$$

From here, usually the junction temperature, T_J, is desired. The first step is to measure the thermocouple voltage with its reference junction at T_R and its measuring junction at T_J, which was done above as V_{meter} (now called V_{RJ} "voltage between reference and the junction"). The next step to achieving this value is to compute the emf voltage of an ice-point (0 °C

NIST where

This equatio

voltage outp

the output v

the data can

compensated

Finally, the j

for the therm

Plotting the t

to the data ca

Therm

are used in fi

thermopower

the voltage p

across the sa

measuring w

to the voltag

point (0 °C) compensated thermocouple at the temperature T_R. This data is provided by NIST where the representing equation is as follows,

$$V_{0R} = F(T_R) \quad \text{(V)} \tag{2.13}$$

This equation can be read "the voltage from 0°C to the reference temperature is the voltage output function of the thermocouple evaluated at the temperature T_R." Plotting the output voltage data versus temperature for the thermocouple and using a curve fit to the data can be used to find this function. Next, compute the emf voltage of an ice-point compensated thermocouple at T_J. Here, the representing equations is as follows,

$$V_{0J} = V_{RJ} + V_{0R} \quad \text{(V)} \tag{2.14}$$

Finally, the junction temperature, T_J, can be calculated from the ice-point calibration data for the thermocouple as,

$$T_J = F(V_{0J}) \quad (^{\circ}\text{C}) \tag{2.15}$$

Plotting the thermocouple data as temperature versus output voltage and using a curve fit to the data can find this function.

Thermocouples are used extensively in the characterization of TE materials. They are used in finding the temperature gradient that is placed across a TE sample for thermopower measurements. Often, these same thermocouple wires are used to measure the voltage produced by the TE material when a temperature gradient is established across the sample. For this measurement, it is necessary to know the thermopower of the measuring wires and to apply a correction to the measured voltage from the sample due to the voltage developed by the wires themselves.

2.6 Seebeck

In 182

metals as in

Thompson (

difference b

difference b

conductor or

known as th

effect. The

conductor is

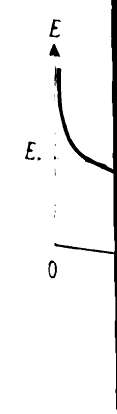

For nor

to the other e

greater veloci

electrons aro

2.6 Seebeck Effect

In 1821, Thomas Seebeck observed the thermoelectric effect using two different metals as in the thermocouple, which is the only way to observe the phenomenon. It was Thompson (Lord Kelvin) who later explained the observed effect. A temperature difference between two points in a conductor or semiconductor results in a voltage difference between these two points. Alternatively stated, a temperature gradient in a conductor or semiconductor gives rise to a built-in electric field. This phenomenon is known as the Seebeck effect. The Seebeck coefficient quantifies the magnitude of this effect. The thermoelectric voltage developed per unit temperature difference in a conductor is called the absolute Seebeck coefficient, also known as thermopower.

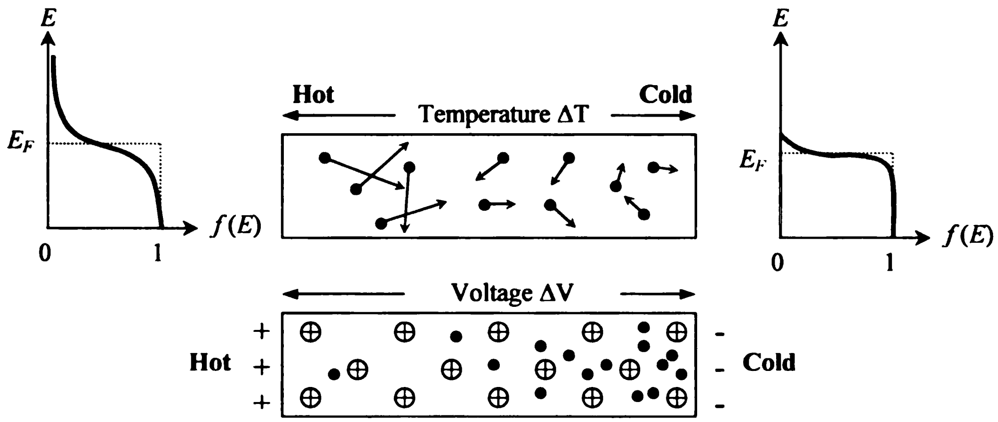

Figure 2-6: Seebeck effect on an aluminum rod

For normal metals, i.e. an aluminum rod, when one end of the rod is heated relative to the other end, the electrons in the hot region have more entropy and therefore have greater velocities than those in the cold region (See Figure 2-6). The conduction electrons around the Fermi energy have a mean speed that has a small temperature dependence

toward the

region and

continue ur

further elec

some time).

difference i

By convent

hot side. Th

term is mis!

thermopow

The av

$g(E) \propto E^1$

where E_{F0} is

distribution

average ener

dependence. This difference in electron energy causes a net diffusion from the hot end toward the cold end. This diffusion leaves behind exposed positive metal ions in the hot region and accumulates electrons in the cold region. The diffusion of electrons will continue until the electric field developed between the ends of the sample prevents any further electron motion from the hot to cold end. At steady state (constant heat flow after some time), the voltage difference across the aluminum rod due to the temperature difference is called the Seebeck effect. The equation for thermopower is shown below.

$$\alpha = \frac{dV}{dT} \quad \text{(V/K)} \tag{2.16}$$

By convention, the sign of α represents the potential of the cold side with respect to the hot side. The coefficient α is also referred to as thermoelectric power even though this term is misleading as it refers to a voltage difference rather than power. By integration of thermopower, the voltage difference across the sample can be found as shown below.

$$\Delta V = \int_{T_1}^{T_2} \alpha \cdot dT \quad \text{(V)} \tag{2.17}$$

The average energy E_{ave} per electron in a metal with the density of states $g(E) \propto E^{1/2}$ is given by

$$E_{ave}(T) = \frac{3}{5} E_{F0}\left[1 + \frac{5\pi^2}{12}\left(\frac{kT}{E_{F0}}\right)\right] \tag{2.18}$$

where E_{F0} is the Fermi energy at 0K and k is Boltzmann's constant. The Fermi-Dirac distribution extends to much higher energies when the temperature is raised so that the average energy per electron is actually greater in the hot end.

For a

the potentia

So, for met

For th

electrons in

K.E. = 1 2m

with higher

diffuse from

normal meta

The di

the hot regio

with the met

scattered, ha

unable to ac

electron mig

the electron

τ. In those r

migrate from

energy deper

following ex

For an electron to diffuse from the hot region to the cold, it has to do work against the potential difference. This work done decreases the average energy of the electron. So, for metals, the Seebeck coefficient is as follows,

$$\alpha \approx -\frac{\pi^2 k^2 T}{2eE_{F0}} \quad \text{(V/K)} \tag{2.19}$$

For the above explanation to be valid, some assumptions were made. First, the electrons in the metal behave as if they were "free". Second, the electron energy E = $K.E.$ = $1/2m_e^*v^2$ and the effective electron mass m_e^* is constant. Finally, the electrons with higher energy have greater mean speeds and longer mean free paths so that they diffuse from the hot to cold region. These assumptions only apply to what are called normal metals (e.g. Na, K, Al, etc.).

The diffusion of electrons from the hot to cold region assumes that the electrons in the hot region have higher speeds. In reality, the interactions of the conduction electrons with the metal ions, the lattice vibrations, and thus on how the conduction electrons are scattered, have to be considered. Except for certain metals, the free electron theory is unable to account for the sign of the thermoelectric effect. It has been found that the net electron migration, hot to cold, or cold to hot, is determined by the energy dependence of the electron concentration, n, the mean free path (MFP), λ, and the mean scattering time, τ. In those metals in which the MFP decreases strongly with the energy, electrons will migrate from the cold to hot and the thermoelectric power is positive. By including the energy dependence of the scattering processes, Mott and Jones [9,10] have derived the following expression for the Seebeck coefficient, where x is a

charge tran

can be scatt

(e.g. Ni). A

2.7 Therm

Ther

ability to c

thermoelec

the charge

modules a

connected

creates a t

thermal er

thermoco

$$\alpha \approx -\frac{\pi^2 k^2 T}{2eE_{F0}} x \quad \text{(V/K)} \tag{2.20}$$

where x is a numerical constant that depends on the energy dependences of various charge transport parameters. This equation does not apply to metals in which electrons can be scattered from one transport band to another transport band as in transition metals (e.g. Ni). A list of thermopower values of some metals is shown in Table 2-2. [11]

Table 2-2: Thermopower of various metals

Metal	Thermopower (μV/K) at 25°C
Al	-1.66
Pb	-1.05
Pt	-5.28
Mo	5.6
Cu	1.83
Ag	1.51

2.7 Thermoelectric Modules

Thermoelectric modules behave similarly to thermocouples in that both have the ability to convert heat energy to electrical energy and vice versa. However, thermoelectric modules are typically made of degenerately doped semiconductors where the charge carriers carry the heat from one end of the semiconductor to the other. The modules are also typically made of many couples electrically connected in series (*n*-type connected to *p*-type) (connecting many thermocouples together electrically in series creates a thermopile). This way, a module for power generation can convert enough thermal energy to electrical energy to provide a considerable amount of power, where as thermocouples do not. For cooling applications, the module can actively transfer enough thermal c

device.

M

connecte

Figure 2-

shows th

flow thro

same dire

generatio

of a stacke

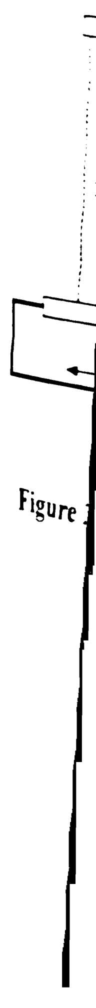

Figure

thermal energy from one side of the module to the other to make a functional cooling device. Thermocouples are typically only used for temperature measurements.

Many thermoelectric modules consist of *p*-type and *n*-type semiconductors connected electrically in series and thermally in parallel as shown in Figure 2-7 and Figure 2-8. Figure 2-7 (a) shows a *pn* module used for cooling applications while (b) shows the same device being used for power generation. By the Seebeck effect, heat flow through this thermoelectric material will tend to move the charge carriers in the same direction as the heat flow. Examples of thermoelectric modules for both power generation and cooling applications are shown in Figure 2-9 where (a) shows an example of a stacked module.

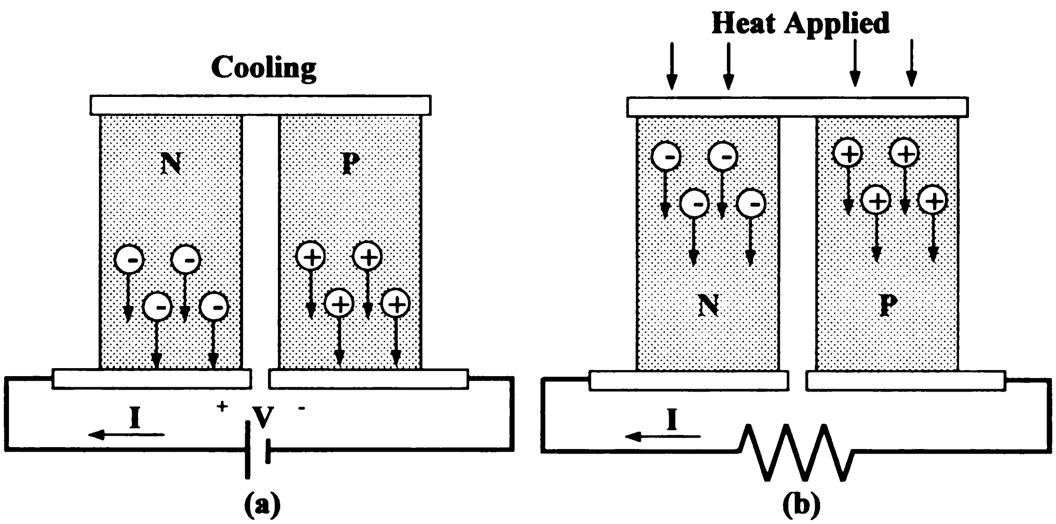

Figure 2-7: PN Thermoelectric Modules. (a) Cooling applications. (b) Power generation.

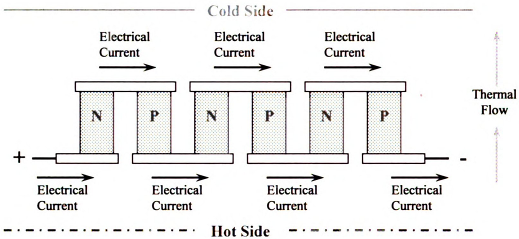

Figure 2-8: Thermoelectric module consisting of many unicouples.

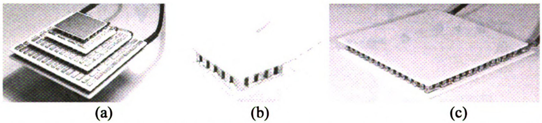

Figure 2-9: Examples of thermoelectric modules. (a) is stacked module, (b) and (c) are modules of difference sizes

This combination of *p*-type and *n*-type materials does not form a diode because the semiconductors are highly doped causing the junctions to be ohmic. A diagram of this behavior can be examined more closely if instead, we look at a connection between a highly doped *n*-type semiconductor and a metal shown in Figure 2-10 where the work function of the metal is smaller than the work function of the semiconductor. In Figure 2-10 (a) electrons are flowing from the metal to the conduction band (CB) of the semiconductor. Current is carried by the electrons near the Fermi level, E_{Fm}, in the metal. When the electrons cross over into the CB of the semiconductor, their energy is E_C plus average kinetic energy (KE). Therefore, there is an increase in the average energy per electron in

environme

Passing an

junction (I

of the mate

the field to

$E_{t\,m}$

Figure 2
absorption

The e

efficiency o

electron in the contact region. The electron must therefore absorb heat from the environment (lattice vibrations) to gain this energy as it moves through the junction. Passing an electron from the semiconductor to the metal results in a release of heat at the junction (Figure 2-10 (b)). There is Joule heating which arises from the finite resistivity of the materials and it is due to the conduction electrons losing their energy gained from the field to lattice vibrations when they are scattered by such vibrations.

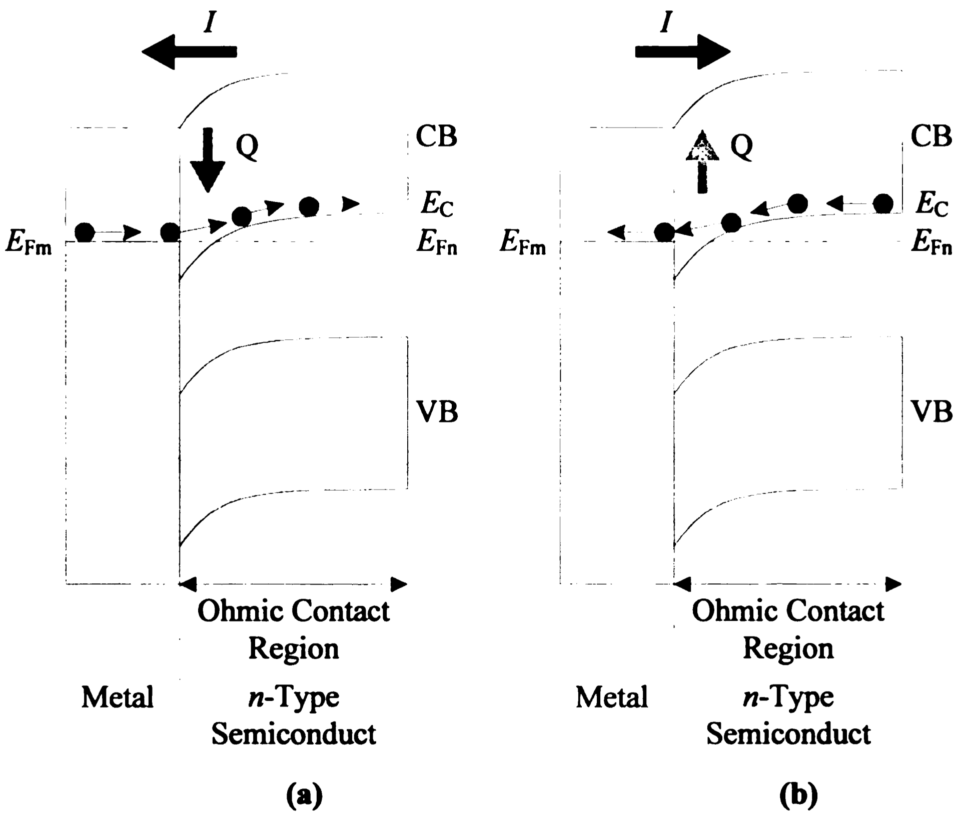

Figure 2-10: (a) Current from an *n*-type semiconductor to the metal results in heat absorption at the junction. (b) Current from the metal to an *n*-type semiconductor results in heat release at the junction. [9]

The efficiency of a thermoelectric generator is titled efficiency, η, while the efficiency of a cooler is titled the coefficient of performance (COP), ϕ. TE devices can

Th

The c

are sh

The limit

the work

Therm

least one m

The equati

resistance

the total ele

thermoelec

resistance h

be scaled without loss of efficiency making the COP derivable from a single TE couple.

The ideal efficiency for power generation (neglecting contact resistance) is as follows,

$$\eta = \frac{\dfrac{\Delta T}{T_{Hot}}}{\left[2 - \dfrac{1}{2} \cdot \dfrac{\Delta T}{T_{Hot}} + \dfrac{4}{Z \cdot T_{Hot}}\right]} \quad \text{(Ideal efficiency)} \tag{2.21}$$

The coefficient of performance for a thermoelectric cooler and its maximum efficiency are shown below

$$\phi = \frac{\alpha_{PN} \cdot T_{Cold} \cdot I - \dfrac{1}{2} \cdot I^2 \cdot R - K \cdot \Delta T}{\alpha_{PN} \cdot \Delta T \cdot I + I^2 \cdot R} \tag{2.22}$$

$$\phi_{\max} = \frac{T_{avg} \cdot \left(\sqrt{1 + Z \cdot T_{avg}} - 1\right)}{\Delta T \cdot \left(\sqrt{1 + Z \cdot T_{avg}} + 1\right)} - \frac{1}{2} \tag{2.23}$$

The limit to the maximum efficiency is called "Carnot Efficiency", which is the ratio of the work to the input heat and is shown below.

$$\eta_c = \frac{\Delta T}{T_{Hot}} \quad \text{(Carnot Efficiency)} \tag{2.24}$$

Thermoelectric modules cannot be made ideally. They will always suffer from at least one major contributor, which is contact resistance between thermoelectric materials. The equations below show how the percentage of contact resistance to the overall resistance of an entire module can degrade the ZT of the module linearly. If we let R be the total electrical resistance of a module and separate it into the resistance of the thermoelectric materials (R_{TE}) and the contact resistance (R_C), and we let the contact resistance be a percentage of the total resistance, the resulting ZT can be found.

This form

materials,

resistance

thermoelec

$$ZT = \frac{\alpha^2 \cdot \mathrm{K}}{R} = \frac{\alpha^2 \cdot \mathrm{K}}{(R_{TE} + R_C)} \tag{2.25}$$

$$\text{Let } R_C = x\% \cdot R$$

$$\text{Then } R = \frac{R_{TE}}{(1 - x\%)}$$

$$ZT = \frac{\alpha^2 \cdot \mathrm{K}}{R_{TE}} \cdot (1 - x\%)$$

This formula shows that if you know the contact resistance and the resistance of the TE materials, then you can determine what the ideal *ZT* value would be. Clearly, low resistance contacts are very desirable and have a major part in research for making thermoelectric devices. [12,13]

3.1 Introd

This

enhancing

descriptior

characteri/

at Michigan

3.2 Renew

In 1

good TE n

thermoele

been don

thermoel

possibie

and the r

or 5 are

could pr

improve

Q

have sh

materia

Chapter 3: History and Current Developments

3.1 Introduction

This section discusses the renewed interest in thermoelectric research. Efforts in enhancing the figure of merit of these TE materials will be briefly described including descriptions of common thermoelectric materials. Finally, measurement techniques for characterizing TE properties will be given along with measurements currently being done at Michigan State University.

3.2 Renewed Interest in TE Research

In 1954, Goldsmid suggested that bismuth telluride (Bi_2Te_3) alloys would make good TE materials [14]. Over the years, Bi_2Te_3 has been one of the best known thermoelectric materials with a *ZT* of about 1 near room temperature. Much effort has been done to increase this *ZT* but without much improvement. A renewed interest in thermoelectrics research (Early 1990s) has been due to predictions of large improvements possible through nanostructured materials due to quantum confinement of charge carriers and the resulting modification of the band structure [15]. Materials with a *ZT* of about 4 or 5 are needed in order to compete with a compressor-based refrigerator, and a *ZT* of 2 could prove to be useful in many applications such as automobiles. However, any improvement in ZT is expected to increase the number of applications of thermoelectrics.

Quantum confinement effects have been realized in thin film devices (TFD) and have shown a great increase in efficiency. However, unlike traditional bulk grown materials, TFDs still have challenges to overcome in order to be useful power generation or coolii

gradient

shown ii

proporti

required

structure

process

33 List

Th

been inv

material

different

material

optimize

This list

by adjus

structure

On

which ex

for coolii

telluride

reduce th

or cooling devices. Such challenges include the ability to have large temperature gradients across them and the need for improvement of manufacturing cost and time. As shown in equation (2.21), the power produced from a TE generator is directly proportional to the temperature gradient established. Therefore, higher gradients are required to yield more power out. Bulk samples may use the benefits of quantum structures found with TFD research but can be made without the complex manufacturing process along with the ability to withstand higher temperature gradients.

3.3 List of TE Materials

The following paragraphs discuss many of the thermoelectric materials that have been investigated over the years. This is a non-exhaustive list of materials and new materials are still currently being discovered. Many of the materials can be used for different operating temperatures and functions. It is also possible to combine different materials in a segmented leg of a TE module so that each material is operated at its optimized temperature range, which improves the overall efficiency of the TE module. This list also helps to show the many ways thermoelectric performance can be enhanced by adjusting the thermal conductivity of materials using quantum confinement, cage-like structures, complex crystal lattices, etc.

One of the most commonly used thermoelectric materials is bismuth telluride which exhibits a $ZT \sim 1$ near room temperature. It is currently made in mass production for cooling applications and for power generation. Usually, it is alloyed with antimony-telluride (Sb_2Te_3) which has the same rhombohedral crystal structure. The alloy helps reduce the thermal conductivity to values as low as $\kappa=1$ W/mK which is a significant contributi

is the lim

well suite

II-I

structure.

a good m

with x=0.

Silic

thermoele

10A nucl

SiGe can

thermoel

means o

operatin

depende

rise to h

efficien

A

low ter

alloyin

fields c

Skutte

contribution toward achieving the high *ZT* value. The main disadvantage of this material is the limited maximum operating temperature of ~470K. Therefore, this material is not well suited for high temperature applications.

II-IV semiconductors such as PbS, PbSe, and PbTe have the cubic NaCl crystal structure. PbTe is a narrow gap semiconductor often used in TE generators because it is a good material for hot side operation around 700K. The standard alloy is $Pb_{1-x}Sn_xTe$ and with x=0.25, the *ZT* is greater than 1 near 800K.

Silicon germanium (SiGe) alloys have been chosen for many radioisotope thermoelectric generators since 1976 where they were first used in space in the SNAP-10A nuclear reactor. In space, its spherical radioactive core serves as a heat source. SiGe can be used up to 1300K without significant degradation and the cold side to the thermoelectric material is maintained by heat fins where heat is flowing out into space by means of radiation. Primary considerations for space applications are reliability and high operating temperatures to take advantage of the T^4 (temperature to the forth power) dependence of radiator heat rejection rates. Therefore, high operating temperatures give rise to higher temperature gradients which correlate to a larger output power and efficiency.

At the other extreme, bismuth-antimony is an alloy for TE devices that operate at low temperatures. The highest ZT for Bi-Sb is 0.6 and it is reached with 10-15% of Sb alloying with Bi. This alloy exhibits a magnetothermoelectric effect where magnetic fields can double the value of the *ZT* for a value greater than 1 near 200K.

The family of skutterudite compounds has also been of great interest recently. Skutterudite is a naturally occurring mineral, $CoAs_3$, with an open, or cage-like structure.

When ato

thermal c

material.

An

similar to

smaller

isobutene,

crystallize

the cage-li

low frequ

have the

of a mate

materials

Ha

MNiSn

by remo

(MNi

interme

electric

known.

several

signifi

When atoms are placed into the interstitial voids, or cages, of these materials, the lattice thermal conductivity can be substantially reduced compared to that of the unfilled material. A *ZT* greater than 1 has been achieved in these materials at 700K.

Another open structure is found in the clathrates which have crystalline structures similar to that of ice that occur when water molecules form a cage-like structure around smaller 'guest molecules'. Common guest molecules are methane, ethane, propane, isobutene, normal butane, nitrogen, carbon dioxide, and hydrogen sulfide. Clathrates crystallize in the cubic system rather than in the hexagonal structure of normal ice. When the cage-like structure of these materials is filled with guest atoms, they strongly scatter low frequency phonons by what is called "rattle" scattering. Low frequency phonons have the highest group velocity and contribute the most to the lattice thermal conductivity of a material. With high Seebeck coefficients and electrical conductivities, clathrate materials are gaining interest for thermoelectric applications.

Half-Heusler alloys are cubic materials (MgAgAs type) with the general formula MNiSn where M is a group IV transition metal (Ti, Zr, or Hf). Half-Heusler is formed by removing the Ni atoms on one of the two Ni sublattices of the full Heusler alloys (MNi_2Sn) and replacing them by an ordered lattice of vacancies. Half-Heusler alloys are intermetallics and exhibit a high negative thermopower (-40 to –250 μV/K) and low electrical resistivities to form materials with some of the highest power factors ($S^2\sigma$) known. Unfortunately, they also exhibit a high thermal conductivity (~10 W/mK) and several efforts are under investigation toward lowering the thermal conductivity without significantly reducing the power factor.

Tell

TAGS hav

TAGS-typ

TAGS-85.

materials.

at 700K. T

mechanica

New

They have

density of

quantum

M

= antimo

LASTT

points n

533°C (

(with m

comple

morph

the ca

values

struct

high

Tellurium (Te), Antimony (Sb), Germanium (Ge), Silver (Ag) alloys known as TAGS have been used successfully in numerous space and terrestrial applications. Basic TAGS-type materials have the general formula of $(AgSbTe_2)_{1-x}(GeTe)x$. TAGS-80 and TAGS-85, 80% and 85% of GeTe respectively, are two of the most commonly studied materials. TAGS-80 exhibits a *ZT* of ~1.85 at 800K and TAGS-85 exhibits a *ZT* of ~1.35 at 700K. TAGS-85 is the preferred TE material because it is more stable and has better mechanical properties than TAGS-80 [16].

New efforts are being made using quantum dot superlattice (QDSL) structures. They have been reported to show enhanced TE device performance due entirely to a high density of quantum nanodots of PbSe composition embedded in a matrix of PbTe. These quantum dots allow electron transport while decreasing the thermal conductivity.

Much of the research at MSU has been on materials called LAST (L = lead (Pb), A = antimony (Sb), S = silver (Ag), and T = tellurium (Te)) for *n*-type bulk materials and LASTT (extra T = tin (Sn)) for *p*-type bulk materials. These materials exhibit melting points near 800°C and therefore target applications with hot side temperatures near 533°C (or 800K which is 2/3 of the melting point. The general formula $AgPb_mSbTe_{m+2}$ (with m=18 to be called LAST-18) is a family of *n*-type bulk cubic compounds with complex composition which combine a set of desirable features, such as isotropic morphology, high crystal symmetry, low thermal conductivity, and the ability to control the carrier concentration. Members of this family can be optimized to produce high *ZT* values (~2) at elevated temperatures. These compounds possess an average NaCl structure. Other materials also being investigated that show promising high *ZT* values at high temperatures are Ag-Sb-Pb-Se, Pb-Sb-Te-Se, Na-Pb-Sb-Te, and K-Pb-Sb-Te. In addition to

quantum m

Ove

several ex

the best Z

a need fo

refrigerat

addition to the creation of the bulk materials, MSU is also investigating embedding quantum nanodots of CdTe into a bulk sample of PbTe. [17]

Over the years, it is apparent that many materials have been investigated with several exhibiting good thermoelectric properties. Figure 3-1 is a graph showing some of the best *ZT* values obtained over a wide temperature range. The graph shows that there is a need for improvement on thermoelectric materials if they are going to replace current refrigeration technology by having average *ZT* values greater than 2.

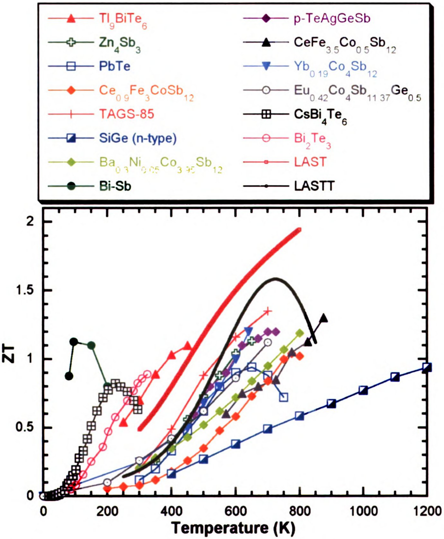

Figure 3-1: Best ZT values obtained for a variety of materials

3.4 Tecl

Tr:

is import

accompli

electrical

and creat

effects as

measurer

understar

made. Tl

devices.

measure (

and techr

disadvant

3.4.1 Ste

A c

(where he

sample) is

of a sampl

gradient al

3.4 Techniques of Characterization

Transport measurements of TE materials has been a main focus in my research. It is important to be able to identify materials with good TE properties. This is accomplished by acquiring accurate temperature dependant data for thermopower and electrical conductivity of the TE samples. Using existing TE measurement techniques and creating new measurement systems requires the knowledge of the thermoelectric effects as well as computer and electrical engineering skills. The goal of the measurements is to not only identify high performance TE materials, but to develop an understanding of the materials to a level where improvements upon the materials can be made. These improvements will be used for developing the materials into functional devices. In the following paragraphs, I discuss various existing techniques developed to measure electrical and thermal properties of TE materials as well as the measurements and techniques currently being used in our lab. Studying the advantages and disadvantages of these methods helps to design better measurements systems.

3.4.1 Steady-State Technique (Thermal Conductivity)

A common technique for low temperature measurements of thermal conductivity (where heat radiated from the sample is much smaller than heat transported through the sample) is the steady-state method [16]. With this technique, heat is applied to one end of a sample for relatively long times in order to establish a steady state temperature gradient along the sample. A diagram of the setup is shown in Figure 3-2.

Figure 3-

By

supplied t

κ can the

A is the c

measurer

If

sufficier

along th

the leng

long sta

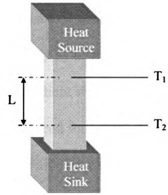

Figure 3-2: Diagram of measuring thermal conductivity using the steady-state technique

By measuring the temperature gradient along the sample, the heat, Q, being supplied to the sample, and by knowing the sample dimensions, the thermal conductivity, κ, can then be calculated. The equation for thermal conductivity is shown below where A is the cross sectional area of the sample, L is the length between the temperature measurements, and ΔT is temperature gradient T_1-T_2.

$$\kappa = \frac{Q \cdot \mathrm{L}}{\mathrm{A} \cdot \Delta T} \tag{3.26}$$

If the sample has high thermal conductivity, then the length of the sample should be sufficiently greater than the diameter. This helps to create a larger temperature gradient along the sample. For low conductivity materials, equilibrium times become very long so the length to area ratio should be kept small. The disadvantage of this technique is the long stabilization period needed for precision measurements.

3.4.2 Ha

The

thermopo

materials

junctions

measurem

method is

current pa

applying a

induced as

cooling at

conductio

[18]. This

for the me

technique

challengin

3.4.3 Pul

The

conductiv

extremely

heater cu

with a sq

3.4.2 Harman Technique (Thermal Conductivity and *ZT*)

The Harman Technique [18] is a measurement of electrical conductivity, thermopower, and thermal conductivity by utilization of the Peltier effect. Because TE materials can create a temperature gradient when electrical current is flowing through the junctions formed to the material, the need for a heat source is eliminated. This measurement allows one to calculate all parameters of *ZT*. A special feature of this method is that *ZT* is given in terms of the ratio of two voltages (voltage produced due to current passing through a resistance and voltage produced due to the Seebeck effect). By applying an electric current through a thermoelectric sample, a temperature gradient is induced as caused by the Peltier heating at one end of the sample and a subsequent Peltier cooling at the other end of the sample. There will also be Joule heating and thermal conduction. From here, it is possible to find the *ZT* using the Harman technique circuit [18]. This circuit (which uses 8 measurement wires connected to the sample) also allows for the measurements of thermopower, electrical resistivity and contact resistance. This technique is only feasible if the two voltages can easily be distinguished, which can be challenging for low *ZT* materials.

3.4.3 Pulse Technique (Thermopower and Thermal Conductivity)

The pulse technique [19] is a method for measurement of thermopower and thermal conductivity. It is very similar to the steady-state technique but does not require an extremely long waiting time. This is an AC method used to avoid offset voltages; the heater current, which is used to create a thermal gradient across the sample, is pulsed with a square wave (See Figure 3-3(a)). This method will produce piecewise exponential signals f

across th

the avera

proportic

plotted (

thermop

determin

Figure 3.

signals for the voltage across the sample (Figure 3-3(b)) and the temperature gradient across the sample (Figure 3-3(b)). When the temperature gradient is small compared to the average temperature of the sample, the voltage across the sample is directly proportional to the temperature gradient across the sample. Here, ΔV versus ΔT can be plotted (Figure 3-3(d)) and the linear slope of the measurements used to determine thermopower. This allows for a large accumulation of data points to more precisely determine the thermopower.

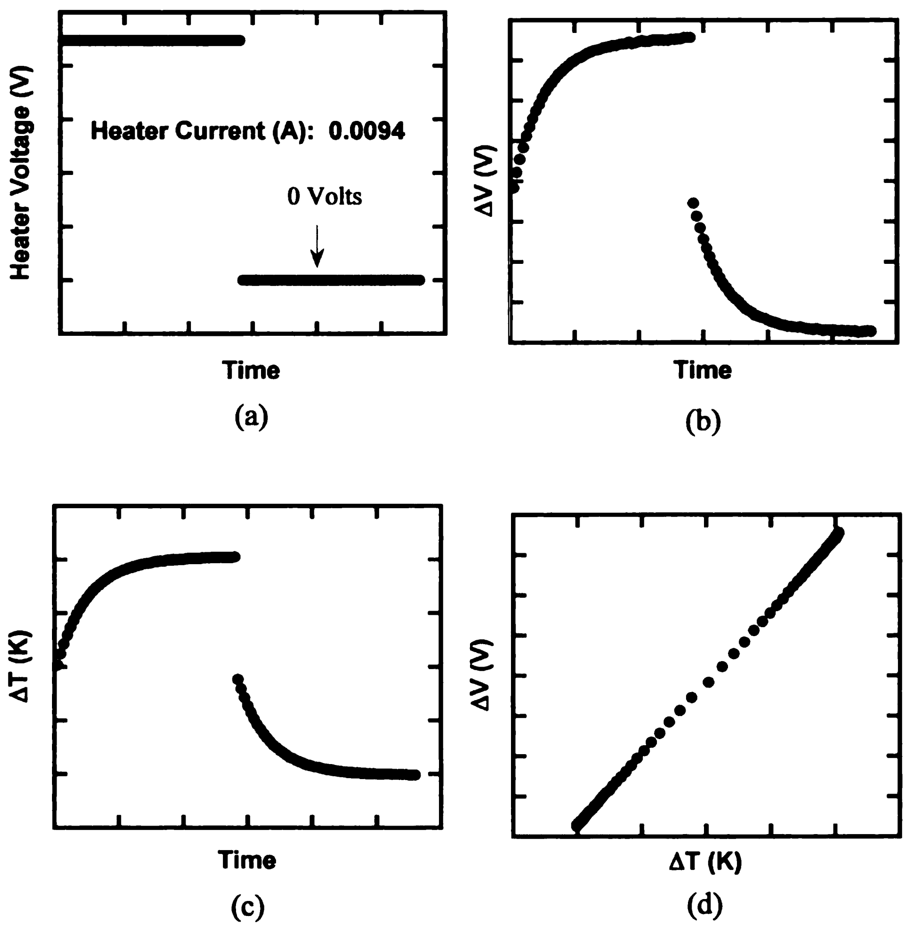

Figure 3-3: Pulse technique example. (a) Plot of heater voltage vs time. (b) Plot of ΔV vs time. (c) Plot of ΔT vs time. (d) Plot of ΔV vs ΔT.

By

may slov

sample v

(several

this stea

faster th

detail in

3.4.4 M

Co

again me

techniqu

step of th

the samp

Without a

without c

involves a

voltage a

contributi

two meas

to the elec

material a

By pulsing the heater on the sample (on and off) the overall sample temperature may slowly rise due to Joule heating. However, the temperature gradient across the sample will reach a steady AC function with constant amplitude after a short time (several minutes). Because the temperature gradient and the voltage gradient maintain this steady state AC function, thermal conductivity measurements can be made much faster than the DC steady-state technique. The pulse technique will be explained in more detail in later sections discussing the Drift System and the Ultra High Temp System.

3.4.4 Modified Harman Technique (*ZT*)

Continuing from the work of Harman, a modified technique [20] was developed to again measure ZT by utilizing only the voltage components in the measurement. In this technique, a switching square wave current source (positive to negative) is used in one step of the measurement. First, a high frequency electrical current signal is put through the sample to prevent the thermoelectric module from developing a temperature gradient. Without a temperature gradient, the electrical conductivity of the sample can be measured without contributions from the Peltier effect. The second part of the measurement involves applying a DC electrical current source through the sample and measuring the voltage across the sample to calculate the resistance. This will of course have contributions from the Peltier effect and the finite resistance of the material. Using the two measurements, one can now separate the voltage due to Seebeck and the voltage due to the electrical resistance of the material. Knowing the DC and AC resistance of the material allows for calculations of the figure of merit, *ZT*. This technique will be discussed

measurem

3.5 Meas

Mic

has many

these mat

systems t

include a

measurem

develope

3.5.1 F

A

Electro

Probe

small

2400

appro

singl

Plac

3-5

discussed in greater detail in later sections involving impedance spectroscopy measurements on thermoelectric materials.

3.5 Measurement Systems at MSU

Michigan State University typically works with bulk thermoelectric materials and has many measurement systems to characterize the temperature dependent properties of these materials (thermopower, electrical conductivity, and thermal conductivity). The systems that are discussed here were used excessively throughout my research and do not include all measurement systems available at MSU. These systems not only provided measurement data on new materials, but were also used to help verify the new systems developed during this research.

3.5.1 Room Temperature Electrical Conductivity Scanning Probe

A common system used to verify electrical conductivity measurements in the MSU Electronic Materials PLD and Characterization Lab is the Room Temperature Scanning Probe (RTSP) shown in Figure 3-4. To measure electrical conductivity of a sample, a small current (typically ~10-50mA) is put through the sample via a Keithley Instruments 2400 current source. The current is a square wave function, 50% duty cycle, at approximately 33Hz. The voltage is then measured along the sample either by using a single probe and moving it along the sample in measured increments, or by simply placing the array of ten pins on the sample and measuring the voltage at each pin (Figure 3-5). This system has three axes of motion (x, y, & z). The x and y direction allow the user to pr

lowering

purposes.

would ca

second pu

temperat

measurem

subtractin

done twen

along the

voltages

The slop

electrica

configur

Then, by

electrica

user to probe over the entire surface incrementally while the z axis is for raising and lowering the spring loaded probes onto the sample. The switching of the current has two purposes. The first is to keep the sample from establishing a temperature gradient, which would cause an error due to the Seebeck voltage developing across the sample. The second purpose is to cancel out any voltage offsets on the measurement wires due to temperature gradients or diode effects. This is accomplished by taking a voltage measurement for a positive current, taking a voltage measurement for a negative current, subtracting the two measurements, and then dividing by two. This process is typically done twenty times and the average of those values is used. By scanning the voltages along the surface of a sample, the electrical conductivity can be found by plotting the voltages versus the probe position and taking the slope ($\Delta V/\Delta x$) as shown in Figure 3-6. The slope can then be used along with the sample dimensions to find an average electrical conductivity. This method is more accurate than the standard four-point probe configuration because many points can be tested along the sample instead of just two. Then, by knowing the sample dimensions, the resistance (R) of the sample is converted to electrical conductivity (σ) of the sample using the following equations.

$$\sigma = \frac{I}{\left(\frac{\Delta V}{\Delta x}\right)} \cdot \frac{1}{\text{area}} \text{ (S/cm)} \tag{3.27}$$

$$\sigma = \frac{1}{R} \cdot \frac{\text{length}}{\text{area}} \text{ (S/cm)} \tag{3.28}$$

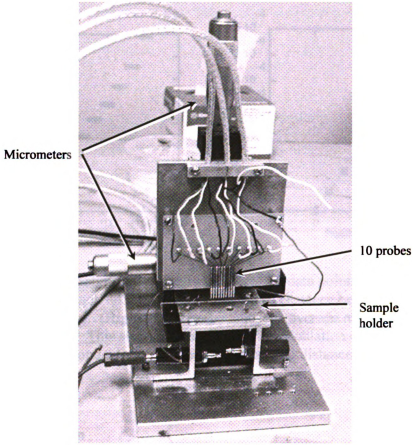

Figure 3-4: Room Temperature Scanning Probe

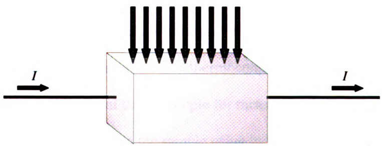

Figure 3-5: Room Temperature Scanning Probe diagram

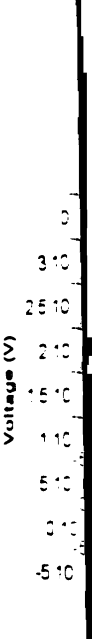

Figure
show
indicate
plotted ve

3.5.2 4-S

Thi

Universit

thermoele

(~$5x10^{-5}$ -

conductiv

T (copper

Separate v

the same l

a diagram

configurat

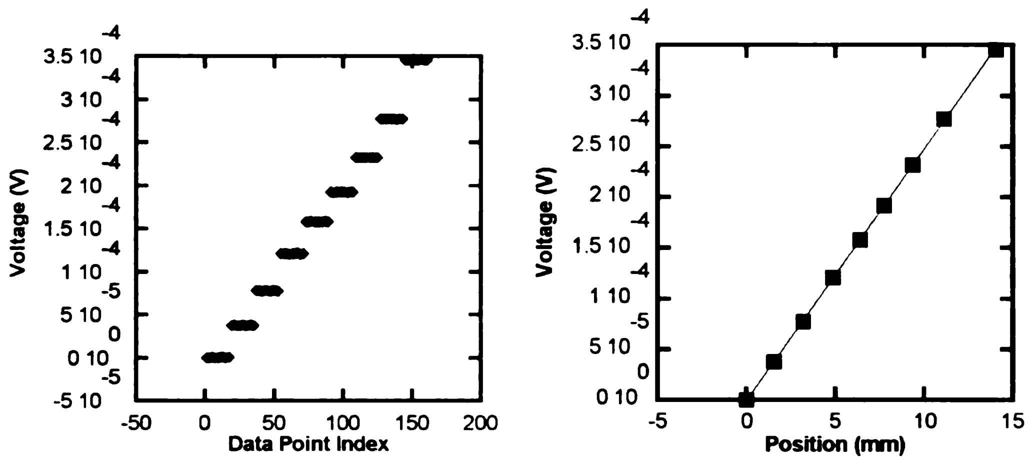

Figure 3-6: (Left) Each probe typically measures 20 data points. Here is an example showing 9 probes each taking 20 measurements. (Distance between probes is not indicated on this graph). **(Right)** Each probe takes the average measured voltage and is plotted versus position. This slope is then used in the calculation of the average electrical conductivity between the measured distances.

3.5.2 4-Sample System

This well established low temperature system (80-400K) at Michigan State University, called the 4-Sample System, is automated to measure properties of thermoelectric materials on four samples at one time in a high vacuum environment (~$5x10^{-5}$ Torr). The system is capable to measure the thermopower, electrical conductivity, and thermal conductivity. The thermocouple used in this system is a Type-T (copper-constantan) differential thermocouple for measuring the temperature gradient. Separate wire leads are connected to the sample using indium or silver paste very close to the same location as where the temperature gradient is being measured. Figure 3-7 shows a diagram of a sample mounted in the 4-Sample system. The method and sample configuration are a variation of the pulse technique. The sample stage is temperature contr lle

lower he

Fi ure

This s ste

samp a

move on

discus ed

3.5.3 Hi

he

condu tiv

Torr). Th

power hr

condu iv

extens e

thermo o

controlled using heaters connected to the stage. Liquid nitrogen (LN_2) is then used to lower the temperature of the stage.

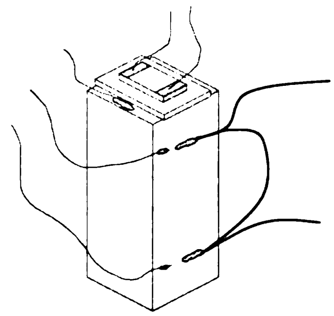

Figure 3-7: Typical mounting of the thermoelectric sample in the 4-Sample System

This system proves to be extremely useful to measure the thermal conductivity of a sample at low to room temperatures. A sample can start in the 4-Sample system and then move on to the High Temp System for higher temperature measurements, which will be discussed next.

3.5.3 High Temperature System (HTS)

The High Temperature System (HTS) [21] measures thermopower and electrical conductivity from room temperature to 700K in a high vacuum environment (~5×10^{-5} Torr). This computer-controlled system was designed to measure the thermoelectric power through a slope measurement technique, also called the pulse technique. Electrical conductivity is measured in the standard four-probe configuration. This system was used extensively to measure bulk thermoelectric samples. The HT System uses single ended thermocouples, which are used in the thermopower and the electrical conductivity measure

3-8 whi

Th

average t

measurements. An example of a sample mounted in the HT System can be seen in Figure 3-8 while Figure 3-9 shows the entire cryostat of the HT system.

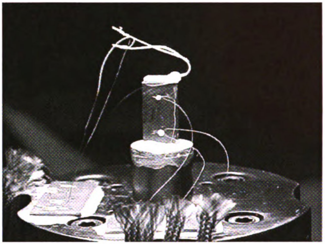

Figure 3-8: Typical sample mounted in HTS

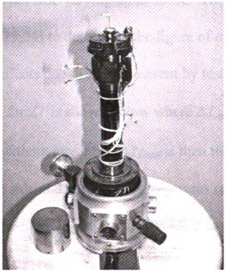

Figure 3-9: HTS Cryostat

The HT system uses heaters on the stage where the sample is mounted to adjust the average temperature of the sample. The heaters are PID (Proportional Band, Integral, Deriv ti

meas re

of ne n

3.5.4 D

ly

typica ly

sizes nd

provi s

efficie ic

desig d

at roo t

adapt H

condit or

condit or

gradie a

a load T

R_{Load} a

ZT_{av}

Derivative) controlled so that the system stays at a maintained temperature while measurements are being taken. The overall system is a good model for the development of new measurement systems.

3.5.4 Device Testing System (DTS)

Systems that are used to measure thermoelectric properties of bulk samples typically lack the capability of fully characterizing a thermoelectric device of various sizes and types (single layer or stacked modules). The Device Testing System (DTS) provides these capabilities [22]. This system measures device thermopower, resistance, efficiency, and power out for varying load and gradient conditions. The DTS was designed to place a large temperature gradient across a module by keeping the cold side at room temperature and the hot side varying up to 900K. The DTS uses a method adapted by Min and Rowe [23,24] to determine the figure of merit for non-short circuit conditions including Joule effects due to Peltier current by testing under varied load conditions. The calculation for ZT is shown below where ΔT_{open} is the temperature gradient across the module without any load. ΔT_{Load} is then the temperature gradient with a load. T_h and T_c are the hot side and cold side temperatures respectively. R_{Module} and R_{Load} are the resistances of the module and the load applied to the module respectively.

$$ZT_{ave} = \frac{\frac{\Delta T_{open}}{\Delta T_{Load}} - 1}{\left[\left(\frac{R_{Module}}{R_{Module} + R_{Load}}\right)\left(\frac{2 \cdot T_h}{T_h + T_c}\right) - \left(\frac{R_{Module}}{R_{Module} + R_{Load}}\right)^2 \left(\frac{T_h - T_c}{T_h + T_c}\right)\right]} \tag{3.29}$$

This system is also provides a large space to perform other experiments at room temperature under high vacuum such as *ZT* measurements using an AC electrical technique discussed in later sections describing impedance spectroscopy measurements on thermoelectric materials. Figure 3-10 shows a picture of the DTS system and all of the main components.

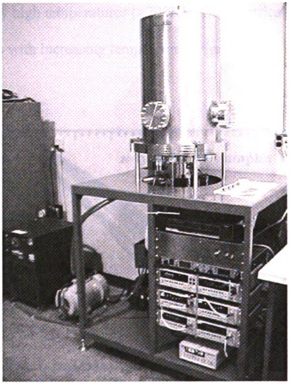

Figure 3-10: Picture of DTS

3.6 Properties of TE materials at MSU

Much of the thermoelectric material being manufactured and tested at Michigan State University behaves very similar to each other. This is due to the fact that the samples are degenerately doped semiconductors. The typical behavior can be seen by examini

of the L

Th

increase

reach a

Howeve

"roll-ov

LAST m

Figu

examining the temperature dependant electrical conductivity and thermopower behavior of the LAST (Pb-Sb-Ag-Te) and LASTT (Pb-Sb-Ag-Te-Sn) materials.

The thermopower of the LAST materials are negative, which indicates *n*-type, and increases in magnitude with increasing temperature (Figure 3-11). Some samples will reach a peak in thermopower and then begin to decrease in magnitude similarly to Bi_2Te_3. However, for high temperature applications, the thermopower doesn't typically reach a "roll-over" point until very high temperatures (>700K). The electrical conductivity of the LAST materials decreases with increasing temperature (Figure 3-12).

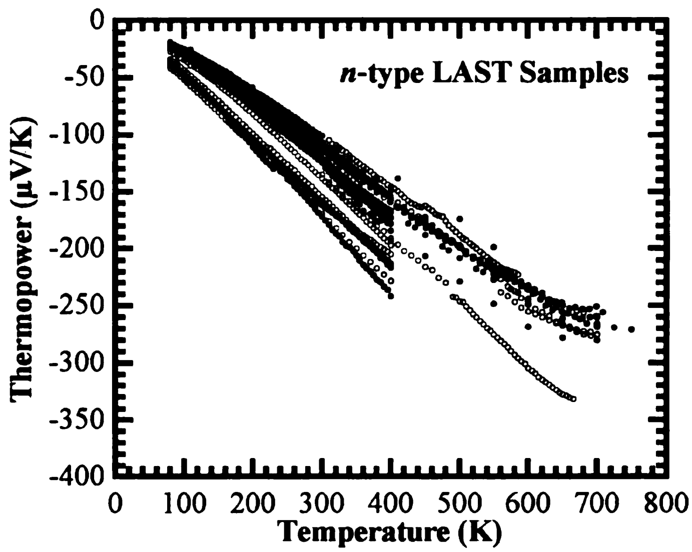

Figure 3-11: Plot of thermopower versus temperature for *n*-type LAST materials

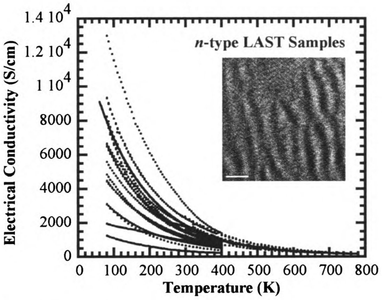

Figure 3-12: Plot of electrical conductivity versus temperature for *n*-type LAST materials

The thermopower for the LASTT materials is positive, which indicates *p*-type, and typically increases with increasing temperature (Figure 3-13). The thermopower can also reach a maximum value and "roll-over" but for high temperature TE materials, this peak in thermopower happens at very high temperatures (>600K). The electrical conductivity for LASTT samples, like the LAST samples, decrease with increasing temperature (Figure 3-14).

igu

gu

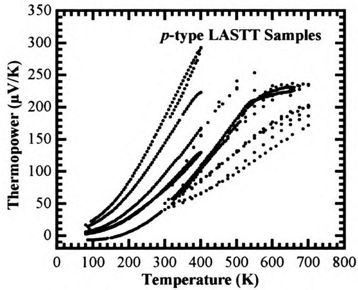

Figure 3-13: Plot of thermopower versus temperature of *p*-type LASTT materials

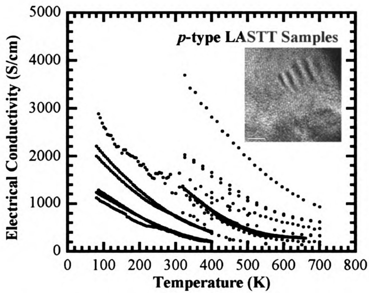

Figure 3-14: Plot of electrical conductivity versus temperature of *p*-type LASTT materials

4.1 In

F

develo

System

conduc

provide

measur

temper

temper

drift in

multiple

T

system

time. In

was also

temperat

examined

4.2 Drif

Th

provide a

Chapter 4: Drift System

4.1 Introduction

For low temperature measurements on thermoelectric materials, a new system was developed as part of this dissertation at Michigan State University called the "Drift" System. This system measures electrical conductivity, thermopower, and thermal conductivity of TE materials for the temperature range of 100K to 300K. This system provided Michigan State with a second low temperature measurement system that could measure four samples at a time. However, unlike the 4-Sample System, which uses PID temperature control, the Drift System slowly, but continuously, rises (drifts) in temperature from 100K to 300K while the system collects data. Allowing this system to drift in temperature provides smooth data at the expense of not being able to take multiple measurements at a single temperature.

The motivation of this system was to not only create another low temperature system but to also experiment with new mounting techniques to reduce the mounting time. Investigations on using a different technique for calculating thermal conductivity was also examined. Finally, the concept of drifting the sample environment in temperature (as opposed to controlling only the temperature of the sample stage) was examined for improved measurements of the thermoelectric samples.

4.2 Drift System Setup and Mounting

The Drift System comprises of a rough vacuum pump and a turbo vacuum pump to provide a high vacuum environment (1×10^{-5} Torr) for thermal isolation shown in Figure

4.1. A

sample

for elec

2182) ar

voltage

sample

7002) is

temper

of the s

of the r

LabVII

4-1. A current source meter (Keithley Instruments 2400) is used to supply power to the sample heater for thermopower measurements as well as to supply current to the sample for electrical conductivity measurements. Four nanovolt meters (Keithley Instruments 2182) are used to measure the voltage across the sample heater, two thermocouples, the voltage developed across the sample when a temperature gradient is applied, and the TE sample for measuring electrical conductivity. A switch system (Keithley Instruments 7002) is used to switch the measurement meters between four different samples. A temperature-monitoring unit (Neocera) uses a calibrated diode to identify the temperature of the sample stage. There is also the chamber for the samples to be measured. A picture of the measurement equipment is shown in Figure 4-2. Finally, there is a computer using LabVIEW software for instrument control and automated data collection.

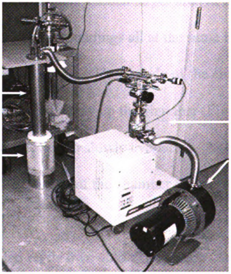

Figure 4-1: Drift System chamber with LN$_2$ dewar and vacuum system

T

inside.

here con

with PII

helps to

controlli

nitrogen

nitrogen

evapora

slowly r

Ea

thermoc

measure

mounted

portable

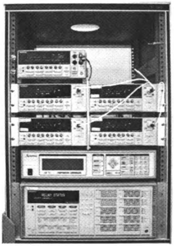

Figure 4-2: Drift System measurement equipment

The measurement chamber is vacuumed sealed with the sample to be measured inside. The chamber is cooled on the outside using liquid nitrogen (LN_2). The advantage here compared to the 4-sample system which uses an internal heater on the sample stage with PID control is that this system has a much larger area of uniform temperature. This helps to make the sample and its surroundings all at the same temperature instead of only controlling the temperature of the stage. The outside of the chamber is placed in liquid nitrogen approximately a third of the way up the chamber (Figure 4-1). The liquid nitrogen is in a dewar and is allowed to slowly evaporate. As the liquid nitrogen evaporates away, the level up the side of the chamber decreases causing the chamber to slowly rise in temperature.

Each sample is mounted on its own gold plated stage using single ended thermocouples (wire diameter = 25.4μm) and a resistor as a sample heater for measurements similar to the HT System. Figure 4-3(left) shows an example of a mounted sample. The idea here was to allow each sample to be pre-mounted to a portable stage under a microscope without interfering with the mountings of other sampl

allows

system

I

the sta

This st

plated

4-5). T

conduc

between

inserted

Figure 4

Figure

w

samples. This stage is much smaller than the one used in the 4-Sample system and allows the experimenter to work in the entire space around the sample. The 4-Sample system only allows for approximately 90 degrees of space around the sample.

Each stage has its own radiation cap, which is gold plated and screwed down onto the stage (Figure 4-3(right)). This keeps the samples from radiating heat to each other. This stage is then mounted to a larger main stage (Figure 4-4). This main stage is gold plated and also has its own gold plated radiation cap to cover all four samples (Figure 4-5). The main stage is mounted to a stainless steel shaft, which has low thermal conductivity. Along the shaft are radiation fins to reduce the thermal radiation flow between the main stage and where the wire connections are made. This long shaft is then inserted into a stainless steel tube where it is vacuum-sealed with a rubber 'O'-ring. (See Figure 4-6)

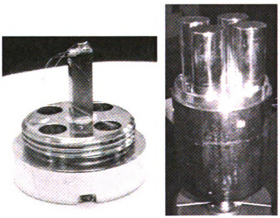

Figure 4-3: (Left) Individual sample stage with a sample mounted. (Right) Main stage without radiation cap shown a four sample stages with their radiation caps on

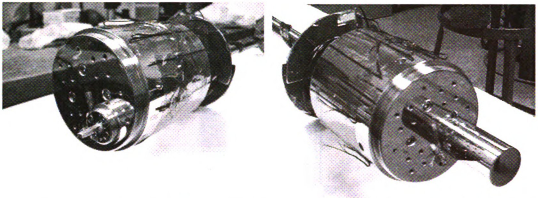

Figure 4-4: (Left) Sample stage on main stage without radiation cap. (Right) Sample stage on main stage with radiation cap.

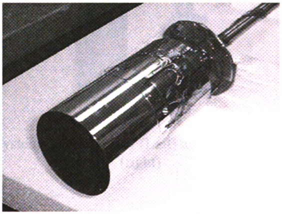

Figure 4-5: Main stage with radiation cap on.

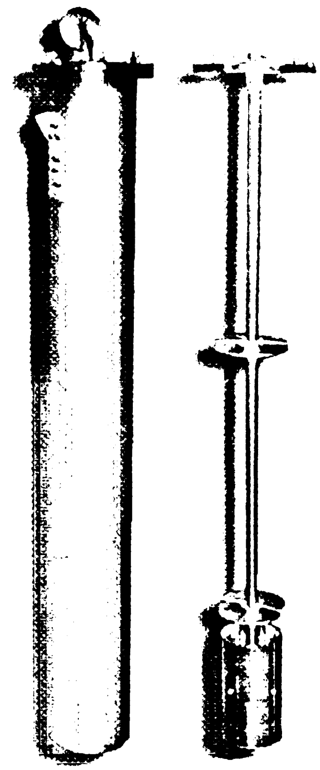

Figure 4-6: Drift System main chamber (Left) and inside shaft with sample stages (right)

The wiring diagram for this system is shown in Figure 4-7. This diagram shows how the four nanovolt meters and the current source are connect to each of the four samples through the switch box. Voltages V_1 and V_2 are used to identify the hot and cold side temperatures, respectively. V_3 is the voltage between the copper wires of the thermocouples for electrical conductivity measurements and to identify the voltage developed across the sample during thermopower measurements.

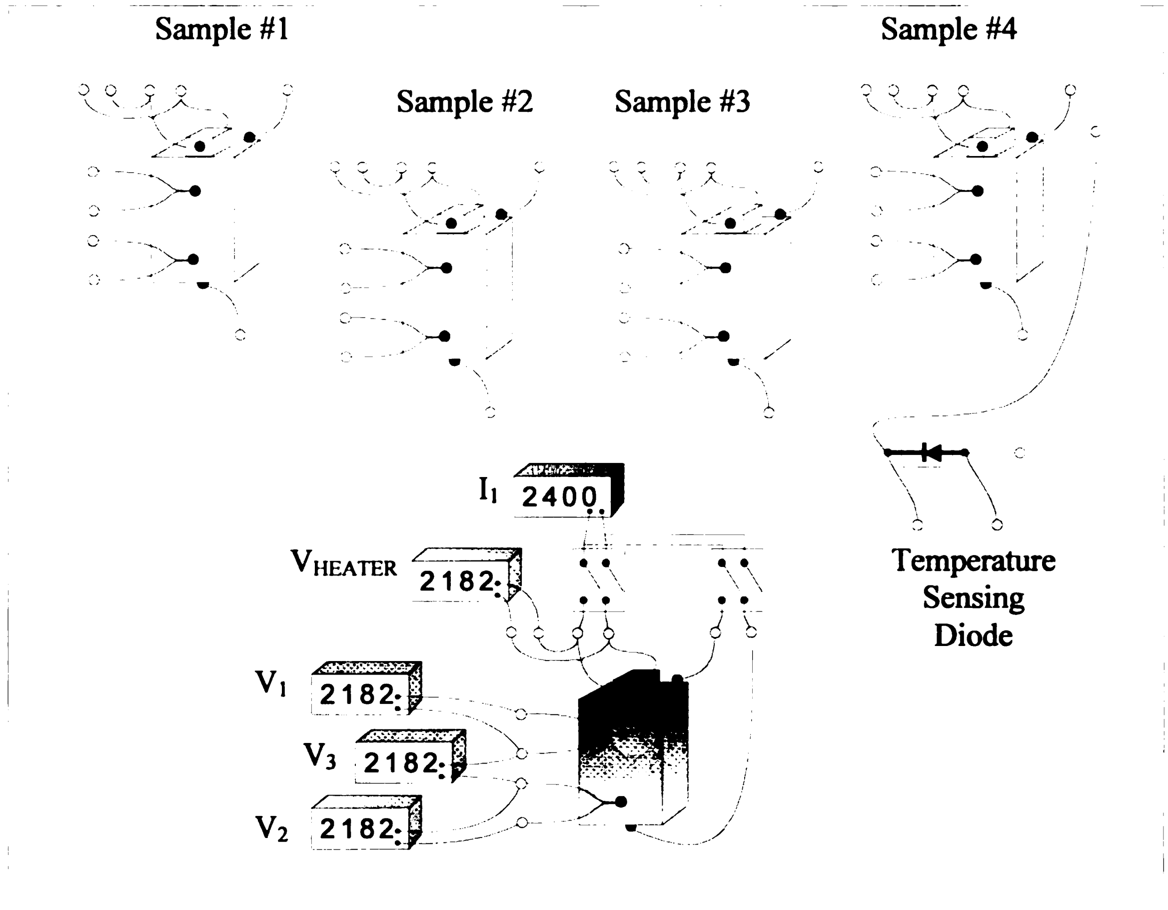

Figure 4-7: Wiring diagram for mounting each sample

4.3 Drift System Automation

Once the Drift System is loaded with the desired samples, the chamber is cooled down to the desired start temperature, and is then to be allowed to slowly rise in temperature. A computer takes control of the measurement process via a personally designed LabVIEW program. This program performs many tasks and is very similar to the HT System software.

4.3.1 Th

Al

together

The on ti

reach a s

before th

gradient

The prog

temperat

heater cu

Th

Typical r

state whe

next stat

calculate

to time a

measurer

be neces

temperat

Be

on and w

data in to

exponenti

4.3.1 Thermal Conductivity Measurements

All sample heaters are connected in series. The sample heaters are pulsed on an off together to establish an AC steady state temperature function across each of the samples. The on time of the heater must be long enough such that the sample being tested can reach a steady state AC function where the temperature gradient reaches steady state before the sample heater changes to the next state. It is important that the temperature gradient stabilizes so that an accurate thermal conductivity measurement can be made. The program keeps track of when the heater is turn on and turned off. By doing so, the temperature gradient and voltage gradient measurements are separated by the state of the heater current.

The Drift System employs a new technique for measuring thermal conductivity. Typical measurements require the samples using the pulse technique to reach a steady state where the temperature gradient levels off before the sample heater changes to the next state. From here, the average max change in temperature gradient is used to calculate the thermal conductivity of the sample. The temperature gradient with respect to time approximates piece-wise exponential curves. It is possible to speed up the measurement by identifying the equation for the exponential curves so that it would not be necessary for the temperature gradient to level off in order to locate the max change in temperature gradient.

Because the program can easily separate the temperature data for when the heater is on and when the heater is off, it is possible to separate the piece-wise temperate gradient data in to a rising exponential function (when heater is turned on) and a falling exponential function (when heater is turned off). The data is then curve fit to an exponentia

are constar

As $t \to \infty$

identifies

constant

temperat

is projec

The diff

the sam

accurat

increas

calcula

makes

experi

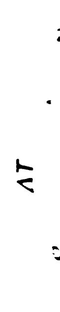

Fig

exponential function such as the one shown here using LabVIEW where A_1, A_2, and A_3 are constants.

$$F(t) = A_1 + A_2 \cdot e^{(-A_3 \cdot t)} \tag{4.30}$$

As $t \to \infty$, the exponential term goes to zero leaving only the A_1 term. This term identifies the temperature that the sample is approaching. The program solves for this constant for both cases where the sample is either rising in temperature or falling in temperature. An example of the curve fitting is shown in Figure 4-8 where the curve fit is projected out further in time where the temperature is stabilized to a constant value. The difference between these two constant values is the appropriate change in ΔT across the sample for a given heater power. Using this method of finding ΔT provides a more accurate calculation of the thermal conductivity of the sample. One reason for the increased accuracy is that instead of just the last few data points being analyzed to calculate ΔT, the entire heating/cooling profile is curve fitted. Using the entire curve makes the calculation less susceptible to glitches in the data. It also helps reduce the experimental measurement time.

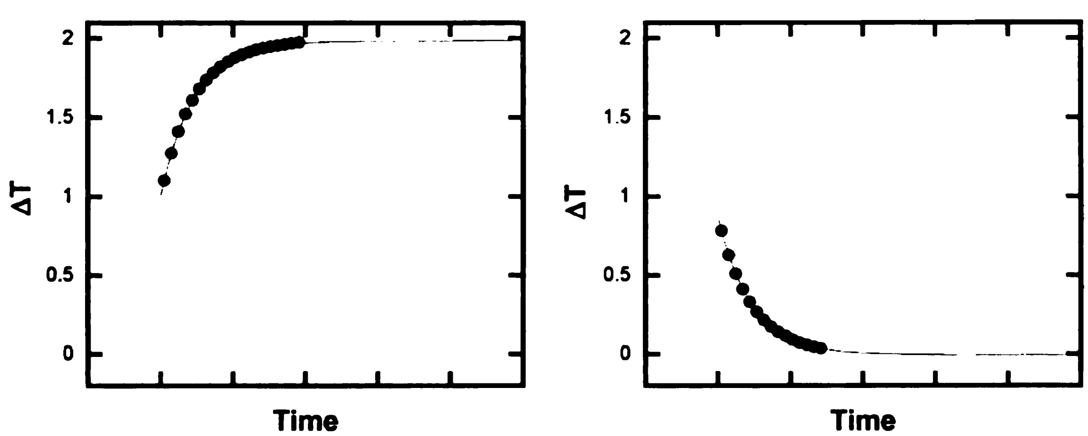

Figure 4-8: Plot of ΔT for sample rising in temperature **(Left)** and falling in temperature **(Right)** with the curve fits projected out further in time.

4.3.2 T

T

measur

as the I

sample

sample.

The sys

(current

the volt

4.3.3 P

A

collected

tempera

heater, a

turned o

The tem

4.3.2 Thermopower and Electrical Conductivity Measurements

The Drift System uses single-ending thermocouples (type-T) for the thermopower measurements. The technique for calculating the thermopower of the sample is the same as the HT System (slope-measurement technique). A resistor is placed on top of the sample as the sample heater. Two thermocouples are placed along the length of the sample. A diagram of a sample mounted for the Drift System is shown in Figure 4-9. The system measures electrical conductivity in the same manner as the HT System (current flipping technique). The current leads are attached to the ends of the sample and the voltage probes are the thermocouple wires.

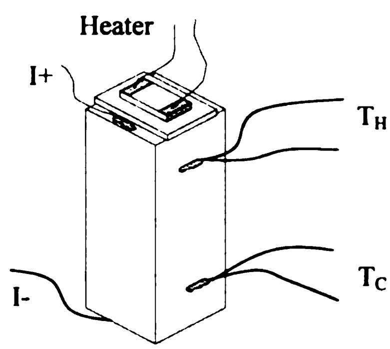

Figure 4-9: Diagram of sample mounted for Drift System

4.3.3 Program Description

As the system is slowly increasing in temperature, data is being continuously collected on each sample. However, each sample is measured at a slightly different temperature. The system will first select a sample to be measured, start pulsing the heater, and then begins collecting data for thermopower calculations. The heater is then turned off (on all samples). After a delay, electrical conductivity of the sample is made. The temperature chosen for these two data points is that average temperature between the start and

system m

the powe

establish

automat

the desi

4.4 Ve

I

In this

autom

boil a

F

con

start and end of the thermopower/electrical conductivity measurement. From here, the system moves on to the next sample and repeats the process. The program also monitors the power into the heater for each sample and keeps track of what current is needed to establish a 1°C across the sample for the thermopower measurements. Adjustments are automatically made to the heater power to keep the temperature gradient within 20% of the desired ΔT.

4.4 Verification of the System

The temperature versus time of a typical Drift System run is shown in Figure 4-10. In this run, the minimum temperature was about 160K. At this temperature, the automated data collection program was initiated while the liquid nitrogen was allowed to boil away.

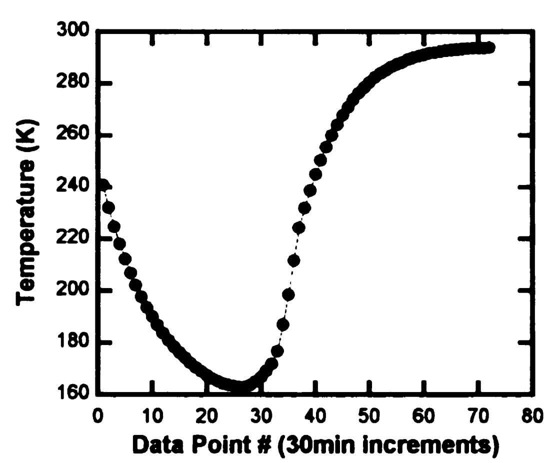

Figure 4-10: Plot of temperature versus time for the Drift System. Automated data collection is started when the temperature reaches a minimum value.

This system used stainless steel as a reference material to test electrical conductivity, thermal conductivity, and thermopower. The most important test for this system is t

gradient a

the separa

shows the

electrical c

plotted ag

experimen

stainless st

Fig

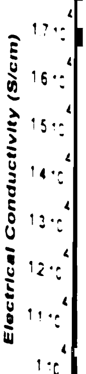

Figure 4-1
(Left)

system is the verification of the thermal conductivity measurements. The temperature gradient across the sample at 163K versus time is shown in Figure 4-11. This plot shows the separation in the data for when the sample is heating up or cooling down. It also shows the temperature gradient to be about 1K. Figure 4-12 shows both plots for electrical conductivity and thermal conductivity versus temperature for the stainless steel plotted against reference data. There is good agreement between reference data and experimental data shown. This system was also able to obtain the thermopower of the stainless steel and is shown in Figure 4-13.

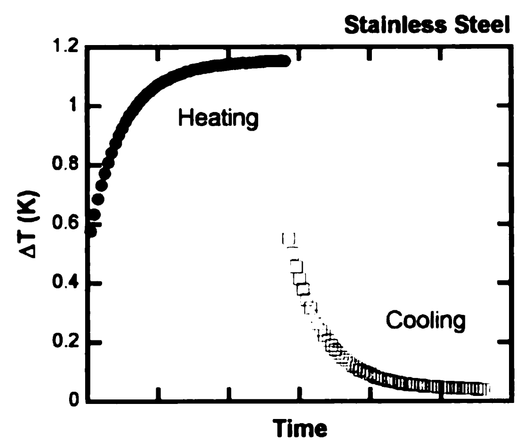

Figure 4-11: Plot of ΔT versus time for heating and cooling of the sample.

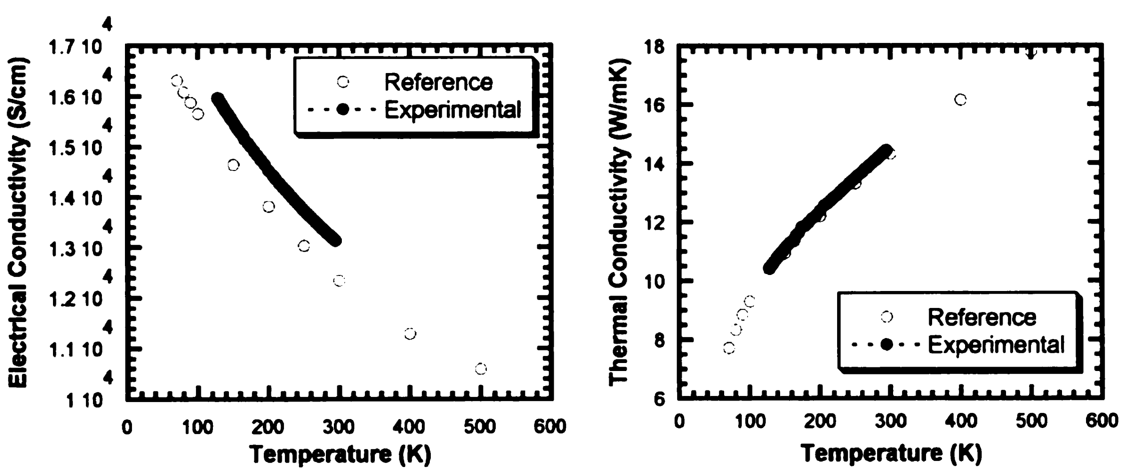

Figure 4-12: Thermal conductivity verification against stainless steel reference sample. (Left) Plot of electrical conductivity versus temperature. (Right) Plot of thermal conductivity versus temperature.

4.5 L

the m

In ad

tempo

Attem

and th

4-14 s

could

minim

goal o

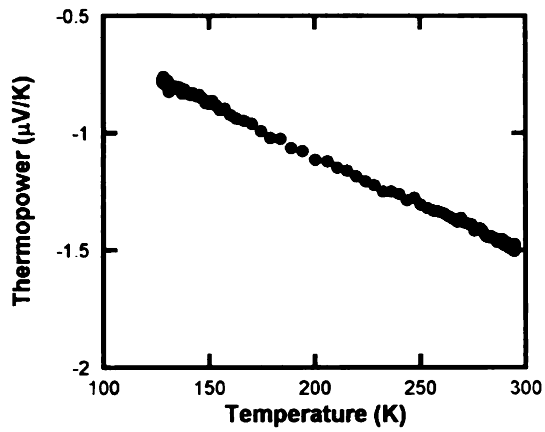

Figure 4-13: Plot of thermopower of stainless steel versus temperature.

4.5 Limitations of the System

The Drift System performed well and was used to test many samples. However, the mounting process for the samples proved to be much more difficult than anticipated. In addition to the long sample mounting times, the system also did not reach low enough temperatures. The goal was for the system to reach liquid nitrogen temperatures (~80K). Attempts were made to increase the thermal conductance between the main sample stage and the outside walls of the chamber that where submerged in the liquid nitrogen. Figure 4-14 shows the addition of aluminum foil to the main stage so that a thermal contact could be made to the walls of the chamber. The addition of the aluminum did bring the minimum temperature down to less than 130K shown in Figure 4-15 but did not reach the goal of less than 100K.

Fi

Figur

4.6 Co

T

TE ma

collecti

use and

system.

curve fi

for an i

lowering

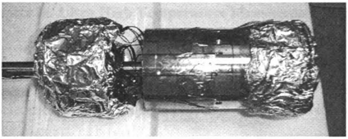

Figure 4-14: Adding aluminum foil to make thermal contact to walls of chamber

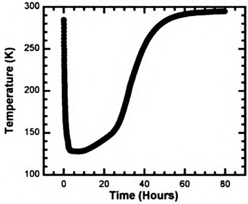

Figure 4-15: Plot of temperature versus time of the Drift System after adding aluminum to the main sample stage.

4.6 Conclusion

The Drift System was assembled and built for low temperature measurements of TE materials. A personally designed LabVIEW program was created for automated data collection. The 'drift' technique for TE measurements proved to be a viable method to use and obtain smooth data. The technique was then applied to a new high temperature system, which is discussed in the next section. A LabVIEW program was created to curve fit the temperature profiles along the sample during thermopower measurements for an improved thermal conductivity measurement. Further investigation is required for lowering the minimum run temperature to at least 100K or below.

5.1 I ro

he

modu s.

700K nd

meası : t

extrap at

There e

meası th

the Ul a I

condu .v

tempe tu

previo . s

how th m

referei : s

5.2 Ul T

T e

temper ar

and dat ac

comme a

of meas e

Chapter 5: Ultra High Temperature Measurement System

5.1 Introduction

The thermoelectrics project is intended for high temperature thermoelectric modules, which may go as high as 900K. The current HT system at MSU can reach 700K and then data is extrapolated up to higher temperatures. A system was needed to measure thermoelectric materials at these higher temperatures to eliminate the need for extrapolation of data, which can provide a false sense of the thermoelectric properties. There is existing research on many systems [25-30]. Presented here is a system that can measure thermoelectric materials from room temperature to 1200°C. This system, called the Ultra High Temp System (UHT System), is used to find thermopower and electrical conductivity on materials never before tested and up to and beyond the necessary temperatures of 300K to 850K. It also employs the 'drift' technique discussed in the previous section. This section describes the components of the system. A description of how the measurements are performed along with verification of the system against a reference sample is provided.

5.2 UHT System

The UHT System is comprised of a large furnace to control the average sample temperature, a sample stage, measurement devices, and a computer for system control and data acquisition. The sample holder with all electrical connections makes use of a commercially available ProbStat by NorECs. The UHT System uses a minimal amount of measurement equipment for the thermopower and electrical conductivity measu

describ

mount

5.2.1 F

T

to creat

of surro

systems

values.

heater is

uses is 1

rate of le

electrica

slowly d

from the

set to a d

measurements. Experiments are also performed under high vacuum. This section will describe each of the components to the system along with how a sample is typically mounted.

5.2.1 Furnace

The UHT System uses a large split tube furnace from ThermCraft (see Figure 5-1) to create a large, uniformly distributed volume of heat around the sample. This technique of surrounding the entire sample holder with a uniform heat is unique to this lab. Current systems heat the sample stage while the surroundings are close to room temperature values. This furnace is rated from room temperature to 1200°C. The power for this heater is 208 VAC single phase (2 legs of a 3-phase network). The maximum current it uses is 19.8 amps. The size of the furnace gives it a large heat capacity and will cool at a rate of less than 2^{o}C/minute. This slow cooling rate allows for thermopower and electrical conductivity measurements to be taken while the overall sample temperature slowly drifts down to a room temperature value naturally. This technique is different from the High Temp System, which uses a small heater inside a vacuum chamber that is set to a desired temperature and controlled using a PID controller.

of the

Platin

contr

tempe

increa

The c

Typic

value

Systen

particu

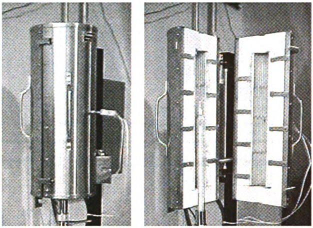

Figure 5-1: ThermCraft split tube furnace

A ThermCraft temperature controller, using PID control, regulates the temperature of the furnace (See Figure 5-2). Two S-Type thermocouples (Platinum - Platinum/Rhodium) are placed into the center of the furnace to monitor temperature. The controller uses on/off switching (pulse train modulation) to maintain the furnace temperature. This temperature controller allows the user to adjust the rate of temperature increase and decrease along with many other important features such as the PID settings. The controller is not computer controlled making the system only semi-automated. Typical measurements are performed by increasing the temperature to a desired max value and then turning off the furnace to cool naturally. This is similar to the Drift System however, unlike the drift system, the temperature can be maintained at a particular level for multiple measurements.

5.2.2 Pr

Th

(see Figu

perr neab

pro ides

elec rical

temj eratu

alon ; wit

high temp

atmc sphe

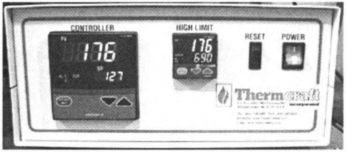

Figure 5-2: ThermCraft temperature controller

5.2.2 ProboStat

The UHT System uses an apparatus called a ProboStat purchased from NorECs (see Figure 5-3). A ProboStat is a measurement cell for electrical properties and permeability studies at high temperatures and in controlled atmospheres. The ProboStat provides a long testing stage so that the sample can be inside the furnace while the electrical connections to the testing equipment remain outside the furnace at a safe temperature. The ProboStat uses S-type thermocouples (Platinum & Rhodium/Platinum) along with platinum measurements wires. Platinum is used because it remains stable to high temperatures without melting and without oxidizing in inert or non-inert atmospheres.

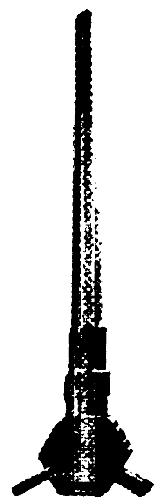

Figure 5-3: NorECs ProboStat

The ProboStat was design to handle long-term temperatures less than 1200°C and is used to measure a single sample. The base of the ProboStat is shown in Figure 5-4 which contains four Swagelok quick connects to 1/8" tubing. Two of the quick connects are for inlet of gasses and two are for exhaust (or vacuum). There are three thermocouple connections (only two are used for this measurement system) and six BNC electrode connections (4 connections are used) are available with the option of being switched either to isolated or ground). The housing of the base is made of nickel-plated brass. The base unit can handle up to 120°C, however, the BNC cables are rated for only 70°C. There is an option to either water or air-cool the top of the base unit, however, it has not been necessary for this measurement system. The top of the base typically has a temperature that does not go above 310K.

A c

connecti

connecti

them to

platinum

cell insi

Platinur

sensor i

measur

sample

explair

is conr

attach

that ar

isolat

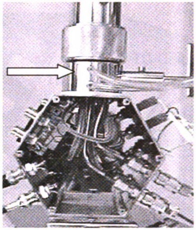

Figure 5-4: Base of Probostat

A diagram of the base of the ProboStat is shown in Figure 5-5 to identify electrical connections. The base unit comes with pre-marked labels next to the electrical connections such as HC, HV, LV, and LC. We can ignore what the letters mean but use them to identify the locations of the electrical connections. For example, a PT-103 platinum resistor (used as a temperature sensor) is placed at the base of the measurement cell inside where the thermocouple connections switch between Platinum (or Platinum/Rhodium) wires and copper wires. The current supplied to this temperature sensor is supplied through the HC connection. The voltage measured across the sensor is measured through the HV connection. LV is used to supply electrical current through the sample and LC is used to supply electrical current to the sample heater (which will be explained in later sections). The thermocouple attached to the "cold" side of the sample is connected to the top thermocouple connections, while the "hot" side thermocouple is attached to the lower thermocouple connection (shown in the diagram). The switches that are shown in the diagram determine if the BNC cables are grounded to the base or isolated. This system uses the isolated case.

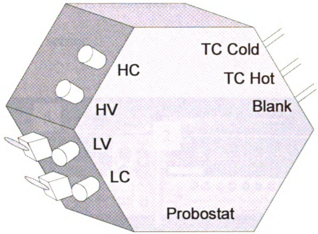

HC	PT-103 10μA current
HV	PT-103 Measure Voltage
LV	Sample Heater Current
LC	Sample Current
Switches	Keep flipped up (isolated shields of BNCs)

Figure 5-5: Diagram for the base of the Probostat unit

5.2.3 Measurement Equipment

Electrical resistance and thermopower measurements involve measuring voltages in the nanovolt range. This requires measurement equipment than can perform in this range. Figure 5-6 shows the five pieces of equipment used for all of the measurements. #1 is Keithley Instruments 2400 current source, which will provide current to the sample and also current to the sample heater. #2, #3, and #4 are Keithley Instruments 2182 nanovolt meters. #2 measures the voltage across the temperature sensor as well as the voltage across the sample. #3 and #4 measures the voltage of the hot side and cold side therm

curre

5.2.

(Rc

app

bet

1 8

tha

pic

thermocouples respectively. #5 is a Lakeshore 10μA current source used to supply current to the temperature sensor.

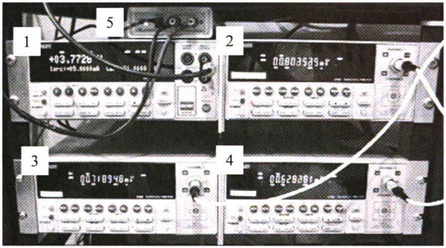

Figure 5-6: Measurement equipment

5.2.4 Vacuum Pump

The UHT System takes measurements under high vacuum. A Varian Task V70LP (Rough and Turbo Pump Package) vacuum pump is used to pump down the ProboStat to approximately 2×10^{-5} Torr. However, the vacuum pressure can only be measured between the pump and the ProboStat (not on the inside of the ProboStat). There is only a 1/8 inch copper tubing for the vacuum line into the ProboStat. Therefore, it is possible that the vacuum pressure inside the ProboStat is higher than the measured values. A picture of the vacuum pump is shown in Figure 5-7.

D.

electrica

connecte

ProboSta

connectio

ground lo

V

Fig

Figure 5-7: Varian vacuum pump

During the initial system tests, the vacuum pump was identified as a source of electrical noise in the measurements of thermopower shown in Figure 5-8. The pump is connected to the ProboStat via a metal hose. To electrically isolate the pump for the ProboStat, a non-conductive clamp and 'O'-ring was used to make the vacuum connection. This considerably helped to reduce the noise, which was likely caused by a ground loop situation.

Volts (μV)

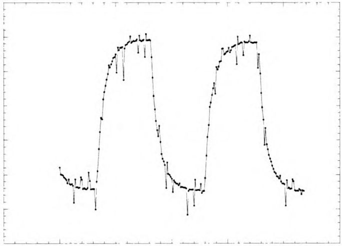

Time

Figure 5-8: Electrical noise in measurements due to vacuum pump connection

5.2.5 Sa

Th

thickness

to moun

top even

Be

appropri

acetone

any resid

sandpape

the samp

current le

nickel la

througho

paste tha

then meas

For

the sampl

temperatu

measuring

with a pie

5.2.5 Sample Mounting

The UHT System is designed to measure bulk TE samples where the width and thickness is 3mm or larger and the height is 5mm or larger. Smaller samples are difficult to mount with all the necessary wires and because the sample must support a heater on top even in the presence of small vibrations (mostly due to the vacuum pump vibration).

Before a sample is mounted, it must first be prepared. Each sample is first cut to an appropriate size using a diamond wheel saw. After the sample is cut, it is cleaned with acetone to remove any dirt and mounting wax followed by a bath in methanol to remove any residue from the acetone. The sample is then lightly polished with fine grit sandpaper. This step can help remove and oxides that may have formed on the surface of the sample. Once the sample is ready to be measured, the ends of the sample where the current leads are attached are nickel-plated using electro-plating processes. This thin nickel layer will help distribute the contact area to insure a uniform electric field throughout the sample and it also acts as a diffusion barrier to help prevent the silver paste that is applied later from diffusing into the sample. Dimensions of the sample are then measured and the sample is ready to be mounted into the system.

For measuring thermopower and electrical conductivity, a heater is placed on top of the sample, two thermocouples are placed along the length of the sample to measure the temperature gradient, and current leads are placed on top and bottom of the sample for measuring electrical conductivity. A diagram of the setup is shown in Figure 5-9 along with a picture of a sample already mounted.

meas

inch

temp

curre

samp

5.3 E

10mA

thermo

The cu

switchi

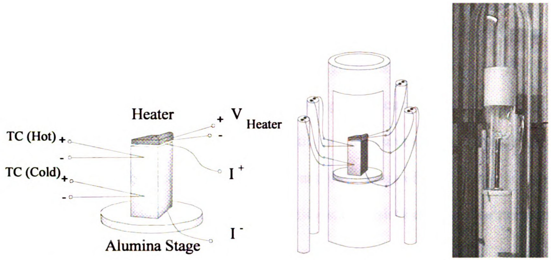

Figure 5-9: Mounting a sample for measurement (TC = thermocouple)

The sample heater is a small platinum resistor typically used for temperature measurements. The thermocouples are Type-S (Platinum - Platinum/Rhodium), 0.003 inch or 0.002 inch in diameter. This thermocouple is a good candidate for this temperature range because it can handle the higher temperatures without oxidizing. The current leads to the sample (I+ and I-) are platinum wires 0.003 inch in diameter. The sample sits on an alumina stage. Colloidal silver pastes is used for all connections.

5.3 Electrical Conductivity Measurement

To measure electrical conductivity of a sample, a small current (typically +/- 10mA) is put through the sample via the current leads and the platinum wires of the two thermocouples measure the voltage across the sample creating a four point measurement. The current is a square wave function, 50% duty cycle, at approximately 33Hz. The switching of the current has two purposes. The first purpose is to keep the sample from establis

voltage

offsets

accomp

measure

by two.

used. F

then con

5.4 Mea

V_1

V_3

V_2

Fig

setup wh

copper w

temperat

establishing a temperature gradient, which would cause an error due to the Seebeck voltage developing across the sample. The second purpose is to cancel out any voltage offsets on the measurement wires due to temperature gradients or diode effects. This is accomplished by taking a voltage measurement for a positive current, taking a voltage measurement for a negative current, subtracting the two measurements, and then dividing by two. This process is typically done ten times and the average of those values is then used. From there, by knowing the sample dimensions, the resistance (R) of the sample is then converted to electrical conductivity (σ) using the equation shown below.

$$\sigma = \frac{1}{R} \cdot \frac{\text{length}}{\text{area}} \text{ (S/cm)} \tag{5.31}$$

5.4 Measuring Thermopower Using a Pulsing Technique

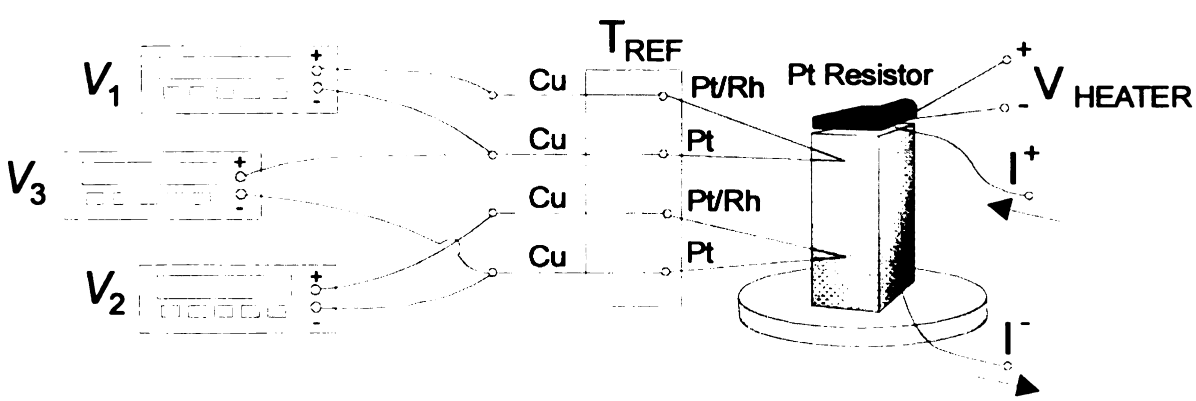

Figure 5-10: Measurement setup

Figure 5-10 shows a diagram of the electrical connections in the measurement setup where V_1, V_2, and V_3 are measured by Keithley nanovolt meters, Cu stands for copper wires, Pt for platinum, Pt/Rh for platinum/rhodium, and T_{REF} stands for reference temperature which is found using a platinum resistor as a temperature sensor. To measure

off. con

After se

a stable

is appro

calculat

data poi

tempera

voltage

System

the calcu

the therm

between

V_1

measure the themopower of a sample, the heater on top of the sample is pulsed on and off, continuously causing the temperature across the sample to increase and decrease. After some period of time, the difference in temperature across the sample will maintain a stable periodic function with a constant offset (no drift). The difference in temperature is approximately 1°K. It is this difference in temperature and voltage that is used in the calculations of thermopower. The advantage of this technique is to be able to use many data points for the calculation of thermopower. This technique eliminates any unknown temperature gradients along the measuring wires. This also eliminates any D.C. offsets in voltage on the measuring wires. This technique is currently used in the High Temp System and is a modified version of the Maldonado technique [19]. The following shows the calculations for V_1 and V_2 and how the difference between those two voltages equals the thermopower of the thermocouples used multiplied by the temperature gradient between the two thermocouples.

$$
\begin{aligned}
V_1 &= \int_{T_R}^{T_H} S_{PtRh}(T)dT + \int_{T_H}^{T_R} S_{Pt}(T)dT = \int_{T_R}^{T_H} \left[S_{PtRh}(T) - S_{Pt}(T)\right]dT \\
V_2 &= \int_{T_R}^{T_C} S_{PtRh}(T)dT + \int_{T_C}^{T_R} S_{Pt}(T)dT = \int_{T_R}^{T_C} \left[S_{PtRh}(T) - S_{Pt}(T)\right]dT
\end{aligned}
\tag{5.32}
$$

$$
\begin{aligned}
V_1 - V_2 &= \int_{T_R}^{T_H} \left[S_{PtRh}(T) - S_{Pt}(T)\right]dT - \int_{T_R}^{T_C} \left[S_{PtRh}(T) - S_{Pt}(T)\right]dT \\
&= \int_{0}^{T_H} S_{TC}(T)dT - \int_{0}^{T_R} S_{TC}(T)dT - \int_{0}^{T_C} S_{TC}(T)dT + \int_{0}^{T_R} S_{TC}(T)dT \\
&= \int_{T_C}^{T_H} S_{TC}(T)dT
\end{aligned}
\tag{5.33}
$$

At the s

V_3 can b

voltage

$$V_3 = \int_{T_R}^{T_H}$$

$$= \int_{0}^{T_H}$$

$$= - \int_{T}^{T}$$

When T_i

$$\int_{T_C}^{T_H} S_{TC}(T)dT \approx S_{TC}(T_{AVG}) \cdot T\Big|_{T_C}^{T_H} = S_{TC}(T_{AVG}) \cdot (T_H - T_C) \tag{5.34}$$

$$T_H - T_C << T_{AVG} \equiv \frac{T_1 + T_2}{2}$$

$$\Rightarrow S_{Sample}(T_H) \approx S_{Sample}(T_C) \;\; \& \;\; S_{Pt}(T_H) \approx S_{Pt}(T_C)$$

$S_{Sample}(T)$ and $S_{Pt}(T_H)$ are a constant.

$$V_1 - V_2 = S_{TC}(T_H - T_C) = S_{TC}(T_{AVG}) \cdot \Delta T \tag{5.35}$$

$$\boxed{V_1 - V_2 = S_{TC}(T_{AVG}) \cdot \Delta T} \tag{5.36}$$

At the same time the temperature gradient is being measured using V_1 and V_2, the voltage V_3 can be used to find the electrical voltage across the sample due to the thermoelectric voltage developed by the sample. This derivation is shown below.

$$\begin{aligned} V_3 &= \int_{T_R}^{T_H} S_{Pt}(T)dT + \int_{T_H}^{T_C} S_{Sample}(T)dT + \int_{T_C}^{T_R} S_{Pt}(T)dT \\ &= \int_0^{T_H} S_{Pt}(T)dT - \int_0^{T_R} S_{Pt}(T)dT - \int_{T_C}^{T_H} S_{Sample}(T)dT + \int_0^{T_R} S_{Pt}(T)dT - \int_0^{T_C} S_{Pt}(T)dT \\ &= -\int_{T_C}^{T_H} S_{Sample}(T)dT + \int_{T_C}^{T_H} S_{Pt}(T)dT \end{aligned} \tag{5.37}$$

When $T_H - T_C << T_{AVG} \equiv \dfrac{T_1 + T_2}{2} \Rightarrow S_{TC}(T_H) \approx S_{TC}(T_C) \quad S_{TC}(T_H)$ is a constant.

Ta

sm

To

eq

coef

the s

func

relat

Whe

const

Taking the sample thermopower, and platinum thermopower to be constant over the small temperature gradient (T_H - T_C) gives

$$V_3 = \left[S_{Pt}(T_{AVG}) - S_{Sample}(T_{AVG})\right] \cdot (T_H - T_C) \tag{5.38}$$

$$\boxed{V_3 = \left[S_{Pt}(T_{AVG}) - S_{Sample}(T_{AVG})\right] \cdot \Delta T} \tag{5.39}$$

To find the thermopower of the sample, ΔT from equation 5.36 (V_1-V_2) can be put into the equation for V_3 as shown below.

$$\begin{aligned} V_3 &= \left[S_{Pt}(T_{AVG}) - S_{Sample}(T_{AVG})\right] \cdot \Delta T \\ S_{Sample}(T_{AVG}) &= S_{Pt}(T_{AVG}) - \frac{V_3}{\Delta T} \\ &= S_{Pt}(T_{AVG}) - \frac{V_3}{\left(\dfrac{V_1 - V_2}{S_{TC}(T_{AVG})}\right)} \\ &= S_{Pt}(T_{AVG}) - \frac{V_3}{V_1 - V_2} \cdot S_{TC}(T_{AVG}) \end{aligned} \tag{5.40}$$

$$\boxed{S_{Sample}(T_{AVG}) = S_{Pt}(T_{AVG}) - \left(\frac{V_3}{V_1 - V_2}\right) \cdot S_{TC}(T_{AVG})} \tag{5.41}$$

The Seebeck coefficient of platinum is known from reference data and the Seebeck coefficient of an S-type thermocouple is provided by NIST. To find the thermopower of the sample, one simply needs to find V_3 / (V_1-V_2). Even though V_3 is some exponential function of time and V_1-V_2 is also some exponential function of time (non-linear), the relationship between V_3 and V_1-V_2 is linear. This can be explained with the following:

When $T_H - T_C << T_{AVG} \equiv \dfrac{T_1 + T_2}{2} \Rightarrow S_{Sample}(T)$ is a constant. Therefore, the $\dfrac{\Delta V}{\Delta T}$ is constant.

will b

best fi

(typica

5.5 Pr

T

LabVIE

controll

material

- P
- C
- C
- S
- S

V_3 is linearly related to V_1-V_2, and when one is plotted versus the other, the result will be linear line. By taking a best fit to this linear function and finding the slope of the best fit, the relationship between V_3 and (V_1-V_2) is found using many data points (typically 200-300 data points). An example of this will be shown in Figure 5-13.

5.5 Program Overview

The system is interfaced to a PC and the data collection is fully automated using LabVIEW software. With the average temperature of the sample being independently controlled, the LabVIEW program performs the following procedures to collect the TE material properties of interest.

- Pulse the sample heater for 3 minutes (approximately 2 pulse periods)
- Get temperature of the base of the thermocouples using Pt Resistor
    - Convert measured resistance ($R_{Pt} = V / I$) to temperature using the following formula:

      $$Temp(R_{Pt}) = 30.098 + 2.3026 \cdot R_{Pt} + 0.0012209 \cdot R_{Pt}^2$$
- Get temperature of sample
    - Use base temperature and voltage of TC_{HOT} to find temperature of the sample
- Start collecting voltages V_1, V_2, and V_3 for 2.2 pulse periods
- Store data

• S

(

• F

The fro

below.

- Main file contains all calculated values from measurements (temperature, thermopower, electrical conductivity, power factor, temperature gradient, etc.)
- Separate files store the V_1, V_2, and V_3 voltage arrays for each measurement taken (This can be used for post processing later if need be)

- Stop pulsing heater, measure electrical conductivity of sample (flipping current method) and store results into main file
- Repeat this process after an arbitrarily set delay

The front panel view of the LabVIEW program for the UHT System is shown below.

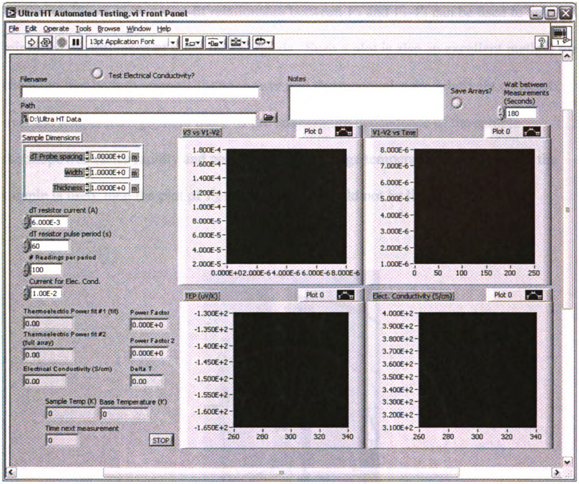

Figure 5-11: Front panel view of the LabVIEW program for the UHT System

5.6 The Built System

The full system (except for the computer) is shown in Figure 5-12. An example is provided of a typical measurement of the UHT system in Figure 5-13. Notice that even though the voltages from the thermocouples are not at a steady oscillating function but rather decreasing in time, the difference between V_1 and V_2 does remain a steady oscillating function along with V_3. This is again because the thermopower of the sample is constant during the period of time the measurement took place and while the sample is slowly drifting down in temperature. Also notice that when plotting V_3 versus V_1-V_2, the

results
minimi
checkin
over th
thermo
sample

results are linear, such a best-fit relationship between V_3 and V_1-V_2 can be used to help minimize the influence of noise in the signals. Such a plot is also an excellent method for checking that both the sample thermopower and thermocouples are relatively constant over the temperature gradient used. If the temperature dependence of the sample thermopower varies rapidly and nonlinearly, and a large temperatre gradient across the sample is used, then the plot of V_3 versus (V_1-V_2) would not be linear.

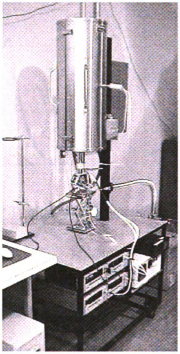

Figure 5-12: UHT System

5.7 Ve

T

sample.

support

are in g

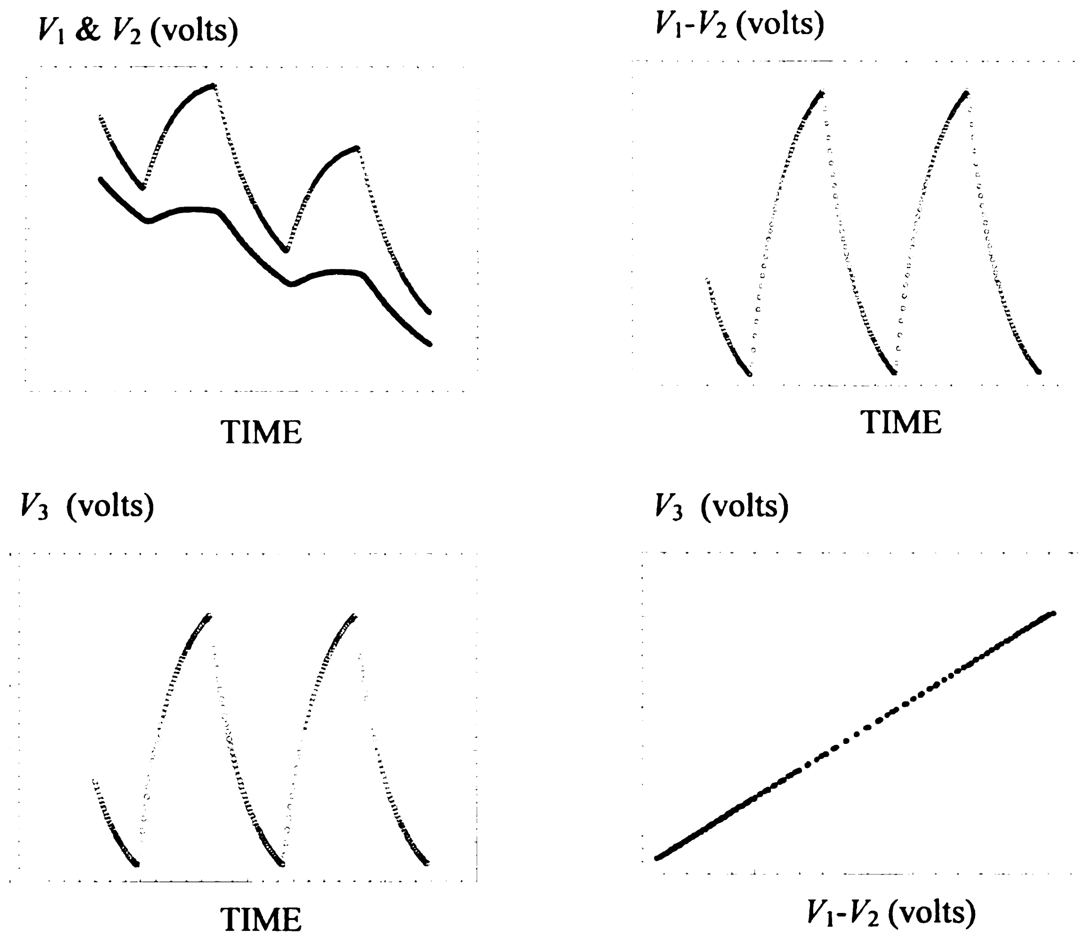

Figure 5-13: Typical data collected for UHT System

5.7 Verification of the UHT System

To test the system up to high temperatures, a platinum wire was used as a reference sample. The wire gauge was 10 mil and was shaped in a way to stand by itself and support a heater as shown in Figure 5-14. The electrical conductivity and thermopower are in good agreement with reference data and are shown in Figure 5-15 and Figure 5-16.

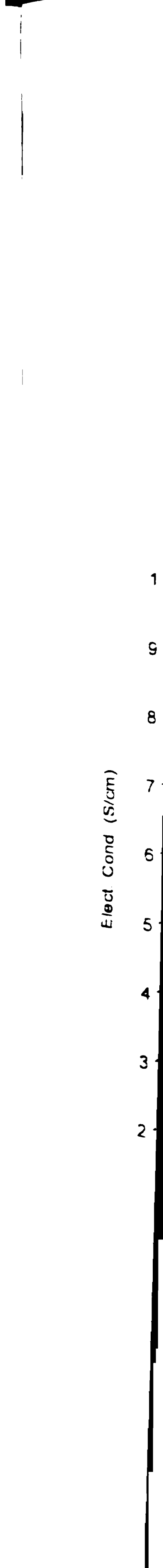
Elect. Cond (S/cm)
1
9
8
7
6
5
4
3
2

Figure 5-14: Platinum wire reference

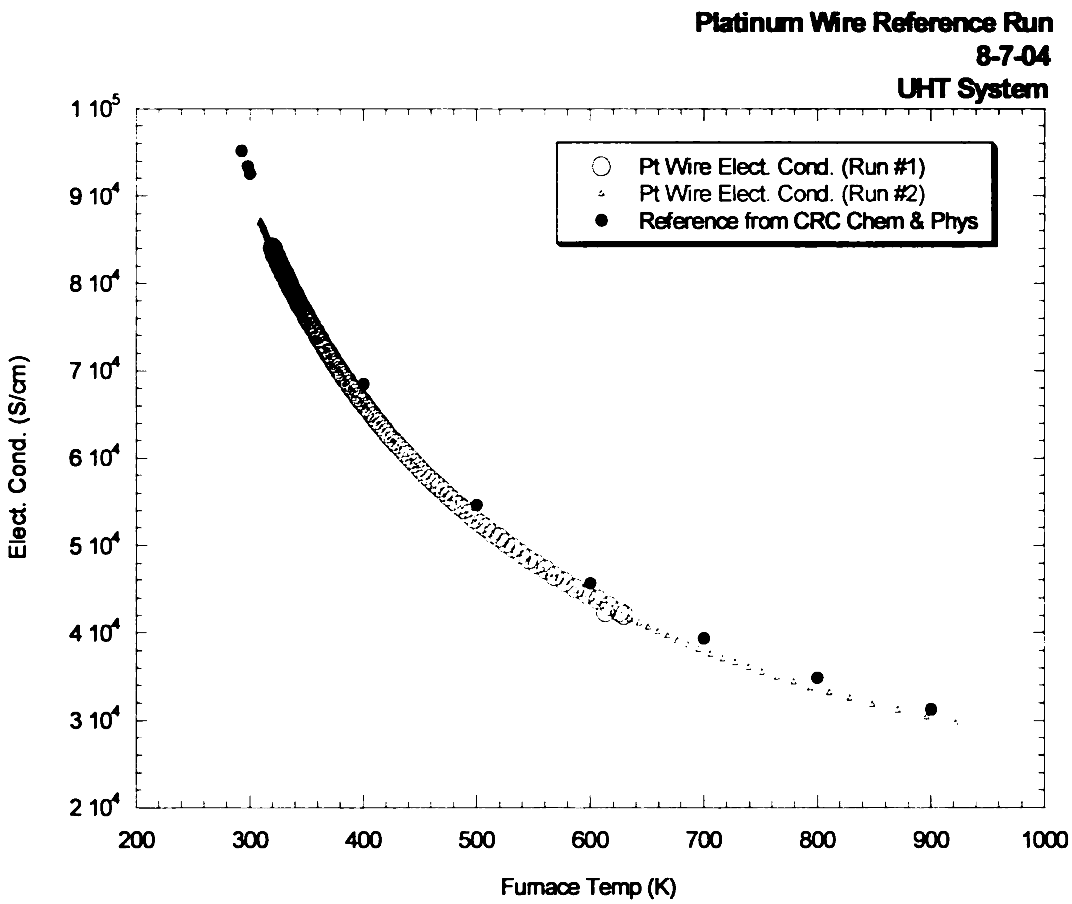

Figure 5-15: Platinum wire electrical conductivity measurements

TEP µV/K

In

made b

compos

Figure 5

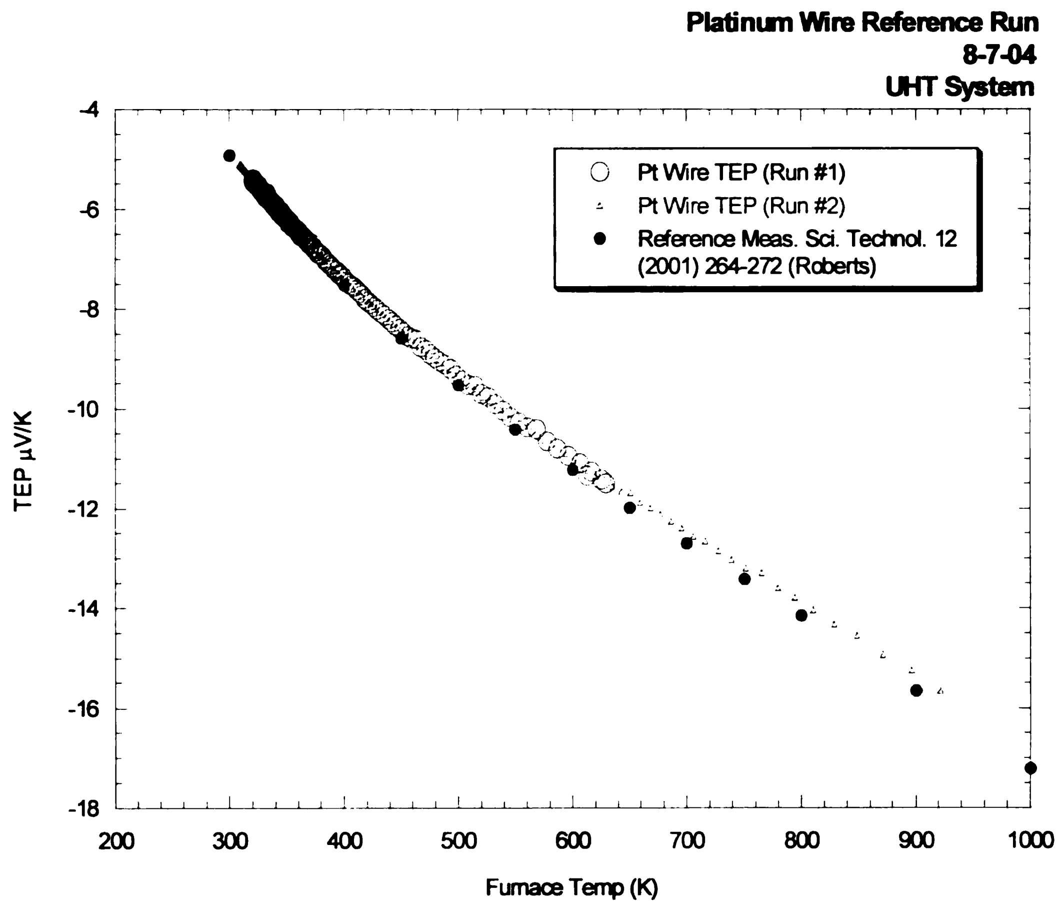

Figure 5-16: Platinum wire thermopower measurements

In addition to testing platinum wire as a reference sample, comparisons where made between data collected by the UHT System and HT System. A LAST sample, with composition $Ag_{0.76}Pb_{18}SbTe_{20}$, was tested and the results are shown in Figure 5-17 and Figure 5-18. These results show an excellent agreement between the two systems.

Figur

Figure

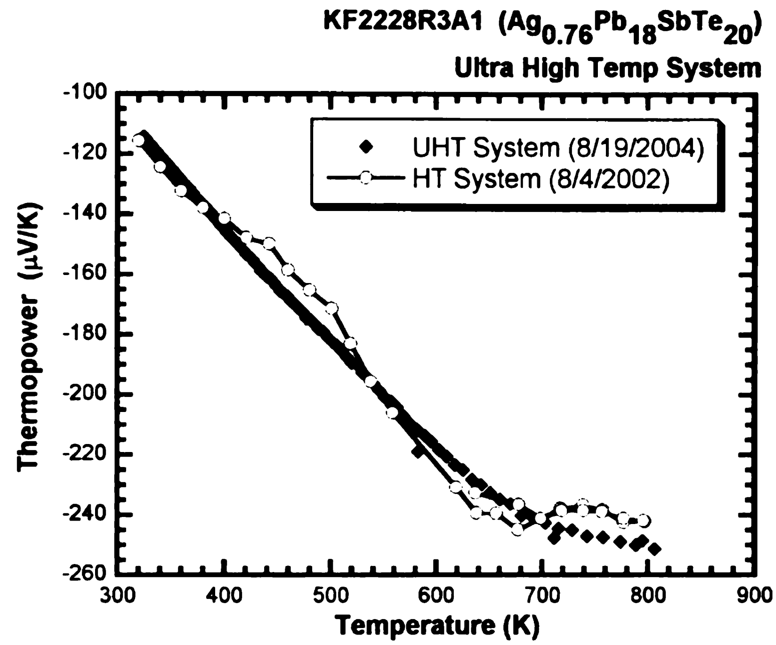

Figure 5-17: Plot of thermopower versus temperature of a LAST sample showing good agreement between the UHT and HT System

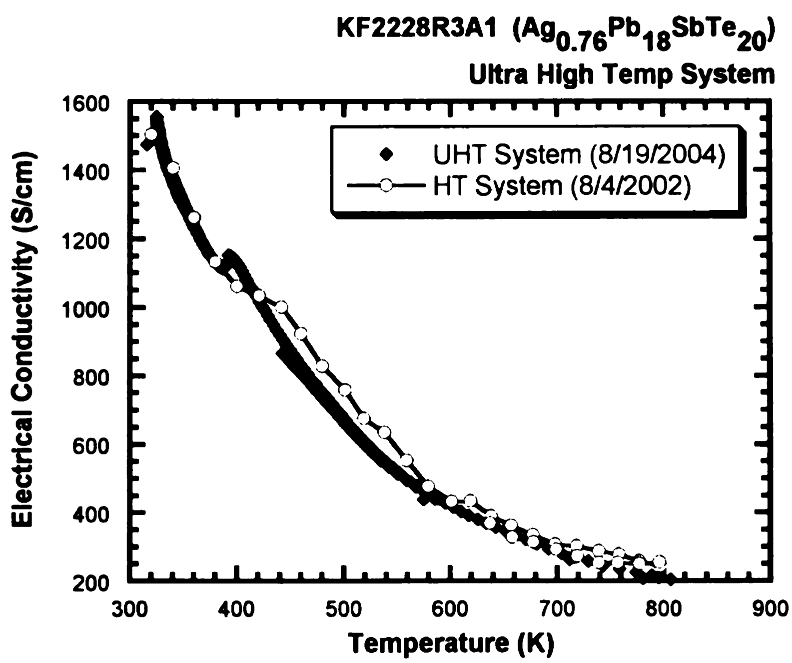

Figure 5-18: Plot of electrical conductivity of a LAST sample showing good agreement between the UHT and HT System

Many samples where tested using the UHT System and data on a new sample that uses potassium in the TE material is shown in Figure 5-19 to provide another example of the high quality data that is obtained from this system.

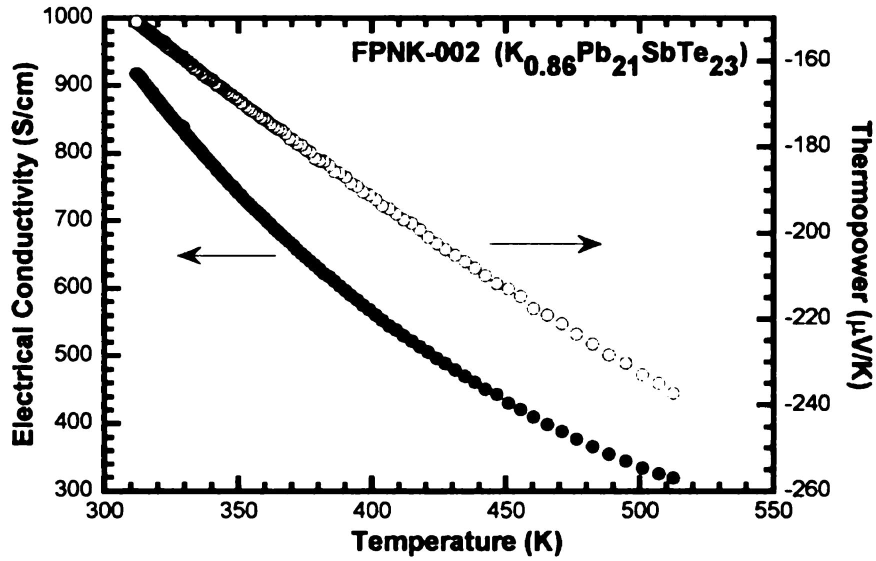

Figure 5-19: Plot of a thermopower and electrical conductivity of a new TE material using potassium using UHT System

5.8 Further Developments and Future Improvements

Upon further developments of the UHT System, with the help of lock-in amplifiers, it was discovered that a significant amount of electrical noise was coming from the furnace, which was due to the 60Hz oscillation in the power lines. When the sample was maintained at a specific temperature, the furnace would be pulsing on and off and ultimately caused an error in the electrical measurements. A high temperature shield made of stainless steel foil was put around the ProboStat and electrically grounded. Figure 5-20 shows the shield in place, which is over the quartz tube of the ProboStat.

Fig

T

electric

accom

to dang

made w

sample

System

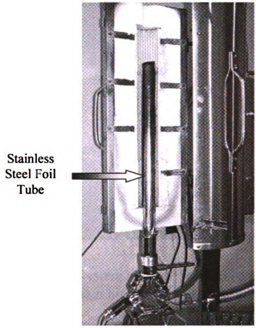

Figure 5-20: Stainless steel foil that is grounded was used as an electrical shield to eliminate noise being emitted from the furnace.

The UHT System was adapted to be able to perform ZT measurements using AC electrical impedance measurements discussed in the following sections. This was accomplished by changing the center sample holder shaft so that four wires could be used to dangle a TE pellet for measurements (see Figure 5-21). This measurement can only be made with the UHT System because the surrounding temperature is modified, not the sample holder like in the current HT System. This is another reason that makes the UHT System a valuable asset to thermoelectric research at MSU.

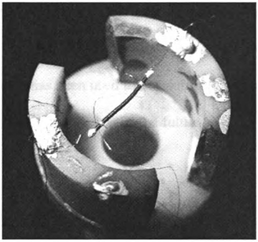

Figure 5-21: Picture of UHT System adapted for ZT direct measurements by dangling a sample in a high temperature environment

A future improvement to the UHT System is to add the capability of back-filling the system with an inert gas such as argon. It has been experimentally discovered that some samples are unstable and outgas at high temperatures in a high vacuum environment. A solution to this would be to first remove the air in the system and then either backfill with argon or possibly provide a continuous flow of argon into the system. This will require a gas flow controller and research into the affects that the argon will have on the thermopower and electrical conductivity measurements. In addition, the background gas would not be suitable for the ZT measurement since it would cause a thermal loss (thermally short the sample) and increase the error in this measurement.

5.9 Conclusion

The UHT System is a valuable asset to Michigan State University's thermoelectric research program by providing measurements of thermopower and electrical conductivity of TE samples up to higher temperatures than previous systems. The unique design of

the sy
which
since
should

the system has allowed it to be adapted for high temperature ZT direct measurements, which is discussed in the following sections. This system has been continuously active since its completion where it has been used to measure a large number of samples and should continue to contribute valuable data in the future.

C

6.1 I

invest

incluc

here is

an AC

utilizir

modul

I

range c

collect

Howev

to calc

This m

temper

T

materia

measur

on the s

thermal

sample

geometr

Chapter 6: Impedance Spectroscopy of Thermoelectric Materials and Devices

6.1 Introduction

Measurements of assembled thermoelectric modules commonly include investigations of the module's output power versus load resistance. Such measurements include non-ideal effects such as electrical and thermal contact resistances. Research here is to analyze the frequency dependent impedance of thermoelectric modules. Using an AC electrical measurement, a model for a thermoelectric module can been developed utilizing electrical circuits for both the thermal and electrical characteristics of the module.

Preliminary measurements were taken at room temperature over the frequency range of 1mHz to 500Hz using lock-in amplifiers. From such measurements, the data collected from commercially available modules can be used for the extraction of ZT. However developing a model to explain the frequency dependent impedance can give rise to calculating the thermal conductivity and thermal capacitance of the module as well. This measurement technique can then be applied to finding ZT of modules at higher temperatures.

The extraction of ZT is extremely important when creating thermoelectric materials. Currently, the accepted method for determining the ZT of a sample is by measuring the temperature dependant data for electrical conductivity and thermopower on the same sample while another sample of the same composition is measured for thermal conductivity. Two samples are required since the required geometry for the sample used in thermal conductivity measurements is vastly different than the required geometry for the electrical conductivity and thermopower measurements. This method cou

dep

the s

of th

6.2 F

the dy

which

from P

<u>Device</u>

thermo

the equ

[45]. I

therma

modul

of the

Stefan

electric

single

a therm

temper

AC mo

could lead to a false sense of ZT. It would be extremely beneficial if the temperature dependant ZT for high temperatures could be found directly. This section will describe the setup and the measurement process for collecting the frequency dependant impedance of thermoelectric materials and devices.

6.2 Existing Research in Scientific Community

There has been a limited amount of research published on observing and modeling the dynamic behavior of thermoelectric materials [31-43]. There were three main articles which did have some insight into this area of research. The first source of material was from Paul Gray. He published a book on The Dynamic Behavior of Thermoelectric Devices in 1960 [44]. This book used extensive mathematical derivations on thermoelectric dynamic behavior in the time domain but it lacked in the ability to apply the equations to experimental data. The next important article came from J. A. Chavez [45]. He published an article called "SPICE model of thermoelectric elements including thermal effects" in 2000. This model used an electro-thermal model to describe TE module behavior in the time domain. The model did not include any thermal capacitance of the TE material and it did not wok in the frequency domain. Finally, a third article by Stefan Dilhaire called "Determination of ZT of PN thermoelectric couples by AC electrical measurement" published in 2002 [46] did show frequency dependant data of a single TE couple attached to copper blocks. The article also provided an AC model using a thermal analysis but lacked in evaluating TE modules and investigations up to high temperatures. However, the article provided a good motivation to further investigate an AC model that would include modeling of complete TE modules, single pellet meas

tempe

6.3 F

a DC

one si

This h

curren

device

voltag

multip

be app

of the

Fi

This m

gradien

be to u

gradien

measurements, and simple unicouples with research into measurements at high temperatures.

6.3 Frequency Dependent Experimental Measurement

A thermoelectric (TE) module is an active device. This can be shown by applying a DC voltage source across the input terminals of the device causing heat to move from one side of the TE module to the other to form a temperature gradient across the module. This heating and cooling is due to the Peltier effect. The heat flow is proportional to the current passing through the device. When there is a temperature gradient across the device, a voltage is developed due to the Seebeck effect. This voltage opposes the voltage source applied to the TE module and is equal to the Seebeck coefficient, α, multiplied by the temperature gradient, ΔT. The electrical behavior of the TE module can be approximated by the circuit shown in Figure 6-1, which shows an electrical resistance of the material, R, in series with a dependent voltage source due to the Seebeck effect.

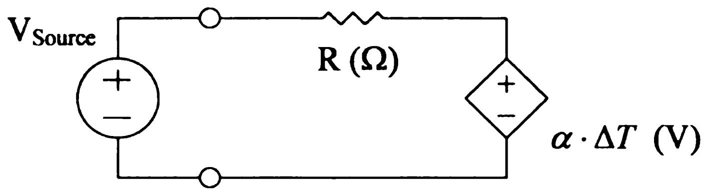

Figure 6-1: Electrical circuit describing the electrical properties of a TE module

This model shows that the impedance of the TE module is dependent on the temperature gradient across the model. One way to find the electrical resistance of the model would be to use an AC electrical source oscillating at a frequency where the temperature gradient could not be established. This would cause the dependent voltage source to approa

freque

allows

of the

interes

freque

6.4 Ex

U

a TE m

AC so

sense

Lock-

in a

mod

approach zero leaving only the electrical resistance. As the AC source approaches zero frequency (DC), the overall resistance increases due to the Seebeck voltage source. This allows one to separate the voltage due to the Seebeck effect from the electrical resistance of the material. This technique can be used to find ZT [47], however, here we are interested in the behavior of the impedance as the frequency transitions from a high frequency down to low frequency (approaching a DC value).

6.4 Experimental Setup

Using two 7165 DSP Lock-In Amplifiers, a frequency sweep can be performed on a TE module using the setup shown in Figure 6-2. One Lock-In is used to provide the AC source voltage signal and to measure the phase and magnitude of the voltage across a sense resistor for calculating the current going through the TE module. The second Lock-In measures the phase and magnitude of the voltage across the TE module.

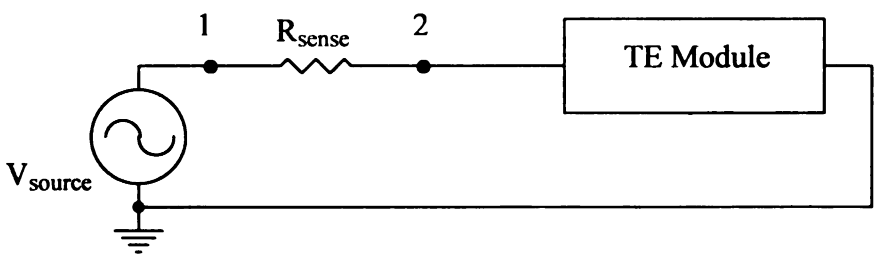

Figure 6-2: Experimental setup for AC measurements

The TE module is suspended by the wires connected to the terminals of the device in a vacuum (1E-6 Torr) so that these wires are the only thermal connection between the module and the measurement equipment. The wires should be small in diameter and long enoug

greate

maint

verific

throug

can be

modul

the re

magni

coord

Alge

Now l

phase

modul

enough so that the thermal resistance of the measurement wires is orders of magnitude greater than the thermal resistance of the TE module. The sense resistor is assumed to maintain a constant value throughout the frequency sweep. This assumption has been verified using an impedance analyzer. Using a small AC voltage so that the current through the TE module is about 10mA(RMS), the phase and magnitude of the impedance can be calculated from the measured phase and magnitude of the voltage across the TE module. Starting with the algebra of complex numbers, if z equals the impedance, a is the real component, b is the imaginary component, θ is the phase angle, and r is the magnitude, then the following shows the representation of impedance in rectangular coordinates or cylindrical coordinates.

Algebra of Complex Numbers [48]:

$$\begin{aligned} z &= a + jb \\ \operatorname{Re} z &= a \\ \operatorname{Im} z &= b \\ a &= r\cos\theta \\ b &= r\sin\theta \\ z &= r(\cos\theta + j\sin\theta) \\ e^{j\theta} &= \cos\theta + j\sin\theta \\ z &= r \cdot e^{j\theta} \end{aligned} \tag{6.42}$$

Now let the phase and magnitude of V_1-V_2, as θ_{sense} and v_{sense}, respectively. Also, let the phase and magnitude of V_2 as θ_2 and v_2, respectively. Then the current into the TE module is as follows.

Now.

From

and th

6.5 L

are us

the sig

ampli

few na

$$
\begin{aligned}
i_{IN} &= \frac{v_{sense} \cdot e^{j\theta_{sense}}}{R_{sense}} \\
&= \frac{v_{sense} \cdot \cos(\theta_{sense}) + j \cdot v_{sense} \cdot \sin(\theta_{sense})}{R_{sense}}
\end{aligned} \tag{6.43}
$$

Now, the impedance of the module, z, can be found as follows.

$$
\begin{aligned}
z &= \frac{v_2 \cdot e^{j\theta_2}}{i_{IN}} = \frac{v_2 \cdot \cos(\theta_2) + j \cdot v_2 \cdot \sin(\theta_2)}{i_{IN}} \\
&= \frac{R_{sense} \cdot v_2 \cdot e^{j\theta_2}}{v_{sense} \cdot e^{j\theta_{sense}}} \\
&= \frac{R_{sense} \cdot v_2}{v_{sense}} \cdot e^{j(\theta_2 - \theta_{sense})}
\end{aligned} \tag{6.44}
$$

From the above equation, the magnitude of the impedance of the module is:

$$
\frac{R_{sense} \cdot v_2}{v_{sense}} \tag{6.45}
$$

and the phase of the impedance is:

$$
\theta_2 - \theta_{sense} \tag{6.46}
$$

6.5 Lock In Amplifier

To measure frequency dependant impedance of TE materials, Lock-in amplifiers are used to get the phase and magnitude of the impedance in a noisy environment where the signal levels can be very low. The following is a description of how Lock-in amplifiers are very useful for this measurement.

Lock-in amplifiers are used to detect and measure very small AC signals down to a few nanovolts. Accurate measurements may be made even when the small signal is obscu

techni

a spec

refere

at 10k

noise

100kH

1000)

noise

a Q=1

kHz (

and th

furthe

with a

bandw

0.5 μV

noise

refere

the res

refere

functio

obscured by noise sources many thousands of times larger. Lock-in amplifiers use a technique known as phase-sensitive detection to single out the component of the signal at a specific reference frequency and phase. Noise signals at frequencies other than the reference frequency are rejected and do not affect the measurement to a certain degree.

Why use a lock-in amplifier? Consider an example signal that is a 10nV sine wave at 10kHz. Amplification is required to bring the signal above the noise. A good low noise amplifier will have about 5 $\mathrm{nV}/\sqrt{\mathrm{Hz}}$ of input noise. If the amplifier bandwidth is 100kHz and the gain is 1000, the output can be expected to be 10 μV of signal (10 nV x 1000) and 1.6mV of broadband noise (5 $\mathrm{nV}/\sqrt{\mathrm{Hz}}$ x $\sqrt{100\mathrm{kHz}}$ x 1000). The signal to noise ratio will be too low to make any measurements. If a bandpass filter is applied with a Q=100 centered at 10kHz, any signal in a 100Hz bandwidth will be detected (10 kHz/Q). The noise in the filter pass band will be 50 μV (5 $\mathrm{nV}/\sqrt{\mathrm{Hz}}$ x $\sqrt{100\mathrm{Hz}}$ x 1000) and the signal will still be 10 μV. Still, an accurate measurement cannot be made, even if further gain is used because the signal to noise ratio is too low. Now use an amplifier with a phase-sensitive detector (PSD). The PSD can detect the signal at 10kHz with a bandwidth as narrow as 0.01 Hz! In this case, the noise detection bandwidth will be only 0.5 μV (5 $\mathrm{nV}/\sqrt{\mathrm{Hz}}$ x $\sqrt{0.1\mathrm{Hz}}$ x 1000) while the signal is still 10 μV. The signal to noise ratio is now 20 and an accurate measurement of the signal is possible.

What is phase-sensitive detection? Lock-in measurements require a frequency reference. Typically an experiment is excited at a fixed frequency and the lock-in detects the response from the experiment at the reference frequency. In the diagram below, the reference signal is a square wave at frequency ω_r. This might be a sync output from a function generator. If the sine output from the function generator is used as a source, the respon

V_{sig}

and θ

signal

diagra

shown

using

waves

response might be the signal waveform shown below. The signal is $V_{sig} \cdot \sin(\omega_r \cdot t + \theta_{sig})$ where V_{sig} is the signal amplitude, ω_r is the signal frequency, and θ_{sig} is the signal's phase. Lock-in amplifiers generate their own internal reference signal usually by a phase-locked-loop (PLL) locked to the external reference. In the diagram below the external reference, the lock-in's reference and the signal are all shown. The internal reference is $V_L \cdot \sin(\omega_L \cdot t + \theta_{ref})$.

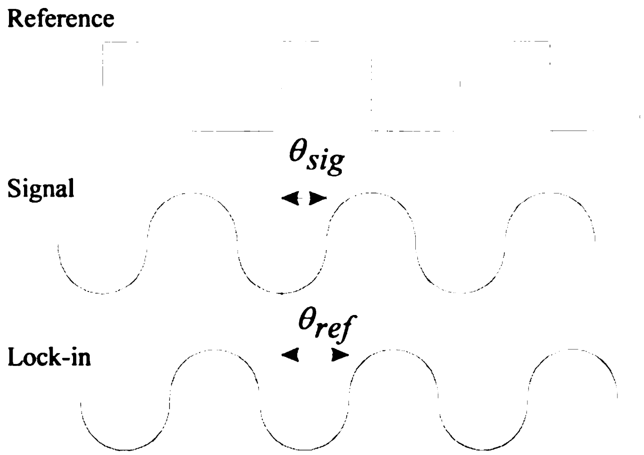

Figure 6-3: Lock-in signal example

The Lock-in amplifies the signal and then multiplies it by the lock-in reference using a PSD or multiplier. The output of the PSD is simply the product of two sine waves.

$$\begin{aligned} V_{PSD} &= V_{sig} \cdot V_L \cdot \sin(\omega_r \cdot t + \theta_{sig}) \cdot \sin(\omega_L \cdot t + \theta_{ref}) \\ &= \frac{1}{2} \cdot V_{sig} \cdot V_L \cdot \cos([\omega_r - \omega_L] \cdot t + \theta_{sig} - \theta_{ref}) - \\ &\quad \frac{1}{2} \cdot V_{sig} \cdot V_L \cdot \cos([\omega_r + \omega_L] \cdot t + \theta_{sig} + \theta_{ref}) \end{aligned} \tag{6.47}$$

The

othe

filte

ω_r

filter

This

6.5.1

phase

θ_{ref}

If θ is

phase

multip

$V_L \cdot$ s

The PSD output is two AC signals, one at the difference frequency $(\omega_r - \omega_L)$ and the other at the sum frequency $(\omega_r + \omega_L)$. If the PSD output is passed through a low pass filter, the AC signals are removed. Normally, this would remove everything, however, if ω_r equals ω_L, the difference frequency component will be a DC signal. In this case, the filtered PSD output will be

$$V_{PSD} = \frac{1}{2} \cdot V_{sig} \cdot V_L \cdot \cos(\theta_{sig} - \theta_{ref}) \tag{6.48}$$

This is a very nice signal. It is a DC signal proportional to the signal amplitude.

6.5.1 Magnitude and Phase

The PSD output is proportional to $V_{sig} \cdot \cos(\theta)$ where $\theta = (\theta_{sig} - \theta_{ref})$. θ is the phase difference between the signal and the lock-in reference oscillator. By adjusting θ_{ref} we can make theta equal to zero, in which case we can measure V_{sig} $(\cos(\theta) = 1)$. If θ is 90°, there will be no output at all. A lock-in with a single PSD is called a single-phase lock-in and its output is $V_{sig} \cdot \cos(\theta)$.

Adding a second PSD can eliminate the phase dependency. If the second PSD multiplies the signal with the reference oscillator shifted by 90°, i.e. $V_L \cdot \sin(\omega_L \cdot t + \theta_{ref} + 90^{\circ})$, its low pass filtered output will be

$$\begin{aligned} V_{PSD2} &= \frac{1}{2} \cdot V_{sig} \cdot V_L \cdot \sin(\theta_{sig} - \theta_{ref}) \\ V_{PSD2} &= \cdot V_{sig} \cdot \sin(\theta) \end{aligned} \tag{6.49}$$

Now

sin(θ

These

oscill

is bec

magni

R mea

and lo

degre

signal

6.6

mod

resis

Now we have two outputs, one proportional to $\cos(\theta)$ and the other proportional to $\sin(\theta)$. If we call the first output X and the second Y

$$X = V_{sig} \cdot \cos(\theta)$$
$$Y = V_{sig} \cdot \sin(\theta) \tag{6.50}$$

These two quantities represent the signal as a vector relative to the lock-in reference oscillator. X is call the 'in-phase' component and Y the 'quadrature' componenet. This is because when θ=0, X measures the signal while Y is zero. By computing the magnitude (R) of the signal vector, the phase dependency is removed.

$$R = \sqrt{\left(X^2 + Y^2\right)} = V_{sig} \tag{6.51}$$

R measures the signal amplitude and does not depend upon the phase between the signal and lock-in reference. A dual-phase lock-in has two PSD's, with reference oscillators 90 degrees apart, and can measure X, Y and R directly. In addition, the phase q between the signal and lock-in reference, can be measured according to;

$$\theta = \tan^{-1}(Y / X)$$

6.6 Example Data using Tellurex Module

The experimental data of the impedance of the commercial Tellurex [49] TE module for power generation is show in Figure 6-4. Notice that for low frequencies, the resistance of the module is much larger than at high frequencies.

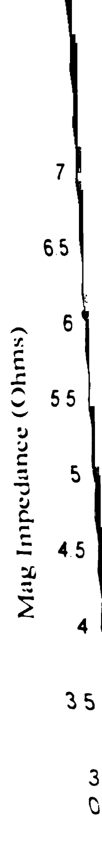

F

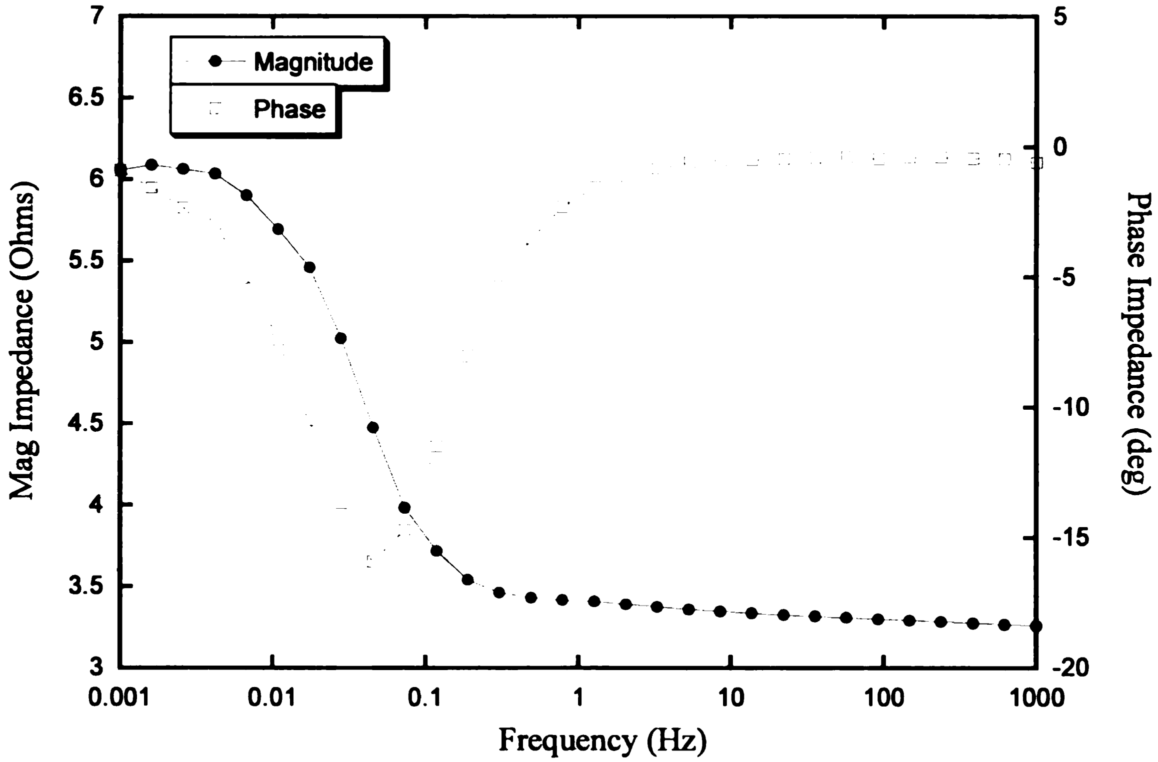

Figure 6-4: Magnitude and phase of the impedance of a Tellurex TE module

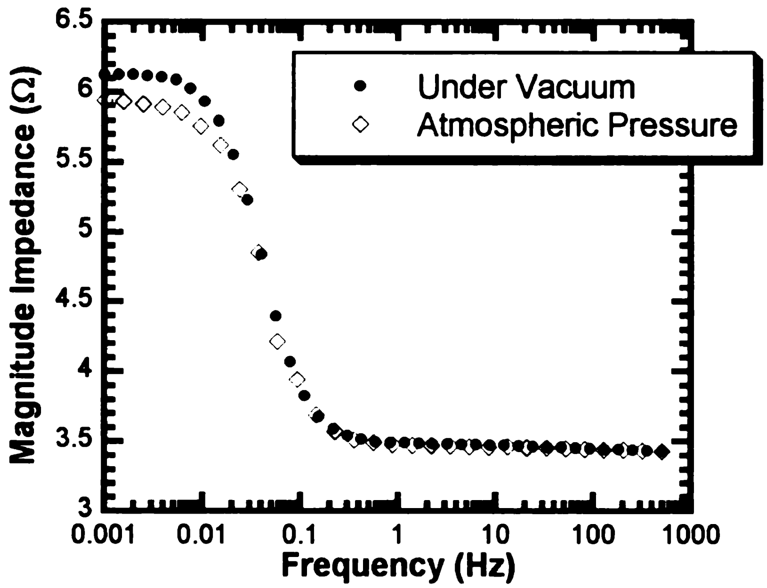

Figure 6-5: Plot of magnitude versus frequency for high vacuum and atmospheric conditions

6.7 An

Neglect

The hea

The volt

The figur

6.7 Analysis of the Data

Neglecting radiation losses, the figure of merit, ZT, of the model is:

$$ZT = \frac{\alpha^2 \cdot \sigma}{\kappa} \cdot T \tag{6.52}$$

The heat flow, Q, and the thermal conductivity can be equated to this:

$$\begin{aligned} Q &= \alpha \cdot T \cdot I \\ \kappa &= \frac{Q}{\Delta T} \cdot \frac{length}{area} \end{aligned} \tag{6.53}$$

The voltage across the terminals of the model equals:

$$\begin{aligned} V &= R_0 \cdot I + \alpha \cdot \Delta T \\ R_{Total} &= \frac{V}{I} = R_0 + \frac{\alpha \cdot \Delta T}{I} \\ \sigma &= \frac{length}{R_0 \cdot area} \end{aligned} \tag{6.54}$$

The figure of merit, ZT, can now be found to be:

$$\begin{aligned} ZT &= \alpha^2 \cdot \frac{length}{R_0 \cdot area} \cdot \frac{\Delta T \cdot area}{\alpha \cdot T \cdot length \cdot I} \\ &= \frac{\alpha \cdot \Delta T}{R_0 \cdot I} \\ &= \frac{R_0 + \frac{\alpha \cdot \Delta T}{I}}{R_0} - 1 \end{aligned} \tag{6.55}$$

$$\begin{aligned} R_{DC} &= R_0 + \frac{\alpha \cdot \Delta T}{I} \\ R_{AC(\Delta T \to 0)} &= R_0 \end{aligned} \tag{6.56}$$

$$ZT = \frac{R_{DC}}{R_{AC}} - 1 \tag{6.57}$$

6.8 Mor

Alo

measurin

This secti

module, a

6.8.1 Sin

A s

diagrame

ends of t

configur

but will

are ther

temper

copper

in the

also b

series

room

smal

Plati

imp

sam

6.8 More Sample Measurement Setups

Along with measuring commercial thermoelectric modules, investigations on measuring the ZT of other thermoelectric materials and configurations have been made. This section describes the setup for measuring ZT on single TE pellets, a pn inline TE module, and unicouples or multicouple modules.

6.8.1 Single Sample ZT Measurements

A single sample of thermoelectric material can be measured for ZT using the setup diagramed in Figure 6-6. In this diagram, there is a sample with electrical contacts at the ends of the material. The setup shows four wires attached to a TE sample, labeled *a*, in a configuration that will include the contact resistance between the wires and the sample but will not include the electrical resistance of the measurement wires. The four wires are then thermally grounded to a reference temperature. This is typically room temperature. At the location of the thermal reference, the wires may change materials to copper wires, which will go to the measurement equipment. A voltage source is shown in the figure to provide the power for the measurement; however, a current source may also be used. If a voltage source is used, a sense resistor of a known value is placed in series with the source in order to calculate the current flowing through the sample. For room temperature measurements, wires labeled *a* may be Copper wires that are very small in diameter such as 25μm. For high temperature measurements, the wires may be Platinum. It is important that the wires have a low thermal resistance. It is also important that the thermopower of the measurement wires is very low compared to the sample being tested. When this is true, the thermopower of the wires can be neglected without a

resistance

accomplis

contacts t

The high

There wil

Sam

For

between th

as the one

measurem

However,

high to low

explained

completely

The voltag

even spark

without acquiring a significant error in the measurement. Except for the small thermal resistance of the measurement wires, the sample is thermally isolated. This is accomplished by hanging the sample by the measurement wires so that there are no other contacts to the sample and also by placing the sample in a high vacuum environment. The high vacuum is used to eliminate thermal loss due to conduction and convection. There will, however, still be losses due to radiation.

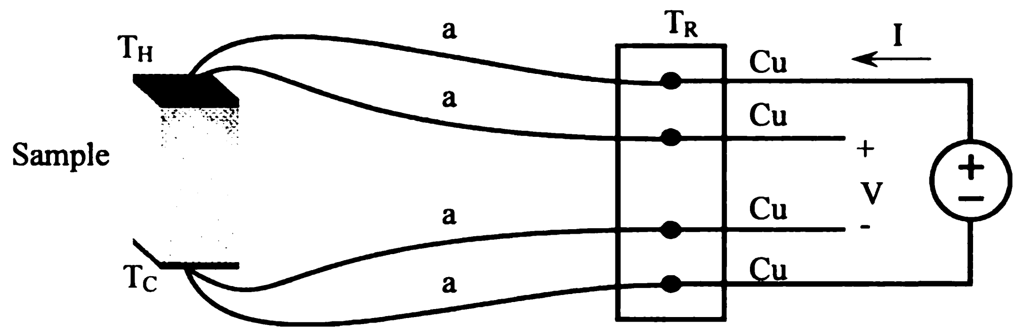

Figure 6-6: Single TE pellet for ZT measurements including contacts

For measurements of single TE pellets which do not include contact resistance between the measurement wires and the sample, a four point configuration is used such as the one diagramed in Figure 6-7. For high frequency measurements and DC measurements, the placement of the probes will not effect the measurement of ZT. However, the AC measurement of the impedance as the frequency is transitioned from high to low frequency will be affected by the placement of the probes. This will be explained in later sections. The sample, which is dangling during the measurement, is completely supported by the wires at the ends of the sample which supply the current. The voltage measurement probes can either be carefully soldered on, silver pasted on, or even spark welded on.

Samp

Figu

A d

sample si

The

platinum c

platinum n

The

electrical c

of the com

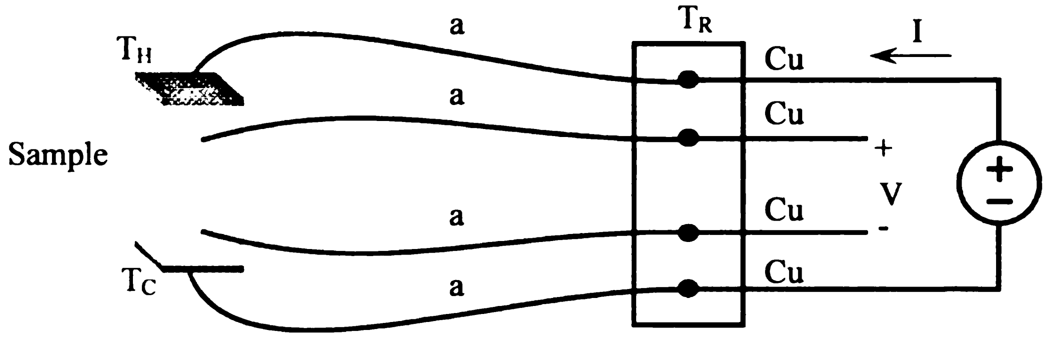

Figure 6-7: Single TE pellet for ZT measurements in four-point configuration

A detailed diagram with dimensions (using variables) is shown in Figure 6-8 for the sample size and voltage probe locations.

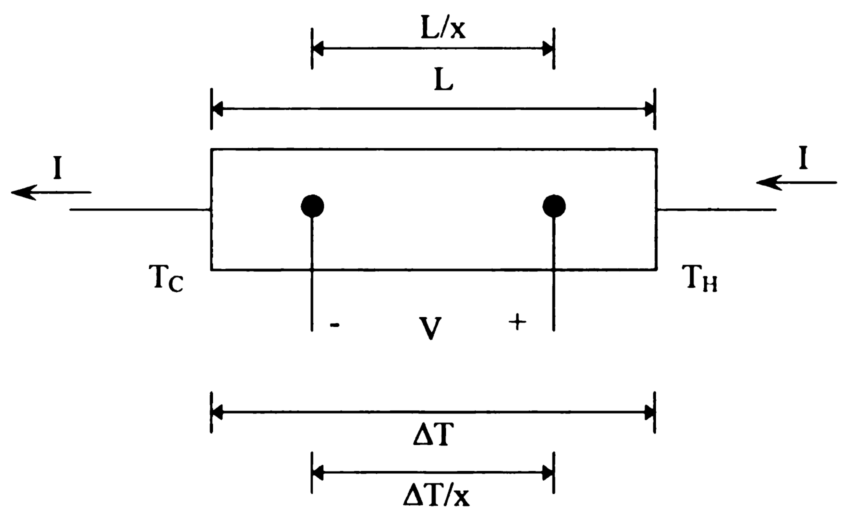

Figure 6-8: Detailed view of a single TE pellet connection

The thermopower of constantan is low enough that the thermopower of the platinum current leads will affect the measurement. Therefore, the thermopower of the platinum must be known and corrected for.

The schematic of the setup is shown in Figure 6-9 where a representation of the electrical circuit and thermal circuit is provided. Figure 6-10 shows the equations for all of the components presented in Figure 6-9.

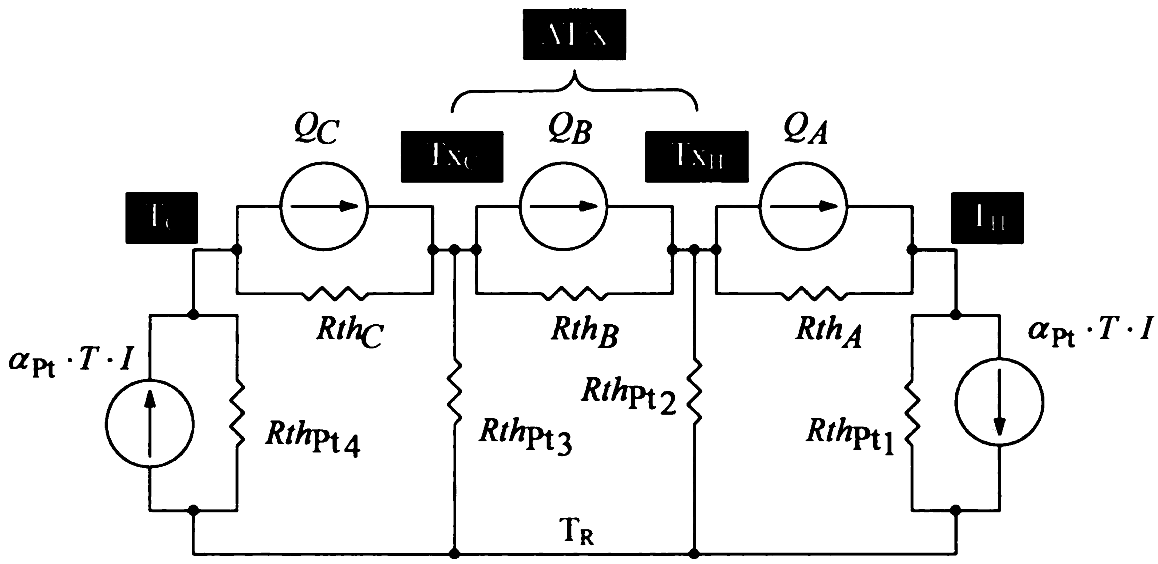

Thermal Circuit

Appendix B: Electrical

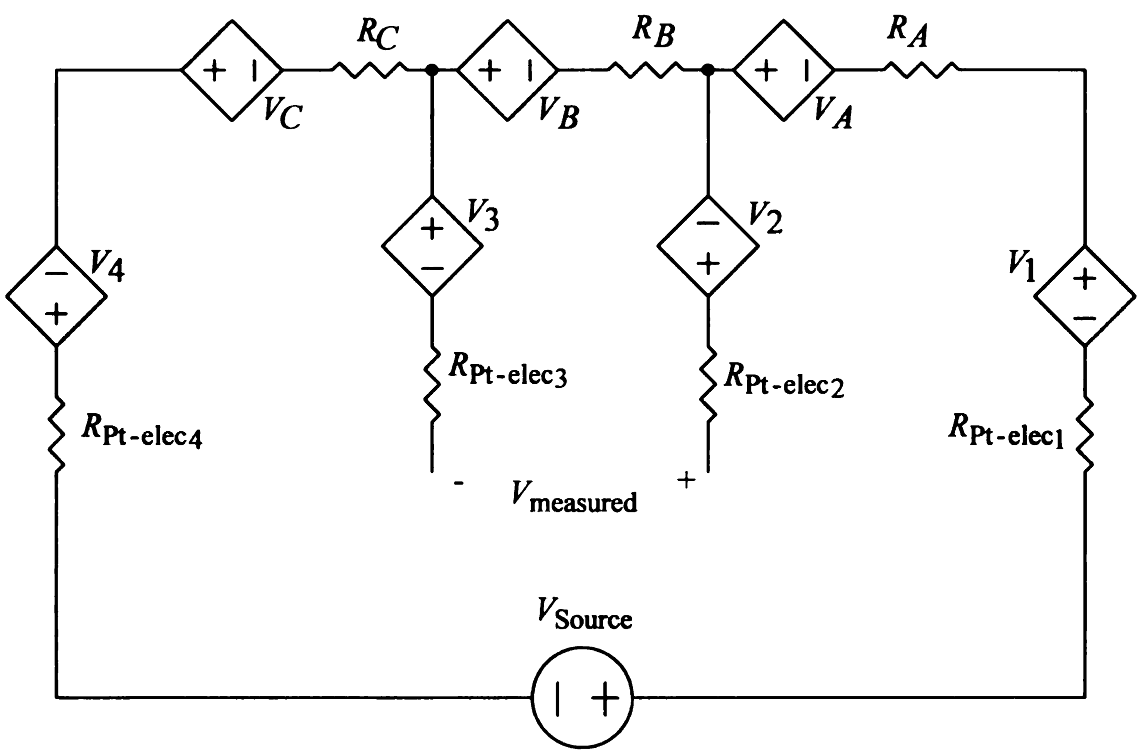

Figure 6-9: Electrical and thermal model of setup

V_1

V_2

$V_3 =$

$V_4 =$

The

schematic

V_{mo}

$$V_1 = \int_{T_R}^{T_H} \alpha_{\mathrm{Pt}} \cdot dT \qquad V_A = \int_{Tx_H}^{T_H} \alpha_{\mathrm{Pt}} \cdot dT \qquad Q_A = Q_B = Q_C = \alpha_{\mathrm{sample}} \cdot I \cdot T$$

$$V_2 = \int_{T_R}^{Tx_H} \alpha_{\mathrm{Pt}} \cdot dT \qquad V_B = \int_{Tx_H}^{Tx_C} \alpha_{\mathrm{Pt}} \cdot dT \qquad Rth_A = Rth_{\mathrm{sample}} \cdot \left(1 - \frac{1}{x}\right) \cdot \frac{1}{n}$$

$$V_3 = \int_{T_R}^{Tx_C} \alpha_{\mathrm{Pt}} \cdot dT \qquad V_C = \int_{Tx_C}^{T_C} \alpha_{\mathrm{Pt}} \cdot dT \qquad Rth_B = Rth_{\mathrm{sample}} \cdot \frac{1}{x}$$

$$V_4 = \int_{T_R}^{T_C} \alpha_{\mathrm{Pt}} \cdot dT \qquad Rth_C = Rth_{\mathrm{sample}} \cdot \left(1 - \frac{1}{x}\right) \cdot \left(1 - \frac{1}{n}\right)$$

$$R_A = R_{\mathrm{sample}} \cdot \left(1 - \frac{1}{x}\right) \cdot \frac{1}{n}$$

$$R_B = R_{\mathrm{sample}} \cdot \frac{1}{x}$$

$$R_C = R_{\mathrm{sample}} \cdot \left(1 - \frac{1}{x}\right) \cdot \left(1 - \frac{1}{n}\right)$$

Figure 6-10: Equations for Figure 6-9

The measured voltage across the constantan wire can be calculated using the schematic from Figure 6-9 and is shown below.

$$\begin{aligned} V_{\mathrm{measured}} &= \int_{T_R}^{Tx_H} \alpha_{\mathrm{Pt}} \cdot dT + I \cdot R_{\mathrm{sample}} \cdot \frac{1}{x} + \int_{Tx_H}^{Tx_C} \alpha_{\mathrm{sample}} \cdot dT + \int_{Tx_C}^{T_R} \alpha_{\mathrm{Pt}} \cdot dT \\ &= \int_{Tx_C}^{Tx_H} \left(\alpha_{\mathrm{Pt}} - \alpha_{\mathrm{sample}}\right) \cdot dT + I \cdot R_{\mathrm{sample}} \cdot \frac{1}{x} \\ &\approx \frac{\left(\alpha_{\mathrm{Pt}} - \alpha_{\mathrm{sample}}\right) \cdot \Delta T}{x} + \frac{I \cdot R_{\mathrm{sample}}}{x} \end{aligned} \tag{6.58}$$

Assumin

the temp

ZT of th

The meas

Now the Z

follows.

Assuming the wire thermal resistance is much larger than the sample thermal resistance, the temperature gradient across the sample can be approximated as follows.

$$\Delta T \approx (\alpha_{\text{sample}} - \alpha_{\text{Pt}}) \cdot I \cdot T \cdot Rth_{\text{sample}} \tag{6.59}$$

ZT of the tested material is found from the basic equations shown below.

$$(ZT)_{\text{sample}} = \frac{\alpha_{\text{sample}}^{2} \cdot \sigma_{\text{sample}}}{\kappa_{\text{sample}}} \cdot T \tag{6.60}$$

$$Q = \alpha_{\text{sample}} \cdot T \cdot I \tag{6.61}$$

$$\kappa = \frac{Q}{\Delta T} \cdot \frac{length}{area} \tag{6.62}$$

$$\begin{aligned}
(ZT)_{\text{sample}} &= \alpha_{\text{sample}}^{2} \cdot \frac{\text{length}}{R_{\text{sample}} \cdot \text{area}} \cdot \frac{\Delta T \cdot \text{area}}{\alpha_{\text{sample}} \cdot T \cdot I \cdot \text{length}} \cdot T \\
&= \alpha_{\text{sample}}^{2} \cdot \frac{1}{R_{\text{sample}}} \cdot \frac{\Delta T}{\alpha_{\text{sample}} \cdot T \cdot I} \\
&= \frac{\alpha_{\text{sample}} \cdot \Delta T}{R_{\text{sample}} \cdot I} \\
&= \frac{\alpha_{\text{sample}}^{2} \cdot Rth_{\text{sample}}}{R_{\text{sample}}} \cdot T
\end{aligned} \tag{6.63}$$

The measured values for R_{DC} and R_{AC} can be calculated below

$$\begin{aligned}
R_{DC} &= \frac{(\alpha_{\text{Pt}} - \alpha_{\text{sample}}) \cdot \Delta T}{x \cdot I} + \frac{R_{\text{sample}}}{x} \\
R_{AC(\Delta T \to 0)} &= \frac{R_{\text{sample}}}{x}
\end{aligned} \tag{6.64}$$

Now the ZT that is measured can be calculated from using the Harman technique as follows.

The abov

measured

of the sam

$$\left[\frac{\alpha_s}{} \right.$$

The above

measurem

always be

$$
\begin{aligned}
(ZT)_{\text{measured}} &= \frac{R_{DC}}{R_{AC}} - 1 \\
&= \frac{\left[\dfrac{(\alpha_{\text{Pt}} - \alpha_{\text{sample}})\cdot \Delta T}{x \cdot I} + \dfrac{R_{\text{sample}}}{x}\right]}{\left[\dfrac{R_{\text{sample}}}{x}\right]} - 1 \\
&= \frac{(\alpha_{\text{Pt}} - \alpha_{\text{sample}})\cdot \Delta T}{R_{\text{sample}} \cdot I} \\
&= \frac{(\alpha_{\text{Pt}} - \alpha_{\text{sample}})\cdot (\alpha_{\text{sample}} - \alpha_{\text{Pt}})\cdot I \cdot T \cdot Rth_{\text{sample}}}{R_{\text{sample}} \cdot I} \\
&= \frac{(\alpha_{\text{Pt}} - \alpha_{\text{sample}})^2 \cdot Rth_{\text{sample}}}{R_{\text{sample}}} \cdot T
\end{aligned} \tag{6.65}
$$

The above equation shows that how the thermopower of the platinum wire affects the measured ZT value. A correction must be made to the measured ZT to get the actual ZT of the sample by introducing a correction factor as follows.

$$(ZT)_{\text{sample}} = (ZT)_{\text{measured}} \cdot \text{Correction}$$

$$\left[\frac{{\alpha_{\text{sample}}}^2 \cdot Rth_{\text{sample}}}{R_{\text{sample}}} \cdot T\right] = \left[\frac{(\alpha_{\text{Pt}} - \alpha_{\text{sample}})^2 \cdot Rth_{\text{sample}}}{R_{\text{sample}}} \cdot T\right] \cdot \text{Correction}$$

$$\boxed{\text{Correction} = \frac{{\alpha_{\text{sample}}}^2}{(\alpha_{\text{Pt}} - \alpha_{\text{sample}})^2}} \tag{6.66}$$

The above equation indicates that in order to correct for the thermopower of the measurement wires, the thermopower of the sample must be known. This may not always be the case. However, typically, samples measured by MSU have large thermopower values in that the thermopower of the platinum voltage probes can be neglected.

6.8.2 Inline PN Module

To create a full working thermoelectric module, *p*-type and *n*-type materials must both be used. Typically the thermoelectric properties as a function of temperature are different between the two types of materials. It is important to test how both materials will work together when combined as a function of temperature. A convenient way to test the combination of the two types is to place them in an inline configuration shown in Figure 6-11 and Figure 6-12. A *pn* inline module is simply a *p*-type and an *n*-type TE sample connected together in a straight line. The two materials are bonded together using a material such as silver paste, solder, or something that will diffuse into both samples to hold them together. In this configuration, the module has the least number of contacts, 1 (*n*-type sample bonded to *p*-type via bonding material). Contact resistance directly effects ZT measurements so by reducing the contacts, the overall contact resistance is reduced and the measured ZT is closer to the actual ZT of the module if there were no contact resistance. The inline configuration also provides a simple and efficient way to make the module. The two TE materials can be placed in a vacuum-sealed quartz tube with the bonding material in between and some added weight to hold the two materials together while it is place in a furnace for the diffusion of the three materials.

Figure 6-11 shows a diagram of the inline module setup which will include the contact resistance between the measurement wires and the sample. Figure 6-12 shows the diagram of the setup where it is in a four-point probe measurement configuration such that the v

materials

increases

opposite.

the samp

hot temp

sample el

dependen

depend o

the bond

electrical

the inline

represent

module is

each of th

measurem

reach the

that the voltage leads do not included any contacts except the bond between the two materials. In both configurations then ends of the module will both tend to either increases or decrease in temperature while the bond between the two materials will do the opposite. Because the materials will have different properties, it is likely that the ends of the sample will not be at the same temperature. The diagram shows this by showing two hot temperatures, T_{H1} and T_{H2}. This is because, even though both samples have the sample electrical current flowing through them, the heat flow through each sample is dependent upon the thermopower. The temperature at the ends of each sample will depend on both the heat flow and the thermal conduction of the material. For modeling, the bond between both samples will be forced to have the sample temperature. Using an electrical circuit to model the thermal behavior, Figure 6-13 shows the thermal circuit of the inline module where a current source represents heat flow and the electrical resistance represents thermal resistance. As long as the temperature gradient along the inline module is much smaller than average temperature of the module, the thermopower along each of the samples can be assumed to be constant. With a constant thermopower, the measurement of ZT should be not affected by the fact that the ends of the sample do not reach the same temperature.

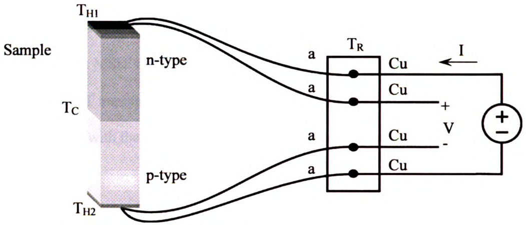

Figure 6-11: Inline TE module including contacts

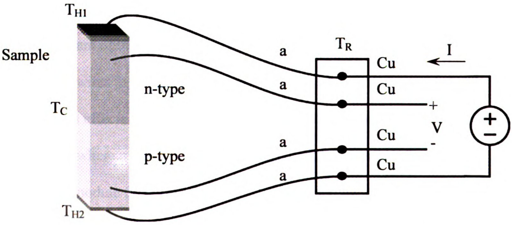

Figure 6-12: Inline TE module in four point probe configuration

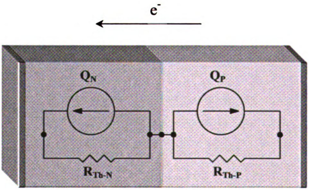

Figure 6-13: Inline module with thermal circuit overlay (DC steady state)

Inline modules are useful for testing ZT using impedance spectroscopy but because of the configuration, the module is not functional for other applications. This module can not be tested in MSU's Device Testing System (which also measures ZT) to verify the results. The ZT measured can be compared to the individual measured properties of each material along with the contact resistance to calculate the predicted ZT value.

6.8.3 Unicouples and Multicouple Modules

Described here is the setup for measuring unicouples and multicouple modules in the standard configuration (electrically in series, thermally in parallel). Figure 6-14 shows the diagram of the setup for measuring a unicouple or a multicouple module. The setup uses four wires to eliminate the resistance of the measuring wires but will include all the non-ideal effects in the module, including contact resistance of each connection. In Figure 6-14, where a unicouple is being measured, there will be four non-ideal contacts in the module that will affect the ZT of the module. This ZT measurement will be the actual ZT of the complete module. Unlike the inline module, the thermal circuit (shown in Figure 6-15) is in parallel instead of in series. The temperature across each of the samples will be the same. However, in this case, the heat flow in each sample will not be solely determined by the individual samples.

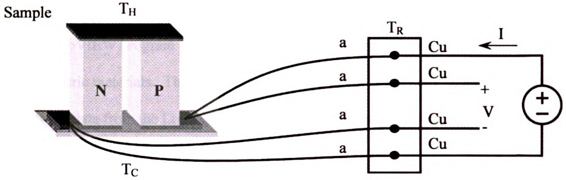

Figure 6-14: Unicouple TE module for ZT measurement

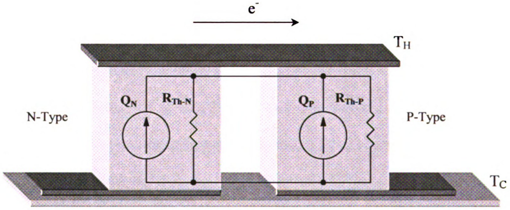

Figure 6-15: Typically unicouple module with thermal circuit overlayed (DC steady state)

The advantage of this setup is that the ZT measurement is performed on a functional module that can also be tested in the Device Testing System for cross comparison.

6.9 System Program

A LabVIEW program was designed to conduct the impedance measurements of the thermoelectric materials. The program controls the setup of the Lock-in amplifiers and collects the data from the Lock-in amplifiers to be organized and stored into a text file for further analysis.

Chapter 7: RC-One Port Method

7.1 Introduction

There has been research on DC electrical measurements and modeling of TE modules by Chavez [45] and AC electrical measurements by Dilhaire [46]. Proposed here is applying an RC-One Port analysis method [50] to provide a simple model that will effectively describe the behavior of a TE module. The first approach to developing a model is to assume that thermal and electrical circuit elements of the module can be in lumped quantities. This approach will provide an overall thermal conductance and thermal capacitance of the module if the average module Seebeck coefficient is known. The model proposed here provides a simple equivalent circuit, which can be analyzed using an electrical simulator such as SPICE. This model makes use of the magnitude and phase of the electrical impedance measured by the lock-in amplifiers at the input terminals of the module and includes fitting parameters of the total electrical resistance, thermal conductance, heat capacitance, and module Seebeck coefficient.

7.2 Development of RC One-Port Model

The RC One-Port model is a model that is based on the impedance of an RC (resistor, capacitor) circuit using a one-port analysis. The model is developed after collecting experimental data on the impedance of a commercially available thermoelectric module. The thermoelectric module is treated like a "black box". From the experimental data, the thermoelectric module appears to be a passive device. It is the experimental data that leads to comparing a thermoelectric module to the impedance of a passive RC circuit.

7.2.1 Comparing Data to Simple RC Circuit

The experimental data collected of the impedance of the commercially available thermoelectric module has similar characteristics to an RC circuit, shown in Figure 7-1. In this figure, Z(s), represents the impedance of the circuit in the s-domain. By inspection of the circuit, the impedance of this circuit will be high and constant for low frequency values (R1+R). For high frequency values, the impedance will be low and constant (R). This behavior is the same as the experimental data collected on the thermoelectric module.

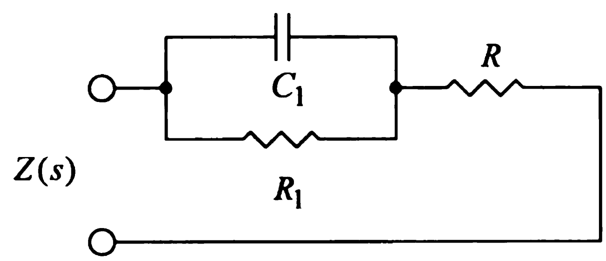

Figure 7-1: RC circuit

The equation for the impedance in the s domain of the circuit shown in Figure 7-1 is shown below where the imaginary value $\sqrt{-1} = j$ and ω is frequency in radians per second.

$$
\begin{aligned}
s &= j\omega \\
\omega &= 2 \cdot \pi \cdot f \qquad (rad/s) \\
Z(s) &= \frac{R \cdot (s + \omega_z)}{(s + \omega_p)} \qquad (\Omega)
\end{aligned}
\tag{7.67}
$$

The equation for the impedance is in terms of the poles and zeros. This indicates that there is a zero and a pole in the impedance function at ω_Z and ω_p, respectively with both the pole and zero being nonnegative and simple. The magnitude and phase of the impedance function in the frequency domain is shown here.

$$|Z(\omega)| = \frac{\omega_Z}{\omega_p} \cdot R \cdot \frac{\sqrt{1+\left(\frac{\omega}{\omega_Z}\right)^2}}{\sqrt{1+\left(\frac{\omega}{\omega_p}\right)^2}} \qquad (7.68)$$

$$Z_{phase}(\omega) = \tan^{-1}\left(\frac{\omega}{\omega_Z}\right) + \tan^{-1}\left(\frac{-\omega}{\omega_Z}\right) \qquad (7.69)$$

The experimental magnitude resistance data is curve fitted to the equation for the magnitude of the impedance for the circuit shown in Figure 7-1. This step can be accomplished by using the Levenberg-Marquardt algorithm in LabVIEW to determine the least squares set of coefficients that best fit the set of input data points (X,Y) as expressed by a nonlinear function y=f(x,*a*) where *a* is the set of coefficients. The results of the curve fitting are display in Figure 7-2. Using the results from the curve fit, the phase of the impedance is then calculated and also plotted with the experimental data in Figure 7-2. By inspection, the experimental data fits extremely well to the impedance equation for the chosen RC circuit.

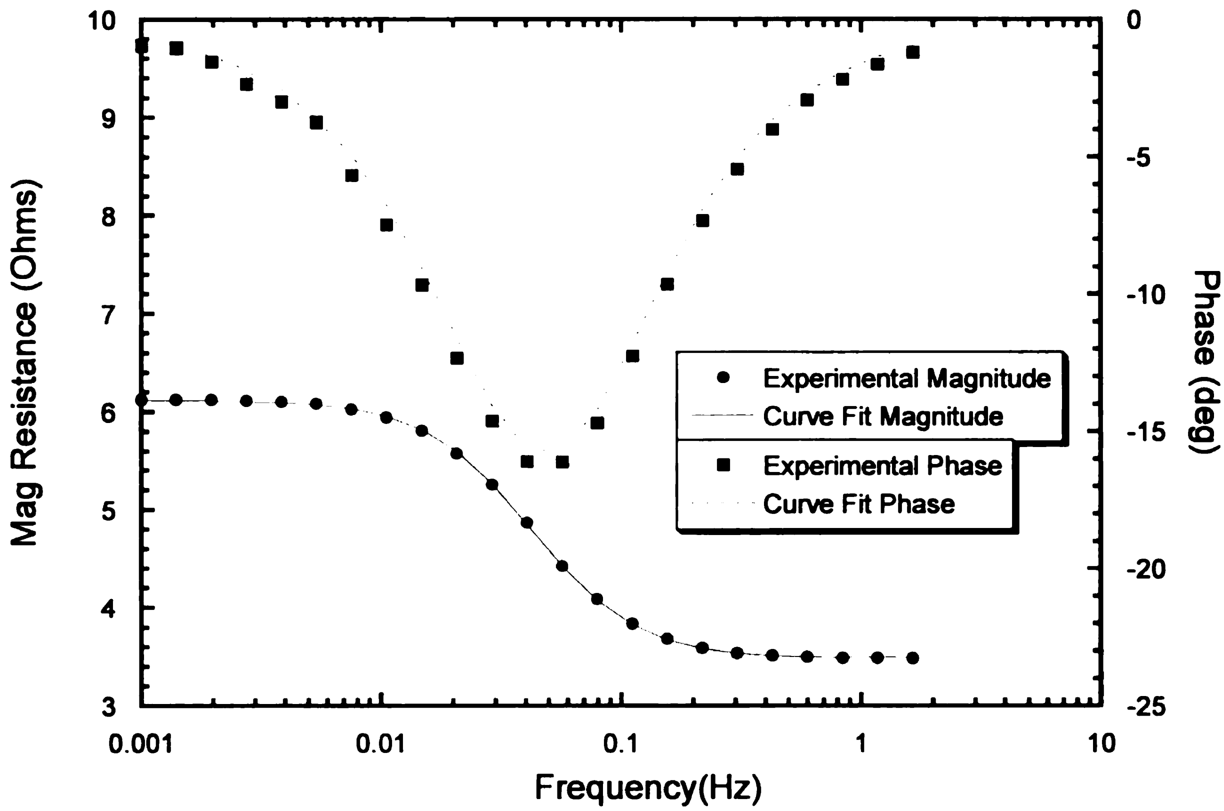

Figure 7-2: Curve fitting experimental data to an impedance equation of the circuit shown in Figure 7-1

The curve fitting routine in LabVIEW provides the values for the pole and zero along with the resistance, R, directly, which is shown here for the experimental data in Figure 7-2.

$$\omega_z = 2\pi \cdot (0.064\,\text{Hz}) \qquad (rad/s)$$
$$\omega_p = 2\pi \cdot (0.037\,\text{Hz}) \qquad (rad/s)$$
$$R = 3.49 \qquad (\Omega)$$

To determine the values for R_l and C_l, the First Foster Technique [51] is used and is described below.

The First Foster Technique can be used to determine an RC circuit that satisfies a real rational impedance function where the poles and zeros are simple, line on the negative real axis, and alternate with each other, the first critical frequency (pole or zero) being a pole. For this situation, the general form of the impedance as a function of s is shown here where H, K, and σ are all real constants with σ representing a critical frequency.

$$Z(s) = H + \frac{K_0}{s} + \sum_{i=1}^{n} \frac{K_i}{s+\sigma_i} \tag{7.70}$$

The general equation can then be written in terms of the critical frequencies as:

$$Z_{RC}(s) = \frac{H \cdot (s+\sigma_{z1}) \cdot (s+\sigma_{z2})\ldots}{(s+\sigma_{p1}) \cdot (s+\sigma_{p2})\ldots} \tag{7.71}$$

Using the above equation, the values for the RC components, shown in Figure 7-3, can be found as follows:

$$\begin{aligned} H &= Z(s)\big|_{s\to\infty} \\ K_0 &= s \cdot Z(s)\big|_{s=0} \\ \hat{K}_i &= (s+\sigma_i) \cdot Z(s)\big|_{s=-\sigma_i} \end{aligned}$$

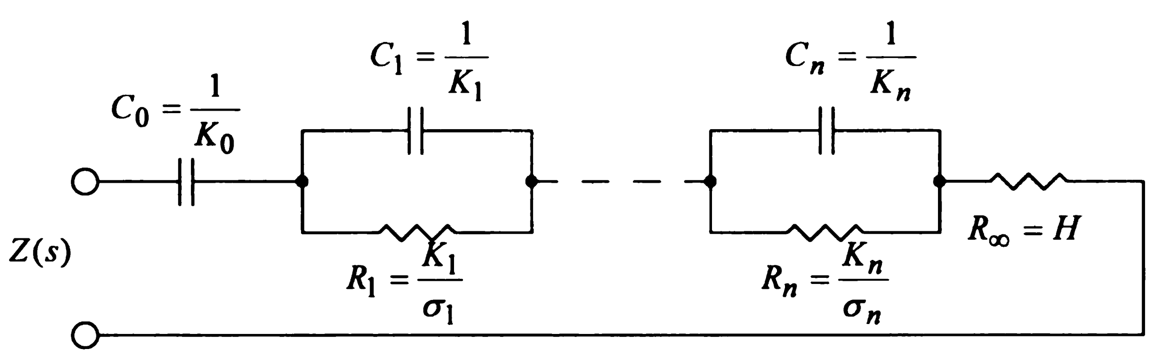

Figure 7-3: First Foster Technique circuit

This technique can be directly applied to the RC circuit representing the thermoelectric module. First, the impedance of the RC circuit is written in terms of the critical frequencies.

$$
\begin{aligned}
Z(s) &= \frac{\omega_Z}{\omega_P} \cdot R \cdot (1 + s/\omega_Z) \cdot \frac{1}{(1 + s/\omega_P)} \\
&= \frac{R \cdot (\omega_Z + s)}{(\omega_P + s)}
\end{aligned}
\tag{7.72}
$$

Using the formulas from the First Foster Technique, the values for H, K_0, and K_1 are found and shown here.

$$
\begin{aligned}
H &= R \\
K_0 &= 0 \\
K_1 &= R \cdot (\omega_Z - \omega_P)
\end{aligned}
$$

Now the RC components of the RC circuit for the TE module are found and shown in Figure 7-4.

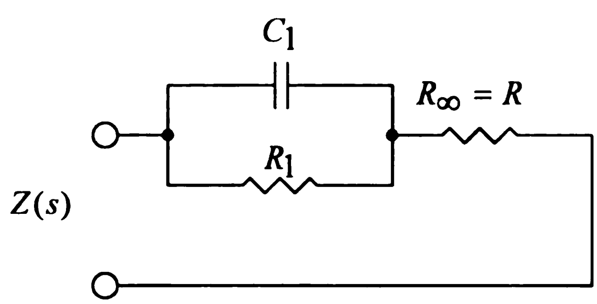

$$C_1 = \frac{1}{R \cdot (\omega_Z - \omega_P)}$$

$$R_1 = \frac{R \cdot (\omega_Z - \omega_P)}{\omega_P}$$

Figure 7-4: Using First Foster Technique for TE Module

Another approach to determining the values for R1 and C1 is to analyze the circuit in the s domain where the impedance of the capacitor will be $1/(s \cdot C_1)$ and manipulate the impedance function until it shows a resistor in series with another resistor in parallel with a capacitor. With a few manipulations of the equation, the values for C_1 and R_1 can be found as shown here.

$$Z(s) = \frac{R \cdot (s + \omega_Z)}{(s + \omega_P)} = \frac{s \cdot R + \omega_Z \cdot R}{s + \omega_P}$$

$$= \frac{s \cdot R + \omega_Z \cdot R + \left[R \cdot \left(s + \omega_P\right) - R \cdot \left(s + \omega_P\right)\right]}{s + \omega_P}$$

$$= R + \frac{R \cdot \left(\omega_Z - \omega_P\right)}{s + \omega_P} \cdot \frac{\left(\frac{\omega_Z - \omega_P}{s \cdot \omega_P}\right) \cdot R}{\left(\frac{\omega_Z - \omega_P}{s \cdot \omega_P}\right) \cdot R}$$

$$= R + \frac{\left[R \cdot \frac{\left(\omega_Z - \omega_P\right)}{\omega_P}\right] \cdot \left[R \cdot \frac{\left(\omega_Z - \omega_P\right)}{s}\right]}{\left[R \cdot \frac{\left(\omega_Z - \omega_P\right)}{\omega_P}\right] + \left[R \cdot \frac{\left(\omega_Z - \omega_P\right)}{s}\right]}$$

$$= R + \frac{R_1 \cdot C_1}{R_1 + C_1} = R + R_1 // C_1$$

$$\text{where } C_1 = \frac{1}{R \cdot (\omega_Z - \omega_P)} \text{ and } R_1 = \frac{R \cdot (\omega_Z - \omega_P)}{\omega_P}$$

Using the curve fitting routine in LabVIEW for the data collected shown in Figure 7-2, the values for R_1 and C_1 are shown here.

$$R_1 = 2.63\,\Omega$$
$$C_1 = 1.65\,\text{F}$$

It is interesting to note the value for C_1. There are not any known capacitances in a thermoelectric module (except for small parasitic capacitances) and typically, an electrical capacitor with a value of 1.65 farads would be very large. The thermoelectric module is effectively storing energy similar to a capacitor. If the thermoelectric module was in a "black box", the user could assume that the "black box" would have this large capacitor inside.

Up to this point, the experimental data has been fitted to an entirely electrical RC circuit. However, the thermoelectric module obviously has a thermal characteristic. The next task is to identify where the thermal properties come into play with the RC circuit. To begin, first start with the steady state circuit for the thermoelectric module, which includes the electrical resistance and the Seebeck dependant voltage source shown in Figure 7-5.

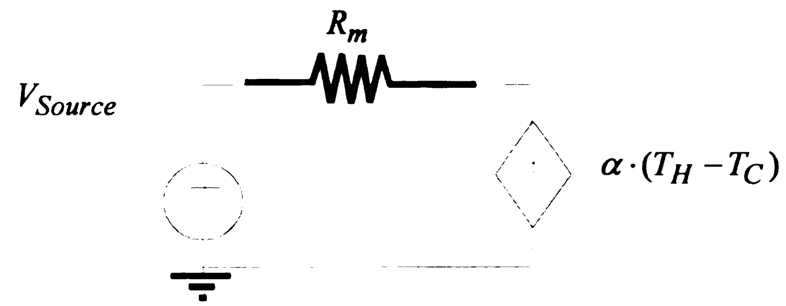

Figure 7-5: Steady state thermoelectric model

The impedance of this circuit is shown in Figure 7-6. The impedance of the steady state thermoelectric model and the impedance of the RC network can be compared. Because the Seebeck dependant voltage source has a negligible effect at high frequencies, the electrical resistance of the module can be set equal to the series resistor found in the RC circuit. This leaves the parallel combination of R_1 and C_1 to be related to the dependant voltage source. R_1 and C_1 must be a representation of the thermal behavior of the TE module that affects the impedance due to the Seebeck effect, which is discussed in the next section.

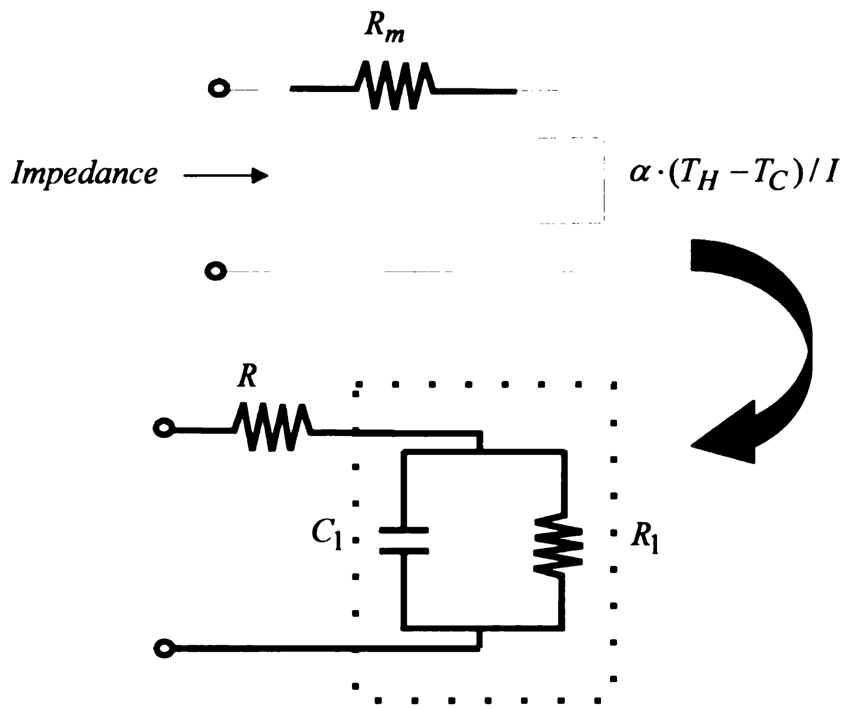

Figure 7-6: Comparison of impedance between circuits

7.2.2 Thermal Impedance

The next task is to relate this electrical impedance of the RC circuit to a thermal impedance [52] of the thermoelectric module. Relating R_1 and C_1 to the dependent voltage source due to the Seebeck effect, the following is found:

$$\frac{\alpha \cdot (T_H - T_C)}{i_{IN}} = R_1 // C_1 = \frac{R_1}{(R_1 \cdot C_1 \cdot s + 1)}$$
$$(T_H - T_C) = \frac{R_1 \cdot i_{IN}}{\alpha \cdot (R_1 \cdot C_1 \cdot s + 1)} \tag{7.73}$$

Thermal impedance can be represented by the temperature gradient across the sample divided by the heat flow, Q. For the thermoelectric module, the heat flow can be defined by $\alpha \cdot i_{IN} \cdot T_{avg}$. Substituting the relation found for the temperature gradient into the thermal impedance equation, the new equation for the thermal impedance is as follows:

$$Z_{Thermal} = \frac{\Delta T}{Q} = \frac{T_H - T_C}{\alpha \cdot i_{IN} \cdot T_{avg}} = \frac{R_1}{\alpha^2 \cdot T_{avg} \cdot (R_1 \cdot C_1 \cdot s + 1)} \tag{7.74}$$

This can be rewritten into a familiar form of a capacitor in parallel with a resistor, which is shown here.

$$Z_{Thermal} = \frac{1}{C_1 \cdot \alpha^2 \cdot T_{avg} \cdot \left(s + \frac{1}{R_1 \cdot C_1} \right)} = \frac{1}{s \cdot C_1 \cdot \alpha^2 \cdot T_{avg} + \frac{\alpha^2 \cdot T_{avg}}{R_1}} = \frac{1}{s \cdot C_{Thermal} + \frac{1}{R_{Thermal}}} \tag{7.75}$$

The values for $R_{Thermal}$ and $C_{Thermal}$ shown here do not represent an electrical resistance and capacitance, but rather a thermal resistance and capacitance where the values for these components are:

$$C_{Thermal} = \alpha^2 \cdot T_{avg} \cdot C_1$$
$$R_{Thermal} = \frac{R_1}{\alpha^2 \cdot T_{avg}} \tag{7.76}$$

Notice that $C_{Thermal}$ and $R_{Thermal}$ are both related to the Seebeck coefficient, α. This indicates that the Seebeck coefficient must be known in order to solve for the thermal resistance and capacitance. From here, the thermal capacitance and thermal conductance of the module can be calculated. It would also be possible to find the thermal conductance if the thermal capacitance is known instead of the Seebeck coefficient.

Figure 7-7 shows the related equivalent circuit found in the above equation to the impedance of the Seebeck dependent voltage source.

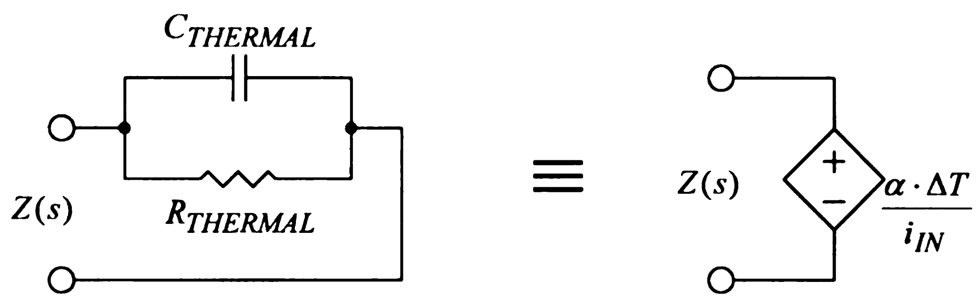

Figure 7-7: Thermal impedance related to electrical impedance

7.2.3 Final Model

The final AC model for the thermoelectric module is shown in Figure 7-8. In this model, the dependent voltage source can be called a temperature dependent voltage source. The following equation also shows how using only the poles and zeros of the impedance can also give ZT of the module.

$$
\begin{aligned}
ZT &= \frac{R_{DC}}{R_{AC}} - 1 \\
&= \frac{R + R_1}{R} - 1 = \frac{R_1}{R} \\
&= \frac{\dfrac{R \cdot (\omega_z - \omega_p)}{\omega_p}}{R} \\
&= \frac{(\omega_z - \omega_p)}{\omega_p} \\
&= \frac{\omega_z}{\omega_p} - 1
\end{aligned}
\tag{7.77}
$$

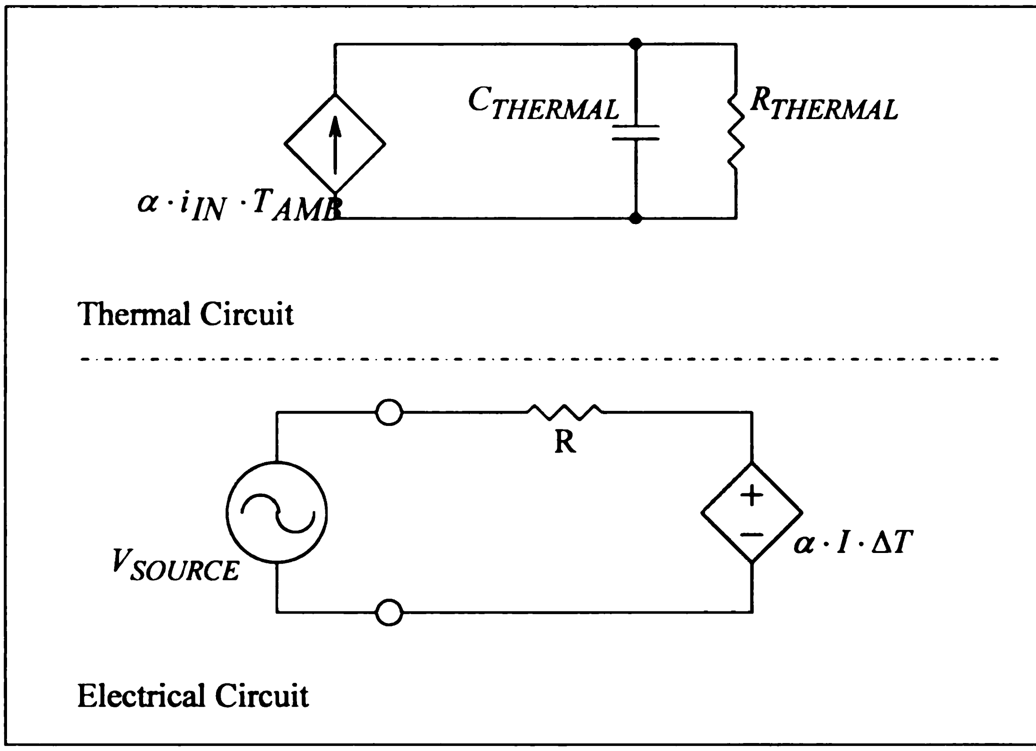

Figure 7-8: AC thermal-electrical model for a TE module

From the Tellurex website [49], the Seebeck coefficient for this module is approximately 0.04604 (V/K). The module consists of 254 pellets, and the size of each pellet is 1mm by 1mm by 1.4mm. With this information the thermal resistance and capacitance can be calculated. The results are shown in Table 7-3.

Table 7-3: AC TEM model results

Seebeck of Module (V/K)	0.04604
Number of Pellets in Module	254
ZT	0.75
Electrical Conductivity (S/cm)	1.02E+03
Seebeck of 1 pellet (V/K)	1.81E-04
Thermal Conductivity (W/m·K)	1.33
Thermal Resistance of Module (K/W)	4.14
Thermal Capacitance (W·s/K)	1.075

7.2.4

The p

progr

panel

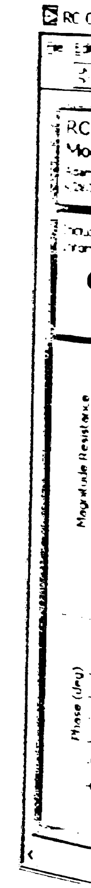

Fi

7.2.4 Final Program for Analyzing Data

The curve fitting program using this RC one-port method was created in LabVIEW. The program first takes the data that was collected by a previously explained LabVIEW program that controlled the impedance measurement experiment. A picture of the front panel view of the program is shown in Figure 7-9.

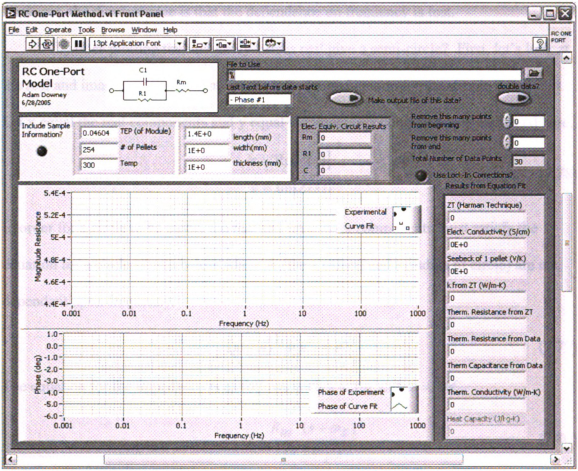

Figure 7-9: Front panel view of the RC One-Port Method LabVIEW program

7.3 Circle Plot

Another possible approach to analyzing the impedance data of the thermoelectric module is to plot the imaginary impedance versus the real impedance, also know as the Nyquist plot. For a thermoelectric module that behaves like the RC circuit, this plot will create a semi-circle. The Nyquist plot is different than the Bode plot in that the Nyquist plot shows visually the relation between the real and the imaginary impedance. However, the disadvantage is that the dependence on frequency is lost.

Why does plotting the imaginary versus real give a semi-circle? First, let's look at the real and imaginary components of the impedance function for the simple RC circuit. Let x equal the real components and y equal the imaginary components as indicated here.

$$\begin{aligned} x &= \mathrm{Re}[Z(s)] \\ y &= \mathrm{Im}[Z(s)] \end{aligned} \tag{7.78}$$

In order for a circle to be made, the real and imaginary components must satisfy the equation for a circle shown below where A (the x offset) and r (radius of circle) are not dependant upon frequency.

$$(x-A)^2 + y^2 = r^2 \tag{7.79}$$

The equation for the impedance is as follows with $s = j\omega$ and $\omega = 2\pi f$,

$$Z(s) = \frac{R_m \cdot (s+\omega_z)}{(s+\omega_p)} \tag{7.80}$$

The frequency at the zero of the impedance function is:

$$\omega_z = \frac{1}{(R_1 \,//\, R_m)\cdot C_1} = \frac{R_1 + R_m}{R_1 \cdot R_m \cdot C_1} \tag{7.81}$$

The frequency at the pole of the impedance function is:

$$\omega_p = \frac{1}{R_1 \cdot C_1} \tag{7.82}$$

Substituting the above equations back into (7.80) and writing the equation in terms of real and imaginary components is shown below.

$$\begin{aligned}
Z(s) &= \frac{R \cdot \left(s + \dfrac{R_1 + R_m}{R_1 \cdot R_m \cdot C_1}\right)}{\left(s + \dfrac{1}{R_1 \cdot C_1}\right)} \\
&= \frac{R \cdot \left(s + \dfrac{R_1 + R_m}{R_1 \cdot R_m \cdot C_1}\right)}{\left(s + \dfrac{1}{R_1 \cdot C_1}\right)} \cdot \frac{\left(s - \dfrac{1}{R_1 \cdot C_1}\right)}{\left(s - \dfrac{1}{R_1 \cdot C1}\right)} \\
&= \frac{R_m \cdot s^2 + \left(\dfrac{-R_m}{R_1 \cdot C_1} + \dfrac{R_m + R_1}{R_1 \cdot C_1}\right) \cdot s - \dfrac{R_m + R_1}{(R_1 \cdot C_1)^2}}{s^2 - \dfrac{1}{(R_1 \cdot C_1)^2}} \\
&\frac{(R_1 \cdot C_1)^2 \cdot R_m \cdot (j \cdot \omega)^2 + (R_m \cdot C_1)(R_1) \cdot (j \cdot \omega) - (R_m + R_1)}{(R_1 \cdot C_1)^2 \cdot (j \cdot \omega)^2 - 1} \\
&= \frac{(R_1 \cdot C_1)^2 \cdot R_m \cdot \omega^2 + R_m + R_1}{(R_1 \cdot C_1)^2 \cdot \omega^2 + 1} + j \cdot \frac{-R_1{}^2 \cdot C_1 \cdot \omega}{(R_1 \cdot C_1)^2 \cdot \omega^2 + 1} \qquad (7.83) \\
&= \mathrm{Re}[Z(s)] + j \cdot \mathrm{Im}[Z(s)]
\end{aligned}$$

The values for the real and imaginary components for this impedance function can be used to satisfy the circle equation where A and r are not dependant upon the frequency as shown here.

From

the c

be R_I

can b

freque

by fin

This fr

curve f

is reac

$$\left(\underbrace{\frac{R_1{}^2 \cdot C_1{}^2 \cdot R_m \cdot \omega^2 + R_m + R_1}{R_1{}^2 \cdot C_1{}^2 \cdot \omega^2 + 1}}_{x} - \underbrace{\frac{2 \cdot R_m + R_1}{2}}_{A}\right)^2 + \left(\underbrace{\frac{-R_1{}^2 \cdot C_1 \cdot \omega}{R_1 \cdot C_1{}^2 \cdot \omega^2 + 1}}_{y}\right)^2 = \underbrace{\left(\frac{1}{2} \cdot R_1\right)}_{r}{}^2 \tag{7.84}$$

From the above equation it is clear that the radius of the circle is $0.5 \cdot R_1$. The center of the circle lies on the x-axis at $0.5 \cdot (2 \cdot R_m + R_1)$. The far most left side of the circle will be R_m while the far most right side of the circle will be $R_m + R_1$. The peak of the circle can be used to identify the capacitor value. This can be explained by identifying the frequency that gives the maximum absolute imaginary impedance. This is accomplished by finding when the derivative of y is zero.

$$\begin{aligned}
\frac{dy}{d\omega} &= 0 \\
\frac{d}{d\omega}\left[\frac{-R_1{}^2 \cdot C_1 \cdot \omega}{R_1 \cdot C_1{}^2 \cdot \omega^2 + 1}\right] &= 0 \\
R_1{}^2 \cdot C_1 \cdot \frac{R_1{}^2 \cdot C_1{}^2 \cdot \omega^2 - 1}{R_1{}^2 \cdot C_1{}^2 \cdot \omega^2 + 1} &= 0 \\
R_1{}^2 \cdot C_1{}^2 \cdot \omega^2 &= 1 \\
\omega_{peak} &= \frac{1}{R_1 \cdot C_1}
\end{aligned} \tag{7.85}$$

This frequency is the same as the pole of the impedance function, ω_p. Therefore, a curve fitting circle fit must be used to identify the frequency where the peak of the circle is reached. Once that is found, the capacitor value can be calculated as follows.

$$C_1 = \frac{1}{R_1 \cdot \omega_{peak}} \tag{7.86}$$

alon

iden

An example of the Nyquist plot is shown with experimental data in Figure 7-10 along with a curve fit to the data that was performed using LabVIEW. The figure identifies the direction of increasing frequency.

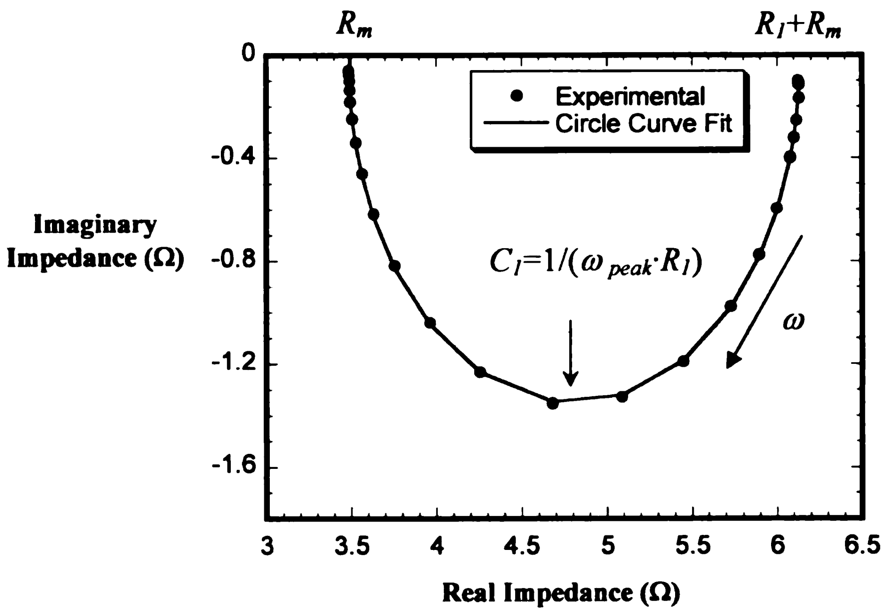

Figure 7-10: Imaginary versus real impedance plot

Chapter 8: Thermal Transmission Line Model

8.1 Introduction

A second approach to modeling a TE module is to model the thermal properties as a distributed thermal resistance and capacitance spread throughout the length of the material using a Thermal Transmission Line Model (Thermal TLINE). This approach is similar to using transmission line theory with electrical cables long enough to propagate an electrical wave. This model, although more complicated than the RC one-port model, can provide a more realistic and detailed description of the thermal and electrical behavior of the module. This is because the model separates out the individual thermal components of the module such as: the thermoelectric pellets, the nickel traces for the interconnects, and the alumina plates attached to the top and bottom of the module. The model provides insight on the effects of thermally grounding one side of the module. The motivation for investigating the use of transmission line theory was the inability of the RC One-Port model to explain the impedance behavior found experimentally with inline modules and single TE pellets.

8.2 Thermal Dynamics

The TE module is composed of thermoelectric material, nickel traces, and ceramic end caps as shown in Figure 8-1. These components (because of their length) must propagate thermal energy through them (heat transfer is not instantaneous).

The f

[53].

materi

length

space (

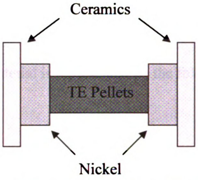

Figure 8-1: Components of a TE module

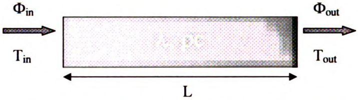

Figure 8-2: Thermal dynamics of a 2-D material

The following variables will be used for the explanation of thermal dynamics.

$$\lambda = \text{thermal conductivity}$$
$$\rho = \text{density}$$
$$\text{c} = \text{specific heat}$$
$$\Phi = \text{heat flow}$$
$$\text{T} = \text{temperature}$$
$$\text{L} = \text{length}$$
$$\text{A} = \text{Area}$$

To being the analysis, first look at the thermal dynamics for a one-dimensional case [53]. Figure 8-2 shows a two dimensional diagram for the thermal dynamics of a material with a given length, L. The equation for temperature throughout a material of length L is a second-order linear differential equation (SOLDE) both dependent upon space (x) and time (t) shown here.

The

For th

possi

that it

new e

Let θ a

The ne

$$\frac{\partial^2 T}{\partial x^2} = \frac{\rho \cdot c}{\lambda} \cdot \frac{\partial T}{\partial t} \quad \text{for } 0 < x < L \tag{8.87}$$

The heat flow through the material is represented by the following equation.

$$\Phi = -\lambda \cdot A \cdot \frac{\partial T}{\partial x} \tag{8.88}$$

For the purposes of the analysis, the assumption will be made that $T = 0$ for $t = 0$. It is possible, with the help of Laplace transform, to rewrite the SOLDE for temperature so that it is based only on space (not on time). To simplify the notation, let $a = \frac{\lambda}{\rho \cdot c}$ so the new equations are now:

$$\frac{\partial^2 T}{\partial x^2} = \frac{1}{a} \cdot \frac{\partial T}{\partial t} \tag{8.89}$$

$$\Phi = -\lambda \cdot A \cdot \frac{\partial T}{\partial x} \tag{8.90}$$

Let θ and ϕ be the Laplace transform of T and Φ respectively, where $s = j\omega$.

$$\begin{aligned} \theta(x,s) &= \int_0^\infty T(x,t) e^{(-st)} dt \\ \phi(x,s) &= \int_0^\infty \Phi(x,t) e^{(-st)} dt \end{aligned} \tag{8.91}$$

The new equations are now only dependent on position and are shown below.

$$\frac{\partial^2 \theta}{\partial x^2} = \frac{s}{a} \cdot \theta \tag{8.92}$$

$$\phi = -\lambda \cdot A \cdot \frac{\partial \theta}{\partial x} \tag{8.93}$$

A s

initi

belo

whe

By in

K_1 an

sampl

This f

dynam

theory

A solution for θ can now be found. By existence and uniqueness of solutions with given initial conditions, there is always exactly one normalized pair of solutions which is shown below (K_1 and K_2 are constants)

$$\theta(x) = K_1 \cdot \cosh(\beta \cdot x) + K_2 \cdot \sinh(\beta \cdot x) \tag{8.94}$$

where

$$\beta^2 = \frac{s}{a} \tag{8.95}$$

By imposing the following boundary conditions,

$$\begin{aligned} \theta_{in} &= \theta(x=0) \\ \theta_{out} &= \theta(x=L) \end{aligned} \tag{8.96}$$

K_1 and K_2 can be solved for in the following way:

$$\begin{aligned} \theta_{in} &= K_2 \\ \theta_{out} &= K_1 \cdot \sinh(\beta \cdot L) + K_2 \cdot \cosh(\beta \cdot L) \\ \phi_{in} &= -\lambda \cdot A \cdot \beta \cdot K_1 \\ \phi_{out} &= \lambda \cdot A \cdot \beta \cdot \left(K_1 \cdot \cosh(\beta \cdot L) + K_2 \cdot \sinh(\beta \cdot L)\right) \end{aligned} \tag{8.97}$$

$$\boxed{\begin{aligned} \theta_{in} &= \cosh(\beta \cdot L) \cdot \theta_{out} + \frac{1}{\lambda A \beta} \cdot \sinh(\beta \cdot L) \cdot \phi_{out} \\ \phi_{in} &= \lambda A \beta \cdot \sinh(\beta \cdot L) \cdot \theta_{out} + \cosh(\beta \cdot L) \cdot \phi_{out} \end{aligned}} \tag{8.98}$$

The above pair of equations for the Laplace of temperature and heat flow into the sample is written in terms of the Laplace of temperature and heat flow out of the sample. This form for the equations will become apparent in the next section where the thermal dynamic equations will be compared to the Telegrapher's equation from transmission line theory.

8.3 C

circui

trans

(G), c

by a s

below

imped

8.3 Comparing Thermal Dynamics with Transmission Line Theory

An electrical transmission line is a distributed parameter network as opposed to a circuit, which consists of lumped elements. A model for a small segment of a transmission line is shown in Figure 8-3 which consists of resistance (R), conductance (G), capacitance (C), and inductance (L) all as units per length such that multiplying them by a small distance, Δx, gives the appropriate units.

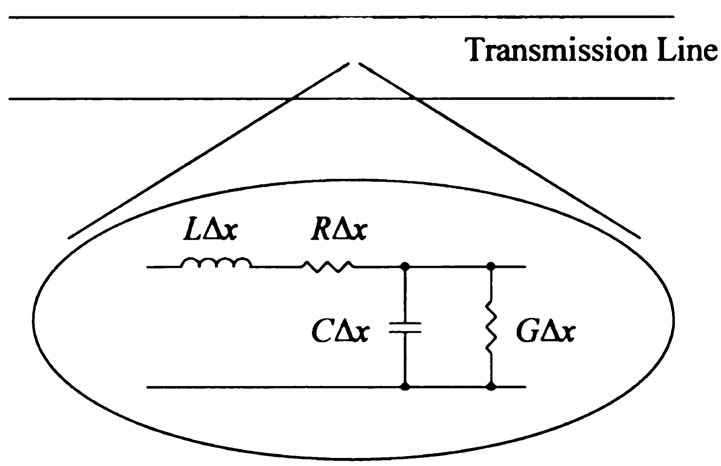

Figure 8-3: Transmission Line Model

Equations for the voltage and current going into a transmission line are shown below where V_L and I_L are the voltage and current across a load, Z_0 is the characteristic impedance, and γ is the propagation constant.

$$\gamma = \sqrt{(R + sL)(G + sC)} \tag{8.99}$$

$$Z_0 = \sqrt{\frac{R + sL}{G + sC}} \tag{8.100}$$

$$\begin{aligned} V_{in}(x') &= V_L \cdot \cosh(\gamma \cdot x') + I_L \cdot Z_0 \cdot \sinh(\gamma \cdot x') \\ I_{in}(x') &= \frac{V_L}{Z_0} \cdot \sinh(\gamma \cdot x') + I_L \cdot \cosh(\gamma \cdot x') \end{aligned} \tag{8.101}$$

The equations above are known as Telegrapher's equations and can be directly compared to the temperature and heat flow equations found with the thermal dynamic equations, which are shown again here.

$$
\begin{aligned}
\theta_{in} &= \theta_{out} \cdot \cosh(\beta \cdot L) + \frac{1}{\lambda A \beta} \cdot \phi_{out} \cdot \sinh(\beta \cdot L) \\
\phi_{in} &= \lambda A \beta \cdot \theta_{out} \cdot \sinh(\beta \cdot L) + \phi_{out} \cdot \cosh(\beta \cdot L)
\end{aligned}
\tag{8.102}
$$

The relation between the thermal dynamics in Laplace form and Telegrapher's equations can be shown be letting the following equalities be true.

$$
\begin{aligned}
\theta_{out} &= V_L \\
\phi_{out} &= I_L \\
\beta &= \gamma \\
\sqrt{\frac{s \cdot \rho c}{\lambda}} &= \sqrt{(R + sL)(G + sC)} \\
\frac{1}{\lambda A \beta} &= Z_0 \\
\sqrt{\frac{1}{\lambda A^2 s \cdot \rho c}} &= \sqrt{\frac{R + sL}{G + sC}}
\end{aligned}
\tag{8.103}
$$

Using the above equalities, an electrical representation of a thermal circuit can be made where the values for R, C, G, and L are as follows.

$$
\boxed{
\begin{aligned}
&R = \frac{1}{\lambda A} \ \ (\mathrm{m}^{-1}) \\
&C = \rho c \mathrm{A} \ \ (\mathrm{m}^{-1}) \\
&G = 0 \ \ (\mathrm{m}^{-1}) \\
&L = 0 \ \ (\mathrm{m}^{-1})
\end{aligned}
}
\tag{8.104}
$$

The relations shown above can be justified. R is the thermal resistance per unit of position. C is the heat capacitance per unit of position. G represents a thermal loss due to thermal conductance. However, a sample that is heated and in a vacuum (neglecting radiation losses) will remain at that temperature and will not cool down. Therefore, it is justified to find that $G = 0$. L represents a thermal inductance. Heat flow is a diffusion process and there is no known thermal inductive component. Therefore, it is also justified to find that $L = 0$.

8.4 Applying Thermal Transmission Line Model

By converting the thermal properties of a sample into an equivalent electrical circuit, the transmission line equations may be used to describe the thermal properties of thermoelectric modules. This can also be applied to inline modules as well as single TE pellets.

8.4.1 Thermal TLINE Model for Commercial Module

The thermal transmission line model can now be applied to each of the elements of the thermoelectric module shown in Figure 8-4. Due to the Peltier effect, an alternating heat flow source will be modeled as an electrical current source. Voltages V_1 and V_2 in this figure indicate temperature at their locations.

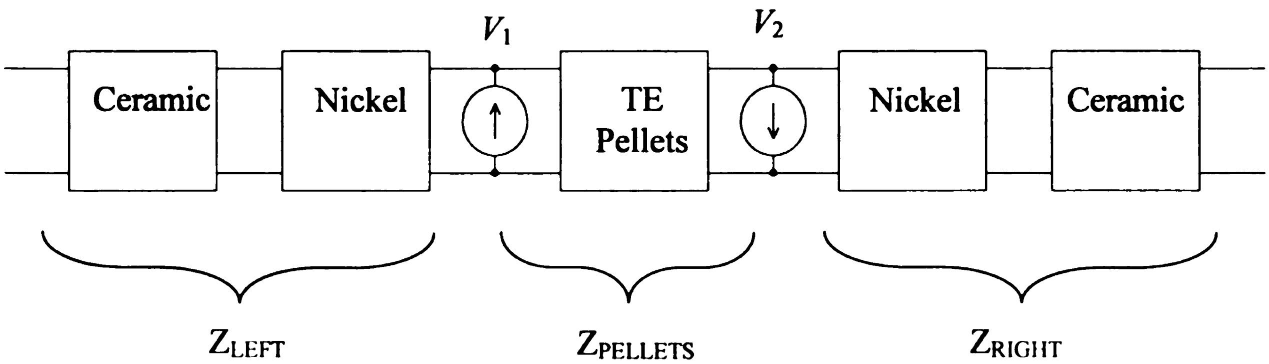

Figure 8-4: Applying Thermal TLINE model

The equation for finding the temperatures indicated by V_1 and V_2 are shown below using a condensed notation and are found using super-position. In this case, Z stands for the thermal impedance.

$$V_1 = i \cdot (Z_{Pellets} \text{ with } Z_{Right}) // Z_{Left} - \left[i \cdot (Z_{Pellets} \text{ with } Z_{Left}) // Z_{Right} \right]_{@V_1}$$
$$V_2 = -i \cdot (Z_{Pellets} \text{ with } Z_{Left}) // Z_{Right} + \left[i \cdot (Z_{Pellets} \text{ with } Z_{Right}) // Z_{Left} \right]_{@V_2}$$

(8.105)

By knowing the dimensions and the thermal properties of the ceramics and the nickel traces used on the TE module, a fit to the data can be achieved using LabVIEW software. Figure 8-5 shows a picture of a commercially available TE module created for power generation that was used to test the Thermal TLINE model.

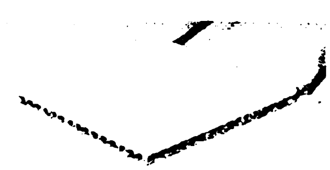

Figure 8-5: Commercially available TE module

The dimensions and thermal properties for the module are separated into the three main components: the ceramics, the nickel traces, and the TE pellets and are shown in Table 8-1.

The v

whic

Table 8-1: Commercially available TE module component properties

	Length (mm)	Width (mm)	Thickness (mm)	Specific Heat (J/K-Kg)	Thermal Conductivity (W/mK)	Density (g/cm³)
Ceramic Side 1	33	30	0.55	850	26	3.9
Ceramic Side 2	30	30	0.55	850	26	3.9
Nickel Trace (each)	3.125	1.25	0.4	444	90.9	8.9
TE Pellet (each)	1.4	1	1			

The values shown in Table 8-1 are used in the Thermal TLINE model using a setup file, which is shown in Figure 8-6.

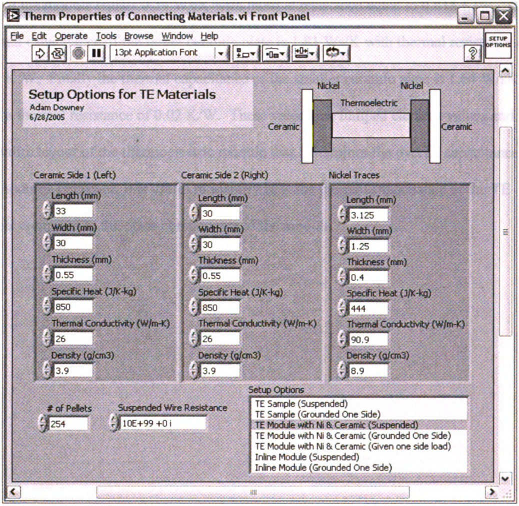

Figure 8-6: Setup LabVIEW vi for commercially available TE module

Using the information on the TE module and using the Thermal TLINE model along with the RC One-Port model to fit the data, it can be seen in Figure 8-7 that the Thermal TLINE model fits well to the experimental data. For this sample, both the Thermal TLINE fit and the RC One-Port fit match the data. However, the RC One-Port model indicates that the thermal capacitance of the module is 1.09 Ws/K without being able to identify where the thermal capacitance is from. The Thermal TLINE model indicates that the thermal capacitance of the TE material alone is 0.67 Ws/K with a thermal resistance equal to 4.07 K/W. Thermal capacitance of the nickel traces on one side of the module equals 0.39 Ws/K with thermal resistance equal to 0.018 K/W. The thermal capacitance of the larger ceramic plate is 1.81 Ws/K with thermal resistance of 0.02 K/W. Finally the thermal capacitance of the smaller ceramic plate is 1.64 W/sK with a thermal resistance of 0.02 K/W. These values are lumped element values and it is the entire layout of the thermoelectric module that determines the overall capacitance of the module. However, it is useful to identify how the thermal capacitance of the TE pellets compares to the other components of the module.

Figu

8.4.2 T

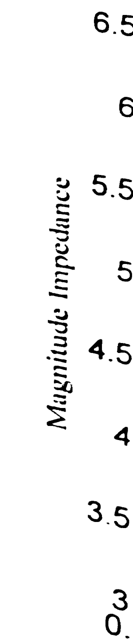

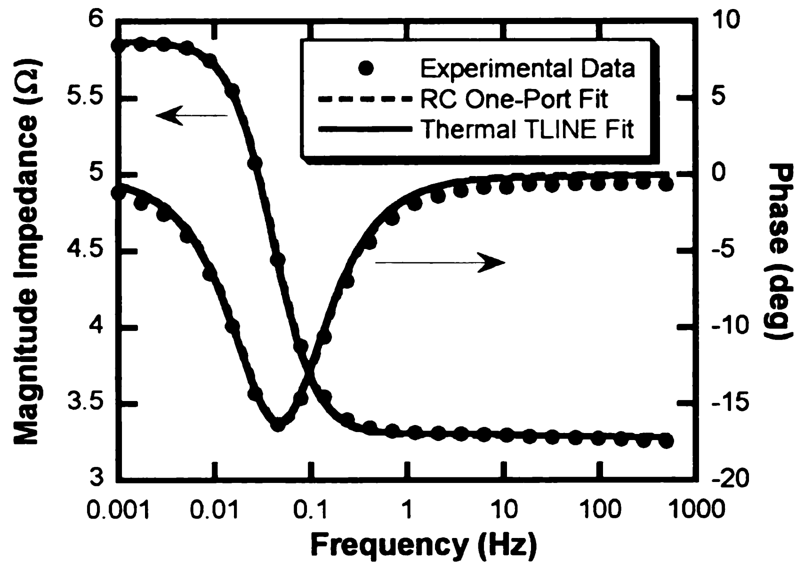

Figure 8-7: Experimental data, RC One-Port fit, and Thermal TLINE fit to data for commercially available TE module

8.4.2 Thermally Grounding One Side of Module

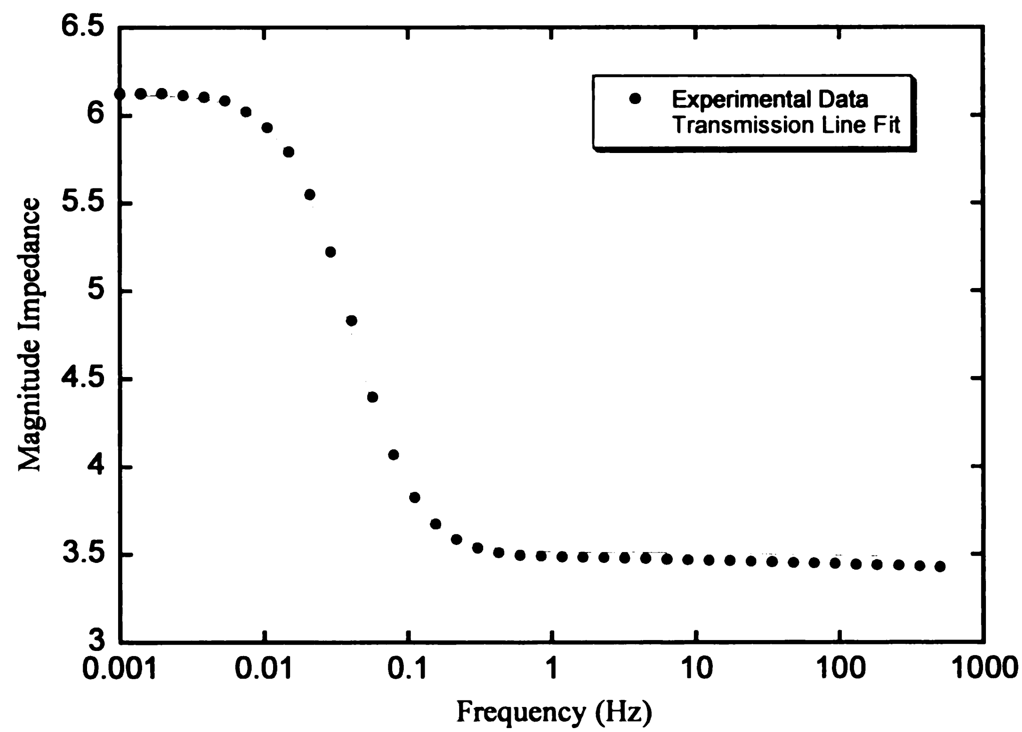

Figure 8-8: Curve fitting thermal transmission line model

An advantage of using the Thermal TLINE model is that the effects of thermally grounding one side of a commercially available TE module can be observed and it is possible to investigate how well the thermal ground is achieved. Figure 8-8 shows data and the Thermal TLINE fit for a different TE module than the one used in Figure 8-7. This module was dangling in a high vacuum environment. Figure 8-9 shows how the data should be theoretically shifted in frequency for this module thermally grounded on one side compared to the module that was not thermally grounded on either side. Figure 8-10 shows experimental data of the module that was thermally grounded to a heat sink using thermal grease compared to the theoretical ideal case. Notice that the experimental data in Figure 8-10 does not agree with the data predicted by the transmission line model. However, the model allows the user to change how it is grounded. For example, instead of an ideal thermal ground, a thermal resistance of 10K/W to ground was used on one side of the module in the Thermal TLINE Model to simulate a theoretical poor thermal ground. The new data predicted by the model, shown in Figure 8-11, agrees well with the experimental data and indicates that a poor thermal ground was established between the TE module and the heat sink.

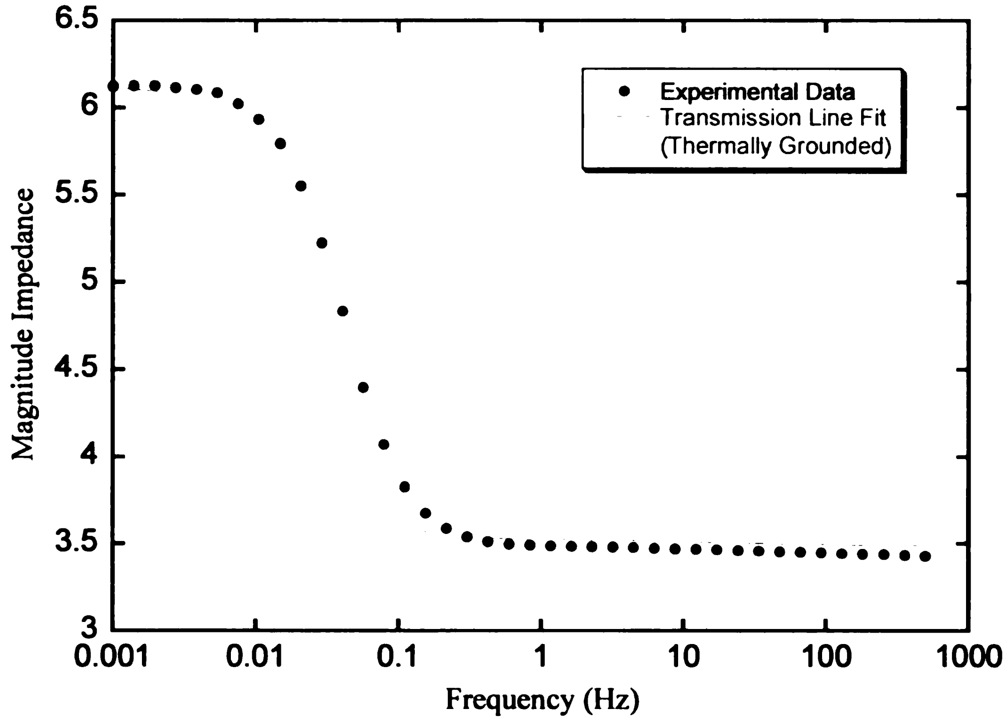

Figure 8-9: Ideal thermal ground one side of TE module

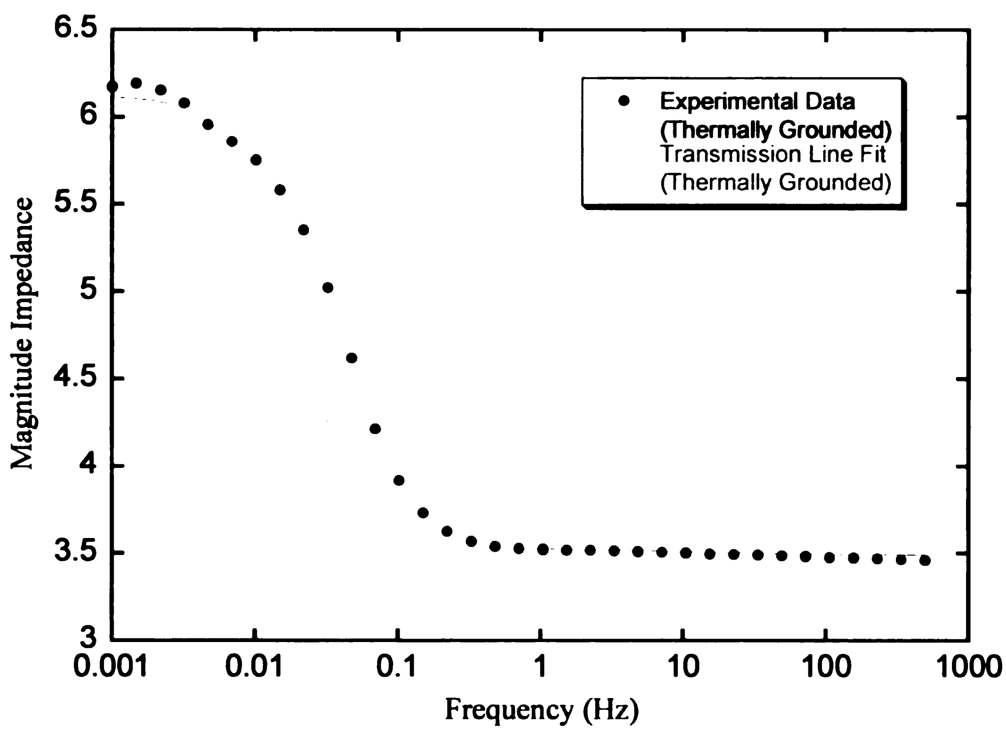

Figure 8-10: Compare ideal thermal ground with experimental data

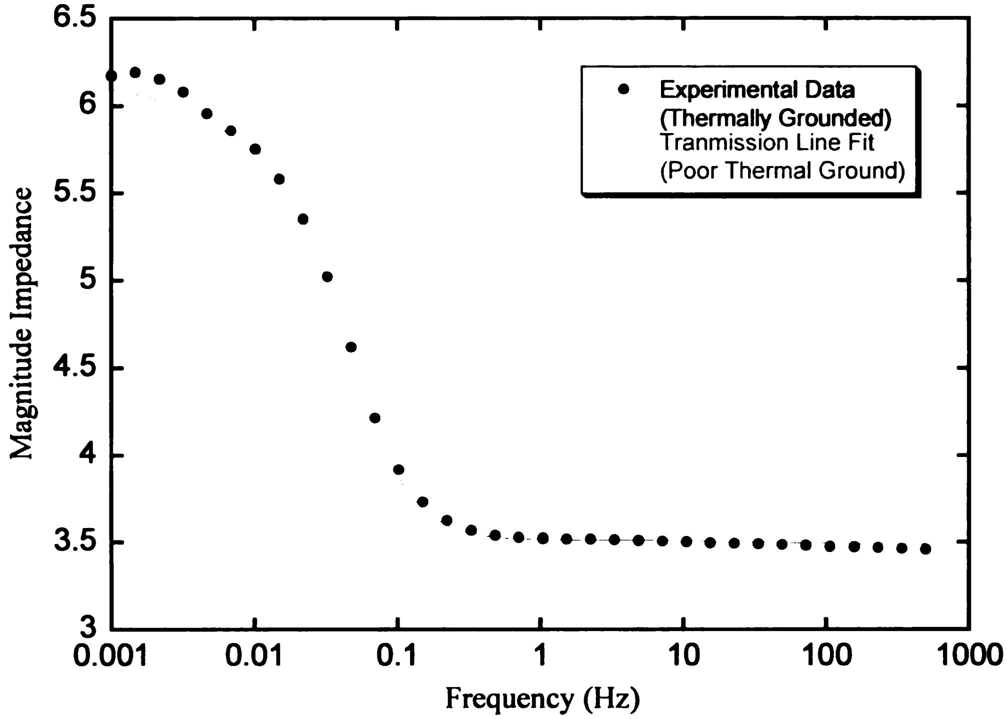

Figure 8-11: Theoretical poor thermal ground compared to experimental data

The Thermal TLINE Model provides much more detailed analysis of the commercially available TE module than the RC One-Port model. It was able to identify where the thermal capacitance and resistance of the module was located along with the corresponding values. The fit to the data was comparable to the fit using the RC-One Port Model. However, the Thermal TLINE Model was able to explain the data collected after attempting to thermally ground one side of the TE module.

8.4.3 TTLM for Inline PN Module

It is important to test materials created by MSU that will be used in the fabrication of a large thermoelectric module. AC frequency measurements were made on an inline module where the n-type sample was LAST (Lead, Antimony, Silver, Tellurium) and the p-type material was LASTT (Lead, Antimony Silver, Tellurium, Tin) bonded together with antimony and without ceramic end caps (see Figure 8-12). This inline module happens to be tested at 600K. After analyzing the impedance spectroscopy data on this inline module, the Thermal TLINE model is a better fit to the data than the RC-One Port Model (see Figure 8-13).

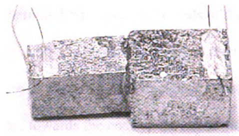

Figure 8-12: Inline TE module using LAST material

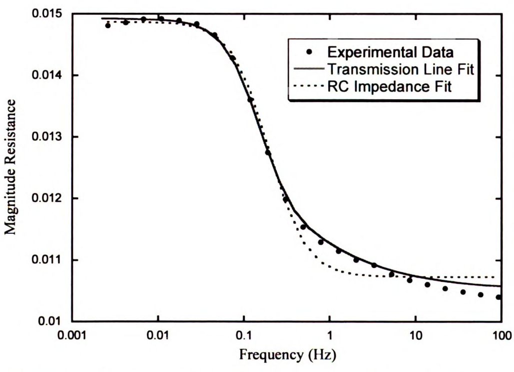

Figure 8-13: Comparison between Transmission Line Model and RC-One Port Model

The experimental data shown in Figure 8-13 shows an interesting behavior as the frequency goes from low frequency to high frequency measurements. Towards the lower frequencies, the impedance behaves similar to the RC One-Port model. However, at high frequencies, the data has a much smoother bend in impedance than the RC One-Port Model. This shape for the data can be expected because the inline module is behaving like a single transmission line with only one source at one end of the line. This is due to the fact that there is not a thermal capacitance at the ends of the module (no ceramics). A possible temperature profile along the length of the inline module (using a low frequency electrical current that is close to the pole of the impedance function) is shown in Figure 8-14. The voltage probes are towards the ends of the inline module where the temperature profile will approximately be in phase with each other.

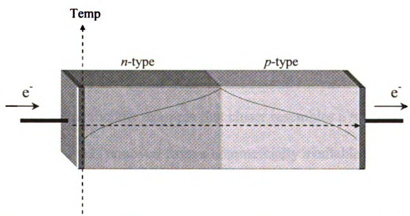

Figure 8-14: Possible temperature profile at one instance in time along the length of an inline *pn* TE module using a low frequency electrical current that is close to the pole of the impedance function

The inline module temperature profile approaches the behavior of an electrical transmission line with a single source at one end and grounded at the other. This can be seen if the inline model is thermally grounded at the ends of the sample as shown in

Figure 8-15. Thermally grounding the ends of the sample shorts out the Peltier Heat flow source at the ends of the sample leaving a thermal circuit shown in Figure 8-16.

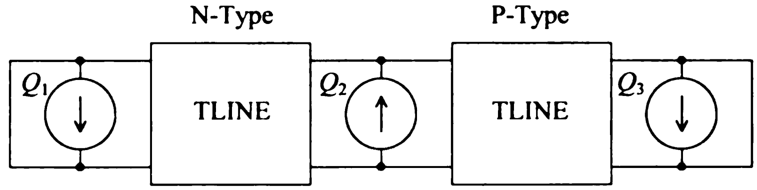

$$Q_1 = \alpha_n \cdot I \cdot T_{avg} \qquad Q_2 = \alpha_{np} \cdot I \cdot T_{avg} \qquad Q_3 = \alpha_p \cdot I \cdot T_{avg}$$

Figure 8-15: Thermal circuit showing the thermally grounded ends of an inline *pn* TE module

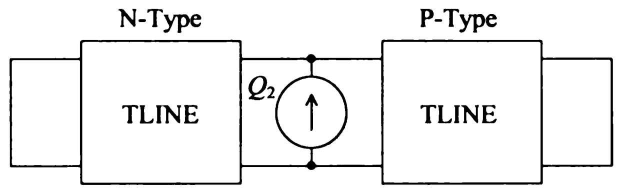

$$Q_2 = \alpha_{np} \cdot I \cdot T_{avg}$$

Figure 8-16: Thermal circuit showing the simplified schematic of Figure 8-15

For another inline module example that closer resembles a reference sample, an n-type and p-type pellet was removed from a commercially available module and bonded together with a solder in the inline configuration shown in Figure 8-17. The overall length of the module is about 3mm. Due to the lack of space (pellet dimensions are 1mm x 1mm x 1.4mm), the voltage probes are at the ends of the sample and will include contact resistance. The data, shown in Figure 8-18 shows a sharp change in impedance at low frequencies and a smooth change in impedance at the higher frequencies (again, which is unlike the RC circuit equivalent). However, the Thermal TLINE model agrees well with this behavior and the percent error between the data and the two models is shown in Figure 8-19 indicating the Thermal TLINE model is a better fit. The data also shows that the frequencies where the magnitude of the resistance transitions from low to high values is at a higher frequency than the full commercially available module. This is expected because there has been a reduction in heat capacitance at the ends of the module by not included the nickel traces or the ceramic end plates. The ZT for this inline module was found to be 0.74. This value is most likely lower than the full module because of contact resistance.

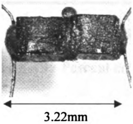

Figure 8-17: *PN* inline module consisting of Bi_2Te_3 from commercially available module and bonded together using woods metal

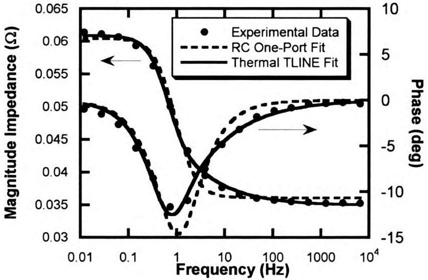

Figure 8-18: Plot of a *pn* inline module consisting of Bi_2Te_3 from commercially available module showing magnitude and phase of the impedance versus frequency

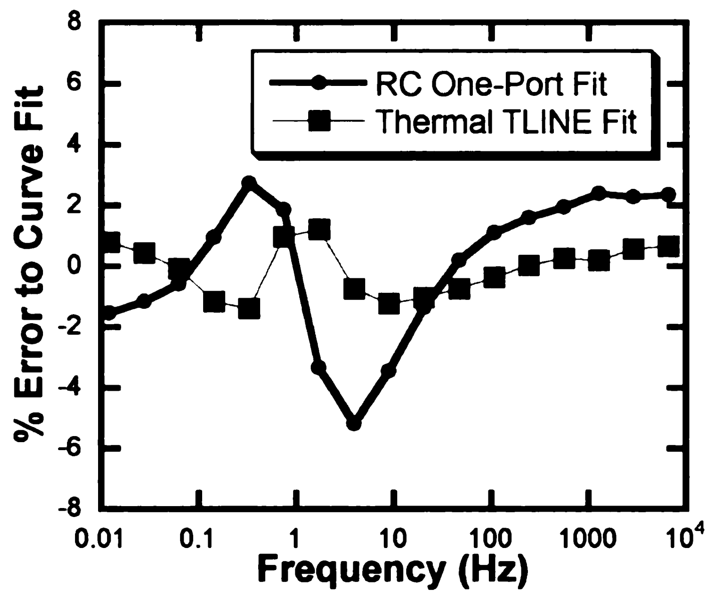

Figure 8-19: Percent error

8.4.4 Thermal TLINE model for single pellet measurements

Impedance spectroscopy measurements have been made on single samples of thermoelectric material created by MSU. An example is shown here using a singe *p*-type pellet created by MSU with a chemical composition of $Na_{0.8}Pb_{20}Sb_{0.6}Te_{22}$ shown in Figure 8-20. Here the voltage probes are within the ends of the sample so contact resistance is not included in the measurement. The magnitude and phase of the impedance for this sample is shown in Figure 8-20 along with the RC One-Port fit and the Thermal TLINE fit.

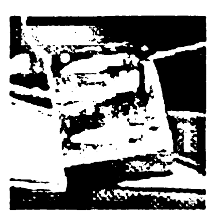

Figure 8-20: Single TE pellet of p-type material ($Na_{0.8}Pb_{20}Sb_{0.6}Te_{22}$)

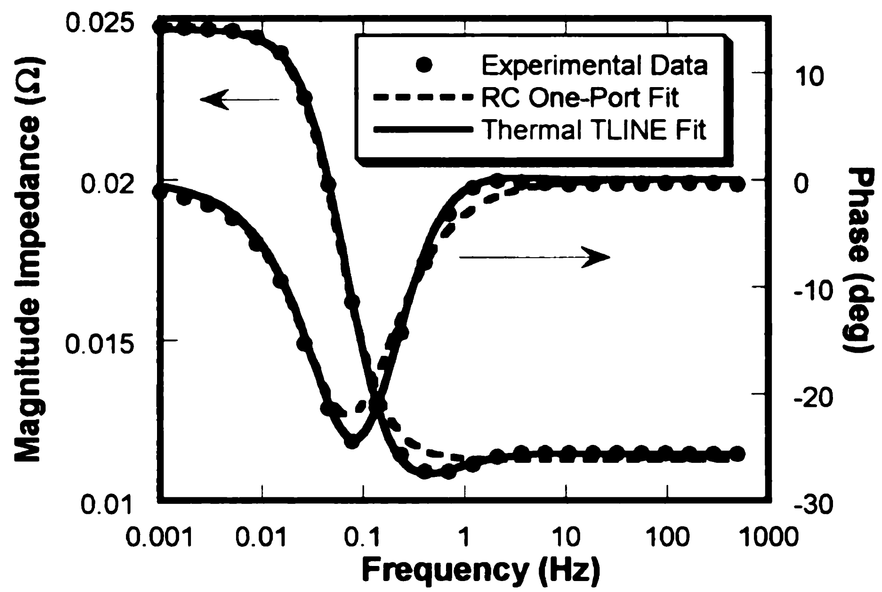

Figure 8-21: Plot of single TE pellet showing magnitude and phase of the impedance measurements of a p-type sample (Na0.8Pb20Sb0.6Te22)

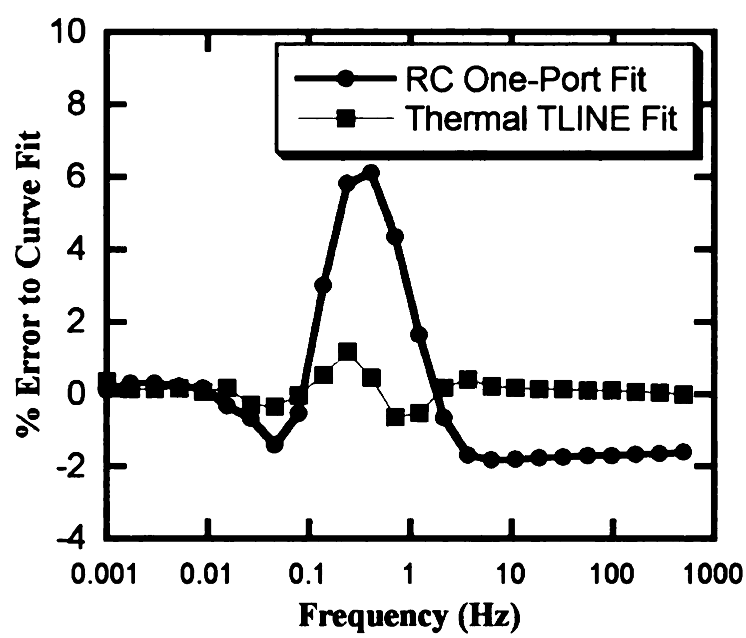

Figure 8-22: Percent error

The data for a single pellet shows a dip where the zero critical frequency would be. This dip in the data is also predicted by the Thermal TLINE model and is due to probe position and the thermal wave developing along the length of the sample. When the probes are at the ends of the sample, the thermal wave at the ends of the sample are always 90 degrees out of phase. But, when the probes are within the ends of the sample, this is not the case. Figure 8-23 shows a possible temperature profile along the length of the sample using a frequency that is close to the pole of the impedance function. Figure 8-24 shows a possible temperature profile along the length of the sample at the frequency where there is a dip in the magnitude resistance data.

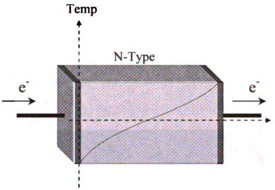

Figure 8-23: Possible temperature profile at once instance in time along n-type sample using a low frequency (close to the pole) voltage source across sample

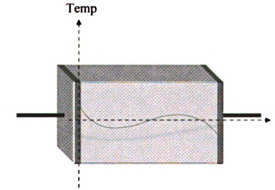

Figure 8-24: Possible temperature profile at one instance in time along n-type sample using a frequency where the dip in the data is created

A LabVIEW program was develop using the Thermal TLINE model to indicate the temperature profile along the length of the sample at a given frequency. Figure 8-25 and Figure 8-26 show the temperature profile along the length of the sample at the frequency where there is a dip in the impedance versus frequency data for two instances in time.

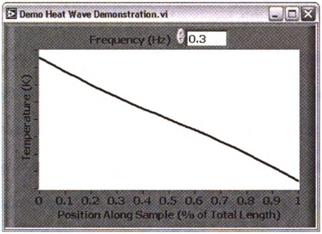

Figure 8-25: LabVIEW program using Thermal TLINE model to indicate temperature profile along the length of the sample at an instance in time where the ends of the sample are at the maximum difference. The frequency of oscillation is at a value where there is a dip in the magnitude versus frequency data

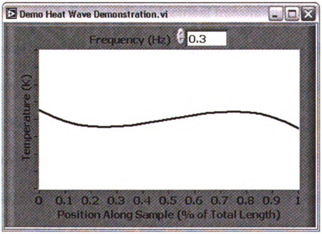

Figure 8-26: LabVIEW program using Thermal TLINE model to indicate temperature profile along the length of the sample at an instance in time when there is a thermal wave. The frequency is at the value where there is a dip in the magnitude versus frequency data.

8.5 Development and Curve Fitting to the Thermal Transmission Line Model

The development of the Thermal TLINE Model involved incorporating many options in the program after impedance spectroscopy data is collected on a TE sample. First, it must include the sample dimensions and optionally the probe positions. Next, the analysis must work with the different types of TE samples such as a full TE module, an inline module, or a single TE pellet. It must also accept different setup configurations such as dangling the sample, thermally grounding one side of the sample, and including the thermal properties of other possible materials in the module such as nickel traces and ceramic end caps. Next, the program needs to be able to curve fit the data to find the appropriate probe positioning. The probe positioning will account for the dip in the data in single pellet measurements. The program must then be able to finally curve fit the data (which involves adjusting the capacitance of the TE material) to find the lowest mean-square-error (MSE). Once that data is curve fitted, output files are created for documentation purposes.

The development of the Thermal TLINE Model first involved creating a program that would simulate the AC behavior of an electrical transmission line in the frequency domain. Once this was established, the model was used to simulate thermal behavior in the frequency domain. Next, to establish a starting point for quickly estimating the electrical resistance, thermal resistance, and thermal capacitance of the thermoelectric samples, the RC One-Port Model is incorporated into the program. Finally, two curve fitting routines are developed to adjust the voltage probe positions and find the correct capacitance value to establish the lowest MSE between the model and the experimental data.

8.5.1 Development of AC model for Electrical Transmission Lines

The first step in the development of the Thermal TLINE model was to simulate the transmission line model for electrical transmission lines. A schematic of using a transmission line in a circuit is shown in Figure 8-27 where an alternating voltage source (V_S) that has a source resistance (R_S) is attached to a transmission line that has a load impedance (R_L).

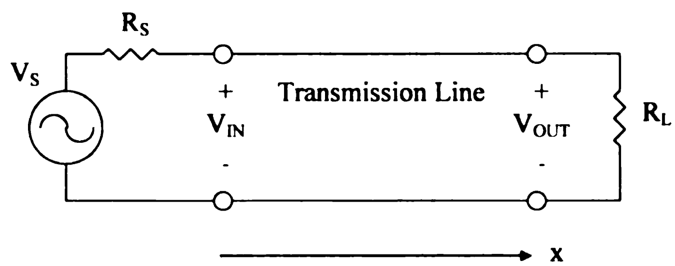

Figure 8-27: Electrical circuit schematic using a transmission line

The equations for the transmission line used in Figure 8-27 are the Telegrapher's equations, which are again shown here.

$$\begin{aligned} V_{in}(x) &= V_L \cdot \cosh(\gamma \cdot x) + I_L \cdot Z_0 \cdot \sinh(\gamma \cdot x) \\ I_{in}(x) &= \frac{V_L}{Z_0} \cdot \sinh(\gamma \cdot x) + I_L \cdot \cosh(\gamma \cdot x) \end{aligned} \tag{8.106}$$

The user starts by knowing the values of the transmission line (*R*, *G*, *C*, and *L*) in units per length along with the total length of the line. The user also inputs either a current or voltage source along with a source resistance. Finally, the user inputs the load impedance and the test frequency. For instance, to test an RG-58 cable, the user can input an AC source voltage of magnitude 1 volt, a source resistance of 50 Ω and a load impedance of 50 Ω. The line parameters for an RG-58 cable 1 meter long are as follows: R = 19.4mΩ, C = 98.4252pF, $G = 0\ \Omega^{-1}$, and L = 246.063nH. A test frequency of

300MHz is chosen. The program first calculates the propagation constant (γ) and the characteristic impedance (Z_0). The impedance into the transmission line can be found as follows where l is the total length of the transmission line.

$$Z_{in} = Z_0 \frac{Z_L + Z_0 \cdot \tanh(\gamma \cdot l)}{Z_0 + Z_L \cdot \tanh(\gamma \cdot l)} \tag{8.107}$$

The open circuit impedance (Z_{io}), where $Z_L \to \infty$, is found using the following.

$$Z_{io} = \frac{Z_0}{\tanh(\gamma \cdot l)} \tag{8.108}$$

The short circuit impedance (Z_{is}), where $Z_L \to 0$, is found using the following.

$$Z_{is} = Z_0 \cdot \tanh(\gamma \cdot l) \tag{8.109}$$

The program divides the transmission line up into 100 pieces. By doing so, the program can calculate the voltage and current into each piece using Telegrapher's equations. This can be used to map out the magnitude of the voltage and the phase of the voltage along the length of the transmission line.

This program also calculates the expected resistance, capacitance, conductance, and inductance values of the transmission line when terminated with a short-circuit and an open-circuit. Using a short circuit test, the resistance and inductance can be found using the following two equations respectively where ω is the frequency radians.

$$R = \mathrm{Re}[Z_{is}] \tag{8.110}$$

$$L = \frac{\mathrm{Im}[Z_{is}]}{\omega} \tag{8.111}$$

Using an open-circuit test, the conductance and capacitance can be found as follows.

$$G = \mathrm{Re}\left[\frac{1}{Z_{io}}\right] \tag{8.112}$$

$$C = \frac{\mathrm{Im}\left[\frac{1}{Z_{io}}\right]}{\omega} \tag{8.113}$$

Figure 8-28 shows the front panel view of the LabVIEW program that models the AC characteristics of a transmission line. The program plots out three graphs. The first graph is the magnitude of the voltage along the length of the transmission line. The second graph plots out the phase of the voltage along the transmission line. The third graph plots out the real voltage across the transmission line at the moment in time when the voltage source (or current source) is at the magnitude and phase that the user set.

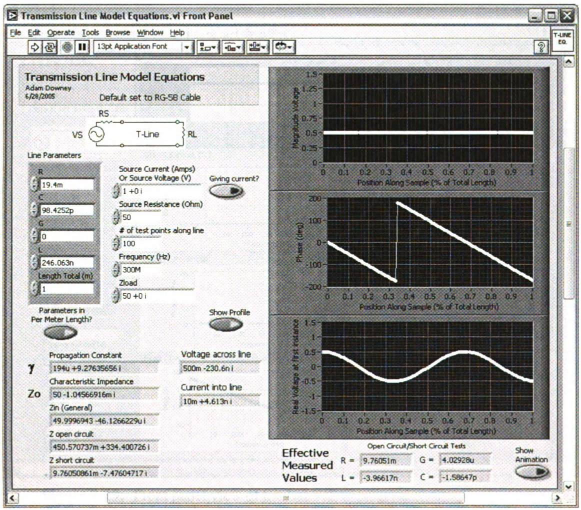

Figure 8-28: Font panel view of the LabVIEW program modeling transmission lines

Another program was created to test the transmission line program by performing a frequency sweep and observing the magnitude of the impedance of the transmission line with a given load versus frequency, the characteristic impedance versus frequency, and the propagation constant versus frequency. Again, a model of an RG-58 cable was used for this test. The main test here was to verify that the impedance of the RG-58 cable would remain 50 Ω over the frequency sweep which it does and can be seen in Figure 8-29.

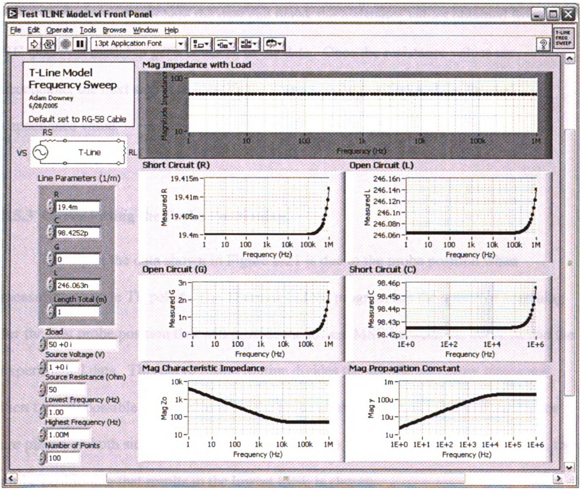

Figure 8-29: Front panel view of the LabVIEW program to test the frequency dependence for the transmission line program. This figure displays an example of testing an RG-58 cable.

8.5.2 Incorporation of RC One-Port Program

The impedance spectroscopy data always should provide a constant resistance for frequencies below the pole and above the zero. The difference between the multiple module configurations is the transition from low to high frequencies between the critical frequencies. The RC One-Port model can estimate the resistance values that will give the constant resistance values at the appropriate locations. For this reason, the RC One-Port model is incorporated into the Thermal TLINE model. This provides a good starting point for the user. From here the user can tweak the resistance values obtained from the RC One-Port model to get a better fit to the data. Once the resistance values are acceptable, the next step is to identify the correct probe position and the thermal capacitance value.

8.5.3 Curve Fitting the Probe Positioning

The dip in the data shown in Figure 8-21 is due to the probe position when measuring a single TE pellet. The Thermal TLINE program has the option of searching for the best probe position that will provide the lowest MSE between the curve fit and the experimental data. This curve fitting routine divides the sample into many pieces and then tries all possible combinations for the probe positioning (assuming that the probes are placed on both sides of the middle of the sample). After all combinations are test, the probe positioning that results in the lowest MSE is chosen.

With the probe position specified as shown in Figure 8-30 where L_t is the total length of the sample and L_1 and L_2 represent the distance from the left and right side of the sample, respectively. The positions are then converted to the percentage of the overall length of the sample.

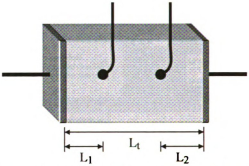

Figure 8-30: Diagram of probe positioning

The transmission line model must include the entire sample, not just the sample between the measurement probes. The values for the electrical resistance, thermal resistance, and thermal capacitance must be known for the entire sample that is measured. This is calculated by knowing the percentage of the total sample that is being measured and using this to increase the component values as follows.

$$\text{Total Value} = \frac{\text{Value Measured}}{\text{\% of Sample Tested}} \tag{8.114}$$

Using the total values for the electrical resistance, thermal resistance, and thermal capacitance, the Thermal TLINE model is applied as if the probes where at the ends of the sample. This model divides the sample into 100 pieces and calculates the complex temperature at each location. By superposition, the difference between the two probe locations can be found using the complex temperatures at the appropriate locations. An example of the program is shown in Figure 8-31. This figure shows what the data would be if the probes were at the ends of the sample or at the user specified locations.

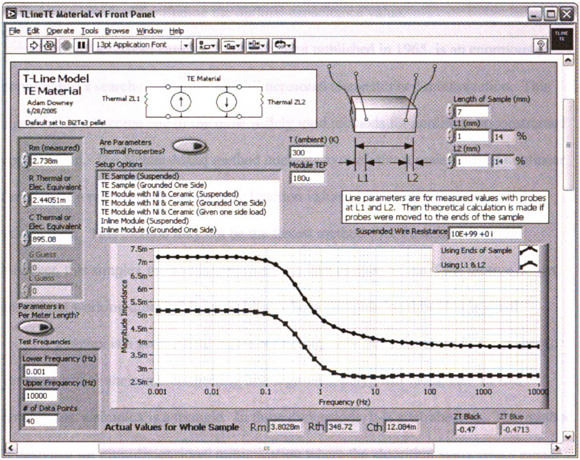

Figure 8-31: Front panel view of the LabVIEW program "TLineTE Material.vi" showing the results of probe positioning

8.5.4 Curve Fitting for Heat Capacitance

After the probe space is determined and the values for R_l and R_m are identified, the next step is to find the capacitance that will best fit the experimental data. The goal is to curve fit to a function where the capacitance has a non-linear effect on the mean-square-error (MSE) between the curve fit and the experimental data. A technique based on the

Nelder-Mead simplex algorithm [54] was used to provide a fairly fast and easily programmed method for finding the optimal capacitance value.

The Nelder-Mead simplex algorithm, first published in 1965, is an enormously popular direct search method for multidimensional unconstrained minimization. This algorithm has become one of the most widely used methods for nonlinear unconstrained optimization. The Nelder-Mead method attempts to minimize a scalar-valued nonlinear function of n real variables using only function values, without any derivative information. This method may not be the fastest method (See Powell's method), however, this simplex method is frequently the best method to use if the motive is "get something working quickly" for a problem whose computational burden is small.

A simplex is a geometrical figure consisting, in N dimensions, of N + 1 points (or vertices) and all their interconnecting line segments, polygonal faces, etc. In two dimensions, a simplex is a triangle. In three dimensions, it is a tetrahedron. This method is designed for multidimensional minimization where the algorithm starts with a guess, that is, an N-vector of independent variables as the first point to try. The algorithm is then supposed to make is own way downhill through the complexity of an N-dimensional topography until it encounters a (local, at least) minimum. The goal is to continuously change the size of the volume of the simplex and diminish it until it is small enough to contain the minimum value of the function within the desired accuracy. The operations of the changing simplex involve contraction, expansion, and reflection to determine new simplex corner points by linear combinations of selected existing corner points. More details can be found in reference [54].

In this case of finding the optimal capacitance that gives the lowest MSE to a specified accuracy, the problem is only 1-dimensional. The simplex algorithm has been modified to take into account that the MSE and the capacitance values are never negative. An example of finding the capacitance value that will give the minimum MSE is depicted in Figure 8-32 where the MSE is simply some function of capacitance, C.

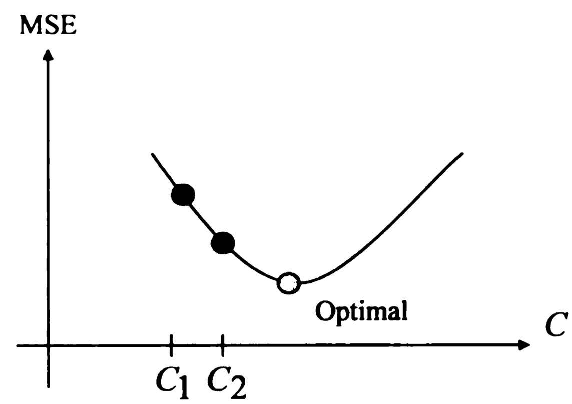

Figure 8-32: Example MSE function versus capacitance values

The algorithm begins by making two guesses for the capacitance value. The first guess comes from the capacitance value found by using the RC One-Port model which will be called C_1. This capacitance value is then used in the Thermal TLINE Model and the MSE is calculated, called M_1. The second guess for the capacitance value is C_2, where $C_2 = C_1 \cdot 1.1$. C_1 is applied to the Thermal TLINE Model where the MSE, M_2, is found. The idea of the algorithm is to quickly surround the optimal capacitance value by the two guesses and then decreases the 'distance' between the two guesses to narrow in on the optimal value.

Because the MSE never becomes negative, the direction of increasing or decreasing the capacitance value must be kept track of, which uses the variable X. Also, the improvement or degradation of the MSE is kept track up using the variable, T, where a value of 1 indicates improvement while 0 indicates degradation. For increasing or decreasing the next capacitance value by a specific factor, the variable Y is used. This algorithm is an iterative process, which begins with the initial two guesses. The two guesses are compared along with the corresponded MSE values. For the next two guesses, $C1_{next}$ will be the previous best guest, and $C2_{next}$ will be the calculated next guess to try. A truth table, found in Table 8-2, provides the logic for determining the variables T_{next}, X, Y, and Z based on the criteria: T, $C_1>C_2$, and $M_1>M_2$.

Table 8-2: Truth table for curve fitting routine

T	$C_1>C_2$	$M_1>M_2$	Next T	X	Y	Z
0	0	0	0	1	-1.2	C1
0	0	1	1	-1	-1.2	C2
0	1	0	0	-1	-1.2	C1
0	1	1	1	1	-1.2	C2
1	0	0	0	1	-0.2	C1
1	0	1	1	-1	-0.2	C2
1	1	0	0	-1	-0.2	C1
1	1	1	1	1	-0.2	C2

From Table 8-2, the value for the next C_1 guess is the best guess from the previous tries.

$$C1_{next} = Z \tag{8.115}$$

The value for the next C_2 is found using the formula shown here.

$$\begin{Bmatrix} C2_{next} = X \cdot Y \cdot (|C_1 - C_2|) + Z & \textit{for} \quad C2_{next} > 0 \\ C2_{next} = 0.4 \cdot Z & \textit{otherwise} \end{Bmatrix} \tag{8.116}$$

The truth table also provides formulas for T_{next}, X, and Y which are shown here.

$$T_{next} = \begin{cases} 0 & for \quad M_1 < M_2 \\ 1 & for \quad M_1 > M_2 \end{cases} \tag{8.117}$$

$$X = \begin{cases} 1 & for \quad (C_1 > C_2) \oplus (M_1 > M_2) = false \\ -1 & for \quad (C_1 > C_2) \oplus (M_1 > M_2) = true \end{cases} \tag{8.118}$$

$$Y = \begin{cases} -1.2 & for \quad T = false \\ -0.2 & for \quad T = true \end{cases} \tag{8.119}$$

From here, the algorithm can then be programmed into LabVIEW where it can interact with the existing models also programmed in LabVIEW. The iteration terminates when the difference in the mean-square-errors between the first and second guess is less than 1E-5. This algorithm is not optimized for speed or efficiency but does provide a curve fitting routine that is relatively fast and achieves the desired accuracy for the purposes of the Thermal TLINE model.

8.5.5 Final Program

The front panel view of the LabVIEW program for the Thermal TLINE fitting is shown in Figure 8-33.

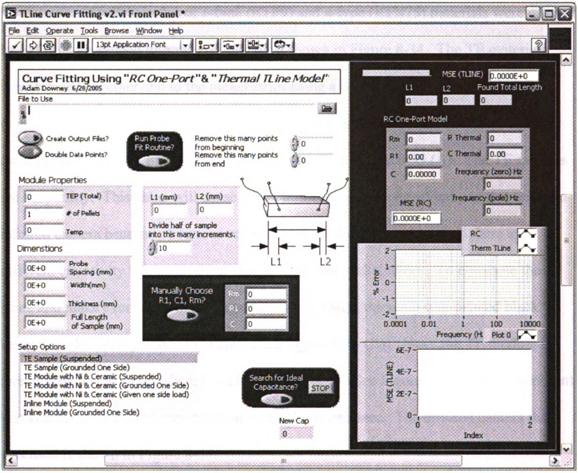

Figure 8-33: Front panel view for the TLINE curve fitting LabVIEW program

8.6 Thermal Imaging

It is well known that applying electricity through a thermoelectric material will cause a temperature gradient to develop. A good way to show this phenomenon is by applying electricity to a TE material and observing the temperature profile with the use of an infrared camera [55]. The use of an infrared camera will also help to verify the dynamic behavior of switching the polarity of the electrical current through the sample over time.

Long, 15mm, samples of *p*-type (ETP9) and *n*-type (ETN75) materials were made by MSU and arranged into the configuration shown in Figure 8-34. The TE materials were bonded together and to the nickel strips using a commercially available, low temperature, "woods metal" solder. The TE module was then placed on a alumina plate for support. A picture of the actual device is shown in Figure 8-35 (A). The TE samples are very shiny. This shine will cause errors in the measurements of temperature with the infrared camera because of various reflections from the surroundings and there are different emissivity values for the n-type, p-type, and nickel traces. To eliminate the shine and make everything at the same emissivity value, the setup was painted black using non-electrically conductive paint (See Figure 8-35 (B)). Next, the TE module is then placed inside a box where it is also painted black (See Figure 8-36). The experiment was conducted at room temperature at atmospheric pressure. The infrared camera that was used is shown in Figure 8-37.

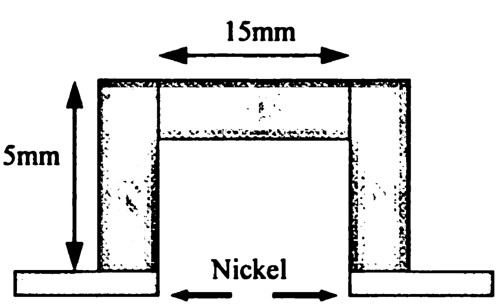

Figure 8-34: TE module setup for thermal imaging

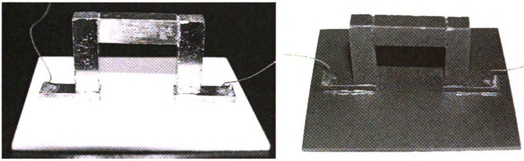

(A) (B)

Figure 8-35: (A) Picture of TE module. (B) Same device painted black

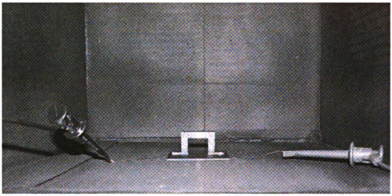

Figure 8-36: TE module place in box painted black

Figure 8-37: Infrared camera

The electricity applied to the TE module was a square wave pulse with a frequency of 0.1Hz. A picture was taken at each second for a duration of 10 seconds and is shown in Figure 8-38. Each picture has a graph of the temperature profile along a line placed on the p-type sample These thermal images provide good evidence of a thermal wave developing in the TE material as predicted by the thermal transmission line model. It is also important to note that there appears to be electrical current crowding happening at the corners of the *pn* interfaces because of the arrangement of the TE pellets. The effects or pros and cons of current crowding are only noted and not discussed in this thesis.

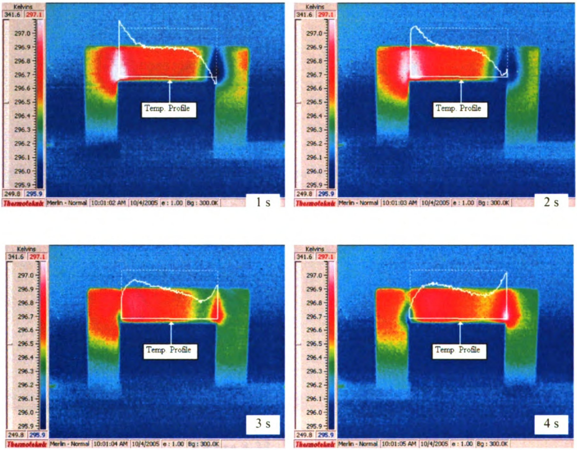

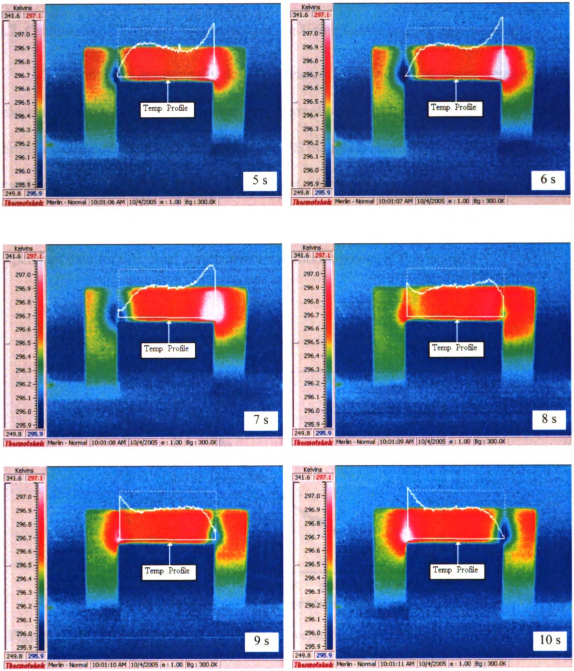

Figure 8-38: Thermal images

8.7 Comparing ZT Direct Measurements to Using Individual Measurements

ZT calculations are typically done by measuring the individual components of ZT (electrical conductivity, thermopower, and thermal conductivity). Measuring ZT directly through the impedance measurements of the TE materials have been compared to the standard method and show excellent agreement. An example is shown using a LAST sample ($Ag_{0.43}Pb_{18}Sb_{1.2}Te_{20}$). Figure 8-39 and Figure 8-40 show the temperature dependant data for electrical conductivity and thermopower of this sample.

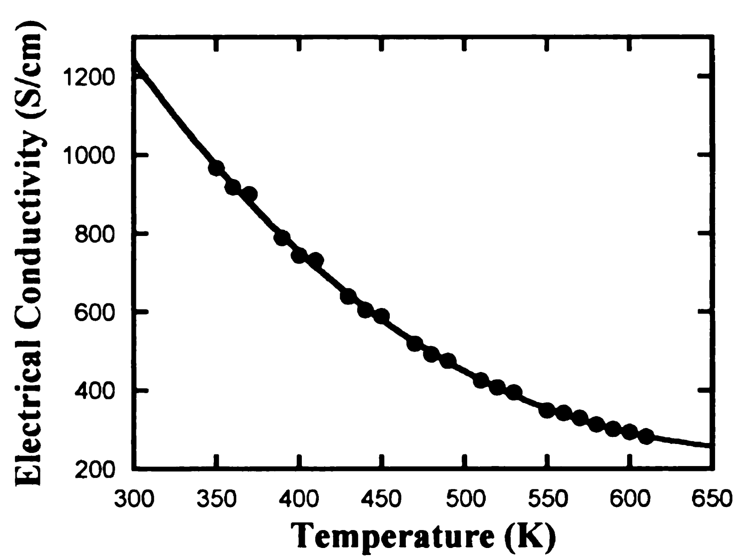

Figure 8-39: Plot of electrical conductivity versus temperature for $Ag_{0.43}Pb_{18}Sb_{1.2}Te_{20}$

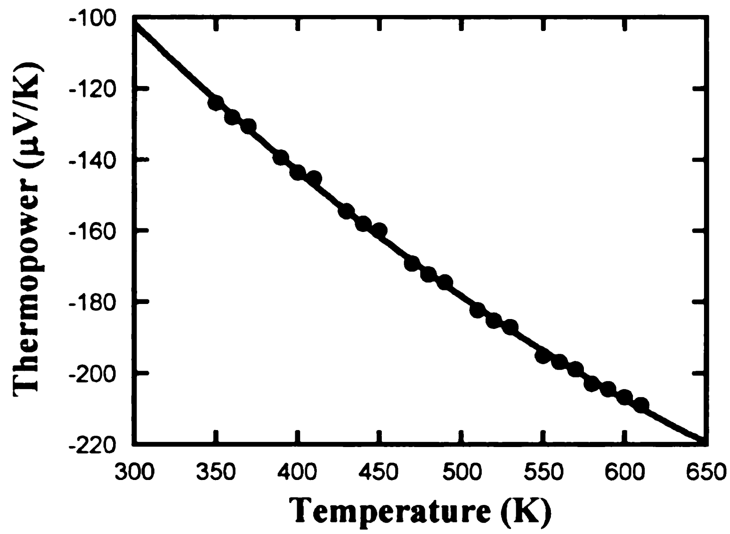

Figure 8-40: Plot of thermopower versus temperature for $Ag_{0.43}Pb_{18}Sb_{1.2}Te_{20}$

The electrical conductivity and thermopower at 300K is 1240 S/cm and -102.2 μV/K. The thermal conductivity of the sample was measured by calculating the power supplied to the heater and dividing it by the temperature gradient across the sample (taking sample dimensions and temperature probe spacing into account). This assumes that all of heat generated by the heater flows through the material and radiation loss is neglected. Using this method at 300K, the thermal conductivity of this sample was found to be approximately 2.12 W/m·K. The resulting ZT at 300 K is then 0.18.

By performing a impedance measurements of the same sample, the ZT is found directly with a value of 0.19 (see Figure 8-41). This shows excellent agreement between the two different methods of obtaining ZT.

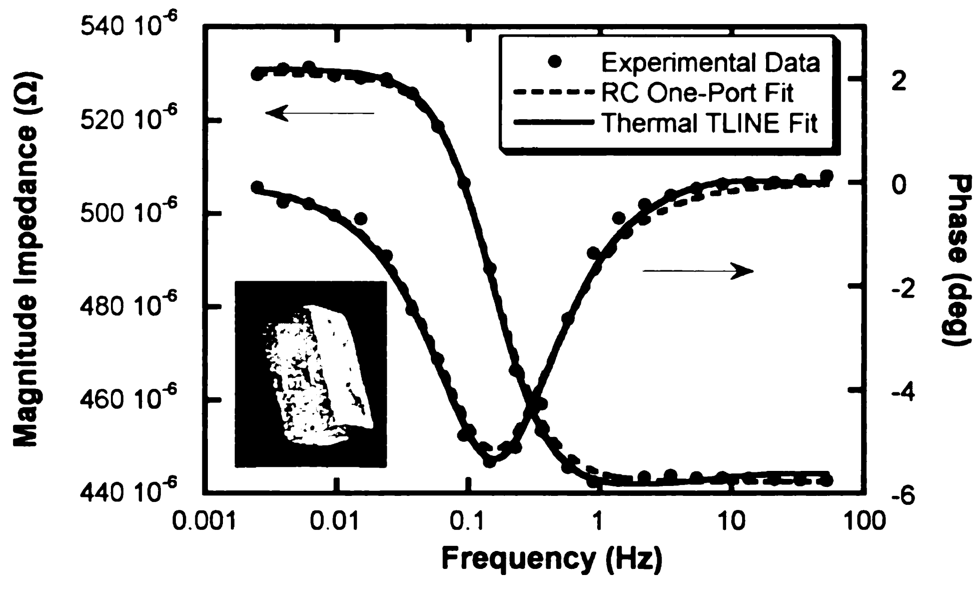

Figure 8-41: Plot of magnitude and phase of the impedance versus frequency for $Ag_{0.43}Pb_{18}Sb_{1.2}Te_{20}$.

Another example is shown using $Ag_{0.29}Pb_{18.61}Sb_{0.28}Te_{19}$. The plot for the temperature dependant electrical conductivity and thermopower data for this sample is shown in Figure 8-42.

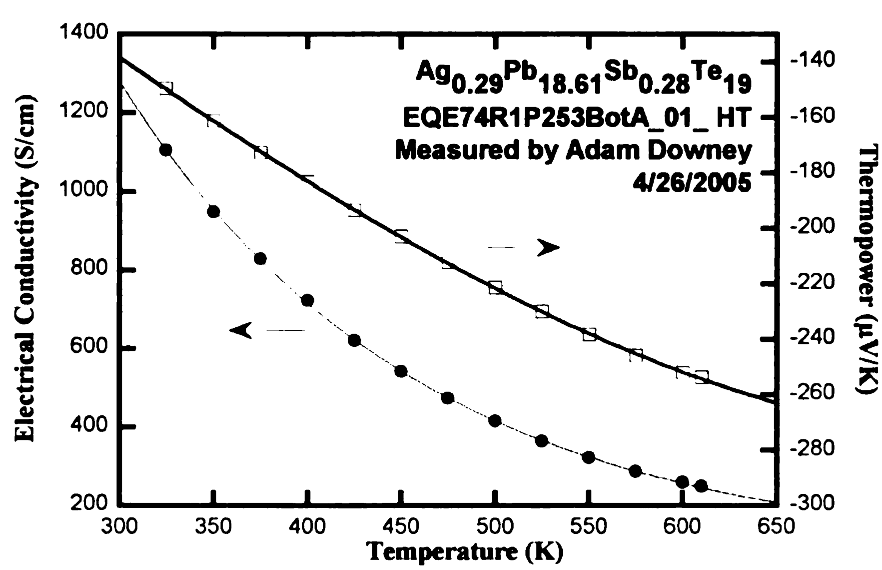

Figure 8-42: Plot of electrical conductivity and thermopower for LAST sample $Ag_{0.29}Pb_{18.61}Sb_{0.28}Te_{19}$

Assuming the lattice contribution to the thermal conductivity at room temperature is 1.3 W/m·K, and by identifying the room temperature value for electrical conductivity to be 1295 S/cm, then the electronic contribution to the thermal conductivity is 0.886 W/m·K, making the total thermal conductivity about 2.19 W/m·K. The thermopower at this temperature is -137 μV/K making the ZT at 300K to be 0.333. A plot of the impedance versus frequency is shown Figure 8-43, which indicates a ZT of 0.33 for this sample. Again, this shows excellent agreement between the two methods of obtaining ZT.

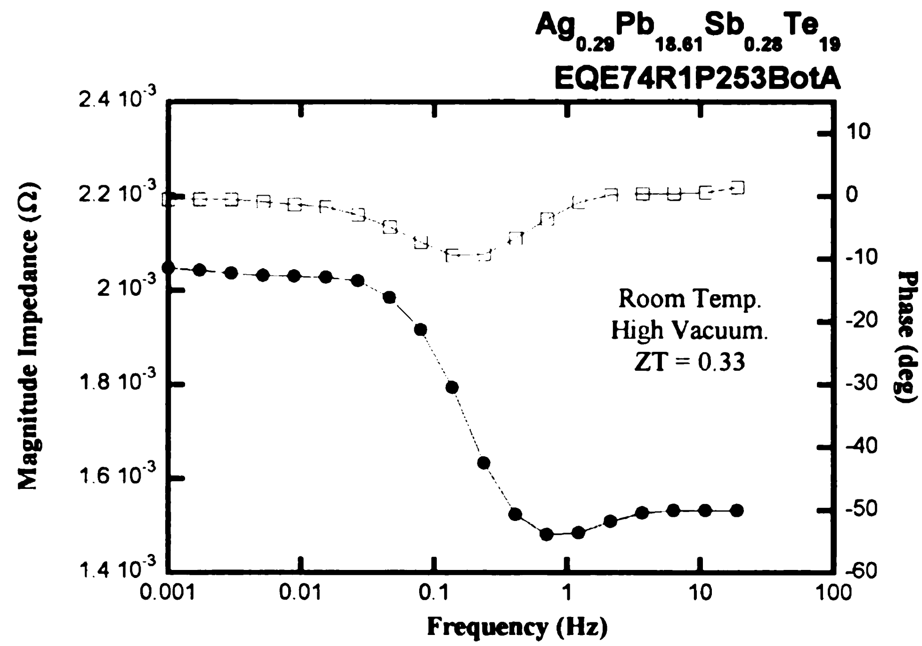

Figure 8-43: Plot of magnitude and phase of the impedance versus frequency for $Ag_{0.29}Pb_{18.61}Sb_{0.28}Te_{19}$

Chapter 9: ZT Measurements at High Temperatures

9.1 Introduction

It is very desirable to be able to measure ZT on thermoelectric materials directly up to high temperatures (800K). For temperature dependent measurements up to these high temperatures, starting at room temperature, the UHT System was used with very little modifications. Only four platinum measurement wires are needed for this measurement along with using the Lock-in amplifiers instead of the Keithley nanovolt meters.

This section will discuss the effects of radiation losses for this particular measurement. It will also evaluate the thermal losses due to the thermal conduction of the measurement wires. Example measurements of TE Materials from MSU will be shown.

9.2 Evaluation of Radiation Losses

Radiation losses are a major factor in the calculation of thermal properties of materials at high temperatures. Radiation happens when there is a temperature difference between the sample and the environment. Optical phonons within the sample can emit photons which carry energy away from the sample. More states within the optical phonon band are occupied at higher temperatures, and radiation increases. It is important to investigate how large a factor radiation plays into the calculation of ZT. One measurement in the calculation of ZT is using the high frequency AC signal applied to the sample to get the electrical conductance of the sample without any Peltier effects. This should not create a temperature gradient across the sample; rather the sample should remain at the same temperature as the surrounding environment. If the sample should rise in temperature due to Joule heating, the entire sample should rise in temperature evenly. This would cause heat to radiate from the sample but would not affect the measurement of electrical resistance. The other measurement for calculating ZT is to use a very low frequency signal, which can be approximated as a DC signal, that would cause a linear temperature gradient profile along the length of the sample. The hot side of the sample will be slightly higher in temperature than the environment causing heat to be radiated from the sample. The cold side of the sample will be colder than the environment allowing heat to be radiated into the sample. A diagram of this is shown in Figure 9-1.

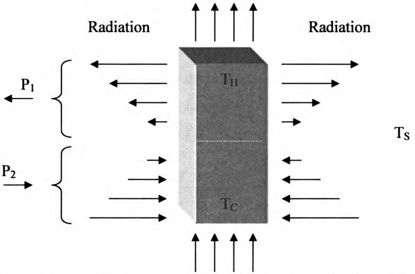

Figure 9-1: Diagram for the steady state analysis of radiation losses for applied DC current

This effect happens at all temperatures, however, radiation is related to temperature to the fourth power. The equation for the power of the heat radiated versus temperature is shown here.

$$P = e \cdot \sigma \cdot A \cdot \left(T^4 - T_S{}^4\right) \quad \text{(W)} \tag{9.120}$$

Where

A = Radiative area (m^2)
P = Power radiated (J/s)
e = emissivity (e = 1 for blackbody)
σ = Stefan - Boltzmann constant ($5.6703 \cdot 10^{-8}$ W/m^{2}K^4)
T = Temperature of radiator (K)
T_S = Temperature of surroundings (K)

To examine the situation shown in Figure 9-2, assume that the temperature gradient across the sample is 1 °C or less. The analysis here does not include Joule heating due to contact resistance and assumes the emissivity is not a function of temperature. Also, it is assumed that the temperature profile along the length of the sample is linear in position as shown in the following equation.

$$T_H = \text{max temp hot side}$$
$$T_C = \text{min temp cold side}$$
$$L = Length$$
$$\Delta T = T_H - T_C$$

$$T(x) = \frac{\Delta T}{L} \cdot x + \left(T_S - \frac{\Delta T}{2}\right) \quad \text{(K)} \tag{9.121}$$

This assumption will prove to be reasonable by the end of this section. Divide the sample into four regions as shown in Figure 9-2 where the sample has been separated into two halves along with also separating the ends of the sample from main body. Now the power being radiated from the sample in each of the four regions can be solved for.

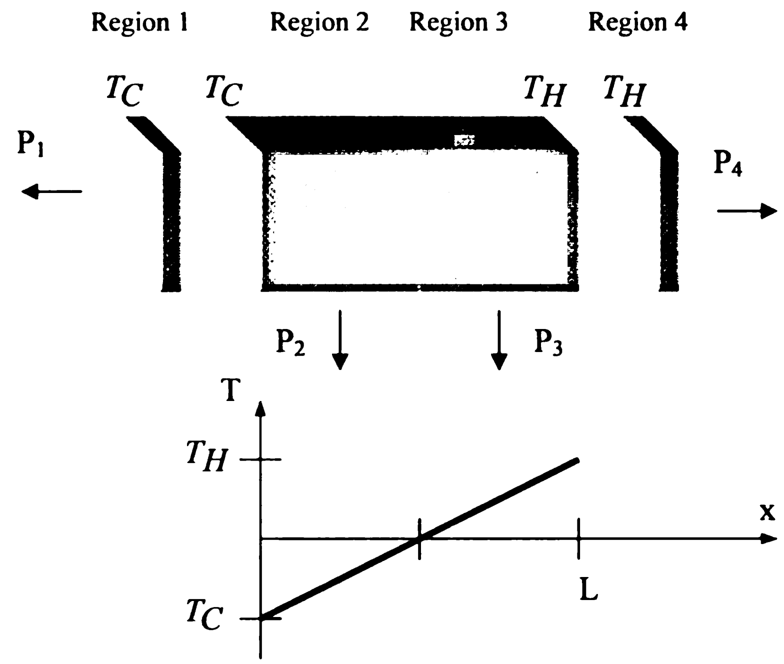

Figure 9-2: Sample divided into four regions. Linear temperature gradient along the length of the sample.

Neglecting the end caps (regions 1 and 4), the power being radiated along the length of the sample is shown here.

$$a = width$$

$$b = thickness$$

$$P_{rad_{2\&3}}(x) = e \cdot \sigma \cdot 2 \cdot (a+b) \cdot \left(T(x)^4 - T_s^{\,4} \right) \quad \text{(W)} \qquad (9.122)$$

Using the chosen temperature profile along the length of the sample, the equation for power radiated now becomes:

$$P_{rad_{2\&3}}(x) = e \cdot \sigma \cdot 2 \cdot (a+b) \cdot \left[\left(\frac{\Delta T}{L} \cdot x + \left(Ts - \frac{\Delta T}{2} \right) \right)^4 - T_s^{\,4} \right] \quad \text{(W)} \qquad (9.123)$$

Taking the derivative of the power radiated will indicate if the power radiated is linearly proportional to the position along the sample.

$$\frac{d}{dx}P_{rad_{2\&3}}(x) = \frac{d}{dx}\left[e\cdot\sigma\cdot 2\cdot(a+b)\cdot\left(\left(\frac{\Delta T}{L}\cdot x+\left(Ts-\frac{\Delta T}{2}\right)\right)^4 - T_S{}^4\right)\right]$$
$$= \frac{e\cdot\sigma\cdot 2\cdot(a+b)}{L^4}\cdot\left[\Delta T\cdot(2\cdot x-L)+2\cdot T_S\cdot L\right]^3\cdot\Delta T \qquad (9.124)$$

Typically for this measurement, the temperature gradient across the sample will be kept small (below 1°C) which will allow the following to be true:

$$\Delta T << 2\cdot T_S$$

When the above statement is true, the derivative of the power radiated now becomes:

$$\frac{d}{dx}P_{rad}(x) \approx \frac{(a+b)}{L}\cdot e\cdot\sigma\cdot 16\cdot T_S{}^3\cdot\Delta T \qquad (9.125)$$

The above equation shows that the derivative of the power radiated is not dependant upon the position. This indicates the power radiated is linearly proportional to position in regions 2 and 3. This is helpful in that the radiation loss will affect the entire length of the sample evenly without altering the linearity of the temperature profile.

Now the total power radiated from each region of the sample can be solved for. The total power at the end of the sample on the cold side, region 1, is as follows:

$$P_1 = e\cdot\sigma\cdot a\cdot b\cdot\left(T(x=0)^4 - T_S{}^4\right) \quad \text{(W)} \qquad (9.126)$$

The total power on the cold half of the sample not including the end of the sample, region 2, is as follows:

$$P_2 = \int_0^{L/2} e\cdot\sigma\cdot 2\cdot(a+b)\cdot\left(T(x)^4 - T_S{}^4\right)\cdot dx \quad \text{(W)} \qquad (9.127)$$

The total power on the hot half of the sample not including the end of the sample, region 3, is as follows:

$$P_3 = \int_{L/2}^{L} e \cdot \sigma \cdot 2 \cdot (a+b) \cdot \left(T(x)^4 - T_S{}^4 \right) \cdot dx \quad \text{(W)} \tag{9.128}$$

The total power at the end of the sample on the hot side, region 4, is as follows:

$$P_4 = e \cdot \sigma \cdot a \cdot b \cdot \left(T(x = L)^4 - T_S{}^4 \right) \quad \text{(W)} \tag{9.129}$$

For the measurement of ZT, the difference in power being radiated from the hot side compared to the cold side must be known. This will give an effective power radiated. This can be done as follows:

$$P_{rad_{eff}} = (P_3 + P_4) - (P_1 + P_2) \quad \text{(W)} \tag{9.130}$$

$$\begin{aligned} P_{rad_{eff}} = \frac{1}{4} \cdot e \cdot \sigma \cdot \Delta T \cdot T_S \cdot \\ \left(L \cdot \Delta T^2 \cdot (a+b) + 8 \cdot L \cdot T_S{}^2 \cdot (a+b) + a \cdot b \cdot \left(4 \cdot \Delta T^2 + 16 \cdot T_S{}^2 \right) \right) \end{aligned} \tag{9.131}$$

Again, the following assumption is made:

$$\Delta T^2 << T_S{}^2$$

When the above statement is true, the effective power radiated is:

$$P_{rad_{eff}} \approx 2 \cdot e \cdot \sigma \cdot \Delta T \cdot T_S{}^3 \cdot (L \cdot a + L \cdot b + 2 \cdot a \cdot b) \quad \text{(W)} \tag{9.132}$$

Using the temperature gradient and the effective power radiated from the sample, an effective radiation resistance can now be found to be:

$$R_{rad_{eff}} = \frac{\Delta T}{P_{rad_{eff}}} = \frac{\Delta T}{2 \cdot e \cdot \sigma \cdot \Delta T \cdot T_S{}^3 \cdot (L \cdot a + L \cdot b + 2 \cdot a \cdot b)} \tag{9.133}$$

$$R_{rad_{eff}} = \frac{1}{2 \cdot e \cdot \sigma \cdot T_S{}^3 \cdot (L \cdot a + L \cdot b + 2 \cdot a \cdot b)} \quad \text{(K/W)} \tag{9.134}$$

Therefore, for small ΔT, the effective radiation resistance is not dependant upon ΔT.

9.2.1 The Effect of Radiation on ZT Measurements

The simplest way to include this new radiation resistance is to go back to the RC One-Port Method and place this added resistance in parallel with the thermal resistance of the sample due to conduction. Instead of ΔT across the sample being

$$\Delta T = \alpha \cdot I \cdot T_{amb} \cdot R_{Thermal} \tag{9.135}$$

The new ΔT will be

$$\Delta T_{new} = \alpha \cdot I \cdot T_{amb} \cdot \frac{R_{Thermal} \cdot R_{Rad}}{R_{Thermal} + R_{Rad}} \tag{9.136}$$

The ZT measured, which includes radiation, can be calculated by

$$ZT_{Rad} = \frac{\alpha \cdot \Delta T_{new}}{R_0 \cdot I} \tag{9.137}$$

Let ZT_{ideal} be the ZT value without radiation losses. Then the percent error between the ZT with radiation losses compared to the ZT without radiation losses is as follows:

$$\text{Percent Error} = \frac{ZT_{ideal} - ZT_{rad}}{ZT_{ideal}} \cdot 100\% = \frac{\Delta T - \Delta T_{new}}{\Delta T} \cdot 100\%$$

$$= \frac{R_{thermal} - \dfrac{R_{thermal} \cdot R_{rad}}{Rtheraml + Rad}}{R_{thermal}} \cdot 100\%$$

$$\text{Percent Error} = \left(1 - \frac{R_{rad}}{R_{thermal} + R_{rad}}\right) \cdot 100\% \tag{9.138}$$

If $R_{Thermal} = R_{Rad}$, then the ZT measured will be exactly half of the correct value (50% error).

9.2.2 Example Calculation (MSU TE Materials)

Currently for the thermoelectrics project at MSU, TE pellet dimensions are: length = 7mm, width = 5mm, and thickness = 5mm. For high temperatures, assume that thermal conductivity of the sample is about 1 W/mK (this is reasonable based of many thermal conductivity measurements). It has been found experimentally that there is an improvement in the ZT measurement by making the sample smaller, which involves cutting the pellet in half to the dimensions shown below.

Table 9-1: Sample specifications

Sample Dimensions	
length (m)	0.005
width (m)	0.005
thickness (m)	0.003

Thermal Cond. (W/mK)	1
Thermal Resistance (K/W)	333.33

The emissivity of the samples are unknown so a value of 1 (worst case scenario) was used in this example. With this sample size, plots were created to estimate the amount of radiation loss and what the thermal resistance is due to radiation. An example of the temperature profile along the length of the sample at 300K is shown in Figure 9-3. Similar profiles will exist at higher temperatures.

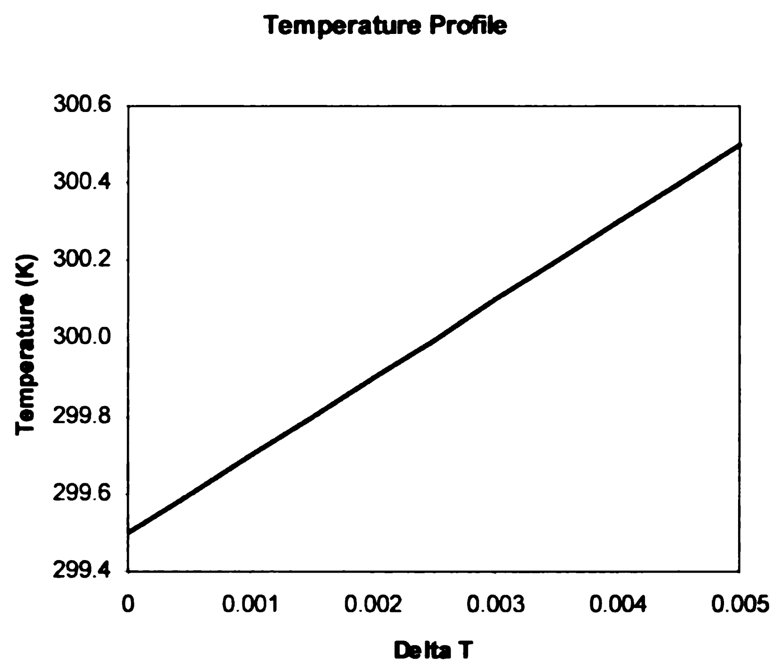

Figure 9-3: Temperature profile at 300K where $\Delta T = 1$

The effective radiated power versus a small range of ΔTs for various surrounding temperatures is plotted and shown in Figure 9-4. The effective radiation resistance versus DT for various surrounding temperatures is plotted and shown in Figure 9-5. Finally, the plot of effective radiation resistance versus surrounding temperature (for small ΔTs) is shown in Figure 9-6

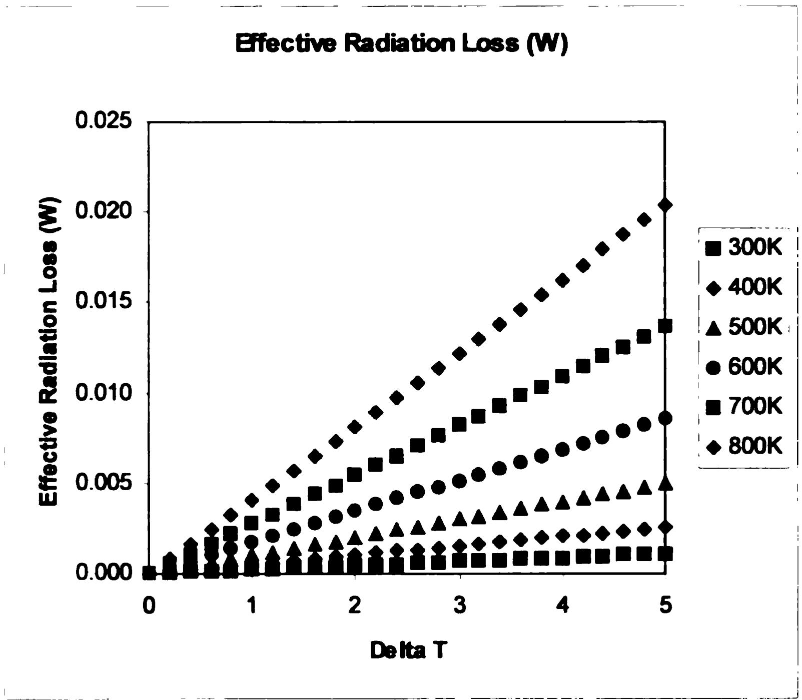

Figure 9-4: Effective radiated power versus ΔT for a specific example

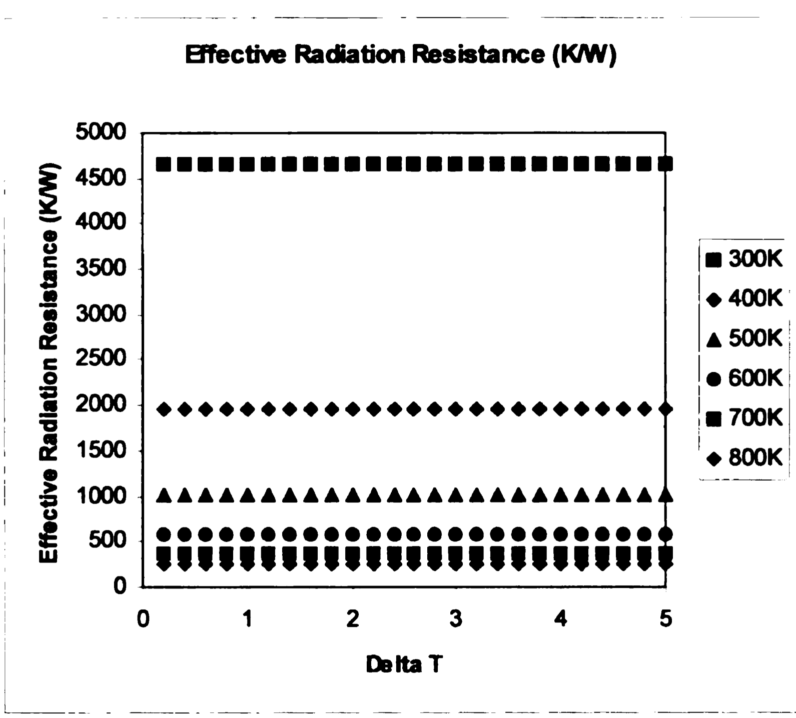

Figure 9-5: Thermal resistance due to radiation for specific example

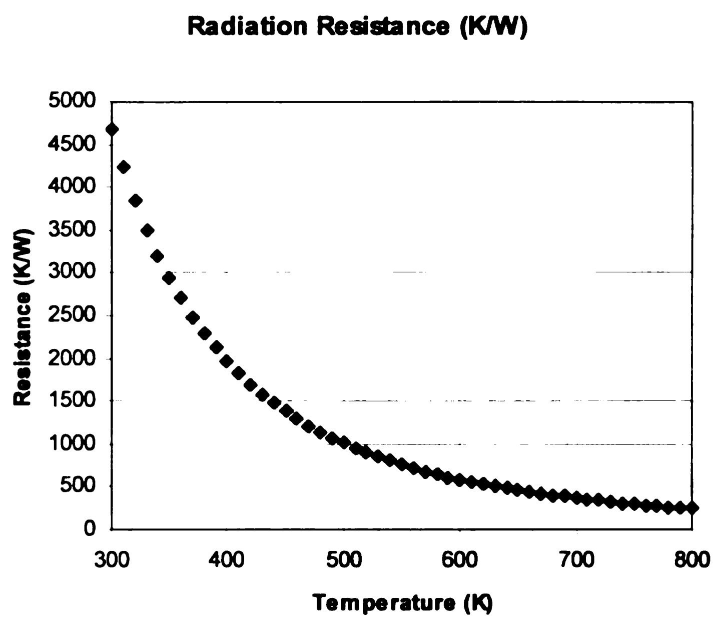

Figure 9-6: Radiation resistance versus temperature for specific example (ΔT is small)

Figure 9-5 and Figure 9-6 illustrates how the thermal resistance due to the radiation loss compares to the thermal resistance of the sample through conduction that was calculated in Table 9-1. For high temperatures, they do fall into the same magnitude range (above 500K, both values are below 1000 K/W). This will dramatically affect the ZT measurement.

If a comparison of measuring ZT at 700K between the ZT including radiation compared to the ZT without radiation is made, the percent error can be found to be as follows:

$$\text{Percent Error (at 700K)} = \left(1 - \frac{370}{333 + 370}\right) \cdot 100\% \approx 47\% \tag{9.139}$$

This indicates that for material properties chosen, there is potentially an enormous error because of radiation in the ZT measurement for this sample. Here the measured ZT value would be 47% less then values indicated in literature.

9.2.3 Example Calculation (Small Constantan Sample)

ZT has been measured of constantan wire. Will radiation effect this measurement if the sample size is small? In the range of 300K to 800K, the thermal conductivity of Constantan ranges from 20 to 40 W/mK. For this example, chose an average value of 30 W/mK to be constant over the temperature range. The emissivity of a constantan metal strip is e = 0.09 [56]. This example will use a small cube of constantan with the following dimensions: length = 6mm, width = 0.5mm, and thickness = 0.5mm. With these dimensions, the thermal resistance due to conduction is 800 K/W. The same linear temperature profile that was used in the previous example will be used here. The effective radiation resistance is plotted versus surrounding temperatures and is shown in Figure 9-7. This plot shows that even at 800K, the thermal resistance due to conduction is much smaller than the effective radiation resistance of the sample.

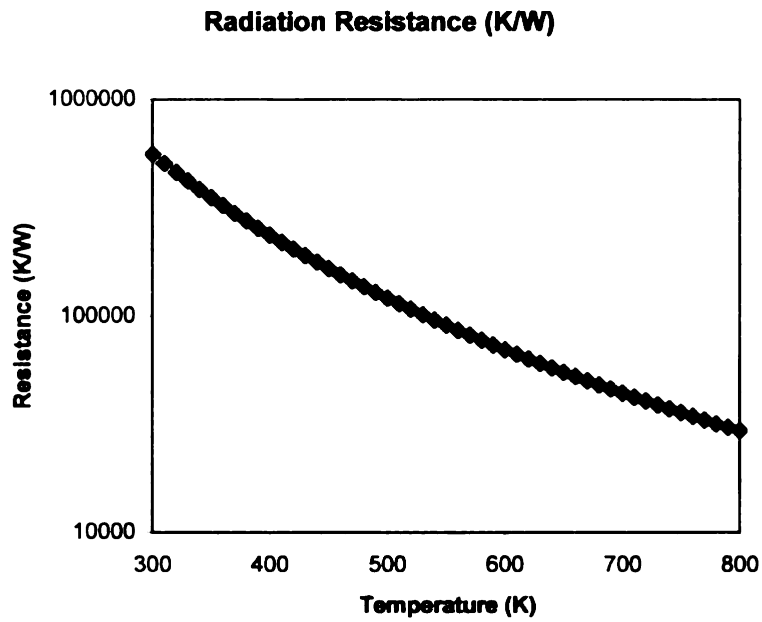

Figure 9-7: Effective radiation resistance versus temperature where $\Delta T = 1$

If a comparison of measuring ZT at 700K between the ZT including radiation compared to the ZT without radiation is made, the percent error can be found to be as follows:

$$\text{Percent Error (at 700K)} = \left(1 - \frac{44000}{800 + 44000}\right) \cdot 100\% = 1.79\% \tag{9.140}$$

This indicates that the ZT measured with radiation losses is 1.79% lower than the expected ZT from literature values.

9.2.4 Can a Correction for Radiation be made to the calculation?

The radiation resistance can be assumed to be in parallel with the thermal resistance due to conduction.

$$ZT_{Rad} = \frac{\alpha \cdot \Delta T_{new}}{R_0 \cdot I} = \frac{\alpha \cdot \left(\alpha \cdot I \cdot T_{amb} \cdot \frac{R_{Thermal} \cdot R_{Rad}}{R_{Thermal} + R_{Rad}} \right)}{R_0 \cdot I} \tag{9.141}$$

Let X be the correction factor.

$$\begin{aligned} ZT_{Rad} \cdot X &= ZT_{Ideal} \\ X &= \frac{R_{Thermal} + R_{Rad}}{R_{Rad}} = 1 + \frac{R_{Thermal}}{R_{Rad}} \end{aligned} \tag{9.142}$$

From here, it is clear that more information about the TE material, such as the thermal conductivity, is still needed in order to get the ideal ZT value. MSU does measure the thermopower of the sample, which may be enough information to use with the ZT measurements and extract the thermal conductivity. The ZT measurement would also require the emissivity to be a known value. This may be accomplished by painting the sample black to make the emissivity equal to ~1. However, a lower emissivity value would be preferred. This shows that radiation effects at higher temperature can adversely effect this measurement. This also suggests that coatings could help ZT values at higher temperatures where radiation losses outweigh conduction losses. This topic will need further development and is not discussed here.

9.3 Thermal Conductivity of the Measurement Wires

For high temperature measurements, a TE sample is mounted in the UHT System so that the material is suspended by two of the measurement wires that attach to the ends of the sample. The wires are stuck to the stage using silver pasted. Small diameter platinum wires (dia = 0.001 inch) are used to mount the sample. The wires must have a thermal resistance that is much higher in magnitude than that of the sample. If the thermal resistances are comparable, then the ZT measurement will be inaccurate. Figure 9-8 shows a typical MSU TE sample being mounted in the UHT System. The wires are at least 1cm long before they are thermally grounded to the stage. The stage is assumed to be at the same temperature as the furnace. Heat will flow from the stage to the cold side of the TE material, and it will flow from the hot side of the TE material to the stage. Here, an example will be given to approximate the thermal resistance of the measurement wires and determine if they cause a significant error in the ZT measurement.

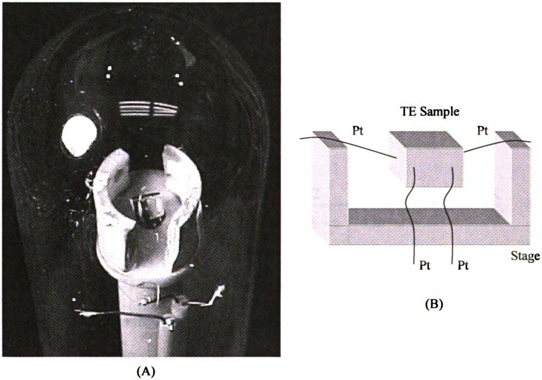

Figure 9-8: (A) Sample mounted in UHT System for ZT meter measurements. (B) Diagram of the sample dangling from the measurement wires attached to the ends of the sample.

The thermal conductivity at 700K for Platinum is ~72 W/mK. The wires attached to the ends of the sample are the shortest at about 1 cm in length. With the wire diameter at 25.4 μm, the thermal resistance of this wire is about

$$R_{Therm_{\mathrm{Pt}}} = \frac{1}{72}\left(\frac{\mathrm{m}\cdot\mathrm{K}}{\mathrm{W}}\right)\cdot\frac{0.01}{\pi\cdot\left(\frac{25.4E-6}{2}\right)^2}\left(\frac{\mathrm{m}}{\mathrm{m}^2}\right) \approx 274{,}000\ \frac{\mathrm{K}}{\mathrm{W}} \tag{9.143}$$

Table 9-1 shows that a typical MSU TE sample would have a thermal resistance of about 333 K/W. This is three orders of magnitude smaller than the resistance of the wires. Therefore, thermal losses up the measurement wires can be neglected for this measurement.

ZT measurements are also taken at room temperature using copper wires. The wires in this case are also 25.4 μm in diameter but the thermal conductivity is 401 W/mK. The wires for these measurements are at least 2 cm in length. The thermal resistance due to this wire is as follows.

$$R_{Therm_{\mathrm{Cu}}} = \frac{1}{401}\left(\frac{\mathrm{m}\cdot\mathrm{K}}{\mathrm{W}}\right)\cdot\frac{0.02}{\pi\cdot\left(\frac{25.4E-6}{2}\right)^2}\left(\frac{\mathrm{m}}{\mathrm{m}^2}\right) \approx 100{,}000\ \frac{\mathrm{K}}{\mathrm{W}} \tag{9.144}$$

Here, a typical MSU TE sample thermal resistance would again be about 3 orders of magnitude less then the measurement wires.

Finally, for a ZT measurement on constantan wire at room temperature, the thermal resistance of a 508 μm diameter constantan wire that is 6 mm in length and with thermal conductivity of 22 W/mK would be

$$R_{Therm_{\text{Constantan}}} = \frac{1}{22}\left(\frac{\text{m}\cdot\text{K}}{\text{W}}\right)\cdot\frac{0.006}{\pi\cdot\left(\frac{508E-6}{2}\right)^2}\left(\frac{\text{m}}{\text{m}^2}\right)\approx 1{,}350 \quad \frac{\text{K}}{\text{W}} \tag{9.145}$$

Here, the resistance of the constantan sample compared to the measurement wires of copper is only two orders of magnitude difference. This can lead up to a 2% error, which is still tolerable for this measurement. However, these types of calculations must be made in order to insure that the ZT measurement is accurate when measuring a sample and any temperature.

9.4 Example Measurements of *ZT* up to Higher Temperatures

Direct ZT measurements have been made at higher temperatures. This was accomplished by suspending a single TE in the UHT System and setting the temperature to higher values in the range of 300K to 700K. The UHT System would be raised to a desired temperature and allowed to stabilize for at least one hour. Monitoring the electrical resistance of the sample could identify temperature stabilization. The TE samples that are tested typically have strong temperature dependence for electrical conductivity and when the electrical resistance of the sample stabilizes, it is assumed that the temperature of the system has stabilized.

Presented here are three examples of comparing ZT direct measurements to using the standard technique of measuring each component of ZT individually. All examples show that the ZT direct method deviates from the standard method more and more as the temperature increases to the higher temperatures. The discrepancies in the data are likely due to radiation effects. The first example shows a direct comparison between using the standard method for obtaining ZT and the ZT direct method. It is shown that the ZT direct method does not reach as high of ZT values as the standard method. The second example shows that the ZT direct method may be less susceptible to radiation than the standard method, where thermal conductivity (including radiation loss) is measured by knowing the heater power on top of the sample and the temperature gradient across the sample (the assumption is all heat flows through the sample). The final example uses *p*-type SiGe sample. In this example, using a reference emissivity value for SiGe helps to correct the ZT data collected by the AC technique.

9.4.1 Comparing ZT measurements Using AgPbSbTe Sample

The sample, EQE74R2P253TopC ($Ag_{0.39}Pb_{20.64}Sb_{0.27}Te_{21}$) was measured using the ZT direct method at several high temperatures. It was then compared to an estimated ZT values obtained by the standard method. The temperature dependant data for electrical conductivity and thermopower of this sample is shown in Figure 9-9.

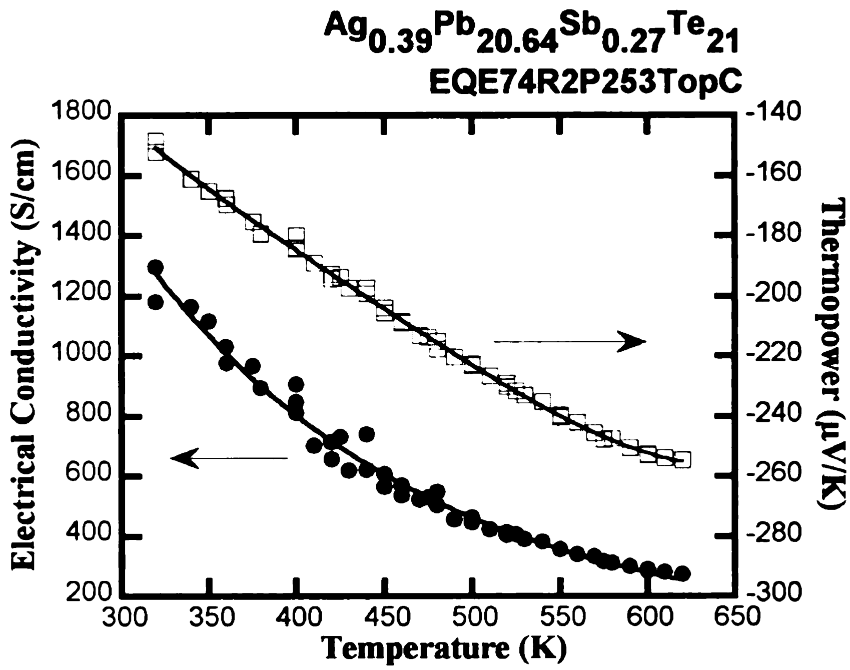

Figure 9-9: Plot of electrical conductivity and thermopower versus temperature for EQE74R2P253TopC

The thermal conductivity was estimated assuming the same lattice contribution to thermal conductivity as the sample published in science for the LAST materials (KF2242R3C $Ag_{0.86}Pb_{18}SbTe_{20}$). The temperature dependant total thermal conductivity of this published material is shown in Figure 9-10 along with the polynomial curve fit to the data. The temperature dependant electrical conductivity of this sample was measured and is shown in Figure 9-11 along with the polynomial curve to fit the data. From here, using the Wiedemann-Franz Law were the Lorenz number is estimated to be 2.28E-8 $W\Omega K^{-2}$ (discussed in Chapter 2 and in reference [7]), the lattice contribution to this total thermal conductivity can be found using the electrical conductivity and is shown in Figure 9-12 along with the curve fit to the data.

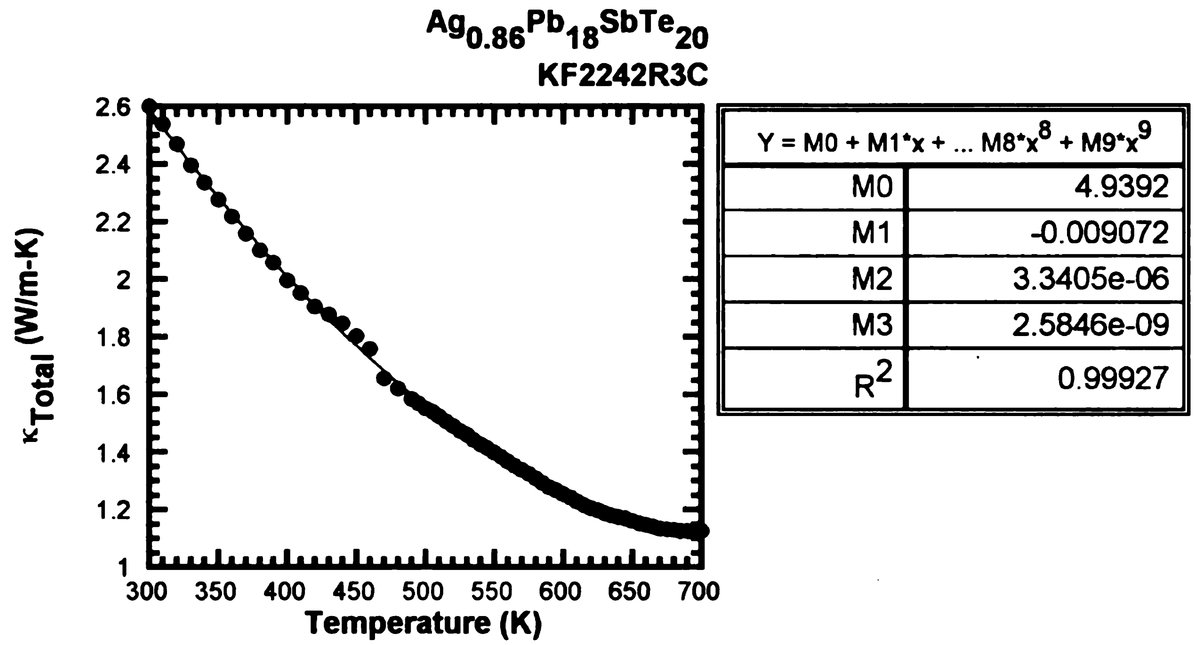

Figure 9-10: Plot of measured thermal conductivity versus temperature of KF2242R3C [6]

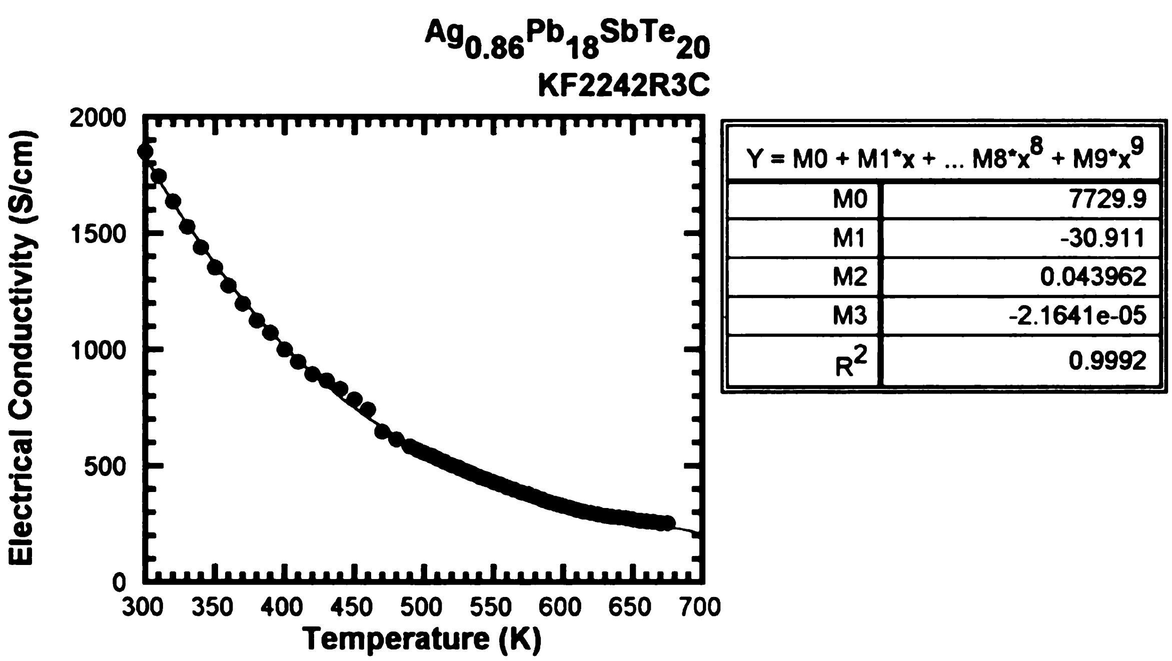

Figure 9-11: Plot of electrical conductivity versus temperature for KF2242R3C

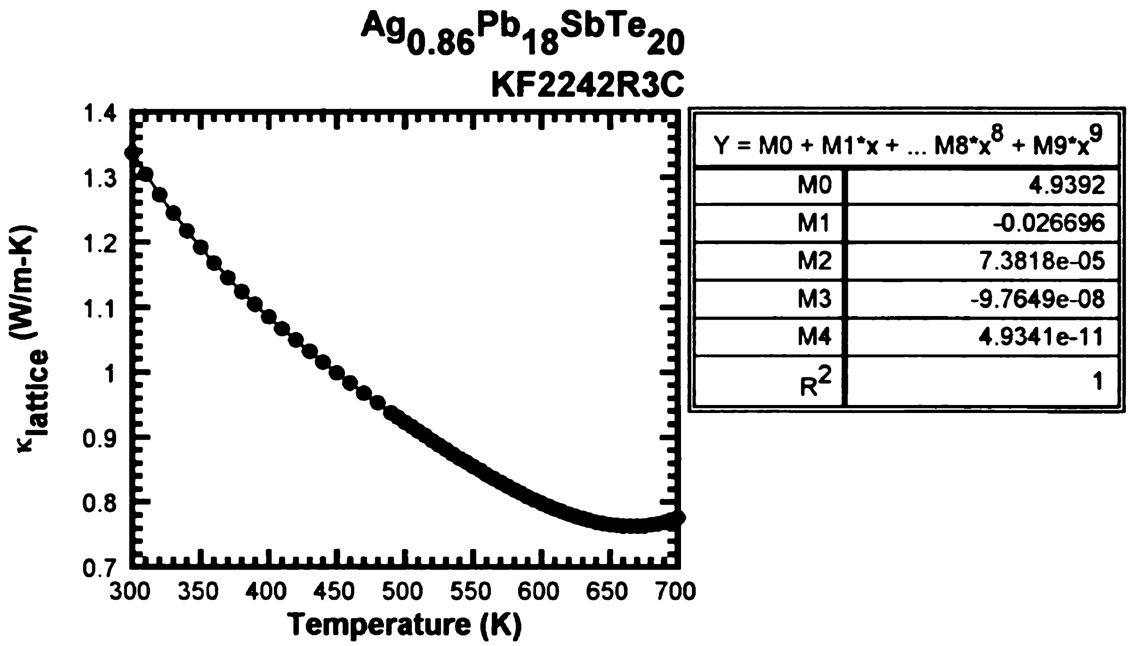

Figure 9-12: Plot of calculated lattice contribution to thermal conductivity versus temperature

By assuming this lattice contribution to the thermal conductivity and knowing the electrical conductivity of this sample, we can again apply the Wiedemann-Franz Law to obtain an estimated thermal conductivity of the sample with will be used in the standard ZT calculation.

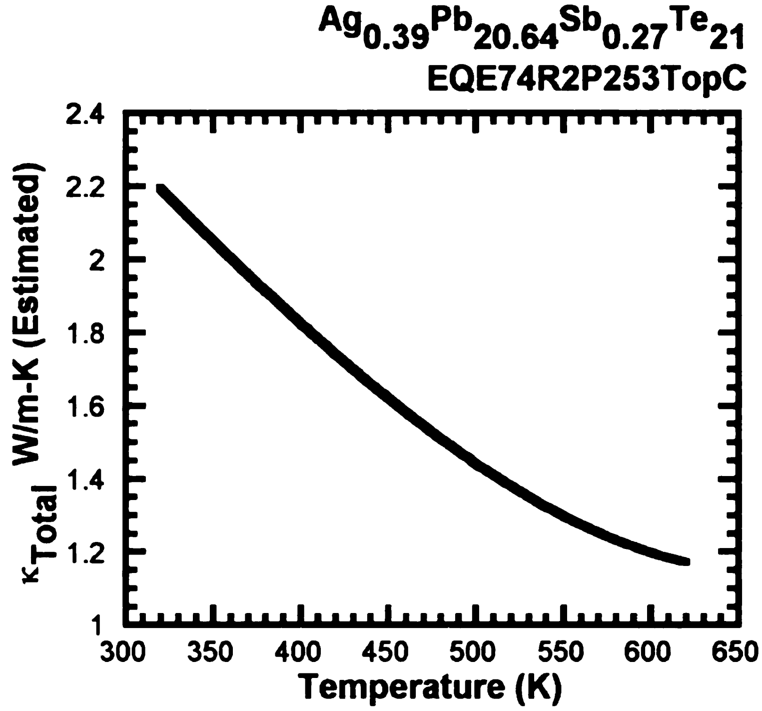

Figure 9-13: Plot of calculated thermal conductivity versus temperature for EQE74R2P253TopC

The sample, EQE74R2P253TopC, was also measured for ZT directly using the impedance of the sample at multiple temperatures. The results of the frequency sweep are shown in Figure 9-14. A plot of the ZT calculations using both methods is shown in Figure 9-15. These data show that ZT direct method measures lower values than the standard method. It also shows that the deviation between the data increases with increasing temperature. It is assumed that this discrepancy between the two methods is caused by inclusion of radiation losses in the ZT direct method.

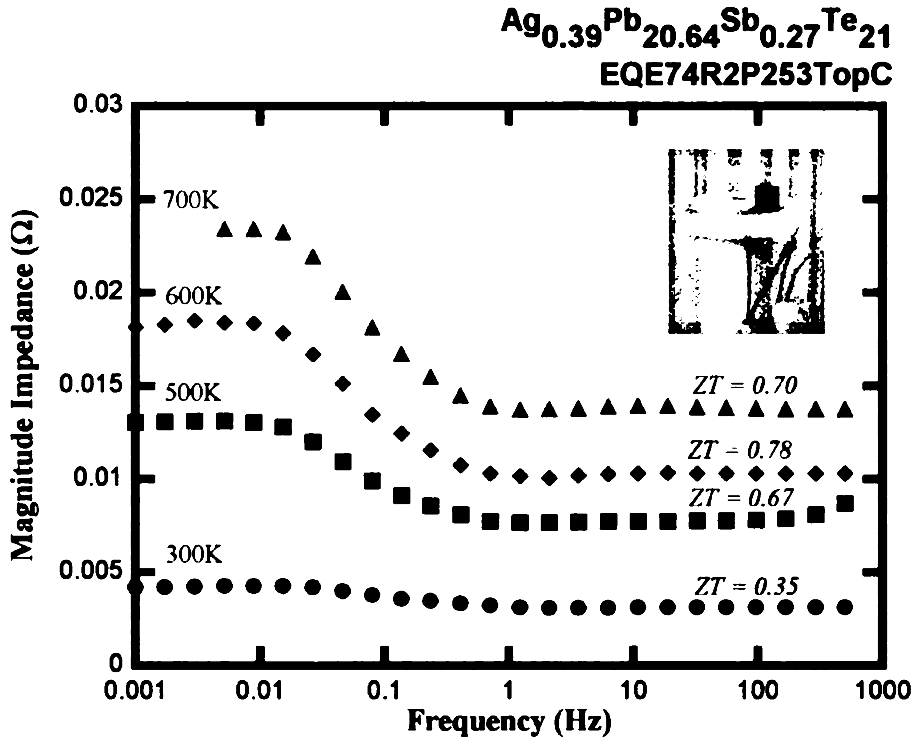

Figure 9-14: Plot of direct ZT measurements using magnitude impedance versus frequency at multiple temperatures for EQE74R2P253TopC

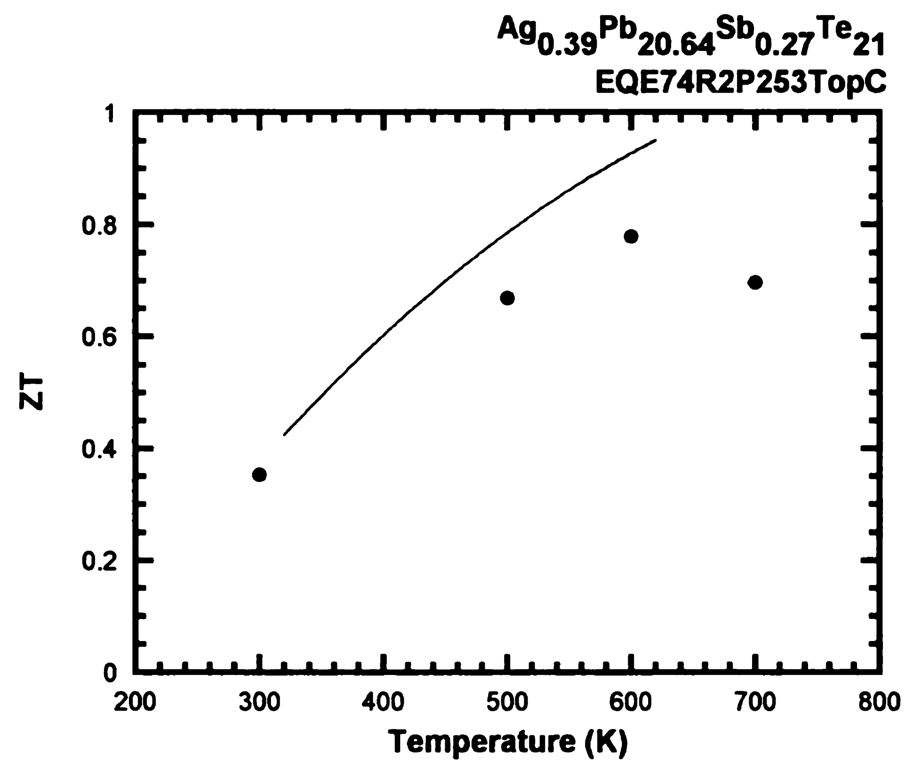

Figure 9-15: Plot of ZT versus temperature. (Line) Estimated ZT using standard measurements of electrical conductivity, thermopower, and thermal conductivity. (Dots) Direct ZT measurements using impedance of the sample

9.4.2 Comparing Radiation Losses using PbTe with Nanoparticals of PbS

The second example uses a PbTe structure with nanoparticals of PbS. The frequency dependant impedance data for multiple temperatures is shown in Figure 9-16. This sample was then measured in the HT system for temperature dependant data for electrical conductivity and thermopower as shown in Figure 9-17. The system also measured the thermal conductivity of the sample (including radiation affects) by measuring the power to the sample heater and measuring the temperature gradient along the length of the sample (assuming all heat produced flows through the sample). This data is shown in Figure 9-18. The rapid rise in thermal conductivity measurements is due to the radiation losses, which have a temperature dependence of T^3.

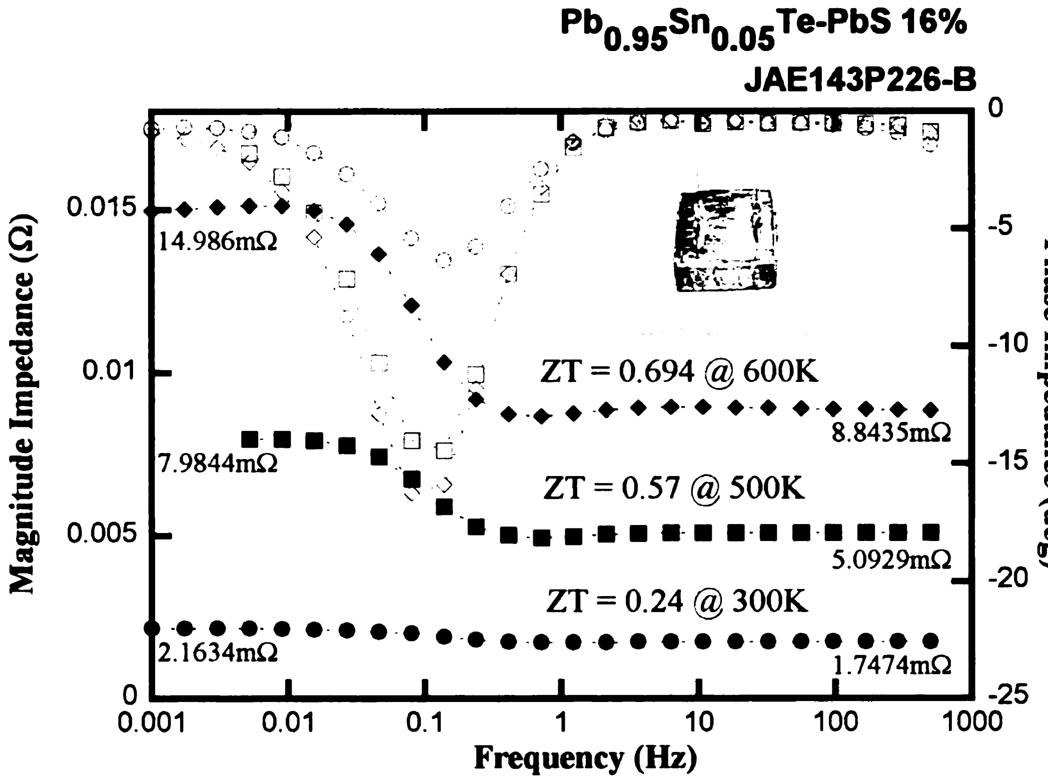

Figure 9-16: Plot of high temperature direct ZT measurements using magnitude impedance versus frequency.

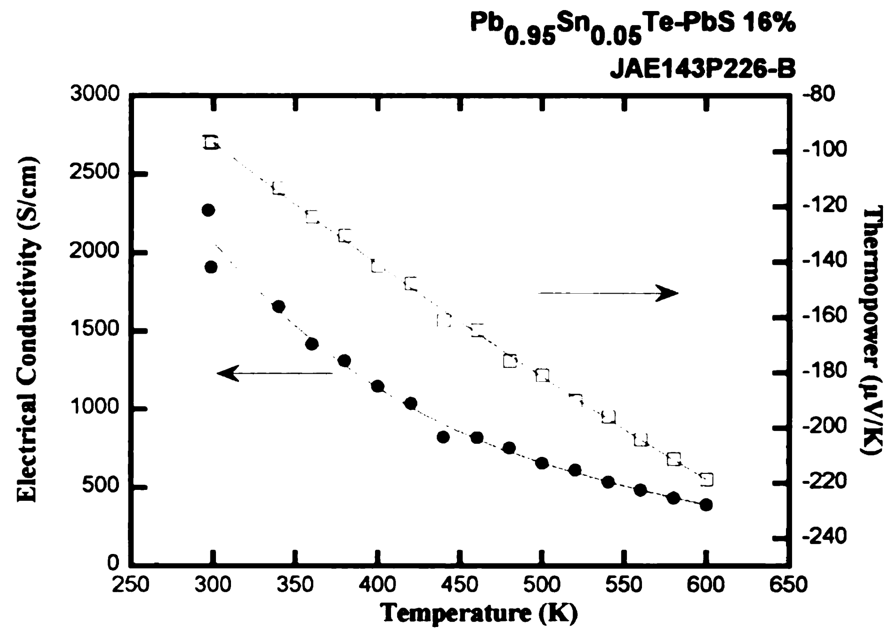

Figure 9-17: Plot of electrical conductivity and thermopower versus temperature for JAE143P226-B

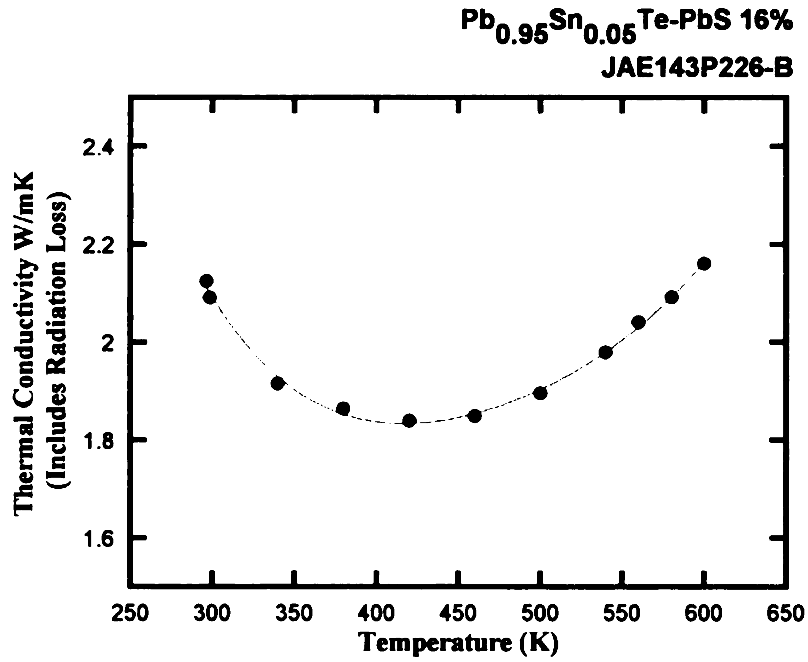

Figure 9-18: Plot of measurement thermal conductivity (including radiation losses) versus temperature for JAE143P226-B

The ZT measured for both methods is shown in Figure 9-19. This data shows that room temperature measurements agree but high temperature measurements disagree with the ZT measuring using the direct method having a higher value. Although it is assumed that both techniques suffer from radiation losses, here it indicates that the radiation effect may have less of an impact on the ZT direct method that using the standard method. It is the radiation effect that prohibits thermal conductivity measurements to be made in this fashion. However, using the ZT direct method may prove to be useful in that the effect is less in this method.

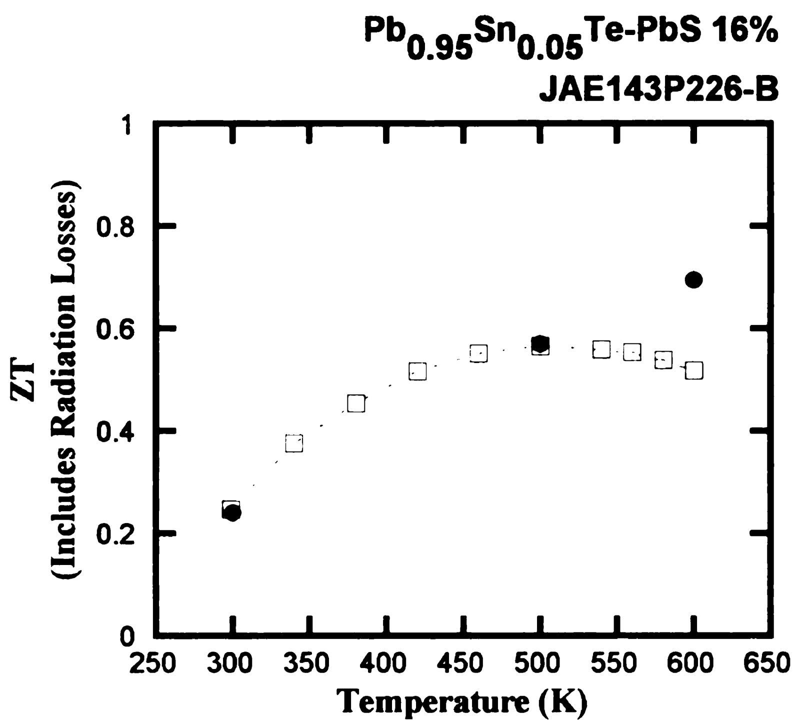

Figure 9-19: Plot of ZT versus temperature. (Squares) ZT calculated using the standard method. (Circles) ZT direct measurements from impedance of the sample.

9.4.3 Testing ZT of *p*-type SiGe and Correcting for Emissivity

The third sample tested for high temperature ZT measurements was a *p*-type $Si_{78}Ge_{22}$ sample provided by Ames Laboratory at Iowa State University. Platinum wires were resistively welded to the sample shown in Figure 9-20(a). The sample was then suspended in the UHT System as shown in Figure 9-20(b). A digital flipping technique (discussed in a later chapter) was used to collect resistor versus frequency at various temperatures and is shown in Figure 9-21. The electrical resistivity of this sample was compared to the data provided by Ames Laboratory and is in excellent agreement as shown in Figure 9-22.

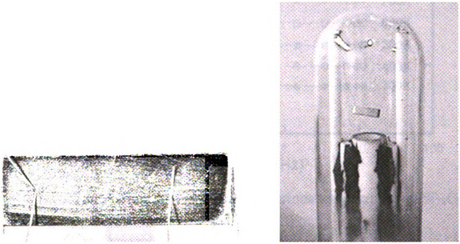

(a) (b)

Figure 9-20: **(a)** $Si_{78}Ge_{22}$ Sample with platinum wires (dia = 0.003 inch) resistive welded to sample. (b) SiGe sample suspended in UHT System.

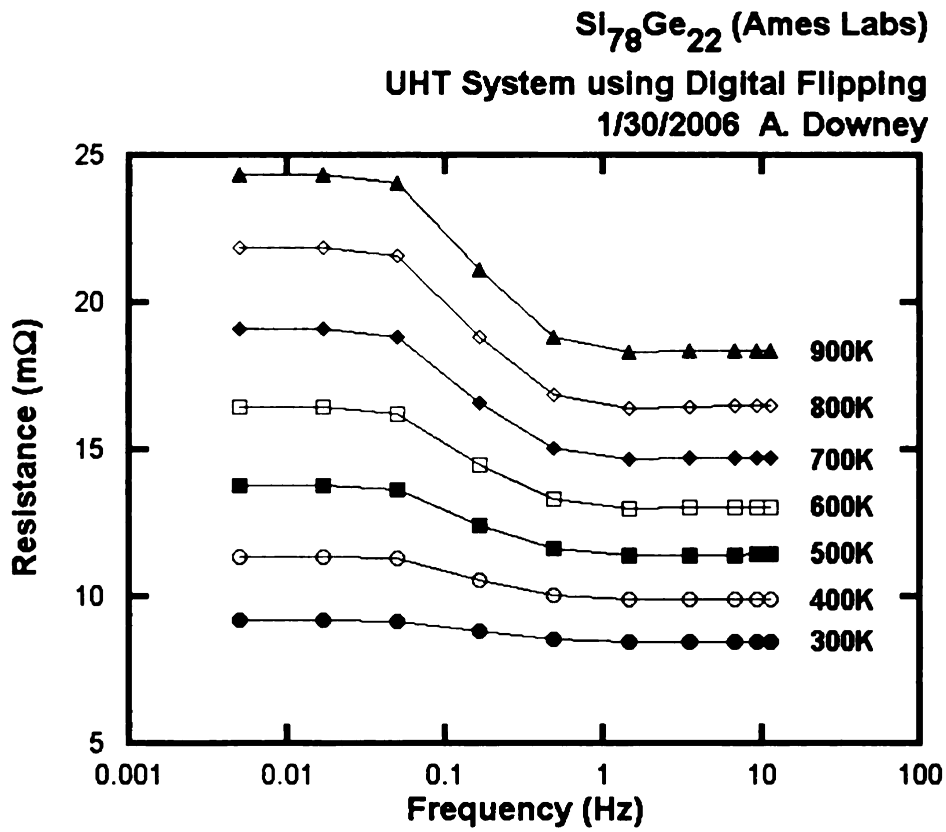

Figure 9-21: Resistance versus frequency at various temperatures of $Si_{78}Ge_{22}$

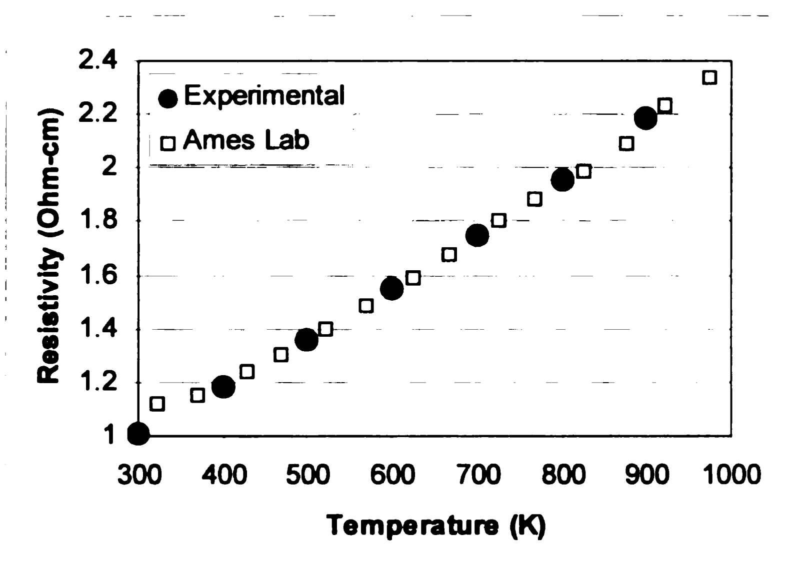

Figure 9-22: Measured resistivity of $Si_{78}Ge_{22}$ sample compared to Ames Lab measurements

By taking the R_{DC}/R_{AC} and subtracting one, the uncorrected ZT value of the sample can be found. The first correction to the ZT value is to account for the thermopower of the platinum measurement wires as discussed in previous sections where the thermopower of both the sample and the measurement wires must be known. This then compared to reference data for *p*-type $Si_{80}Ge_{20}$ data [57] due to a lack of data published for $Si_{78}Ge_{22}$. The results are shown in Figure 9-23 where it is again clear that the measured ZT value deviates from the traditional ZT measurement method at the higher temperatures due to radiation loss. However, a correction can be made to the ZT value by taking into account the sample dimensions and the emissivity of SiGe. A highly doped sample of SiGe was published to have an emissivity value of 0.7 over the temperature range tested [58]. When this value is used along with the correction method discussed previously, the data more closely matches reference data as shown in Figure 9-24. There is still a slight deviation at the highest temperature tested which could be due to surface roughness, emissivity value changing versus temperature, or the fact that the reference data is for $Si_{80}Ge_{20}$

.

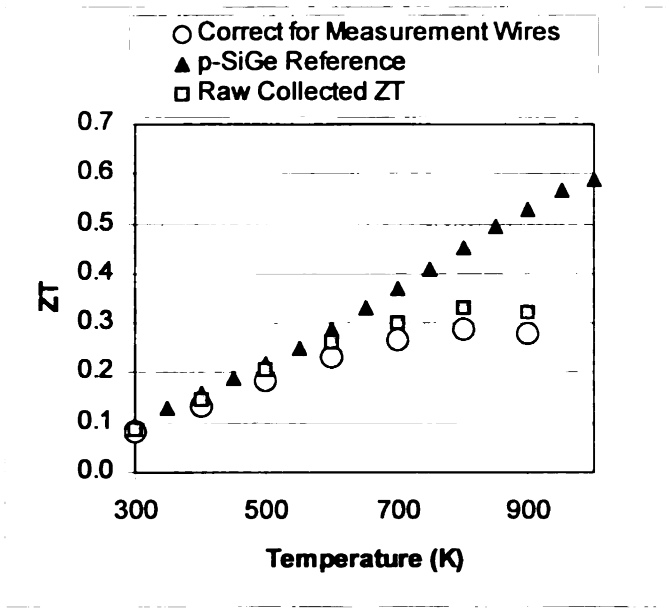

Figure 9-23: ZT values measured versus temperature compared to *p*-type $Si_{80}Ge_{20}$. This plot shows the raw ZT value collected and the ZT correct for the measurement wires.

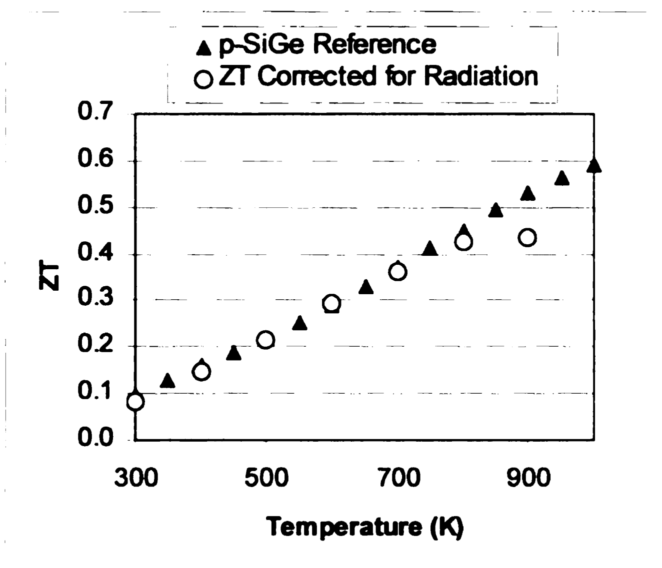

Figure 9-24: Measured ZT of $Si_{78}Ge_{22}$ that has been corrected for radiation losses using an emissivity value of 0.7

Chapter 10: ZT of Constantan

10.1 Introduction

There are many researchers involved in thermoelectrics, however, an accepted reference material with high ZT values has not been established for confirming measurements of thermopower and ZT. One possible reason for this is the difficulty in manufacturing identical thermoelectric samples. This presents difficulties in verifying new techniques for investigating thermoelectric material properties except by having a sample measured by many different companies in a "round-robin" approach. Thermocouples, however, have been well characterized and their output voltage versus temperature has been published by NIST (National Institute of Standards and Technology). Presented here is a suggestion to use constantan (copper 55%, nickel 45%), which is used in a Type-T and Type-E thermocouple, as a reference material because it has a relatively high thermopower and low thermal conductivity compared to other thermocouple materials (copper, iron, chromel, alumel, platinum). By using published data from various sources, it is possible to calculate the ZT of constantan. The ZT is large enough to be measured by the ZT meter and can be used as a reference material.

10.2 Establishing Constantan as a reference material

NIST provides the output voltage versus temperature for a Type-T thermocouple where one material is copper and the other material is constantan (See Figure 10-1). The thermopower of a Type-T thermocouple can be found by taking the derivative of this output voltage with respect to the temperature shown in Figure 10-2. The thermopower of a thermocouple is equal to the difference in thermopowers of each of the wires shown in equation the equation below. In this case, copper has a positive thermopower and constantan has a negative thermopower.

$$S_{\text{Type T}} = S_{\text{Copper}} - S_{\text{Constantan}} \tag{10.146}$$

The thermopower of copper has been published by Roberts [59] where the data and polynomial curve fit to the data is shown in Figure 10-3. This data is used to extract the thermopower of constantan shown in Figure 10-4. This thermopower of constantan can be used as a reference for other systems that measure thermopower directly such as MSU's High Temperature (HT) system [21]. See Appendix B for thermopower and electrical conductivity measurements made with MSU's HT System. The electrical conductivity of constantan is 52 μΩcm according to Goodfellow with temperature coefficient of +/-0.00002 (K^{-1}). The thermal conductivity of constantan comes from two published sources, one for low temperature values [60], and the other for high temperature values [61] (see Figure 10-5). The figure of merit, ZT, for constantan can now be found using equation the equation below and the results are shown in Figure 10-6.

$$ZT = \frac{\alpha^2 \cdot \sigma}{\kappa} \cdot T \tag{10.147}$$

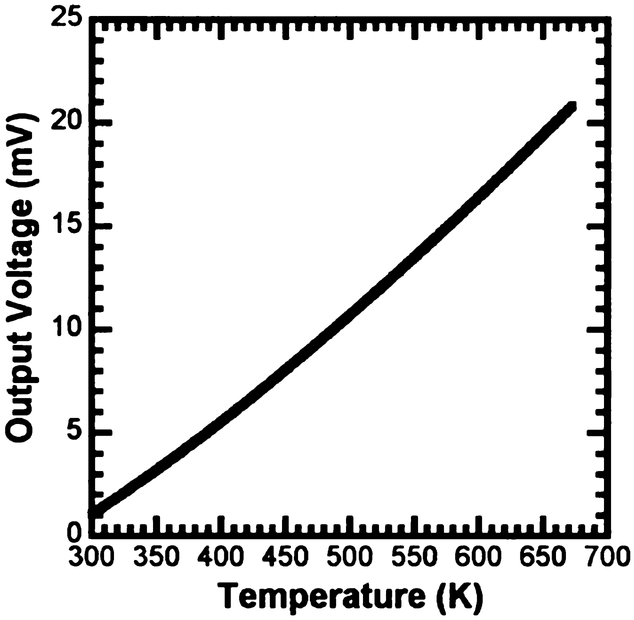

$Y = M0 + M1{*}x + \ldots M8{*}x^8 + M9{*}x^9$	
M0	-52.523572
M1	0.758629334
M2	-0.00496786397
M3	1.71724575e-05
M4	-2.75241767e-08
M5	-2.66892886e-12
M6	9.15755819e-14
M7	-1.61535312e-16
M8	1.24985525e-19
M9	-3.79293207e-23
R	0.999999999

Figure 10-1: Output voltage for Type-T thermocouple from NIST

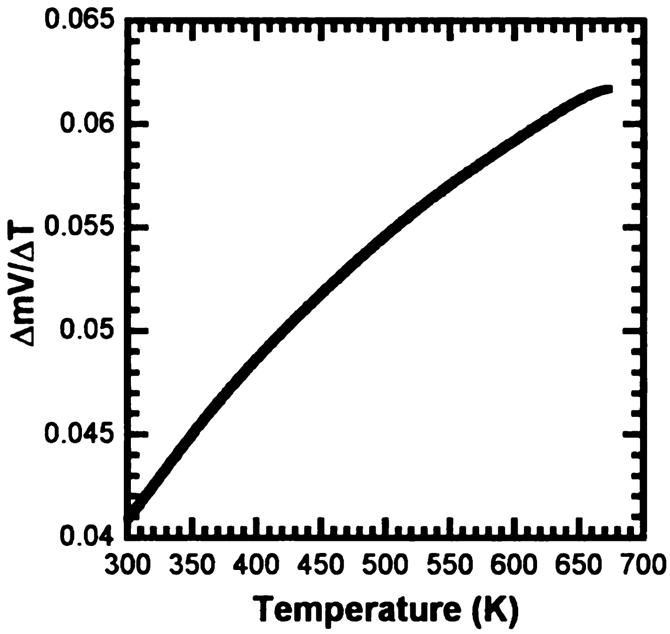

Figure 10-2: Thermopower of Type-T thermocouple from derivative

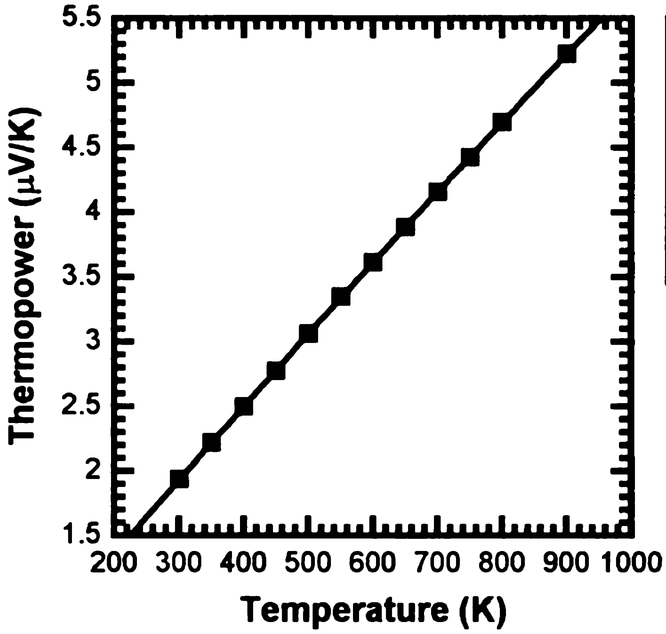

$Y = M0 + M1*x + \ldots M8*x^8 + M9*x^9$	
M0	0.183706027
M1	0.00596025885
M2	-3.93945306e-07
M3	3.89026595e-15
R	0.999992681

Figure 10-3: Thermopower of copper from Roberts (squares) with curve fit on top (line)

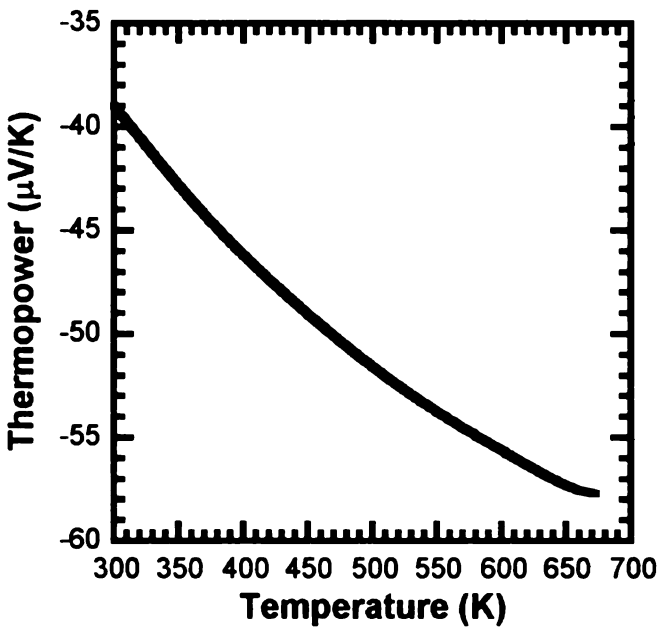

$Y = M0 + M1*x + \ldots M8*x^8 + M9*x^9$	
M0	-996.557489
M1	13.9463863
M2	-0.0801583144
M3	0.000222554832
M4	-2.45151607e-07
M5	-2.17858754e-10
M6	9.67057136e-13
M7	-1.11899956e-15
M8	5.37574211e-19
M9	-7.46944001e-23
R	0.999999984

Figure 10-4: Thermopower of constantan based on published thermopower of copper and NIST data for Type-T thermocouple

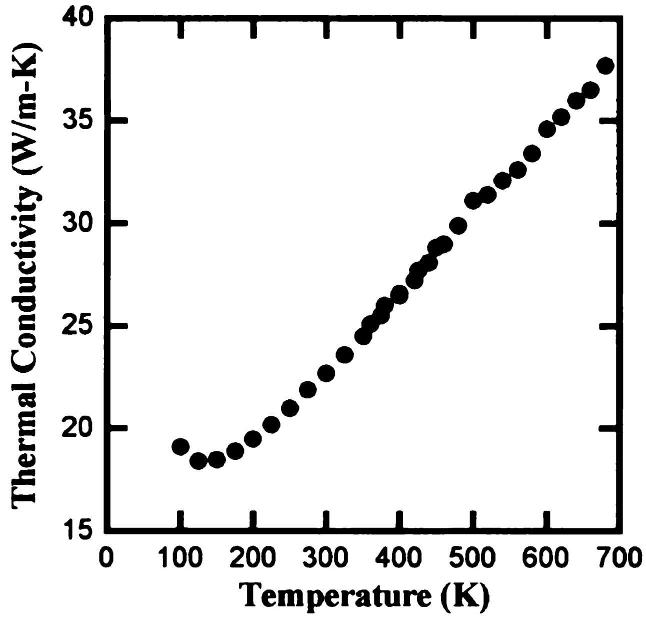

Y = M0 + M1*x + ... M8*x^8 + M9*x^9	
M0	25.1070348
M1	0.0329667566
M2	-0.0032442501
M3	3.98412407e-05
M4	-2.29936572e-07
M5	7.63354855e-10
M6	-1.5345749e-12
M7	1.84630541e-15
M8	-1.22465673e-18
M9	3.44812305e-22
R	0.999682374

Figure 10-5: Thermal conductivity of constantan from two published sources

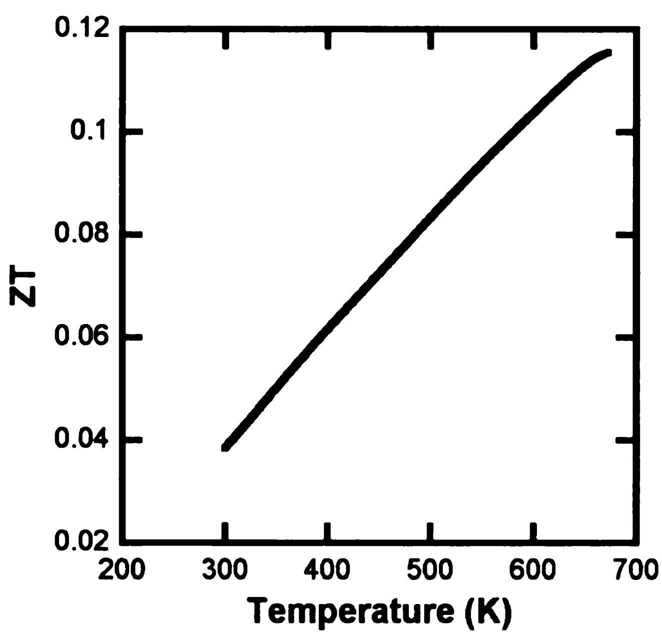

Y = M0 + M1*x + ... M8*x^8 + M9*x^9	
M0	0.0426568885
M1	0.00562630239
M2	-8.22857225e-05
M3	4.57839727e-07
M4	-1.1546815e-09
M5	8.00159646e-13
M6	2.55604704e-15
M7	-6.75897139e-18
M8	6.39615537e-21
M9	-2.24621516e-24
R	0.999999999

Figure 10-6: Calculated ZT of constantan

10.3 Measurement of Constantan

A small sample of constantan wire was used measured using the single TE sample configuration shown in Figure 10-7. For high temperature ZT measurements, the Ultra High Temp system was utilized. Because of the higher temperatures, platinum wires are used for the current leads and voltage leads connected to the sample.

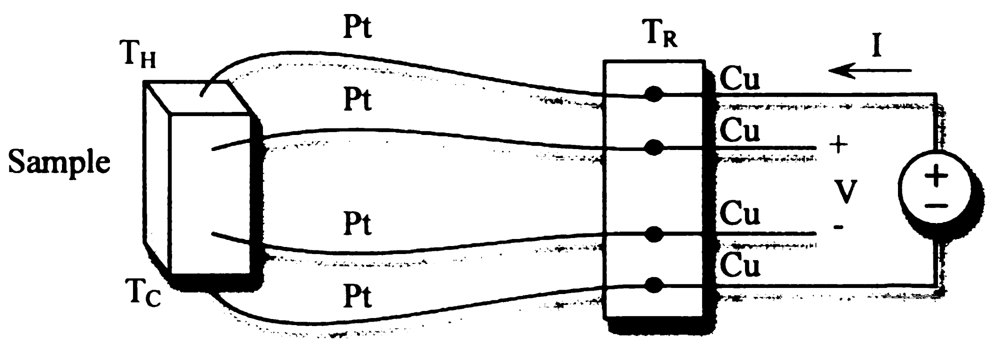

Figure 10-7: Setup for single TE pellet

A detailed diagram with dimensions (using variables) is shown in Figure 10-8 for the sample size and voltage probe locations.

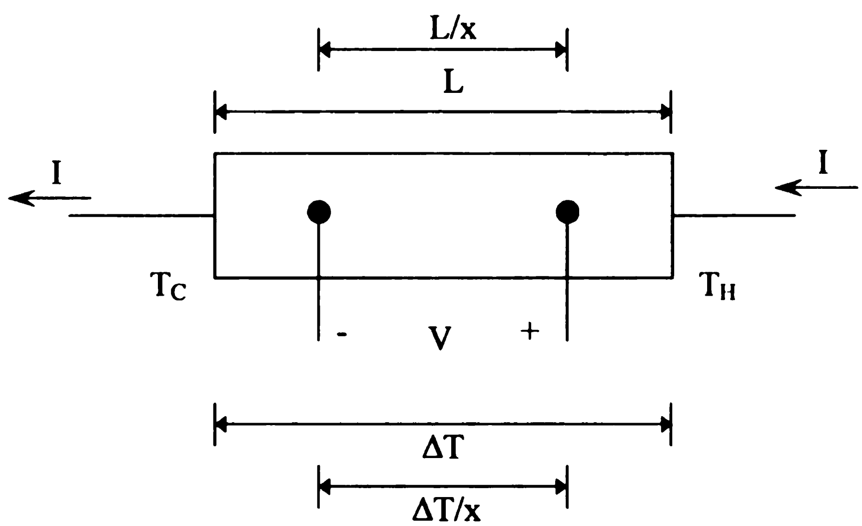

Figure 10-8: Detailed view of a single TE pellet connection

The thermopower of constantan is low enough that the thermopower of the platinum current leads will affect the measurement. Therefore, the thermopower of the platinum must be known and corrected for. Published data on the thermopower of platinum is shown in Figure 10-9 along with the polynomial curve fit.

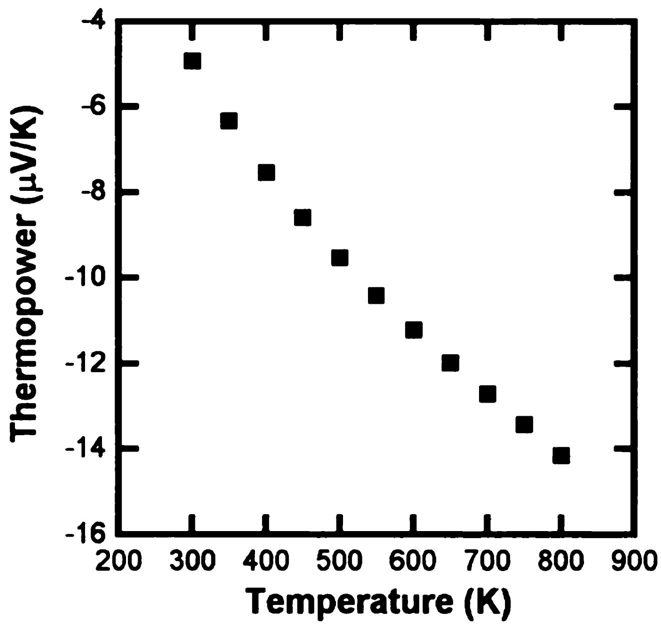

Y = M0 + M1*x + ... M8*x^8 + M9*x^9	
M0	118.724984
M1	-2.10073889
M2	0.0167153763
M3	-7.86175678e-05
M4	2.35649658e-07
M5	-4.64450512e-10
M6	6.00944332e-13
M7	-4.92071067e-16
M8	2.31451138e-19
M9	-4.7677029e-23
R	0.999999716

Figure 10-9: Thermopower of platinum from published data (Roberts)

The schematic of the setup is shown in Figure 10-10 where a representation of the electrical circuit and thermal circuit is provided. Figure 10-11 shows the equations for all of the components presented in Figure 10-10.

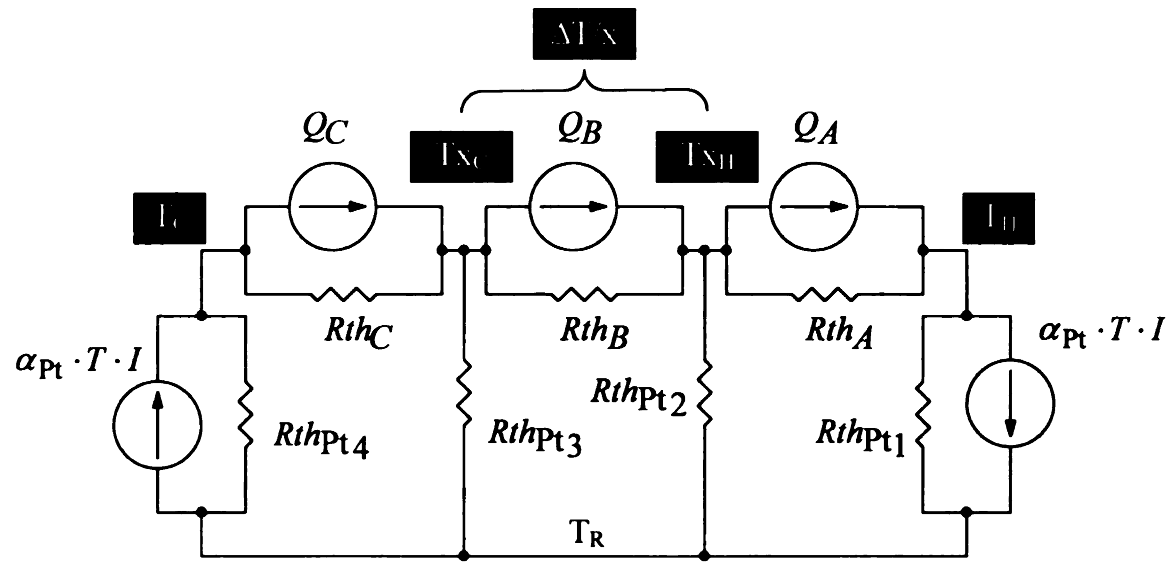

Thermal Circuit

Appendix D: Electrical

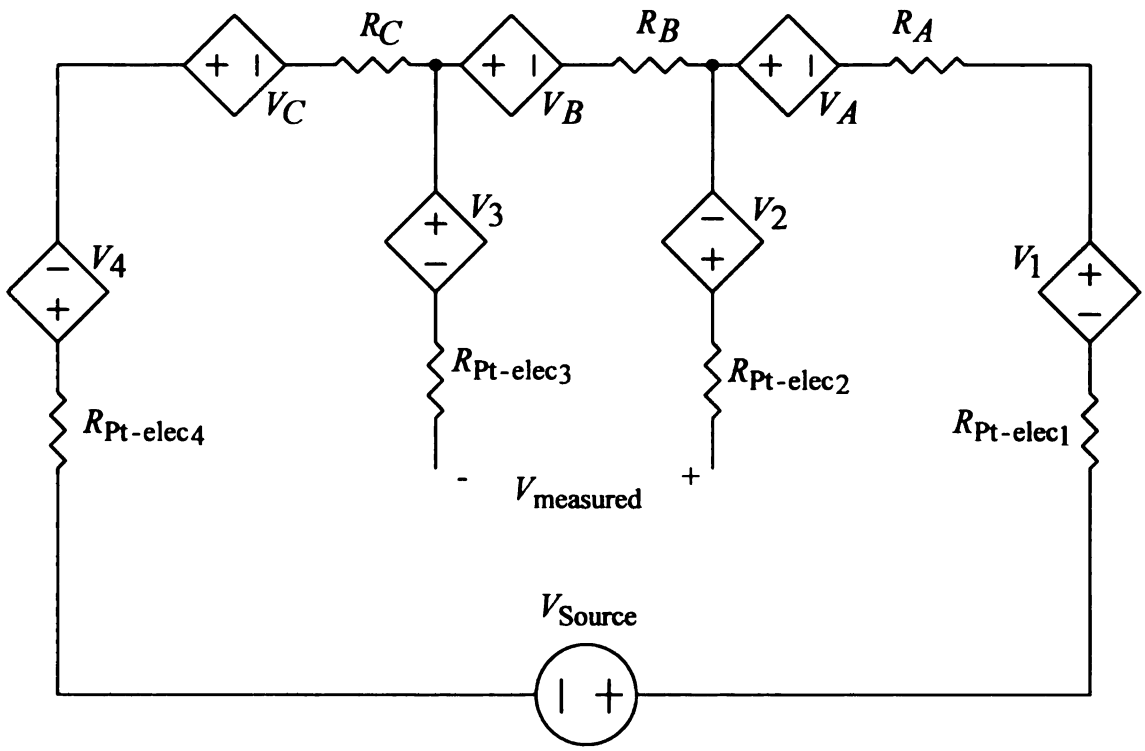

Figure 10-10: Electrical and thermal model of setup

$$V_1 = \int_{T_R}^{T_H} \alpha_{Pt} \cdot dT \qquad V_A = \int_{Tx_H}^{T_H} \alpha_{Pt} \cdot dT \qquad Q_A = Q_B = Q_C = \alpha_{sample} \cdot I \cdot T$$

$$Rth_A = Rth_{sample} \cdot \left(1 - \frac{1}{x}\right) \cdot \frac{1}{n}$$

$$V_2 = \int_{T_R}^{Tx_H} \alpha_{Pt} \cdot dT \qquad V_B = \int_{Tx_H}^{Tx_C} \alpha_{Pt} \cdot dT \qquad Rth_B = Rth_{sample} \cdot \frac{1}{x}$$

$$V_3 = \int_{T_R}^{Tx_C} \alpha_{Pt} \cdot dT \qquad V_C = \int_{Tx_C}^{T_C} \alpha_{Pt} \cdot dT \qquad Rth_C = Rth_{sample} \cdot \left(1 - \frac{1}{x}\right) \cdot \left(1 - \frac{1}{n}\right)$$

$$V_4 = \int_{T_R}^{T_C} \alpha_{Pt} \cdot dT \qquad R_A = R_{sample} \cdot \left(1 - \frac{1}{x}\right) \cdot \frac{1}{n}$$

$$R_B = R_{sample} \cdot \frac{1}{x}$$

$$R_C = R_{sample} \cdot \left(1 - \frac{1}{x}\right) \cdot \left(1 - \frac{1}{n}\right)$$

Figure 10-11: Equations for Figure 10-10

The measured voltage across the constantan wire can be calculated using the schematic from Figure 10-10 and is shown below.

$$\begin{aligned} V_{measured} &= \int_{T_R}^{Tx_H} \alpha_{Pt} \cdot dT + I \cdot R_{sample} \cdot \frac{1}{x} + \int_{Tx_H}^{Tx_C} \alpha_{sample} \cdot dT + \int_{Tx_C}^{T_R} \alpha_{Pt} \cdot dT \\ &= \int_{Tx_C}^{Tx_H} \left(\alpha_{Pt} - \alpha_{sample}\right) \cdot dT + I \cdot R_{sample} \cdot \frac{1}{x} \qquad (10.148) \\ &\approx \frac{\left(\alpha_{Pt} - \alpha_{sample}\right) \cdot \Delta T}{x} + \frac{I \cdot R_{sample}}{x} \end{aligned}$$

Assuming that wire thermal resistance is much larger than the sample thermal resistance, the temperature gradient across the sample can be approximated as follows.

$$\Delta T \approx \left(\alpha_{\text{sample}} - \alpha_{\text{Pt}}\right) \cdot I \cdot T \cdot Rth_{\text{sample}} \tag{10.149}$$

ZT of the tested material is found from the basic equations shown below.

$$(ZT)_{\text{sample}} = \frac{\alpha_{\text{sample}}^{2} \cdot \sigma_{\text{sample}}}{\kappa_{\text{sample}}} \cdot T \tag{10.150}$$

$$Q = \alpha_{\text{sample}} \cdot T \cdot I \tag{10.151}$$

$$\kappa = \frac{Q}{\Delta T} \cdot \frac{length}{area} \tag{10.152}$$

$$\begin{aligned}
(ZT)_{\text{sample}} &= \alpha_{\text{sample}}^{2} \cdot \frac{\text{length}}{R_{\text{sample}} \cdot \text{area}} \cdot \frac{\Delta T \cdot \text{area}}{\alpha_{\text{sample}} \cdot T \cdot I \cdot \text{length}} \cdot T \\
&= \alpha_{\text{sample}}^{2} \cdot \frac{1}{R_{\text{sample}}} \cdot \frac{\Delta T}{\alpha_{\text{sample}} \cdot T \cdot I} \\
&= \frac{\alpha_{\text{sample}} \cdot \Delta T}{R_{\text{sample}} \cdot I} \\
&= \frac{\alpha_{\text{sample}}^{2} \cdot Rth_{\text{sample}}}{R_{\text{sample}}} \cdot T
\end{aligned} \tag{10.153}$$

The measured values for R_{DC} and R_{AC} can be calculated below

$$\begin{aligned}
R_{DC} &= \frac{\left(\alpha_{\text{Pt}} - \alpha_{\text{sample}}\right) \cdot \Delta T}{x \cdot I} + \frac{R_{\text{sample}}}{x} \\
R_{AC(\Delta T \to 0)} &= \frac{R_{\text{sample}}}{x}
\end{aligned} \tag{10.154}$$

Now the ZT that is measured can be calculated from using the Harman technique as follows.

$$
\begin{aligned}
(ZT)_{\text{measured}} &= \frac{R_{DC}}{R_{AC}} - 1 \\
&= \frac{\left[\dfrac{(\alpha_{\text{Pt}} - \alpha_{\text{sample}}) \cdot \Delta T}{x \cdot I} + \dfrac{R_{\text{sample}}}{x}\right]}{\left[\dfrac{R_{\text{sample}}}{x}\right]} - 1 \\
&= \frac{(\alpha_{\text{Pt}} - \alpha_{\text{sample}}) \cdot \Delta T}{R_{\text{sample}} \cdot I} \\
&= \frac{(\alpha_{\text{Pt}} - \alpha_{\text{sample}}) \cdot (\alpha_{\text{sample}} - \alpha_{\text{Pt}}) \cdot I \cdot T \cdot Rth_{\text{sample}}}{R_{\text{sample}} \cdot I} \\
&= \frac{(\alpha_{\text{Pt}} - \alpha_{\text{sample}})^2 \cdot Rth_{\text{sample}}}{R_{\text{sample}}} \cdot T
\end{aligned}
\tag{10.155}
$$

The above equation shows that how the thermopower of the platinum wire affects the measured ZT value. A correction must be made to the measured ZT to get the actual ZT of the sample by introducing a correction factor as follows.

$$(ZT)_{\text{sample}} = (ZT)_{\text{measured}} \cdot \text{Correction}$$

$$\left[\frac{\alpha_{\text{sample}}{}^2 \cdot Rth_{\text{sample}}}{R_{\text{sample}}} \cdot T\right] = \left[\frac{(\alpha_{\text{Pt}} - \alpha_{\text{sample}})^2 \cdot Rth_{\text{sample}}}{R_{\text{sample}}} \cdot T\right] \cdot \text{Correction}$$

$$\boxed{\text{Correction} = \frac{\alpha_{\text{sample}}{}^2}{(\alpha_{\text{Pt}} - \alpha_{\text{sample}})^2}} \tag{10.156}$$

The above equation indicates that in order to correct for the thermopower of the measurement wires, the thermopower of the sample must be known. This may not always be the case. However, typically, samples measured by MSU have large thermopower values in that the thermopower of the platinum voltage probes can be neglected.

10.4 Experimental Results

Constantan wire was tested for ZT using the Ultra High Temp system. A picture of the mounted sample is shown in Figure 10-12.

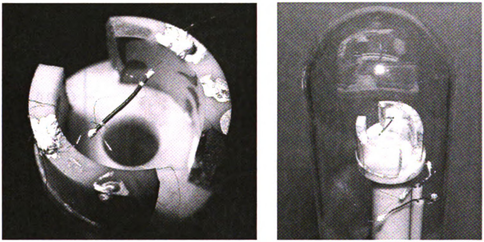

Figure 10-12: Mounting constantan wire for ZT measurement

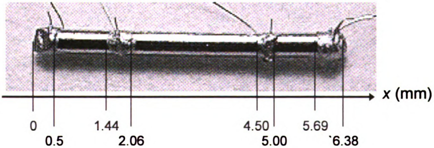

Figure 10-13: Constantan wire (dia = 0.02" = 0.508mm) probe spacings

Several sample temperatures were investigated, and once thermal stabilization was achieved, a frequency sweep for impedance measurements was initiated. The results of the magnitude and phase of the impedance at various temperatures are shown in Figure 10-14 and Figure 10-15.

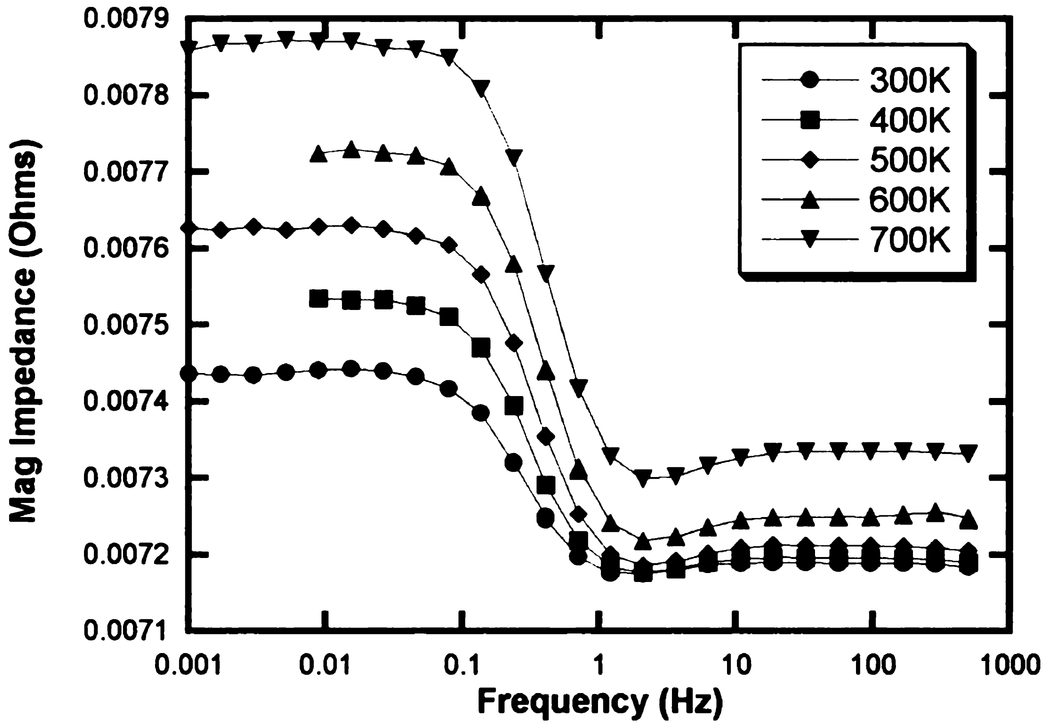

Figure 10-14: Magnitude of impedance versus frequency at multiple temperatures

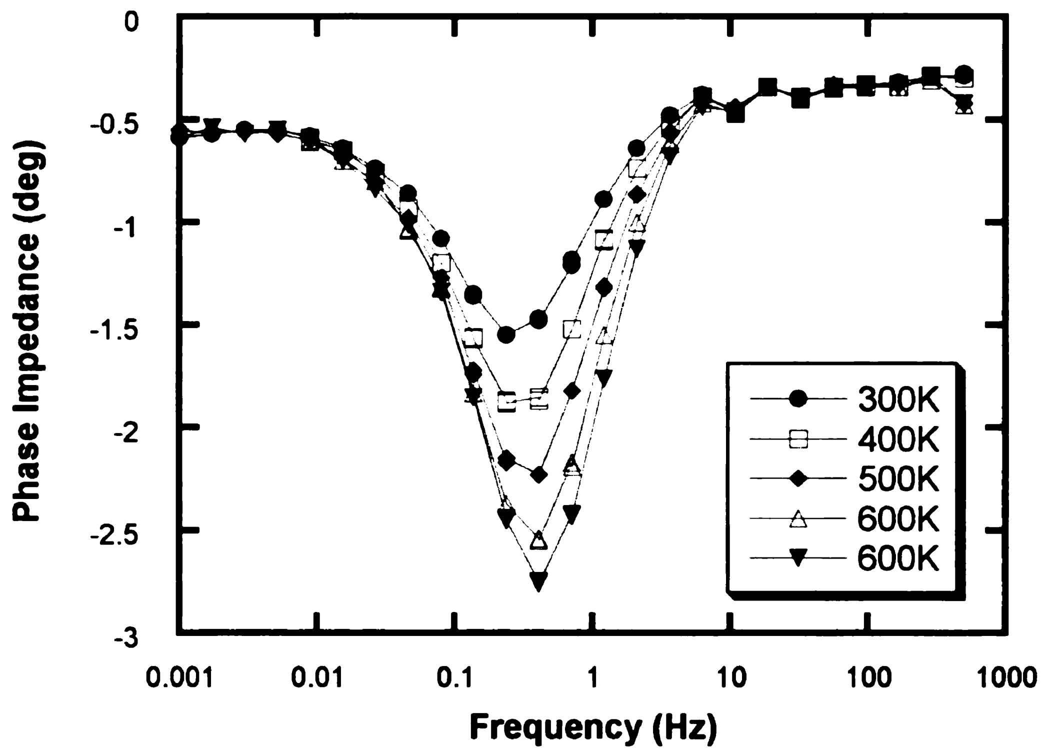

Figure 10-15: Phase of impedance versus frequency at multiple temperatures

By knowing the thermopower of the constantan wire and the platinum, the correction factor can be found and is shown in Figure 10-16 with the polynomial curve fit.

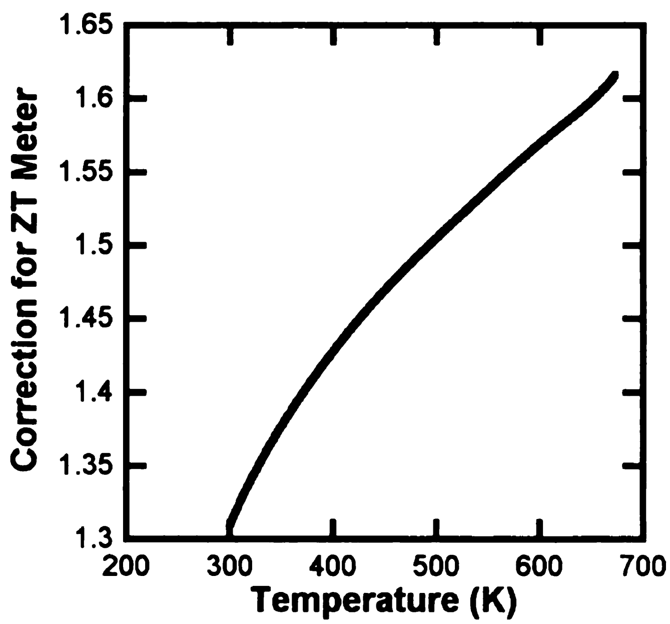

$Y = M0 + M1*x + ... M8*x^8 + M9*x^9$	
M0	-11.5835284
M1	0.17105912
M2	-0.000927986297
M3	2.47244562e-06
M4	-2.58138734e-09
M5	-2.35767787e-12
M6	9.334039e-15
M7	-9.27187619e-18
M8	2.97000378e-21
M9	2.58485063e-25
R	0.999999993

Figure 10-16: Correction factor for measuring constantan using platinum wires

Using the correction factor and the measured impedance measurements of the constantan wire, the ZT was found and is shown in Figure 10-17

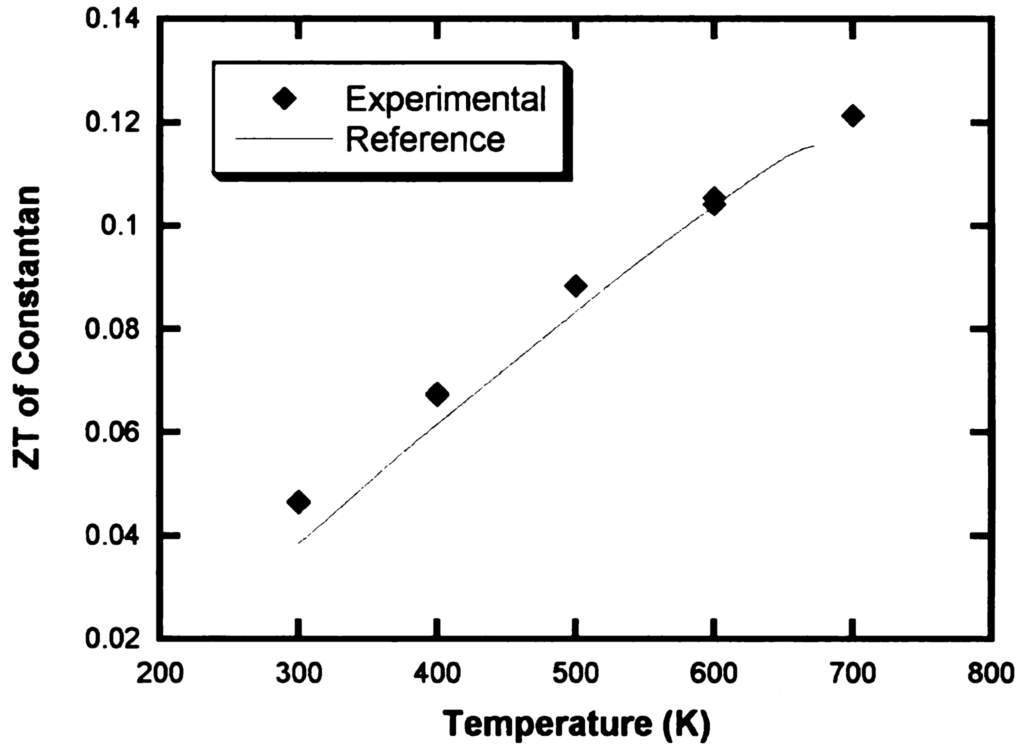

Figure 10-17: Experimental results for measuring ZT of constantan

Chapter 11: Rapid ZT Measurements

11.1 Introduction

ZT measurements using the AC impedance sweep requires measurements at very low frequencies. If the samples are too long or have too large of a thermal conductivity and thermal capacitance, this can cause the frequency range of the experiment to be below the range of the measuring equipment. This section will discuss the option of changing the sample dimensions in order to shift the frequency range up to a high range. This will not only help the measurement equipment, but it will also help speed up the measurement time by not requiring as low of a frequency measurement.

Frequency shifting will be helpful for rapid ZT measurements, however, there is still more that can be done to increase the speed of a ZT measurement. One possibility is to measure ZT based on the phase of the impedance alone. This section will describe how the phase of the impedance can be used to calculate ZT. Furthermore, it will show how the maximum phase angle of the impedance over the appropriate frequency range can also be used to calculate ZT. If measurements are measured at this frequency of maximum phase angle only, the time required for ZT measurements can be dramatically decreased.

11.2 Frequency Shifting by Sample Dimensions

Measuring the ZT of thermoelectric materials requires very low frequency measurements. This is due to the fact that TE materials have very low thermal conductivity values. When measuring a large commercially available thermoelectric module such as one from Tellurex, the alumina plates on the module account for most of the heat capacitance and this also lowers the frequency required to measure the impedance. It is approximately the product of the thermal resistance and the thermal capacitance of the module that determines the frequency range need for the measurement. A potential way to increase the frequency range of a Tellurex module would be to remove the Alumina plates. When measuring single pellets, unicouple, or multicouple modules made at MSU, it is the thermal resistance and thermal capacitance of the material that drives the frequency range. In this case, the sample dimensions can be altered to increase the frequency range of the impedance to a more time saving range. To simplify this analysis, a lumped element model will be used for the single pellets. This allows for calculations to be made using the RC one-port method. The results from this analysis will be good enough to describe how the frequency range can be shifted up so that measurements can be made faster. In some cases, this will also help to keep the range in a workable range for the measurement equipment.

It has been shown for the RC One-Port model that for the circuit shown in Figure 7-1, R_1 depends on the thermal resistance, thermopower, and the ambient temperature, while C_1 depends on the heat capacitance, thermopower, and ambient temperature shown here.

$$C_1 = \frac{C_{Thermal}}{\alpha^2 \cdot T_{avg}} \qquad R_1 = \alpha^2 \cdot T_{avg} \cdot R_{Thermal} \tag{11.157}$$

The pole of the impedance function, ω_p, determines the approximate lower frequency point where measurements at frequencies lower than this point should give a constant value for the magnitude of the impedance. The pole is related to R_1 and C_1 as shown here and can also been shown that it is simply related to the thermal resistance and heat capacitance of the material.

$$\omega_p = \frac{1}{R_1 \cdot C_1} \quad \text{(rad/s)}$$

$$= \frac{1}{\alpha^2 \cdot T_{avg} \cdot R_{Thermal} \cdot \dfrac{C_{Thermal}}{\alpha^2 \cdot T_{avg}}} \tag{11.158}$$

$$\omega_p = \frac{1}{R_{Thermal} \cdot C_{Thermal}} \quad \text{(rad/s)} \tag{11.159}$$

In order to make sure that a sample can be measured in the frequency range of the measurement equipment, the sample dimensions can be adjusted to increase ω_p.

Thermal resistance depends on the length and cross sectional area of the sample while heat capacitance depends on the volume of the sample. Figure 11-1 shows an example of the effects on changing the sample size where we let r be the thermal conductivity and c be heat capacity. The product of thermal resistance and heat capacitance of the sample is examined. Figure 11-1 (a) and (b) show that changing the cross sectional area of the material does not change the time constant, τ. However, when the sample length is reduced, as shown in Figure 11-1 (c), the τ is dramatically reduced. The equation below shows that τ is inversely related to the square of the length of the sample. Therefore, reducing the sample length in half will increase the frequency by four.

$$
\begin{aligned}
\tau &= \frac{1}{R_{\text{Therm}} \cdot C_{\text{Therm}}} \\
&= \frac{1}{\left(r \cdot \dfrac{\text{length}}{\text{width} \cdot \text{thickness}}\right) \cdot (c \cdot \text{length} \cdot \text{width} \cdot \text{thickness})} \\
&= \frac{1}{r \cdot c \cdot (\text{length})^2}
\end{aligned}
\tag{11.160}
$$

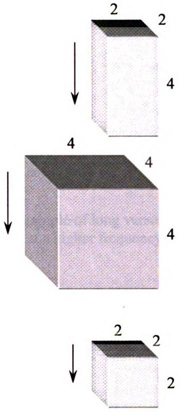

(a)

$$
\begin{aligned}
R_{\text{Therm}} &= r \cdot \frac{\text{length}}{\text{area}} = r \cdot \frac{4}{2 \cdot 2} \\
C_{\text{Therm}} &= c \cdot \text{volume} = c \cdot 2 \cdot 2 \cdot 4 \\
\tau_a &= R_{\text{Therm}} \cdot C_{\text{Therm}} = 16rc
\end{aligned}
$$

(b)

$$
\begin{aligned}
R_{\text{Therm}} &= r \cdot \frac{\text{length}}{\text{area}} = r \cdot \frac{4}{4 \cdot 4} \\
C_{\text{Therm}} &= c \cdot \text{volume} = c \cdot 4 \cdot 4 \cdot 4 \\
\tau_b &= R_{\text{Therm}} \cdot C_{\text{Therm}} = 16rc
\end{aligned}
$$

(c)

$$
\begin{aligned}
R_{\text{Therm}} &= r \cdot \frac{\text{length}}{\text{area}} = r \cdot \frac{2}{2 \cdot 2} \\
C_{\text{Therm}} &= c \cdot \text{volume} = c \cdot 2 \cdot 2 \cdot 2 \\
\tau_c &= R_{\text{Therm}} \cdot C_{\text{Therm}} = 4rc
\end{aligned}
$$

Figure 11-1: Adjusting sample dimensions to change the frequency range of the impedance.

If TE materials are improved by reducing the thermal conductivity, sample sizes will need to be smaller in order to keep the dynamic impedance behavior within the frequency range of the measurement equipment. The limiting factor with this will be placing voltage probes along the length of the sample without interfering with each other for a four-point measurement.

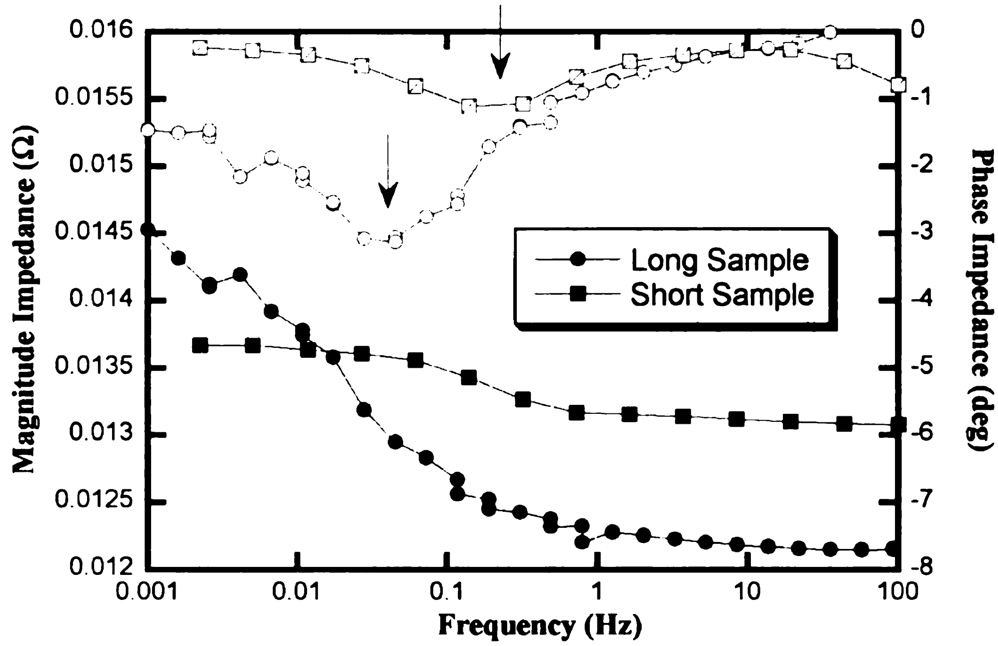

Figure 11-2: Example of long versus a short sample showing that the minimum phase occurs at a higher frequency of a short sample versus a long sample.

11.3 Phase Angle with Simple RC Circuit

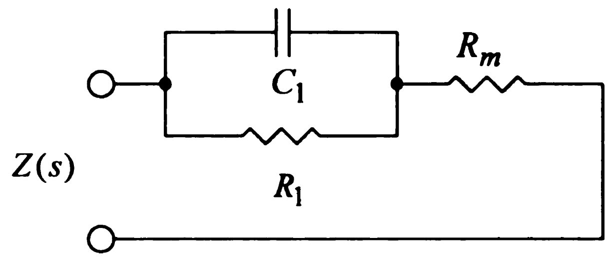

Figure 11-3: RC circuit

The evaluation of using the phase of the impedance begins by looking at a simple RC circuit that was used in the RC One-Port method. The real and imaginary components of the impedance have been solved for in a previous chapter and the result is shown again here.

$$\begin{aligned} Z(s) &= \frac{(R_1 \cdot C_1)^2 \cdot R_m \cdot \omega^2 + R_m + R_1}{(R_1 \cdot C_1)^2 \cdot \omega^2 + 1} + j \cdot \frac{-R_1^{\,2} \cdot C_1 \cdot \omega}{(R_1 \cdot C_1)^2 \cdot \omega^2 + 1} \\ &= \mathrm{Re}[Z(s)] + j \cdot \mathrm{Im}[Z(s)] \end{aligned} \tag{11.161}$$

The phase of the impedance can now be found using the arctangent of the imaginary components divided by the real components, which are shown below.

$$\begin{aligned} \theta(s) &= \tan^{-1}\left(\frac{\mathrm{Im}[Z(s)]}{\mathrm{Re}[Z(s)]}\right) \\ \theta(\omega) &= \tan^{-1}\left(\frac{\dfrac{-R_1^{\,2} \cdot C_1 \cdot \omega}{(R_1 \cdot C_1)^2 \cdot \omega^2 + 1}}{\dfrac{(R_1 \cdot C_1)^2 \cdot R_m \cdot \omega^2 + R_m + R_1}{(R_1 \cdot C_1)^2 \cdot \omega^2 + 1}}\right) \\ &= \tan^{-1}\left(\frac{-R_1^{\,2} \cdot C_1 \cdot \omega}{(R_1 \cdot C_1)^2 \cdot R_m \cdot \omega^2 + R_m + R_1}\right) \end{aligned} \tag{11.162}$$

Now that the phase of the impedance function is found in terms of frequency, the minimum phase (absolute maximum phase angle) can be found by taking the derivative of the phase function and solving for where it equals zero.

$$\begin{aligned} \frac{d}{d\omega}\theta(\omega) &= \frac{d}{d\omega}\tan^{-1}\left(\frac{-R_1^{\,2} \cdot C_1 \cdot \omega}{(R_1 \cdot C_1)^2 \cdot R_m \cdot \omega^2 + R_m + R_1}\right) \\ &= \frac{R_1^{\,2} \cdot C_1 \cdot \left(R_m \cdot \omega^2 \cdot R_1^{\,2} \cdot C_1^{\,2} - R_m - R_1\right)}{\left\{\begin{matrix} R_m^{\,2} \cdot (\omega \cdot R_1 \cdot C_1)^4 + 2 \cdot (R_m \cdot \omega \cdot R_1 \cdot C_1)^2 + 2 \cdot R_m \cdot \omega^2 R_1^{\,3} \cdot C_1^{\,2} + R_m^{\,2} + \ldots \\ 2 \cdot R_m \cdot R_1 + R_1^{\,2} + \omega^2 \cdot R_1^{\,4} \cdot C_1^{\,2} \end{matrix}\right\}} \end{aligned} \tag{11.163}$$

Finding where the derivative equals zero is as follows:

$$\frac{d}{d\omega}\theta(\omega) = 0 \rightarrow \left(R_m \cdot \omega^2 \cdot R_1{}^2 \cdot C_1{}^2 - R_m - R_1\right) = 0 \tag{11.164}$$

Now the frequency that will give the absolute maximum phase angle can be solved for and is shown here.

$$\omega_{|\theta|\max} = \sqrt{\frac{R_1 + R_m}{R_m \cdot R_1{}^2 \cdot C_1{}^2}} \tag{11.165}$$

Applying this result back into the phase function will give the solution for the absolute maximum phase.

$$\theta\left(\omega_{|\theta|\max} = \sqrt{\frac{R_1 + R_m}{R_m \cdot R_1{}^2 \cdot C_1{}^2}}\right) = |\theta|_{\max} = \tan^{-1}\left(\frac{-R_1{}^2 \cdot C_1 \cdot \sqrt{\frac{R_1 + R_m}{R_m \cdot R_1{}^2 \cdot C_1{}^2}}}{(R_1 \cdot C_1)^2 \cdot R_m \cdot \frac{R_1 + R_m}{R_m \cdot R_1{}^2 \cdot C_1{}^2} + R_m + R_1}\right)$$

$$|\theta|_{\max} = -\tan^{-1}\left(\frac{1}{2} \cdot \sqrt{\frac{R_1{}^2}{R_m \cdot (R_1 + R_m)}}\right) \tag{11.166}$$

The above equation can be rewritten to find $|\theta|_{\max}$ in terms of *ZT* where ZT has been shown to be

$$ZT = \frac{R_1}{R_m} \tag{11.167}$$

Using this ZT, we find the magnitude

$$
\begin{aligned}
|\theta|_{\max} &= -\tan^{-1}\left(\frac{1}{2}\cdot\sqrt{\frac{R_1{}^2}{R_m\cdot(R_1+R_m)}}\right) \\
&= -\tan^{-1}\left(\frac{1}{2}\cdot\sqrt{\frac{R_1{}^2}{R_m{}^2\cdot\left(\frac{R_1}{R_m}+1\right)}}\right) \\
&= -\tan^{-1}\left(\frac{1}{2}\cdot\sqrt{\frac{ZT^2}{(ZT+1)}}\right) \\
&= -\tan^{-1}\left(\frac{1}{2}\cdot ZT\cdot\sqrt{\frac{1}{(ZT+1)}}\right)
\end{aligned}
\tag{11.168}
$$

A computer math program was used, such as MathCAD, to solve the above equation to give:

$$
ZT = -2\cdot\tan\left(|\theta|_{\max}\right)\cdot\left[-\tan\left(|\theta|_{\max}\right)\pm\sqrt{\tan^2\left(|\theta|_{\max}\right)+1}\right] \tag{11.169}
$$

Since ZT is not a negative quantity, we can neglect one of the terms above to give:

$$
ZT = -2\cdot\tan\left(|\theta|_{\max}\right)\cdot\left[-\tan\left(|\theta|_{\max}\right)+\sqrt{\tan^2\left(|\theta|_{\max}\right)+1}\right] \tag{11.170}
$$

Now ZT has be solved in terms of $|\theta|_{\max}$. If one is measuring the circuit shown in Figure 11-3 which is similar to the circuit model of the Tellurex module, one only needs to locate the absolute maximum phase and take a measurement at this frequency. Of course, the first time a thermoelectric module is tested, a full frequency sweep would be desired which can take several hours. But once a module has been characterized and the frequency of absolute maximum phase angle can be approximated, only a few measurements about this point will be needed, which might only take several minutes instead of hours. A plot is provided to show ZT versus maximum absolute phase angle in Figure 11-4.

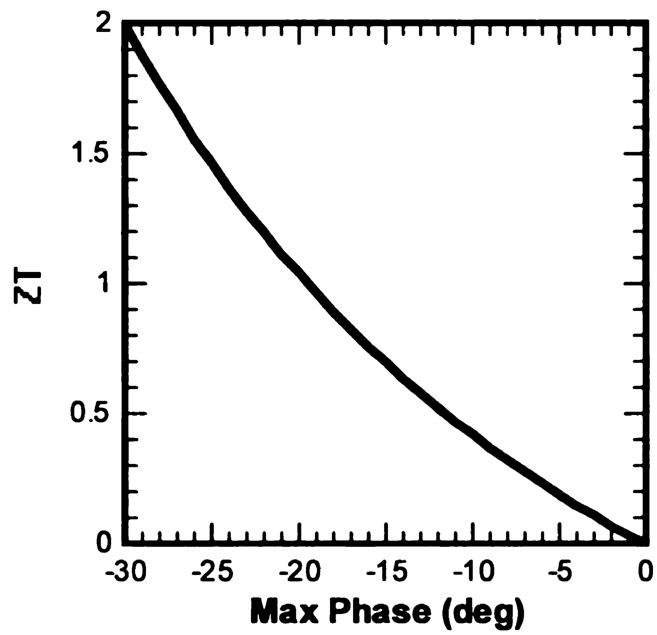

Figure 11-4: ZT versus max absolute phase angle for RC circuit equivalent

11.4 Phase Analysis for Thermal TLINE model

Many thermoelectric devices do not behave exactly like the simple RC circuit such as single pellets, unicouples, and modules with only a few couples. These devices behave more like the Thermal TLINE model. In this case, the absolute maximum phase angle cannot be used to determine the ZT directly. The following will show why.

Three different measurements where simulated using LabVIEW where all three samples would have the same ZT value. The first was a sample that exhibited the circuit shown in Figure 11-3. The second and third were samples that behaved like the conditions explained in the thermal transmission line model (TTLM) where the measurement probes were at the ends of the sample and with the measurement probes not at the ends of the sample respectively. It can be shown by computer simulations that plotting the phase versus frequency indicates that each measurement has a different absolute maximum phase angle. The sample with the probes at the end with TTLM characteristics shows the least maximum absolute phase angle. Next in order is the sample representing the RC-circuit. The sample with the highest maximum absolute phase angle is the one with the probes not at the ends of the sample. The frequency at this maximum absolute phase angle is not of interest at this point because this does not influence the ZT of the material. It can also be shown that after plotting the phase versus log frequency (Figure 11-6) for the three measurements, the area under the curves for all three measurements is approximately equal for a given ZT value. The exact areas under the curves for the transmission line circuits could not be found because values used in the simulation become large enough that they reach the limitation of the software.

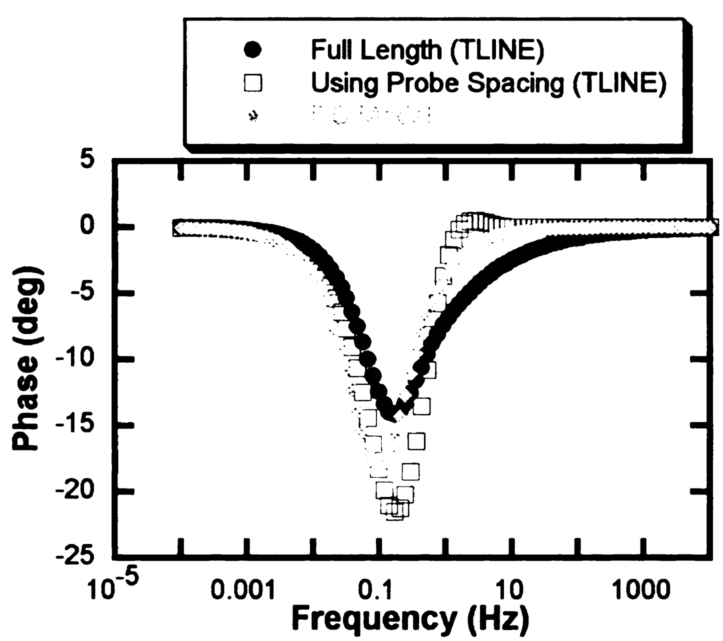

Figure 11-5: Phase versus Frequency. Absolute maximum phase angle is different for the three measurements even though the ZT value is the same.

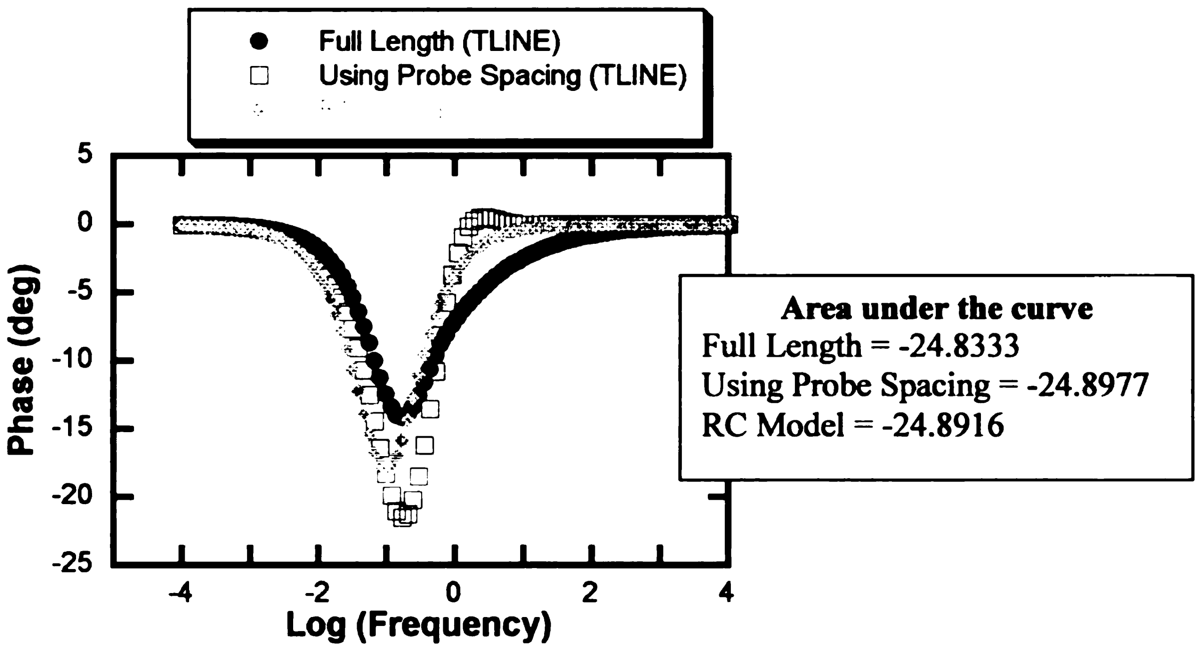

Figure 11-6: Phase versus Log Frequency. Area under the curve for all three cases is approximately equal for a given ZT value.

11.4.1 Area Under the Phase Plot

What is the area under the curve? Since the areas for all three cases appear to be approximately equal, only mathematically calculate the area under the curve to the RC circuit. This will prove to me much simpler than the calculations using transmission line theory. First, start with the equations for the magnitude and phase of the RC circuit.

$$|Z(\omega)| = \frac{\omega_z}{\omega_p} \cdot R \cdot \frac{\sqrt{1+\left(\frac{\omega}{\omega_z}\right)^2}}{\sqrt{1+\left(\frac{\omega}{\omega_p}\right)^2}} \tag{11.171}$$

$$Z_{phase}(\omega) = \tan^{-1}\left(\frac{\omega}{\omega_z}\right) + \tan^{-1}\left(\frac{-\omega}{\omega_z}\right) \tag{11.172}$$

$$\omega_p = \frac{1}{R_1 \cdot C_1}$$

$$\omega_z = \frac{R_1 + R_m}{R_1 \cdot R_m \cdot C_1} \qquad (11.173)$$

Integrating the phase with respect to the log of frequency can be very challenging. However, the use of standard techniques for plotting magnitude and phase as shown below in a Bode plot can be employed. In such plots, at low frequency values where the capacitance is considered to be open-circuit, the magnitude is a straight, horizontal line. This line continues up until the frequency of the pole. At this point, the line bends downward at a slope of -20dB/decade. This continues until the line reaches the frequency of the zero. At this point, the capacitor is considered to be short-circuited which gives a constant magnitude as frequency increases. The phase can be separated into two plots (one for pole and one for the zero) that will be added together to get the final result. The first plot of phase will look at the pole of the impedance function. Starting from low frequencies, the phase begins at an angle of 0°. Then at one decade before the pole of the impedance function, the angle decreases at a rate of -45°/decade. This line will continue until it reaches one decade past the zero of the impedance function where it will level off at -90°. The second plot is of the zero of the impedance function where again it starts at 0° at the low frequencies. When the frequency reaches one decade before the zero of the impedance function, the phase angle increases at a rate of 45°/decade. The phase will increase until one decade past the zero of the impedance function is reached where it will remain at 90°. The addition of the two plots is then highlighted and shown in Figure 11-7. For this particular example, the phase made an isosceles triangle. This does not have to be the shape. It could turn out to be a trapezoid.

It should also be noted here that this technique is simply an approximation to the actually phase and magnitude but it should still help in the understanding and calculation of the area under the phase versus log frequency plot.

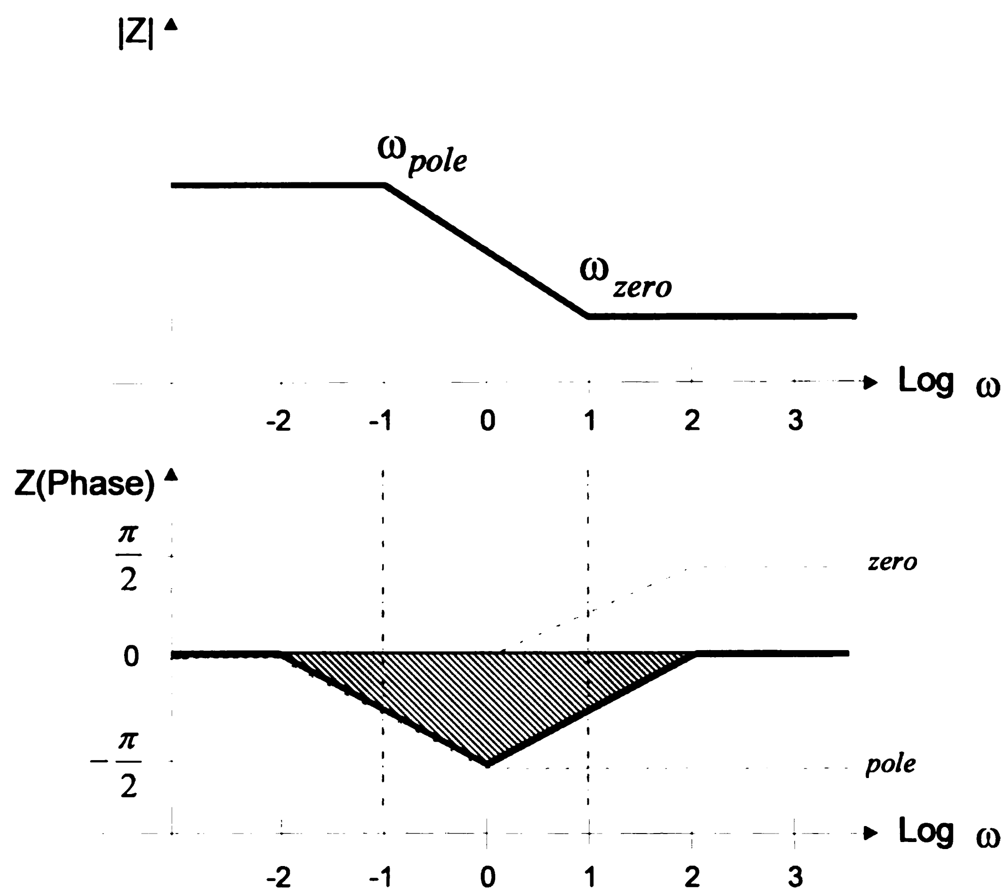

Figure 11-7: Phase and Magnitude plots versus log frequency

From Figure 11-7, the area under the phase plot can visually be calculated, which is shown here.

$$\begin{aligned} Area &= -\left[\log(\omega_p) - \log(\omega_z)\right] \cdot \frac{\pi}{2} \\ &= -\frac{\pi}{2} \cdot \log\left(\frac{R_1 + R_m}{R_m}\right) \end{aligned} \tag{11.174}$$

From the plots shown and the equation above, it is clear that the area is independent of log frequency and the thermal capacitance.

11.4.2 Applying a Correction to the Absolute Maximum Phase for ZT Calculations

The equation for the area can then be used to correct for the maximum phase angle. This is accomplished by first collecting a full frequency sweep across the sample to get a ZT value which identifies the values for R_l and R_m. This full sweep will also identify the maximum absolute phase angle. Because the integration of phase with respect to log frequency is the same for RC circuit model and the Thermal transmission line model, the theoretical maximum phase angle can be calculated for the sample as if it were behaving like the RC circuit model. To correct the phase so that the formula for finding ZT using the phase for the RC circuit model can be used. Let X be a correction factor to the measured phase.

$$X = \frac{|\theta|_{\max_{\text{RC model}}}}{|\theta|_{\max_{\text{TTLM}}}} \tag{11.175}$$

So that

$$|\theta|_{\text{measured}} \cdot X = |\theta|_{\text{corrected}} \tag{11.176}$$

Now the formula for ZT can be used as follows.

$$ZT\left(|\theta|_{\text{corrected}}\right) = -2 \cdot \tan\left(|\theta|_{\text{corrected}}\right) \cdot \left[-\tan\left(|\theta|_{\text{corrected}}\right) + \sqrt{\tan^2\left(|\theta|_{\text{corrected}}\right) + 1} \right] \tag{11.177}$$

Now the maximum phase can again be used to find the ZT of the sample.

Chapter 12: Measuring Resistance of a TE Module using Alternating Digital Pulses at Various Frequencies

12.1 Introduction

The modified Harman technique has shown that finding the AC resistance and DC resistance of a TE module can be used to find the *ZT* of the module. A commercially available Z-meter has been developed by RMTLTD [62] that uses a high frequency digital square wave signal for the AC resistance and a low frequency digital square wave signal for the DC resistance of the module. My investigations have been performing a full frequency sweep of the module using a single harmonic sine wave. This technique requires the use of lock-in amplifiers for identifying the magnitude and phase of the impedance and can take a considerable amount of time to perform the experiment. Here, the investigation is to examine the resistance of the module using alternating digital pulse (50% duty cycle) at various frequencies and to learn under what conditions this technique can be used for obtaining the *ZT* of the module.

Pulsing the current through the sample will introduce harmonic frequencies into the module, which may affect the measurement. This method of measuring resistance will not include the phase of the impedance. This section will explain the experimental setup, the automated data collection program, and the results of the experiments. Finally, the results will show that using digital square wave signals can be used to obtain the *ZT* of thermoelectric materials under certain conditions.

12.2 Automated Program

The experiment uses a commercially available TE module for power generation and is utilized at room temperature. Measurements where taken for the module exposed to atmosphere as well as in a high vacuum environment. A four-point probe method was used for the resistance measurement.

The experiment uses the same technique that is used to measure electrical conductivity of the TE samples already discussed where a digital current source is flipped positive and negative at a high frequency. Before each flip of the current source, the voltage across the module is recorded and used for the calculation of resistance. Here, the modification of this process is that the duration of the current pulse is increased to create a lower frequency of flipping. This is accomplished by placing a delay (in seconds) between when the current pulse is switched, and when the voltage is measured. Immediately after the voltage is measured, the current source is flipped and the procedure is repeated. A part of this work, a LabVIEW program was created to perform this experiment which interfaced with a Keithley 2400 current source and a Keithley 2182 nanovolt meter. The front panel to the user interface of the LabVIEW program is shown in Figure 12-1. This program allows the user to enter the amplitude of the current, the set of delay values, and the number of measurements for each set of delay values. It then records the calculated resistance value of the module at each frequency. It is important to note that although exact delay values where used, there were additional delays from the measurement equipment that were not taken into account. Therefore, the exact frequencies are not precisely know for this experiment and only trends in the data from high to low frequencies should be examined.

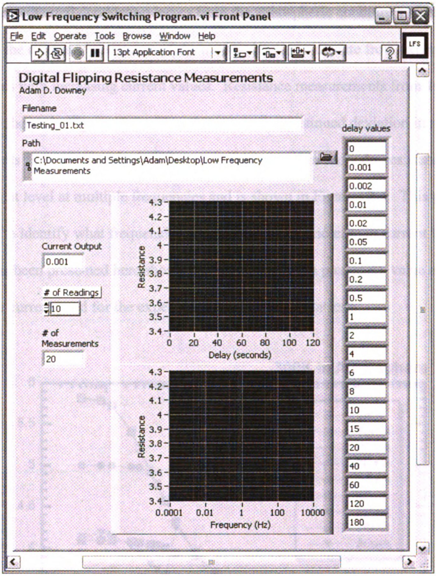

Figure 12-1: Front panel view of LabVIEW program for automated data collection of the resistance of the TE module for various frequencies.

12.3 Room Temperature Measurements in Atmosphere

Experiments on the module were done at room temperature in atmospheric conditions. Figure 12-2 shows a plot of the measured resistance versus frequency for multiple current values (1mA - 80mA). The expected results showing a ZT value of ~0.71 for this module are when electrical currents are lower than 30mA. The lower ZT value is due to thermal conduction losses from the atmospheric conditions. Between 30 and 40mA, the measured resistance of the module begins to deviate from expected results and increases with increasing current values. Resistance measurements from 100mA to 260mA are shown in Figure 12-3. This plot shows the continued deviation in resistance measurements from the expected results. A plot is created in show the resistance value versus current level at multiple frequencies and is shown in Figure 12-4. This plot is convenient to identify what frequencies are affected by the increase in current level. The data that has been presented here shows that in order to get a proper ZT value of the module, the current used for the experiment must be 30mA or less.

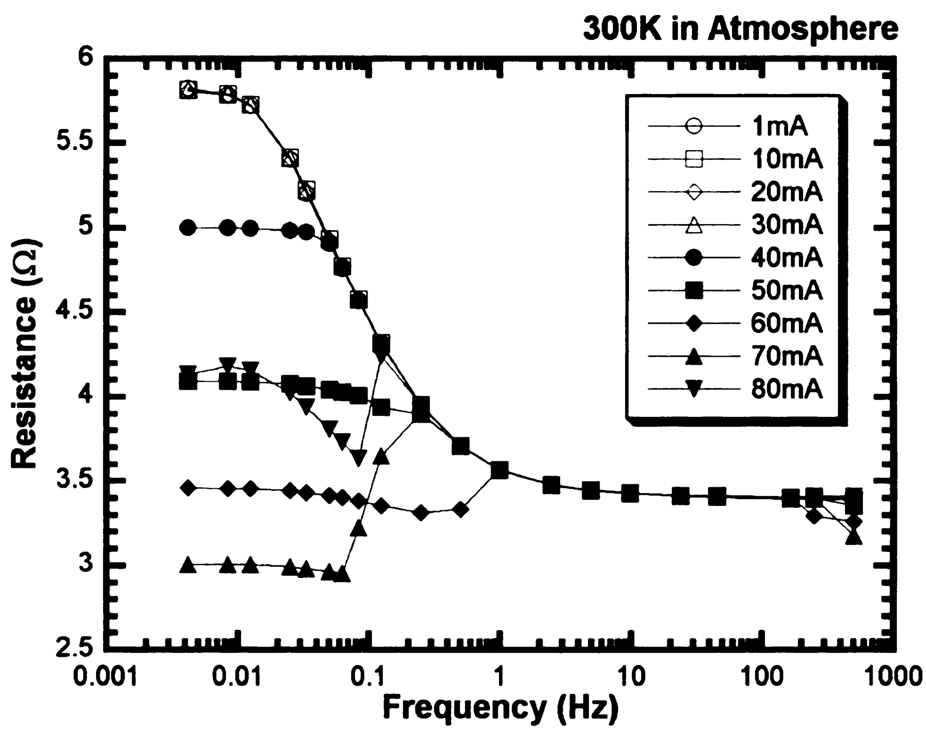

Figure 12-2: Plot showing resistance measurements of a module in atmosphere using multiple current values (1mA - 80mA).

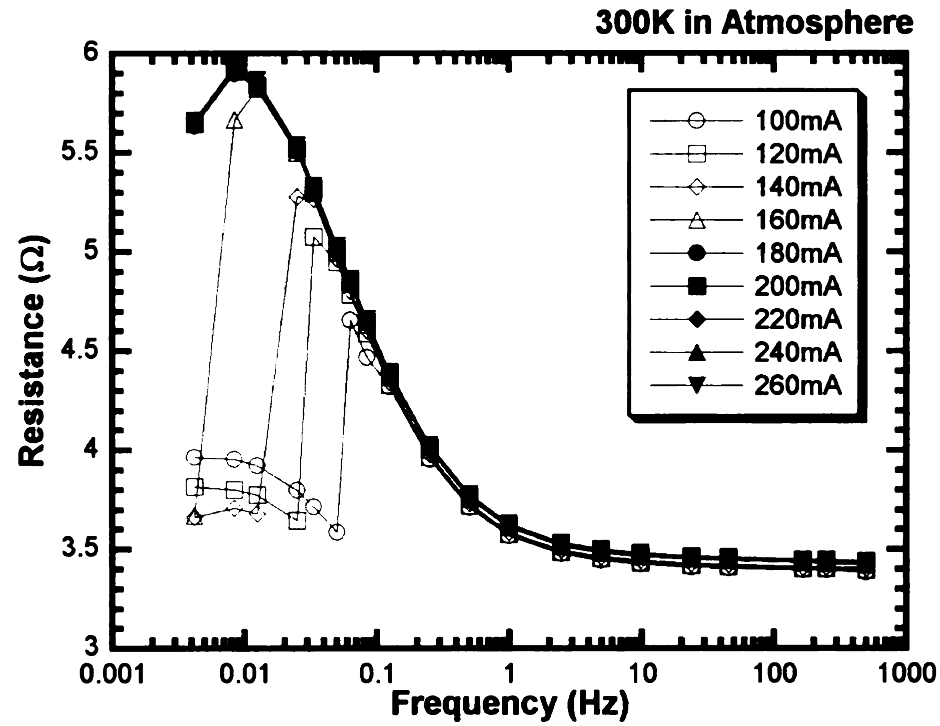

Figure 12-3: Plot showing resistance measurements of a module in atmosphere using multiple current values (100mA - 260mA).

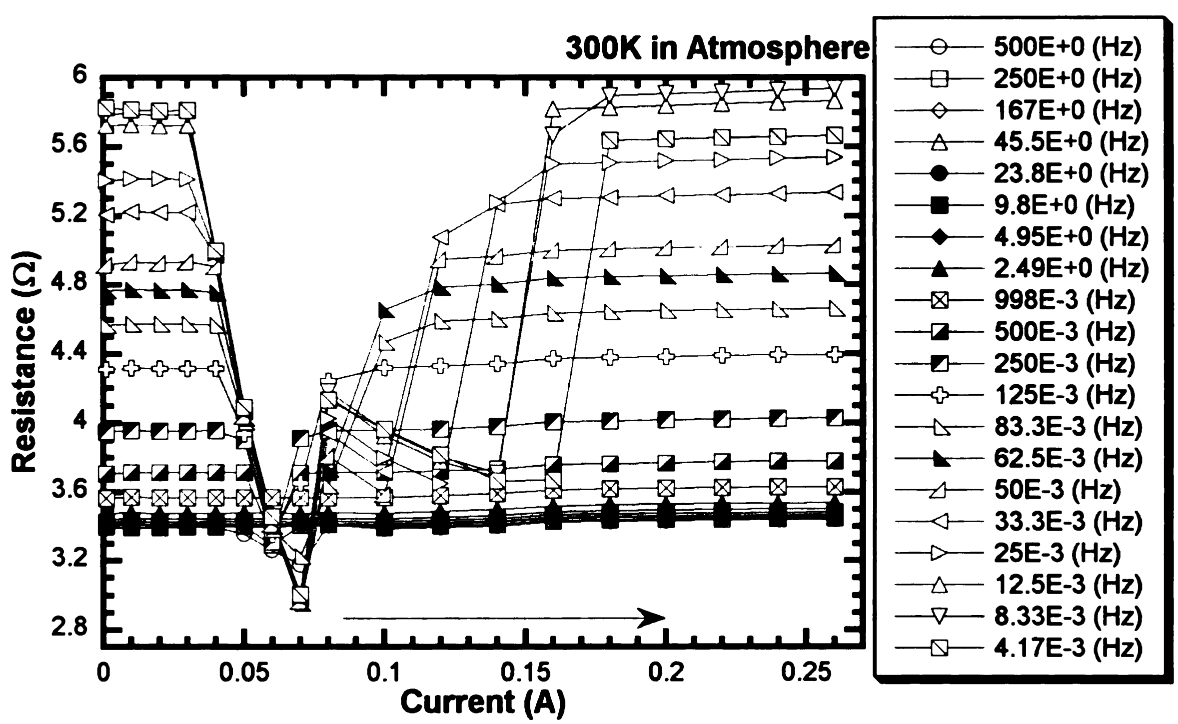

Figure 12-4: Plot showing resistance measurements of a module in atmosphere at each frequency versus multiple current values (1mA - 260mA).

12.4 Room Temperature Measurements in High Vacuum

The same experiment was repeated on the module except in this case; the module is place in a high vacuum environment (1×10^{-6} Torr). This time, the measured ZT of the module is ~0.77. This is in good agreement with expected ZT of this power generation device at room temperature. This ZT value can be clearly identified using currents up to 50mA as shown in Figure 12-5 and Figure 12-7. Using current levels higher than 50mA results in a deviation in the resistance plot from expected values as shown in Figure 12-6. Again, a plot of resistance versus current for multiple frequencies is created to show the behavior of the resistance for the module using currents up to 500mA (Figure 12-8). The data presented here shows that accurate ZT measurements can be made when current values are 50mA or less.

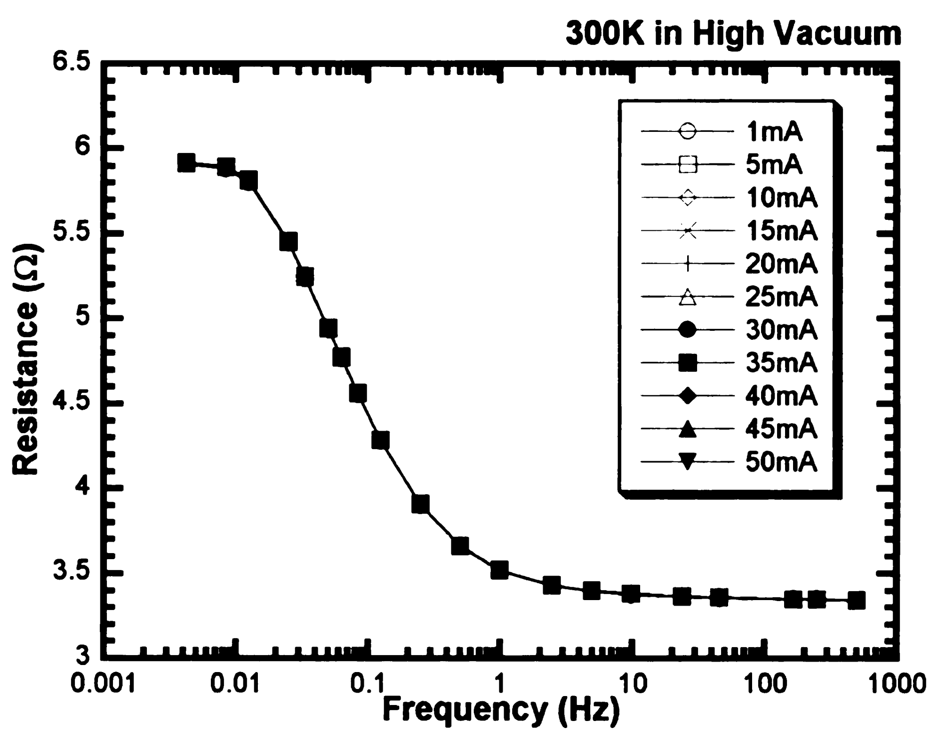

Figure 12-5: Plot showing resistance measurements of a module in high vacuum using multiple current values (1mA - 50mA).

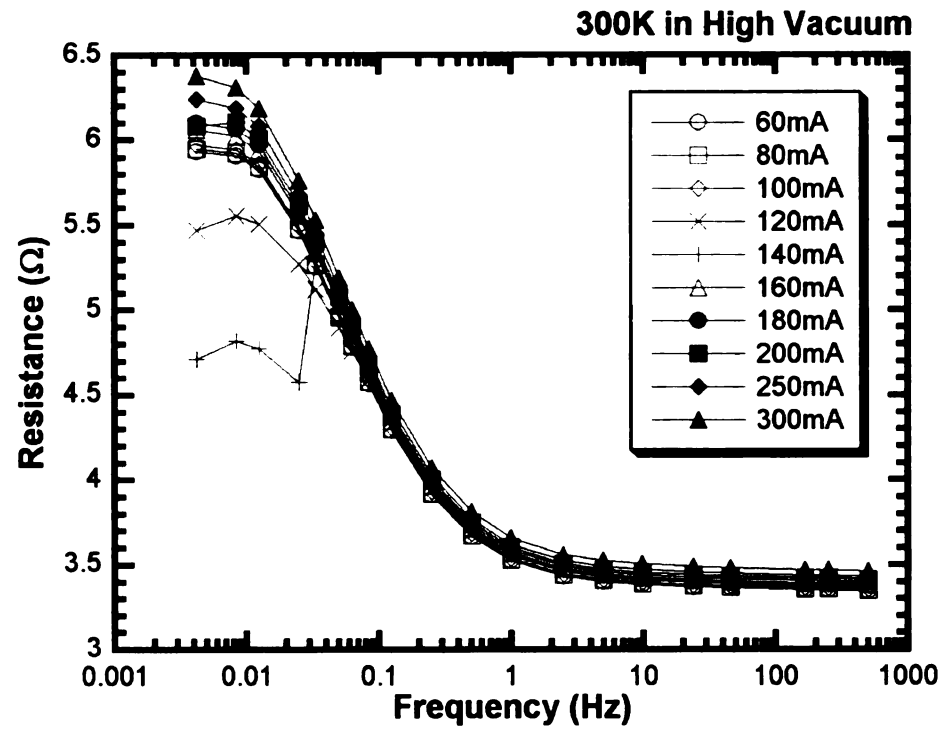

Figure 12-6: Plot showing resistance measurements of a module in high vacuum using multiple current values (60mA - 300mA).

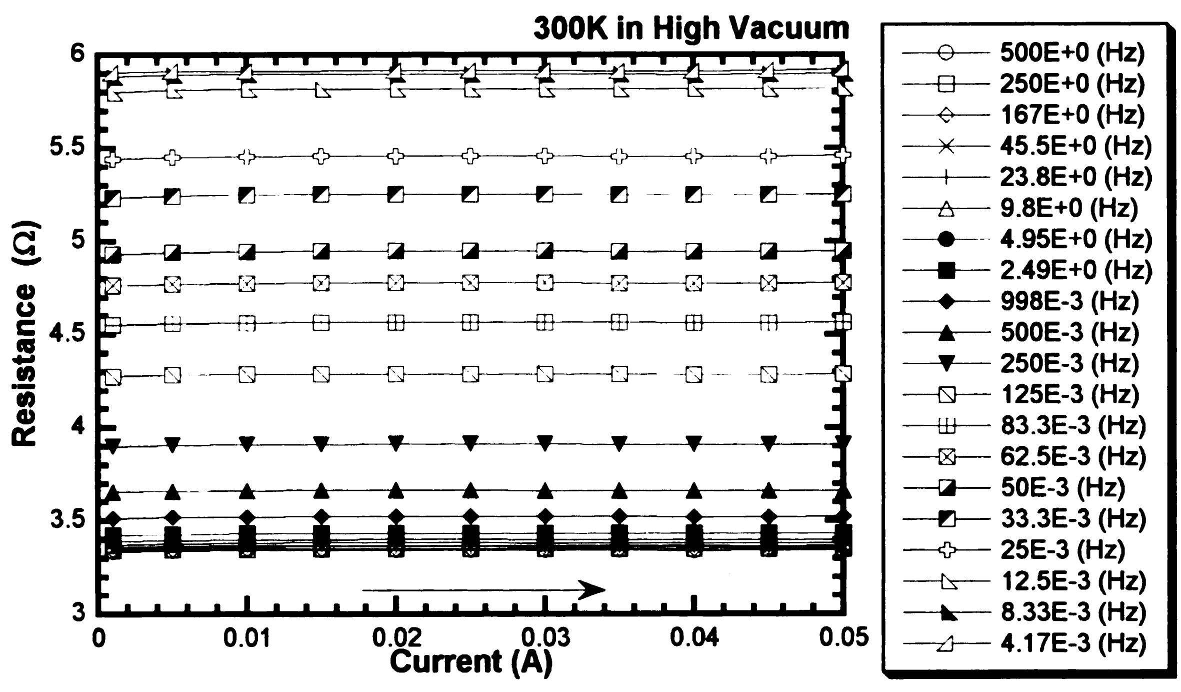

Figure 12-7: Plot showing resistance measurements of a module in high vacuum at each frequency versus multiple current values (1mA - 50mA).

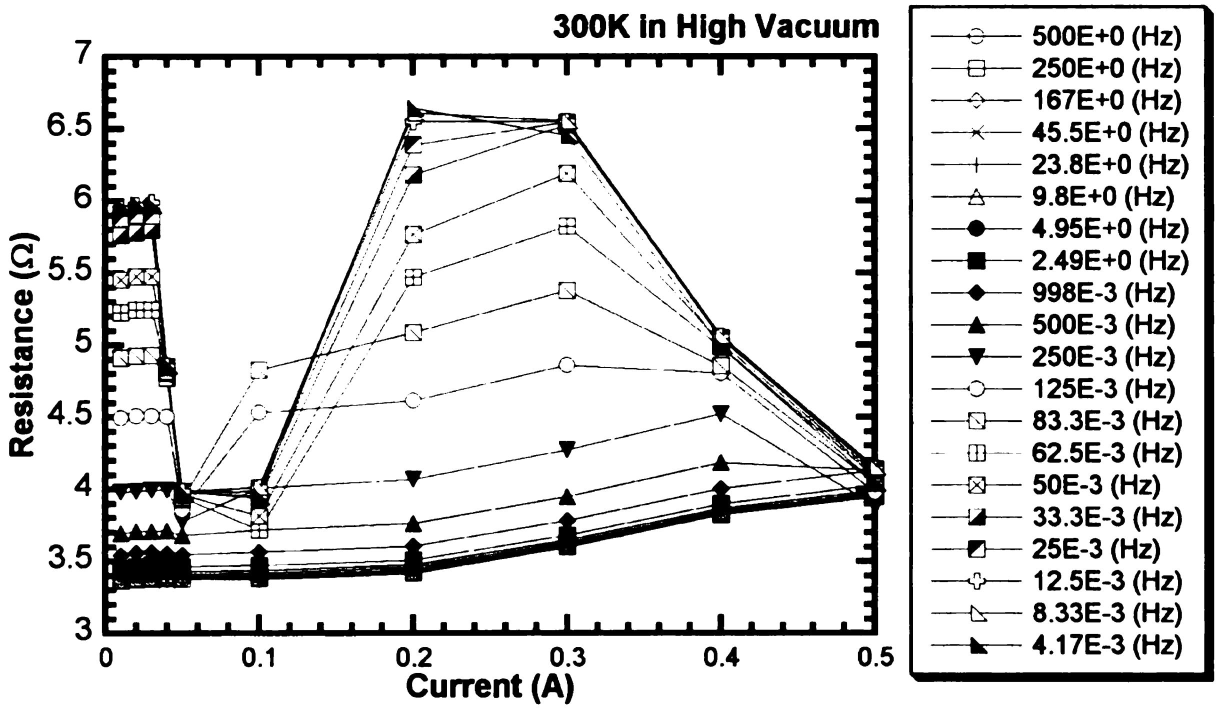

Figure 12-8: Plot showing resistance measurements of a module in atmosphere at each frequency versus multiple current values (1mA - 500mA).

12.5 Monitoring the Voltages

The voltages across the module was examined versus time for several frequencies and current levels to identify any unexplained behavior due to using digital square wave signals. Using a small current value of 10mA, three delays of 1, 2, and 15 seconds where tested and the results are shown in Figure 12-9, Figure 12-10, and Figure 12-11, respectively. These plots show expected behavior for the resistance of the module. For short delays, the Peilter effect does not contribute as much as for long delays. This can be seen in the plots where the voltages rises and falls exponentially are much more apparent for longer delay values. The jump in the voltage as the current is flipped is due to the finite resistance of the module. For larger current values such as 140mA and 500mA, the voltage behavior was also as expected (a jump with the current is flipped followed by an exponential rise or fall). There was no indication of noisy data to explain the results shown above where high current values affect the ZT measurement.

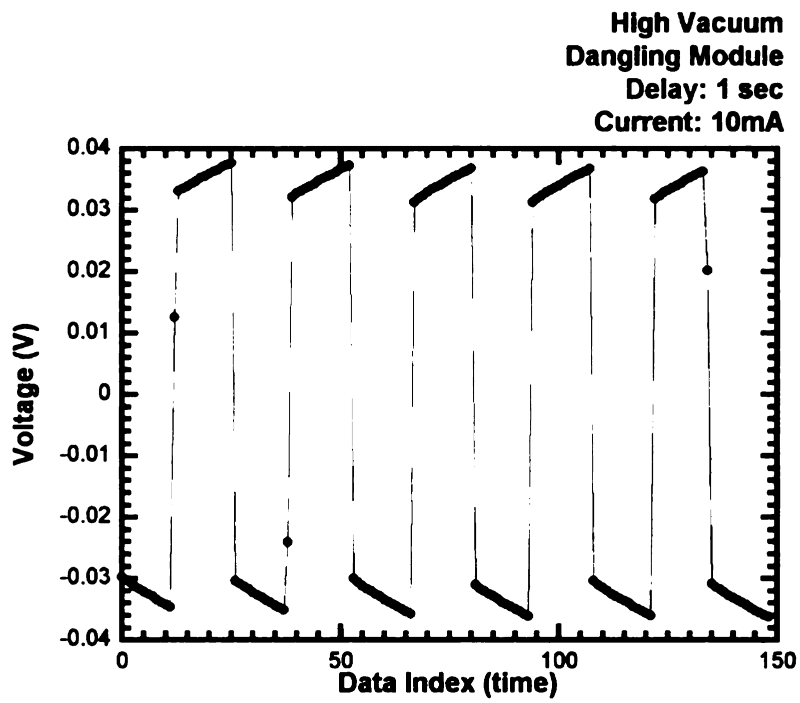

Figure 12-9: Plot of voltage versus time across TE module using a 1 second delay and 10mA.

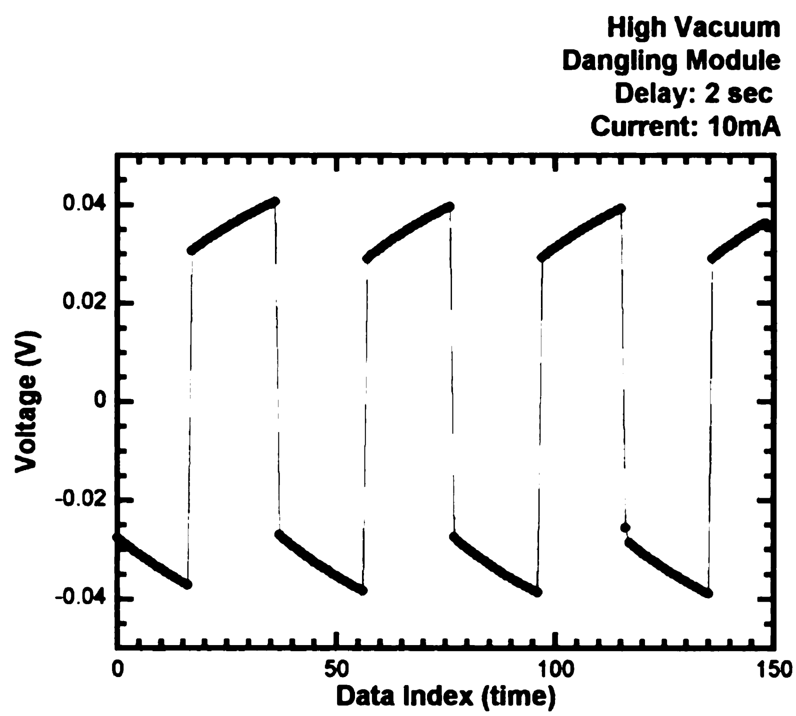

Figure 12-10: Plot of voltage versus time across TE module using a 2 second delay and 10mA.

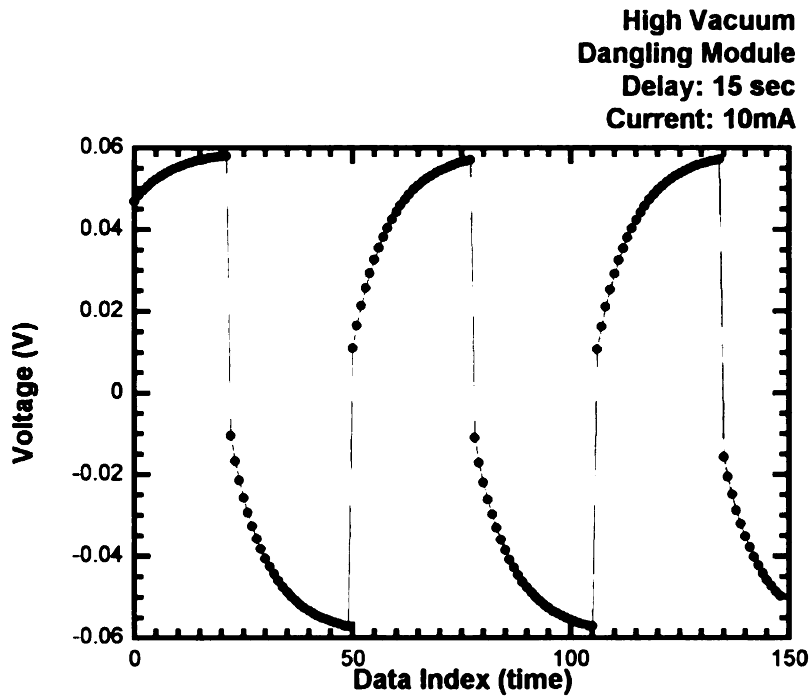

Figure 12-11: Plot of voltage versus time across TE module using a 15 second delay and 10mA.

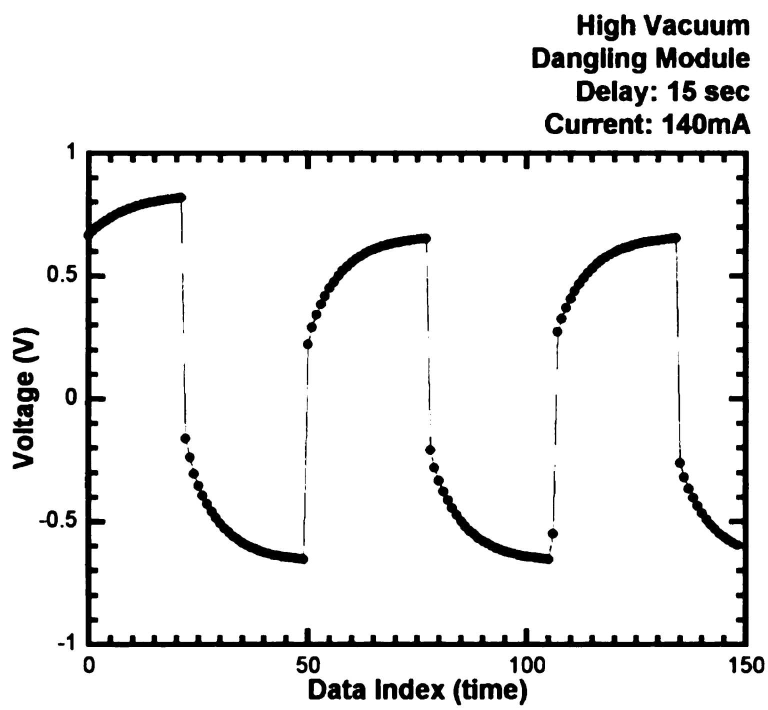

Figure 12-12: Plot of voltage versus time across TE module using a 15 second delay and 140mA.

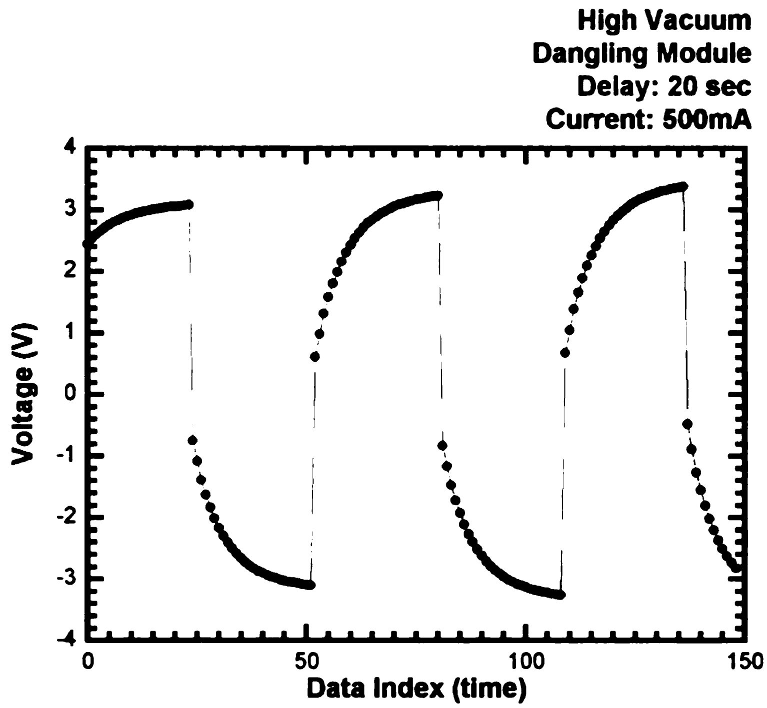

Figure 12-13: Plot of voltage versus time across TE module using a 20 second delay and 500mA.

12.6 Conclusion

Based on experimental evidence, it is viable to use a digital square wave current signal to obtain the ZT value. For measurements taken in atmosphere, there must be a correction factor applied to the ZT value obtained to account for thermal losses due to conduction and convection. For both high vacuum or atmospheric conditions, careful considerations must be made on the amplitude of the current used. Current values must be kept small. The errors in the resistance measurements for high current values are likely due to the Joule heating at the electrical contacts between to the TE material. By using small current levels, the effect of Joule heating is dramatically reduced ($Q = i^2 \cdot R$).

Chapter 13: ZT Machine

13.1 Introduction

In searching for the best thermoelectric material, many variables are present in the manufacturing process such as chemical composition, cooling rate profile, cold and hot pressing of the samples, environment conditions, etc. This leads to a vast number of samples being made in order to optimize each variable in the process. These process variables affect the strength of the materials, the brittleness, and of course the thermoelectric properties. In the beginning of large-scale production of the TE materials, the heating/cooling profiles along with chemical composition were changed to give samples that did not contain voids and cracks and were robust enough to handle for measurements. An example of a scaled up LAST material were cracking occurred is shown in Figure 13-1.

Figure 13-1: Picture of 100g ingot of LAST material sliced up into 5mm thick coins. This picture shows the cracking in the sample throughout the ingot and is affected by the cooling profile.

From this point, the materials are investigated for hardness and electrical conductivity. Based on typical measurements of good TE materials, higher electrical conductivity warrants higher ZT performance. For a given TE crystal structure, the thermal properties due to the crystal lattice will remain approximately the same for different doping levels.

The TE crystal can be doped with different concentrations of impurities to adjust the electrical conductivity. The Wiedemann-Franz Law states that the thermal properties due to the electrons increases linearly with increasing electrical conductivity. Because the thermal properties due to the crystal lattice remains constant for the multiple doping levels, the ZT of the material can increase with increasing electrical conductivity. Measurements on electrical conductivity alone are not enough to determine a trend in thermoelectric performance against the different variables. It is also possible that a brittle sample will outperform a strong, non-brittle sample. It has been determined that measurements of ZT at room temperature would be an important measurement to add to the existing one for screening out good TE materials from the bad. For example, based on previous measurements, a good n-type material for this project would have a ZT>0.2 at room temperature. Once this is achieved, the samples can then be measured for temperature dependant properties in other systems at MSU. In addition of measuring ZT, rapid measurements are needed to increase the throughput of TE development. For a full frequency sweep using lock-in amplifiers, it would typically take approximately 16 hours per sample to measure (not including sample mounting time). A faster method can be employed for measuring ZT because this ZT measurement does not have to be as accurate as the AC full frequency sweep. For this measurement, only a single low frequency measurement and a high frequency measurement is needed to calculate ZT. The transition from high to low frequency is not needed. The lock-in amplifiers can be removed from the measurement and replaced by a Keithely 2400 source meter and 2182 nanovolt meter. The lock-in amplifiers provided a large reduction in noise for the electrical measurement; however, removing the lock-amplifiers will allow many samples to be measured at the same time. By removing the lock-amplifiers and not performing a full frequency sweep, this system can measure 16 samples of LAST material (5mm x 5mm x 7mm) in less then 4 hours. Having this system meets a reasonable goal of screening approximately 30 samples per week. This will help in the development of manufacturing good TE materials by providing a fair amount of feedback to the developers.

This section will describe a new system at MSU for measuring the ZT and electrical conductivity of 16 TE material samples at one time. The method for the measurement will be explained along with a computer program overview. The assembled system will be shown and finally, example data is provided included data from a commercially available TE module that is used as a reference sample to verify the accuracy of the system.

13.2 Method of Measurement

This system uses an existing technique called the Modified Harman Technique [63]. This technique simply states that ZT can be found by measuring a high frequency resistance (R_{AC}) such that no temperature gradient is established and a low frequency resistance (R_{DC}) such that the electrical current is effectively DC. With these measurements, ZT is found as follows.

$$ZT = \frac{R_{DC}}{R_{AC}} - 1 \tag{13.178}$$

Previous impedance spectroscopy measurements on the TE materials have helped in the development of this system. For example, small copper wires can be used at room temperature to provide current to the sample and for the measurement probes as long as the wires have a much higher thermal resistance than the sample being measured. Using wires with low thermal resistance will reduce the accuracy of the ZT measurement. The wires connected to the ends of the sample must cover the entire end of the sample to insure a uniform electric field across the sample. The end contacts must also be a reasonably low thermal resistance. High resistance contacts, especially if one contact has a different resistance than the other, can cause an uneven joule heating at the contacts and again reduce the accuracy of the ZT measurement. Finally, AC measurements are needed to examine the transition from high frequency to low frequency resistance values so that the phase of the impedance can also be examined. However, for just looking at high frequencies and low frequency measurements where the resistance values do not change for a small change in frequency, a square pulse may be used. This is also based on experimental evidence. Experimentally, it has been found that using small electrical currents through the sample (~10mA) can provide a good ZT measurement. High current values (>100mA) have been found to give an error in the ZT measurement. It is extremely beneficial to use a square wave pulse for rapid ZT measurements. Using a square wave pulse for the current eliminates the need for the lock-in amplifier (assuming the signal to noise ratio is at a reasonable level). This also eliminates the time that the lock-in amplifier takes to "lock" on to the signal.

All 16 samples are connected electrically in series. Each sample is thermally isolated from each other by using long wires connected between the samples, which are mounted to a metal disk that acts as a thermal grounding point.

13.2.1 Mounting Current Leads

All of the 16 samples are mounted as shown in Figure 13-2. Copper wires that are about 3cm long are used to dangle the sample in a vacuum from a thermally grounded location. The wires going to the ends of the sample are first attached to a thin copper foil that covers the entire end of the sample. The copper foil is then soldered to the sample using "woods metal" solder.

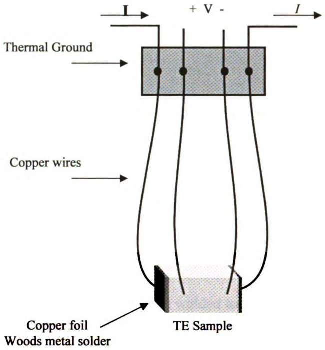

Figure 13-2: Diagram of TE sample mounted for ZT measurements

13.2.2 Mounting Voltage Probes

Resistive welding is being used to connect copper wire voltage probes to the TE materials for electrical conductivity measurements. This technique is very useful since it is fast, easy to precisely place a contact point, creates a very small contact, and makes a strong contact that will not fall off. An example of a resistive weld is shown in Figure

13-3, and Figure 13-4, and Figure 13-5. Other techniques of attaching voltage probes involves either soldering the wires to the sample, which is a little challenging to get a small solder spot, or by silver painting the wire to the sample, which is very difficult to get a strong bond without making the contact are large (~1-2mm). Figure 13-5 shows that the contact are is not much larger than the diameter of the wire. There is also no spill over like there can be with silver paint.

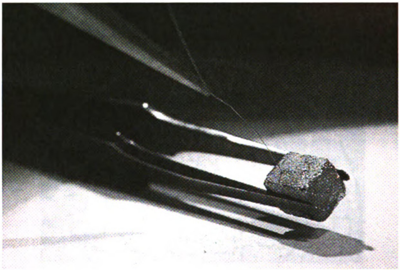

Figure 13-3: Copper wire (0.003" in diameter) welded to a LAST TE material (5mm x 5mm x 7mm)

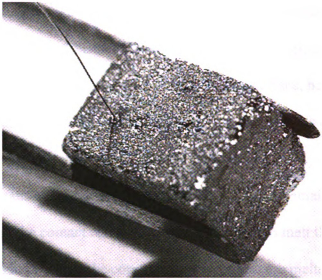

Figure 13-4: Close-up of Figure 13-3

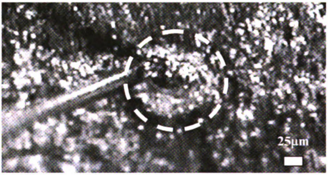

Figure 13-5: Microscopic image of copper wire welded to LAST sample showing the small size of the contact area

Resistance welding uses the resistance of the parts in the current path to generate heat energy for welding. Bulk resistance is a function of sample geometry and resistivity, which is a material property. Contact resistances occur at the contact between the electrode and the sample and normally includes the following two contributions: constriction resistance and film resistance. When two metal surfaces each with a certain roughness are brought into contact, the real contact are of the mutually deformed asperities is much smaller than the apparent area as long as the normal pressure is below the yield stress of the softer material. When a current runs through the interface, the current flow lines bundle together passing through the separated conducting spots of real contact. This constriction of the electric current by the contact spots reduces the volume of the metal used for electrical conduction locally at the interface, hence giving rise to a resistance named the constriction resistance. The film resistance is due to less-conductive surface films such as oxides, oil and water vapor, etc.

With a short pulse of electricity that comes from a commercial spark welder (HotSpot shown in), the contact resistance heats up enough to melt the thermoelectric material. With slight pressure, the copper wire moves into the melted material. When the pulse is done, the melted material cools and it bonded to the copper wire. It has been experimentally found that a 15-volt charge can be placed in line with the wire (0.003" diameter copper), the thermoelectric sample, and a 2-ohm resistor to get a good strong contact between the copper and the TE material.

Figure 13-6: HotSpot thermocouple welder

13.2.3 Measurement Process

The ZT Machine system is setup for two separate sets of measurements, the high frequency and the low frequency. For all measurements, the current (I) through all of the samples is a square wave function ($F(t)$) with a 50% duty cycle. The function oscillates between a positive and negative value, a, which is typically around 10mA. This function is plotted in Figure 13-7. Another function, $G(t)$, defines the time when a voltage measurement is taken. For all measurements, the current through the sample is constant for a specified length of time. At the end of the of this time period, a voltage measurement is taken. When the measurement is complete, the current switches to the negative value where the process is repeated.

For high frequency measurements (roughly 33Hz to 1Hz), each sample is measured for 10 periods at each frequency before switching to the next sample. The technique for this measurement is the same as the flipping method used in all MSU systems for measuring electrical conductivity. Before the current is flipped, a single voltage measurement data point is collected and recorded. The voltage for the negative current is subtracted from the voltage for the positive current and then divided by two. This gives a single resistance value for one of the ten periods. Once all samples have been measured over the high frequency range, the system switches to take low frequency measurements. For this measurement, after the current has maintained a particular value for the specified length of time, and average of 10 voltage measurements are made on each sample before the current is switched to the negative value. This is accomplished by using a 7002 controller with a switch card inside to allow the nanovolt meter to switch between measuring each sample. Each frequency is measured using 4 cycles of F(t). It is this measurement method that saves time for measuring ZT of many samples.

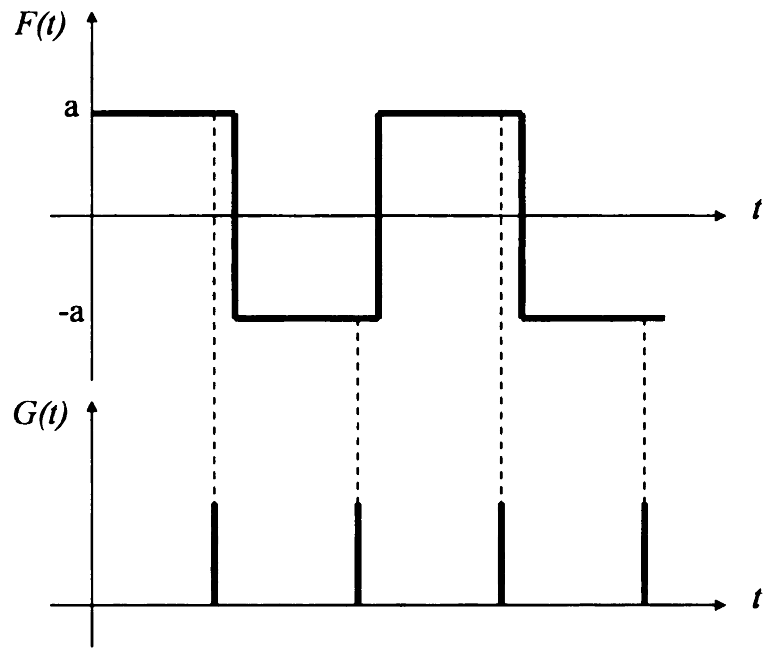

Figure 13-7: Plot of current through sample and measurement locations

13.3 The Assembled System

The assembled system consists of a Keithley 2400 current source meter, a Keithlely 2182 nanovolt meter, a Keithley 7002 controller, a computer using LabVIEW to automate the measurements, a vacuum pump, and the measurement chamber. The measurement chamber is the Drift System that has been modified. Figure 13-8 shows the inside of the measurement chamber held up with a ring stand where 16 samples are mounted for ZT measurements. Eight samples are mounted on a ring towards the top of the chamber (also shown in Figure 13-9) and another eight samples are mounted at the bottom of the chamber (also shown in Figure 13-10). The samples are mounted to a circuit board with pins that plugs into another circuit board with sockets. Each removable circuit board holds two samples. This allows the samples to be mounted with care under a microscope before loading them into the chamber.

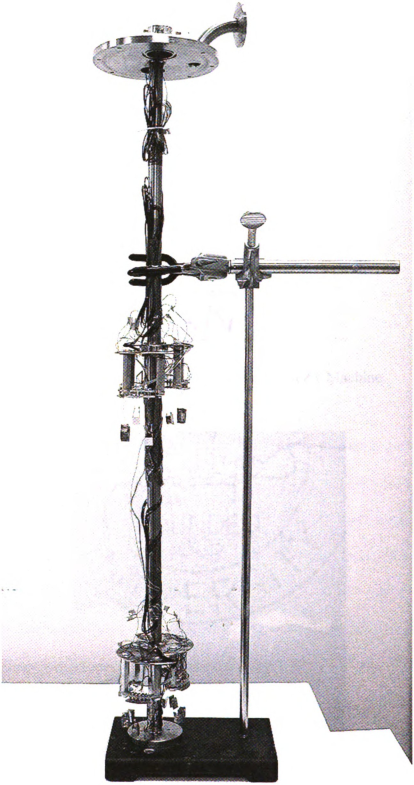

Figure 13-8: Assemble ZT Machine (Inside view with 16 samples mounted)

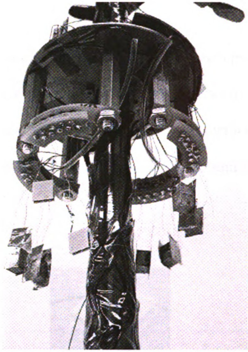

Figure 13-9: Top 8 samples mounted in ZT Machine

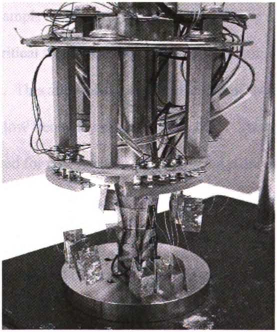

Figure 13-10: Bottom 8 samples mounted in ZT Machine

13.4 Example Data

Example data has been provided to show how the system performs. A Marlow Industries small thermoelectric module was used as a reference material for testing the ZT machine. The module uses 34 Bismuth-Telluride pellets with nickel traces and Alumina plates that make the overall size of the module: 6.6mm by 6.6mm by 2.16mm (See Figure 13-11)

Figure 13-11: Small TE module from Marlow Industries

The data for this sample is shown in Figure 13-12. Before a measurement is taken, it is unclear where the critical frequencies will be for the module. Therefore, many frequencies are sampled. This allows for a clear indication of the high frequency AC resistance, R_{AC}, and the low frequency measurements, R_{DC}. The transition between R_{AC} and R_{DC} should be ignored for now because a square wave pulse was used for the measurement. The square wave pulse consists of many frequencies and may give rise to a large error if one was to analyze the data for the transition frequencies. From the graph, the values for R_{AC} and R_{DC} can be observed and the calculation of ZT can be measured using Harman's formula.

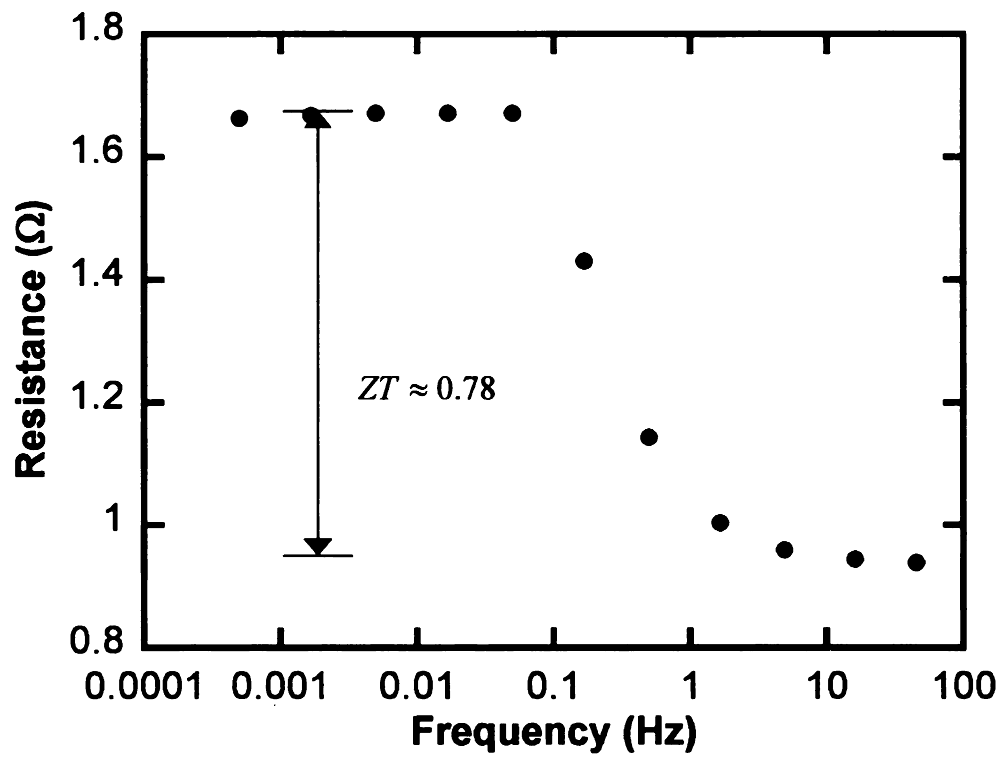

Figure 13-12: Resistance versus frequency plot for Bi_2Te_3 Marlow Industries TE module

Data from a single pellet of LAST material has been tested and an example of the data is shown in Figure 13-13. This shows that the system will work for measuring the ZT of the thermoelectric pellets created at MSU for rapid analysis.

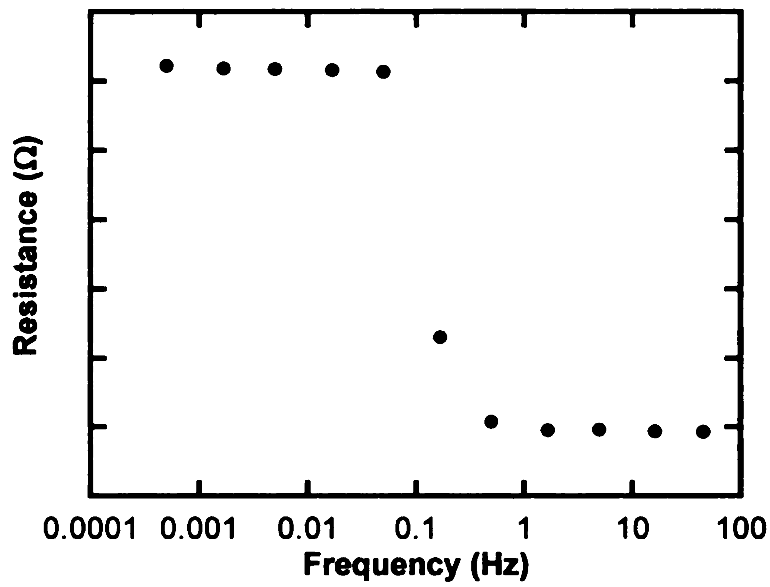

Figure 13-13: Resistance versus frequency for single LAST pellet

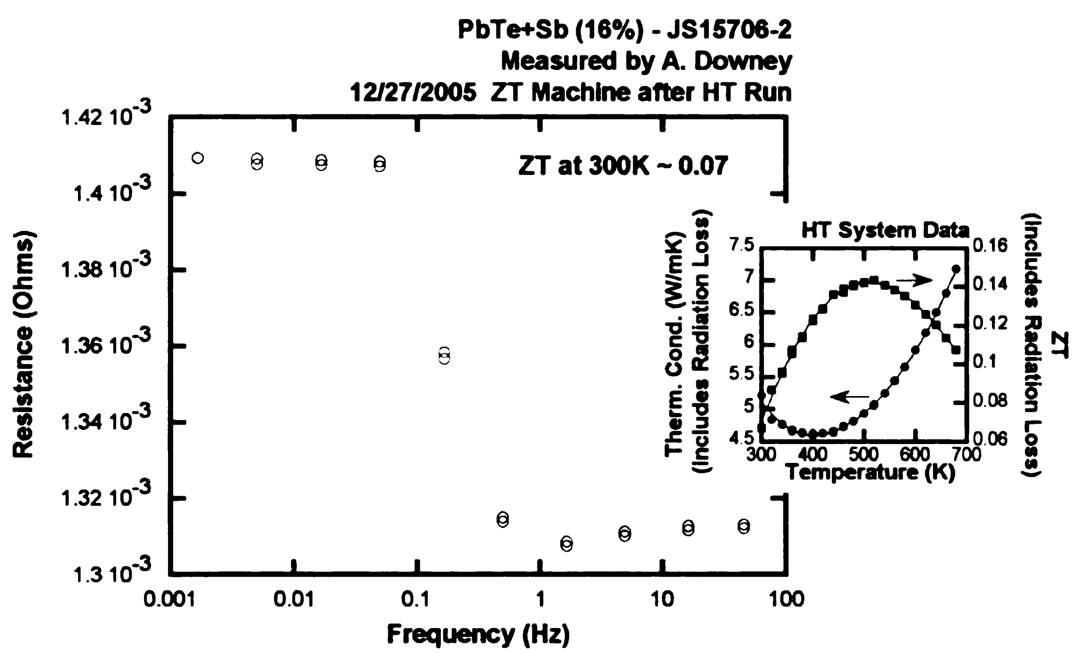

Figure 13-14: Resistance versus frequency for single pellet PbTe+Sb(16%). Here, ZT value is 0.07. HT System gets the same ZT value using measured thermal conductivity at room temperature.

13.5 Conclusion

The system has been able to measure the *ZT* of 32 samples in one week at room temperature. At this speed, many samples where tested of the LAST materials to help identify potentially good TE materials. A plot showing the *ZT* values of a generous amount of LAST samples is shown in Figure 13-15. From here, samples with ZT values greater than 0.2 were then tested for temperature dependant thermopower and electrical conductivity. The data also suggests that increasing the electrical conductivity of the materials tends to increase the ZT of the material. Overall, this system will prove to be very useful in the development of making and screening TE materials.

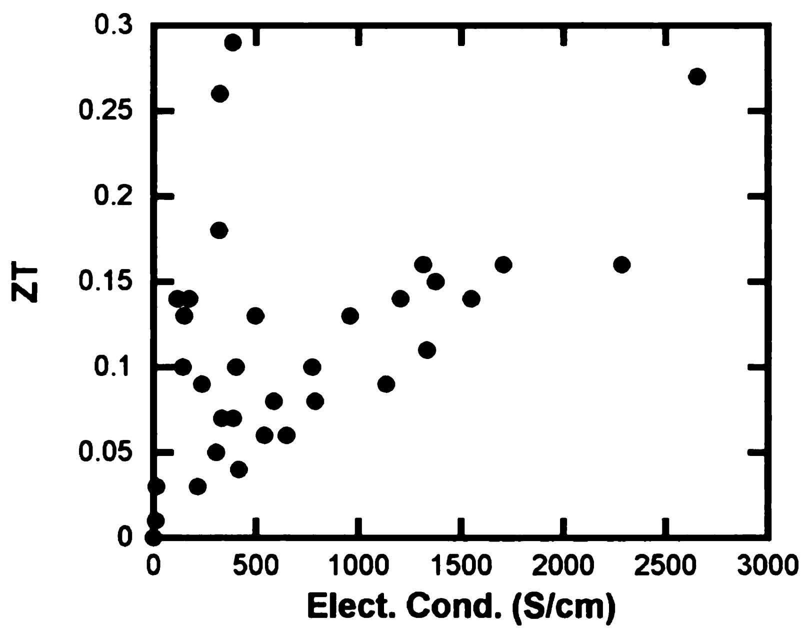

Figure 13-15: Plot of room temperature ZT values for many TE samples of LAST composition where different compositions and heating/cooling profiles where used in the manufacturing process.

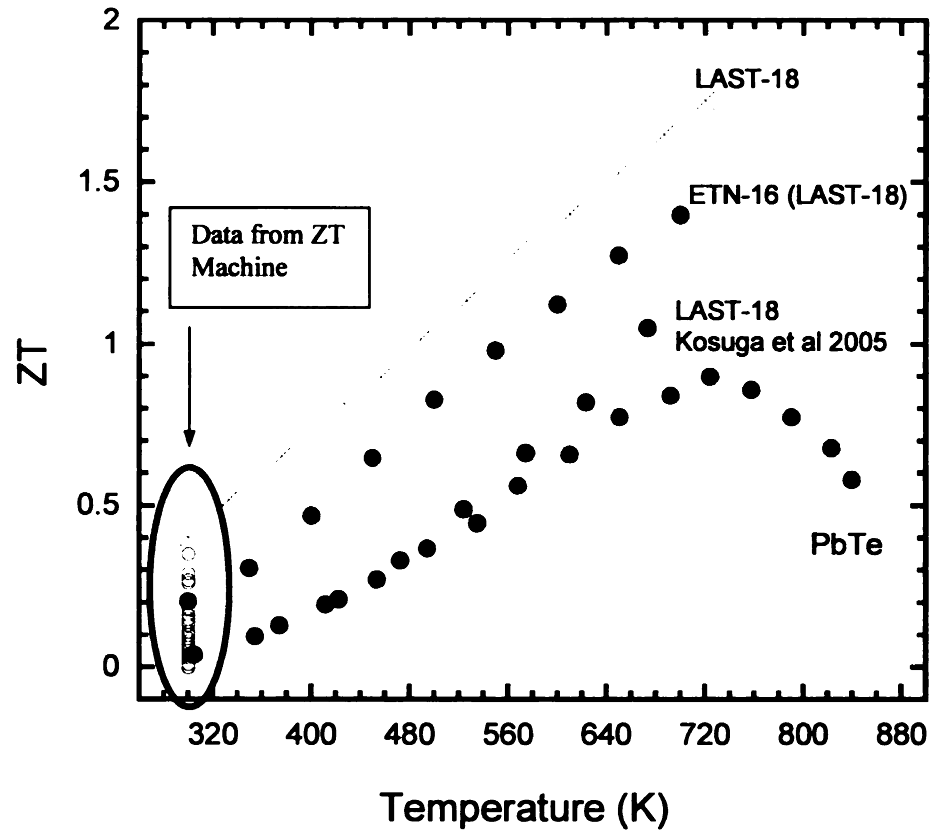

Figure 13-16: Plot of temperature dependant ZT values for LAST materials and PbTe. This shows how the ZT results compare at room temperature.

Chapter 14: Conclusion/Future Work

14.1 Conclusion

Advancements in thermoelectric research have been made by the development of new thermoelectric measurement systems and thermoelectric modeling discussed in this thesis. Some of these advancements include using a thermal drifting technique during thermopower measurements, measurements of thermopower and electrical conductivity at higher temperatures, and the investigations of measuring ZT directly both at room temperature and high temperatures. The performance and validation of each of the systems developed have been presented by testing reference materials. With these new systems, more confidence in the measurements of thermoelectric materials can be had by measuring a thermoelectric sample in multiple systems as a cross check. The analyses of measuring ZT directly lead to the creation of the ZT Machine. This system has proved to be very useful in the rapid analysis of thermoelectric samples in searching for the optimal synthesis technique.

A list of contributions to the thermoelectrics measurement laboratory at MSU includes the following:

Major Contributions

- Drift System
    - Assembly of the system
    - Design of the automated computer control via LabVIEW
    - New curve fitting technique for measuring thermal conductivity
    - Testing and validation of the system
- Ultra High Temp System
    - Assembly of the system
    - Design of the automated computer control via LabVIEW
    - Testing and validation of the system

- ZT Meter Using AC Method
    - Assembly of the system
    - Design of the automated computer control via LabVIEW
    - Testing and validation of the system

- ZT Machine Using Digital Pulses
    - Assembly of the system
    - Design of the automated computer control via LabVIEW
    - Testing and validation of the system

- Other LabVIEW Programs
    - RC-One Port Model with curve fitting
    - AC Transmission Line Model
    - Thermal Transmission Line Model with curve fitting

- H3LT (Hogan's Heroes High & Low Temp) System
    - Assembly of the system
    - Design of the automated computer control via LabVIEW
    - Testing and validation of the system

- Measurements of Thermoelectric Materials
    - Thermopower (80K to 900K)
    - Electrical Conductivity (80K to 900K)
    - Thermal Conductivity (80K to 400K)
    - ZT Direct (300K to 800K)

Minor Contributions

- Room Temperature Scanning Probe
    - Made software improvements

- Enhancement of Impedance analyzer LabVIEW program
    - Modified program for more functionality

- Room Temperature Thermopower Measurement System

In addition to the above contributions to the thermoelectrics research at MSU, this work has also been presented to the scientific community through an oral presentation and publication of the RC One-Port model at the 24th International Conference of

Thermoelectrics [64]. The Thermal TLINE model was orally presented with publication at the Fall 2005 Materials Research Society (Materials and Technologies for Direct Thermal-to-Electric Energy Conversion) [65]. Finally, data collected through our collaboration with the MSU Chemistry Department has been published for the investigation of new bulk materials [66,67,68,69,70,71].

14.2 Future Work

There are many opportunities for future work and some have already begun. One topic of interest is more experiments with direct ZT measurements at high temperatures to reduce radiation losses. One study is the effect of different coatings around the TE sample. Another is to measure temperature dependant emissivity of a sample to calculate radiation losses in ZT measurements at high temperatures. Also, include a study on how surface roughness affects radiation loss of these TE samples. Incorporated with this work would be to also expand on the Thermal TLINE model to include radiation losses.

Another future study would be to add more automation to the ZT Machine to reduce the sample preparation/mounting time. When massive quantities of thermoelectric materials are being made for large power generation devices, an automated ZT measuring system would prove to be very useful in this industrial type application for rapid analysis.

More investigations are being studied on finding the optimal chemical formula and the TE material synthesis process in which the ZT machine is being used to get larges amounts of statistical data. This data can be used investigate patterns to identify trends in the manufacturing process which would be used to improve the performance of the TE materials.

Finally, new systems developed will be used to study segmented thermoelectric legs of a module. Investigations of measuring ZT directly under large temperature gradients will be needed for these types of modules.

Appendix A: Properties of Materials

Table A-1: Thermal conductivities of various materials

	Thermcal Conductivity (W/mK)		
Material	25 °C	125 °C	225 °C
Platinum	71	71	72
Antimony	18.5		
Air	0.024		
Aluminum	250	255	250
Brass	109		
Copper	401	400	398
Nickel	91		
Stainless Steel	16	17	19
Constantan	22		
Niobeum	53.7		
Silver	429		
Alumina (Al_2O_3)	26-35		
Alumina Nitride (AlN)	175-190		

Table A-2: Emissivity values of various materials

Material	Emissivity
Carbon Black Paint NS-7	0.88
Aluminum (Commercial Sheet)	0.09
Buffed Copper	0.03
Copper with thick oxide layer	0.78
Constantan metal strip	0.09
Nickel Polished	0.072

Appendix B: Constantan Wire

B.1 Introduction

Constantan wire was used as a reference material. The thermopower and electrical conductivity was tested on a constantan wire sample (dia = 0.015") in MSU's HT System from 300K to 700K.

B.2 Setup

Figure B-1 (a) shows constant wire shaped in a manner to be able to support itself along with a platinum resistor heater on top. Figure B-1 (b) shows the wire now mounted in the HT System using two Type-E thermocouples.

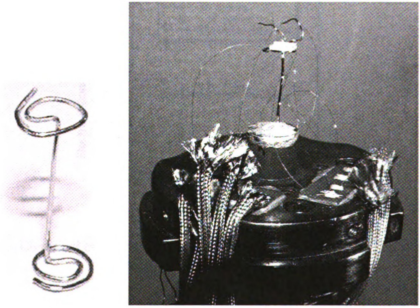

(a) (b)

Figure B-1: Constantan wire (a) mounted in HT system (b) for thermopower and electrical conductivity measurements

B.3 Results

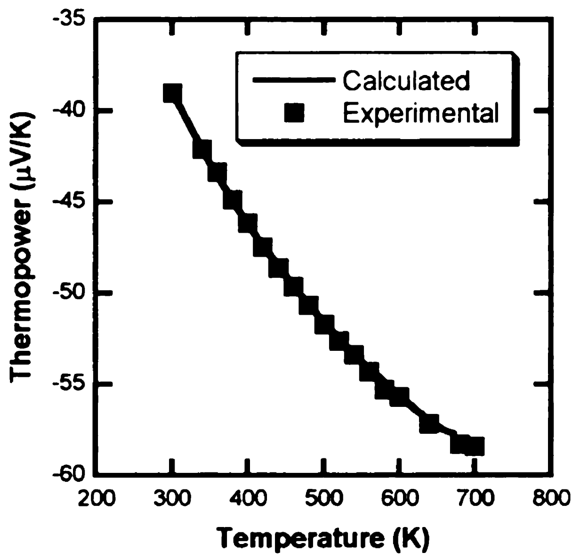

Figure B-2: Thermopower of constantan found experimentally using MSU's HT System and compared to the calculated thermopower

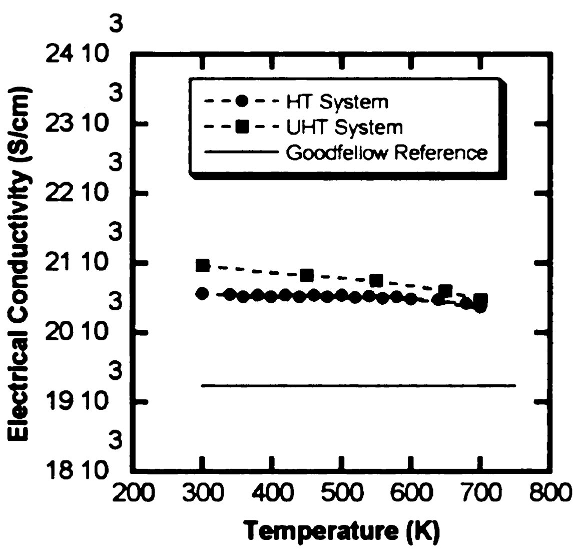

Figure B-3: Electrical conductivity of constantan measured with HT System, UHT System, and from Goodfellow

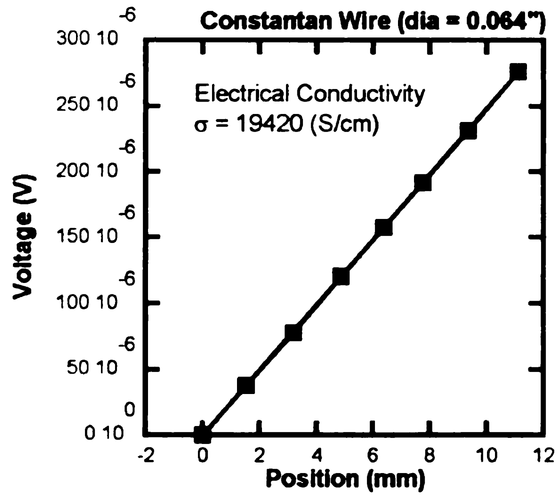

Figure B-4: Room Temp Scanning Probe measurement on constantan wire

Appendix C: Radiation Losses of Sim's HT System and High Temperature ZT Measurements

C.1 Introduction

This Chapter gives details for radiation losses attributed to Sim' HT System as well as High Temperature ZT measurements using an AC technique. Calculated radiation losses can become very complicated because of the many unknown variables (emissivity, exact temperature of surroundings, etc.). This chapter explores a reasonable approach to calculating the approximate radiation losses and provides an insight to the effects of radiation for small temperature gradients across the sample.

C.2 Evaluation of Radiation Losses

Radiation losses are a major factor in the calculation of thermal properties of materials at high temperatures. Radiation happens when there is a temperature difference between the sample and the environment. It is important to investigate how big of a factor radiation plays into the calculation of ZT. A diagram of a sample mounted in Sim's HT System is shown in Figure C-1.

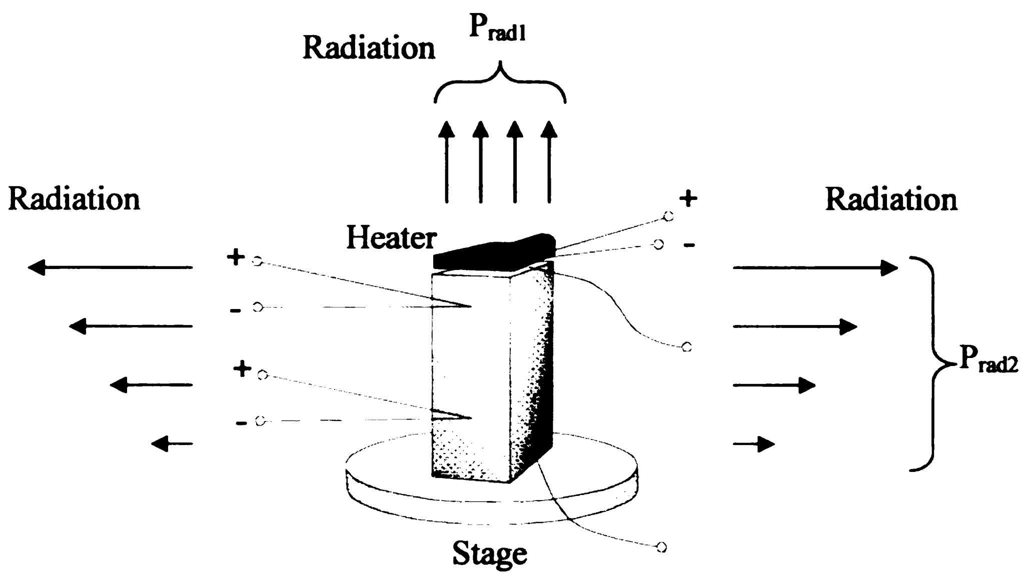

Figure C-1: Diagram showing radiation losses in the HT System

This figure shows a sample with a heater on top which is in a high vacuum environment (1E-5 Torr). The sample is also covered by a cap which will be assumed to be the same temperature as the stage the sample is mounted to. From the diagram, there are two main sources of radiation loss. One is radiation from the sample heater and the other is the sample itself radiating heat. These two sources of radiation can be analyzed separately and then added together to get the total radiation loss from the setup.

Radiation Equation

Radiation losses happen at all temperatures, however, radiation is related to temperature to the fourth power. The equation for the power, in Watts, of the heat radiated versus temperature is shown here.

$$P = e \cdot \sigma \cdot A \cdot \left(T^4 - T_S{}^4\right) \quad \text{(W)} \qquad \text{(C.179)}$$

Where we let

A = Radiative area (m^2)
P = Power radiated (J/s)
e = emissivity (e = 1 for blackbody)
σ = Stefan - Boltzmann constant ($5.6703 \cdot 10^{-8}$ W/m^{2}K^4)
T = Temperature of rdiator (K)
T_s = Temperature of surroundings (K)

Radiation of Sample Heater

Calculating the radiation loss from the sample heater alone is explained here. The heater is assumed to be at the temperature ΔT for the entire surface. The radiative surface area of the sample heater is the entire surface minus the area where the heater is in contact with the sample. Therefore, the radiative surface area of the sample heater is as follows.

A_H = radiative surface are of the heater
a = width of sample
b = thickness of sample (C.180)

$$AH = 2 \cdot (L_H \cdot W_H + L_H \cdot T_H + W_H \cdot T_H) - (a \cdot b)$$

$$P_{rad_1}(x) = e_H \cdot \sigma \cdot A_H \cdot \left(T(x)^4 - T_s^4\right) \quad \text{(W)}$$

$$P_{rad_1}(x) = e_H \cdot \sigma \cdot A_H \cdot \Delta T \cdot \left(4 \cdot T_s^3 + 6 \cdot T_s^2 \cdot \Delta T + 4 \cdot T_s \cdot \Delta T^2 + \Delta T^3\right) \quad \text{(W)}$$
(C.181)

When $\Delta T << T_s$ is true, the above equation can be approximated to the following.

$$P_{rad_1}(x) \approx e_H \cdot \sigma \cdot A_H \cdot \Delta T \cdot \left(4 \cdot T_s^3\right) \quad \text{(W)} \qquad \text{(C.182)}$$

Radiation of Sample

To examine the effects of radiation on only the sample, assume that the temperature gradient across the sample is 1 °C or less. Also, assume that the temperature profile along the length of the sample is linear to position with the equation shown here. This assumption will prove to be reasonable by the end of this section.

ΔT_{probe} = Temp gradient between measurement probes

Lp = Distance between measurement probes

L = Length of sample

ΔT = Temp gradient across entire sample

$T(x)$ = Temp along length of sample versus position (x = 0 to L)

$$\Delta T = \frac{L}{Lp} \cdot \Delta T_{probe} \quad \text{(K)} \tag{C.183}$$

$$T(x) = \frac{\Delta T}{L} \cdot x + T_S \quad \text{(K)} \tag{C.184}$$

Neglecting the ends of the sample, the power being radiated along the length of the sample is shown here.

A_S = Radiative surface area of sample (do not include ends of sample)

$$P_{rad_2}(x) = e_S \cdot \sigma \cdot A_S \cdot \left(T(x)^4 - T_S{}^4 \right) \quad \text{(W)} \tag{C.185}$$

Using the chosen temperature profile along the length of the sample, the equation for power radiated now becomes:

$$P_{rad_2}(x) = e_S \cdot \sigma \cdot A_S \cdot \left(\left(\frac{\Delta T}{L} \cdot x + T_S \right)^4 - T_S{}^4 \right) \quad \text{(W)} \tag{C.186}$$

Taking the derivative of the power radiated will indicate if the power radiated is linearly proportional to the position along the sample.

$$\frac{d}{dx}P_{rad_2}(x)=\frac{d}{dx}\left[e_S\cdot\sigma\cdot A_S\cdot\left(\left(\frac{\Delta T}{L}\cdot x+T_S\right)^4-T_S{}^4\right)\right]$$
$$=\frac{e_S\cdot\sigma\cdot 4\cdot A_S}{L^4}\cdot[\Delta T\cdot x+T_S\cdot L]^3\cdot\Delta T \quad \text{(C.187)}$$

Typically for this measurement, the temperature gradient across the sample will be kept small (below 1°C) which will allow the following to be true:

$$\Delta T << T_S$$

When the above statement is true, the derivative of the power radiated now becomes:

$$\frac{d}{dx}P_{rad_2}(x)\approx\frac{A_S}{L}\cdot e_S\cdot\sigma\cdot 4\cdot T_S{}^3\cdot\Delta T \quad \text{(C.188)}$$

The above equation shows that the derivative of the power radiated is not dependant upon the position. This indicates the power radiated is linearly proportional to the position. This is helpful in that the radiation loss will affect the entire length of the sample evenly without altering the linearity of the temperature profile.

Because the temperature along the length of the sample is not constant, the power radiated must be integrated over the length of the sample. Now the total power radiated from the sample can be solved for as follows.

$$a = width$$
$$b = thickness$$
$$A_S = 2\cdot a\cdot L+2\cdot b\cdot L=2\cdot L\cdot(a+b)$$

$$P_{rad_2}=\int_0^L e_S\cdot\sigma\cdot 2\cdot(a+b)\cdot\left(T(x)^4-T_S{}^4\right)\cdot dx \quad \text{(W)} \quad \text{(C.189)}$$

$$P_{rad_2}=\int_0^L e_S\cdot\sigma\cdot 2\cdot(a+b)\cdot\left(\left(\frac{\Delta T}{L}\cdot x+T_S\right)^4-T_S{}^4\right)\cdot dx \quad \text{(W)} \quad \text{(C.190)}$$

$$P_{rad_2} = e_s \cdot \sigma \cdot \frac{2}{5} \cdot (a+b) \cdot L \cdot \left(\Delta T^3 + 5 \cdot \Delta T^2 \cdot T_s + 10 \cdot \Delta T \cdot T_s^{\,2} + 10 \cdot T_s^{\,3} \right) \quad (\mathrm{W}) \tag{C.191}$$

When $\Delta T << T_s$ is true, the above equation can be approximated as follows.

$$P_{rad_2} \approx e_s \cdot \sigma \cdot 4 \cdot (a+b) \cdot L \cdot \left(T_s^{\,3} \right) \quad (\mathrm{W}) \tag{C.192}$$

Now, the total effective radiation power is the sum of power radiated from the heated plus the power radiated from the sample as follows.

$$P_{rad_{eff}} = P_{rad_1} + P_{rad_2} \tag{C.193}$$

When $\Delta T << T_s$ is true, the total power radiated can be approximated as follows.

$$\begin{aligned} P_{rad_{eff}} &\approx \left[e_H \cdot \sigma \cdot A_H \cdot \Delta T \cdot \left(4 \cdot T_s^{\,3} \right) \right] + \left[e_s \cdot \sigma \cdot 4 \cdot (a+b) \cdot L \cdot \left(T_s^{\,3} \right) \right] \\ &= 4 \cdot \sigma \cdot \Delta T \cdot T_s^{\,3} \cdot \left(A_H \cdot e_H + L \cdot e_s \cdot (a+b) \right) \quad (\mathrm{W}) \end{aligned} \tag{C.194}$$

Using the temperature gradient and the effective power radiated from the sample, an effective radiation resistance can now be found to be:

$$R_{rad_{eff}} = \frac{\Delta T}{P_{rad_{eff}}} = \frac{\Delta T}{4 \cdot \sigma \cdot \Delta T \cdot T_s^{\,3} \cdot \left(A_H \cdot e_H + L \cdot e_s \cdot (a+b) \right)} \tag{C.195}$$

$$R_{rad_{eff}} = \frac{1}{4 \cdot \sigma \cdot T_s^{\,3} \cdot \left(A_H \cdot e_H + L \cdot e_s \cdot (a+b) \right)} \quad (\mathrm{K/W}) \tag{C.196}$$

So for small ΔT, the effective radiation resistance is not dependant upon ΔT.

C.3 Comparing Radiation from ZT measurements and Sim's HT System

For comparing the radiation loss of Sim's HT System to the radiation loss of high temperature ZT measurements using an AC technique, the following equation was used for the radiative power loss of the ZT measurement.

$$P_{radZT_{eff}} \approx 2 \cdot e_s \cdot \sigma \cdot \Delta T \cdot T_s^{\ 3} \cdot (L \cdot a + L \cdot b + 2 \cdot a \cdot b) \quad \text{(W)} \qquad \text{(C.197)}$$

Using the temperature gradient and the effective power radiated from the sample, an effective radiation resistance can now be found to be:

$$R_{radZT_{eff}} = \frac{\Delta T}{P_{radZT_{eff}}} = \frac{\Delta T}{2 \cdot e_s \cdot \sigma \cdot \Delta T \cdot T_s^{\ 3} \cdot (L \cdot a + L \cdot b + 2 \cdot a \cdot b)} \qquad \text{(C.198)}$$

$$R_{radZT_{eff}} = \frac{1}{2 \cdot e_s \cdot \sigma \cdot T_s^{\ 3} \cdot (L \cdot a + L \cdot b + 2 \cdot a \cdot b)} \quad \text{(K/W)} \qquad \text{(C.199)}$$

For a comparison of the effective radiation conductivity between the sample and the environment, an example sample was chosen and is shown in the next page. The emissivity for the sample and the sample heater was chosen to be 1. A small temperature gradient was used in this analysis. For this specific example, the HT system radiation loss was more than 3 times greater than if the sample was measured using the AC technique for ZT measurements.

MathCAD File:

Heater

Dimensions (m)

$Lh := 0.0041$

$Wh := 0.00487$

$Th := 0.00067$

Emissivity $eh := 1$

Radiative Surface area of heat
Excluding spot touching sample.

$Ah := Lh \cdot Wh \cdot 2 + Lh \cdot Th \cdot 2 + Wh \cdot Th \cdot 2 - W \cdot T$

Sample

Dimensions (m)

$L := 0.0075$

$W := 0.00225$

$T := 0.002825$

Probe Spacing (m)

$Ps := 0.002906$

Emissivity $es := 1$

Radiative Surface Area

$As := 2 \cdot L \cdot W + 2 \cdot L \cdot T$

Temperature of Surroundings (K)

$Ts := 300, 310 .. 700$

Stefan Boltzmann Constant (W/m^2K^4)

$\sigma := 5.6703 \cdot 10^{-8}$

Temperature Gradient across Sample

$ddT := 0, \frac{20}{10} .. 20 \quad dT(ddT) := \frac{L}{Ps} \cdot ddT$

$$PradHT(Ts, ddT) := 4 \cdot \sigma \cdot dT(ddT) \cdot Ts^3 \cdot (Ah \cdot eh + L \cdot es \cdot W + L \cdot es \cdot T)$$

$$PradZT(Ts, ddT) := 2 \cdot es \cdot \sigma \cdot dT(ddT) \cdot Ts^3 \cdot (L \cdot T + L \cdot W + 2 \cdot W \cdot T)$$

$$kradHT(Ts, ddT) := \frac{PradHT(Ts, ddT)}{dT(ddT)} \cdot \frac{L}{W \cdot T}$$

$$kradZT(Ts, ddT) := \frac{PradZT(Ts, ddT)}{dT(ddT)} \cdot \frac{L}{W \cdot T}$$

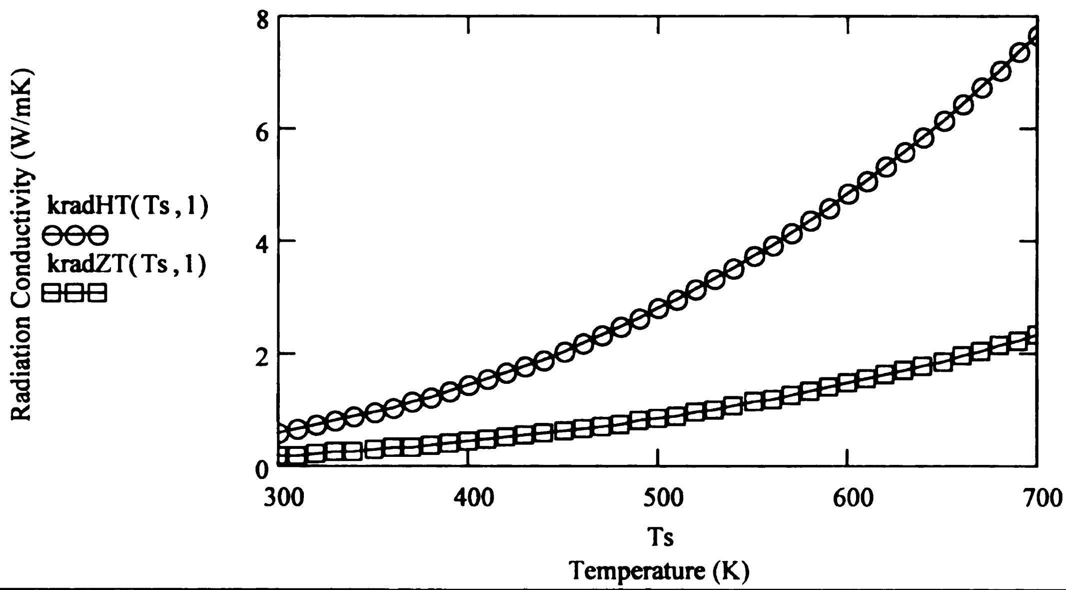

Appendix D: Useful Programs

D.1 Frequency Sweep Generator (Program)

There have been many times when a series of frequency test points where needed such as the AC impedance spectroscopy test or even when analyzing the data in LabVIEW. A LabVIEW program was created to generate a list of test frequencies by indicating the minimum frequency, the maximum frequency, the number of total test frequencies, and finally, the sweep mode (linear or logarithmic). A picture of the front panel to the program is shown in Figure D-1. The LabVIEW code can be seen in Figure D-2.

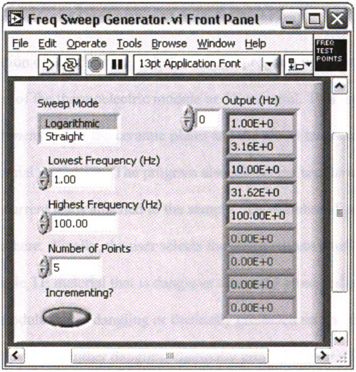

Figure D-1: LabVIEW front panel for "Frequency Sweep Generator.vi"

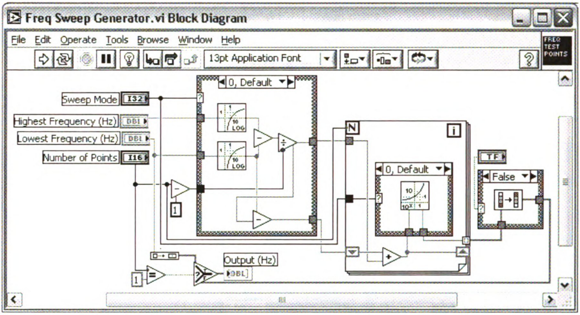

Figure D-2: LabVIEW code for "Frequency Sweep Generator.vi"

D.2 Thermal Properties of Connecting Materials (Program)

For the creation of the Thermal TLINE model, a program was created to input the standard properties of the thermoelectric module or TE material. This program allows the user to input the dimensions of the ceramic plates and the nickel traces along with the corresponding thermal properties. The program also allows the user to adjust the wire impedance of the current leads attached to the sample. The number of pellets used in the module is inputted here. Finally, the user selects the measurement configuration, such as, is the sample a single TE material that is dangle or thermally grounded on one side, is the sample an inline module that is dangling or thermally grounded on one side, or is the sample a full module that is either dangling, thermally ground on one side, or one side has a thermal resistance to ground. A picture of the front panel to this program is shown in Figure D-3.

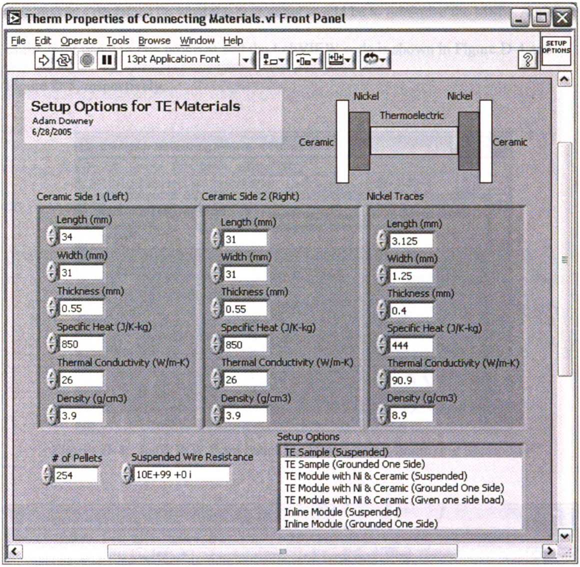

Figure D-3: LabVIEW front panel for "Therm Properties of Connecting Materials.vi"

D.3 Triangular Minimizing Method (Program)

For curving fitting data to the Thermal TLINE module, a triangular minimization technique was used but in only one dimension. The program keeps track of three items: the initial guesses of the answer, the corresponding MSE for those guesses, and a toggle to show if the guesses have been improving or degrading. The output of the program then makes a decisions on what the next guess would be to minimize the MSE. A picture of the front panel to this program and the LabVIEW code is shown in Figure D-4 and Figure D-5, respectively.

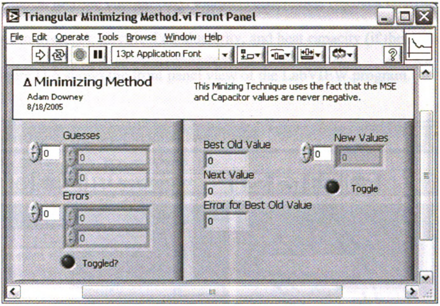

Figure D-4: LabVIEW front panel for "Triangular Minimizing Method.vi"

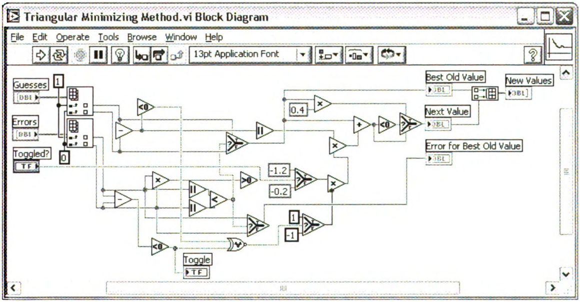

Figure D-5: LabVIEW code for "Triangular Minizing Method.vi"

D.4 Converting Impedance Properties of a TE module to Actual Properties

A program was created to convert the measured impedance properties of a thermoelectric module and convert it to the actual properties of the module such as ZT, thermal resistance, thermal conductivity, thermal capacitance, Seebeck coefficient of a single pellet (on average), electrical conductivity, and heat capacity (if the mass density is known). Figure D-6 shows the front panel view of the LabVIEW program.

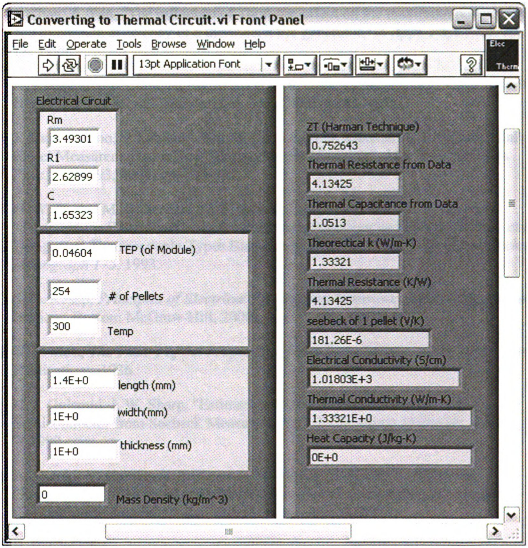

Figure D-6: Front panel view of the LabVIEW program "Converting to Thermal Circuit.vi"

References

[1] A. F. Ioffe, *Semiconductor Thermoelements and Thermoelectric Cooling.* Infosearch Ltd. 1957.

[2] G. Mahan, "Good Thermoelectrics," Solid State Physics, vol 5.1, 1998.

[3] H. J. Goldsmid, *Electronic Refrigeration.* New York: Plenum, 1964.

[4] S. O. Kasap (2001), *Thermoelectric Effect in Metals: Thermocouples.* [Online]. Available: http://Materials.Usask.Ca

[5] J. Chen, Z. Yan, "The influence of Thomson effect on the maximum power output and maximum efficiency of a thermoelectric generator," *J. Appl. Phys.*, vol. 79, no. 11, 1996.

[6] K. F. Hsu et al., "Cubic AgPb(m)SbTe(2+m) Bulk Thermoelectric Materials with High Figure of Merit," *Science*, vol. 303, 2004, pp. 881-821.

[7] J. Short, S. Loo, S. Lal, K.F. Hsu, E. Quarez, M.G. Kanatzidis, T. Hogan, "Hall Effect Measurements on New Thermoelectric Materials", *Mat. Res. Soc. Sym. Proc.,* Vol. 793, 2004, pp. 323-332.

[8] G. W. Burns, M. G. Scroger, G. F. Strouse, M. C. Croarkin, W. F. Guthrie, "Temperature-Electromotive Force Reference Functions and Tables for the Letter-Designated Thermocouple Types Based on the ITS-90," *Natl. Inst. Stand. Technol. Monograph 175*, 1993.

[9] S. O. Kasap, *Principles of Electrical Engineering Materials and Devices*, Revised Edition. Boston: McGraw-Hill, 2000.

[10] N. F. Mott, *The Theory of the Properties of Metals and Alloys.* New York: Dover Publications. 1936.

[11] H. J. Golsmid, J. W. Sharp, "Estimation of the Thermal Band Gap of a Semiconductor from Seebeck Measurements," *J. Electronic Materials.*, vol. 28, no. 7, 1999.

[12] A. Suzuki, Y. Hasegawa, T. Komine, H. Morita, H. Shirai, Y. Ishikawa, "Investigation of physical and electric properties of silver pastes as a binder for thermoelectric materials," *Rev. Sci. Instrum.*, vol. 76, 2005.

[13] E. F. Chor, J. Lerdworatawee, "Quasi-Two-Dimensional Transmission Line Model (QTD-TLM) for Planar Ohmic Contact Studies," *IEEE Trans. Electron Devices*, vol. 49, no. 1, Jan. 2002.

[14] H.J. Goldsmid, "The use of semiconductors in thermoelectric refrigeration," *Bri. J. Appl. Phys.*, vol. 5, Nov. 1954.

[15] L. D. Hicks, M. S. Dresselhaus, "Effect of quantum-well structures on the thermoelectric figure of merit", *Phys. Rev. B*, vol. 47, no. 19, pg. 727-731, 1993.

[16] R. Taylor, *CRC Handbook of Thermoelectrics,* ed. D. M. Rowe, CRC Press, Inc., 1995.

[17] M. G. Kanatzidis, *et. al.*, "Thermoelectric Materials: Solid State Synthesis," *Naval Res. Rev.*, vol. 48, no. 4, 1996.

[18] T. C. Harman, J. H. Cahn, and M. J. Logan, "Measurement of Thermal Conductivity by Utilization of the Peltier Effect," *J. Appl. Phys.*, vol. 30, no. 9, Sept. 1959.

[19] O. Maldonado, "Pulse method for simultaneous measurement of electric thermopower and heat conductivity at low temperatures", *Cryogenics*, vol. 32, no. 10, 1992.

[20] T. C. Harman, J. M. Honig, *J. Appl. Phys.,* vol. 13, 1962, p. 440.

[21] S. Loo, *Transport Characterization of New High Temperature Quaternary Thermoelectric Materials and Devices*, Ph.D. Thesis, Michigan State University, 2003.

[22] J. Short, *A New System Debeloped to Characterize Thermoelectric Devices for Power Generation Applications,* Master Thesis, Michigan State University, 2005.

[23] G. Min, D. M. Rowe, and K. Kontostavlakis, "Thermoelectric figure of merit under large temperature differences," *J. Phys. D,* vol. 37, 2004, pp. 1301-1304.

[24] G. Min, D. M. Rowe, "A novel principle allowing rapid and accurate measurement of a dimensionless thermoelectric figure of merit," *J. Meas. Sci. Tech.*, Vol. 12, 2001, pp. 1261-1262.

[25] F. Chen, "Low-frequency ac measurement of the Seebeck coefficient," *Rev. Sci. Instrum.*, vol. 72, no. 11, 2001, pp. 4201-4206.

[26] A. T. Burkov, A. Heinrich, P. P. Konstantinov, T. Nakama, K. Yagasaki, "Experimental set-up for thermopower and resistivity measurements at 100-1300K," *Meas. Sci. Technol.,* vol. 12, 2001, pg. 264-272.

[27] A. L. Pope, R. T. Littleton, T. M. Tritt, "Apparatus for the rapid measurement of electrical transport properties for both "needle-like" and bulk materials," *Rev. Sci. Instrum.*, vol. 72, no. 7, July 2001, pp. 3129-3131.

[28] R. T. Littleton IV, *et. al.*, "High Temperature Transport Probe for Thermopower and Resistivity Measurements," *Materials Research Society Symposium Proceedings*, 1998.

[29] Z. Zhou, C. Uher, "Apparatus for Seebeck coefficient and electrical resistivity measurements of bulk thermoelectric materials at high temperature," Rev. Sci. Instrum., vol. 76, 2005.

[30] M. Putti, M. R. Cimberle, A. Canesi, C. Foglia, A. Siri, "Thermopower measurements of high-temperature superconductors: Experimental artifacts due to applied thermal gradient and a technique for avoiding them," *Phys. Rev. B*, vol. 58, no. 18, Nov. 1998.

[31] R. Buist, "A new methodology for testing thermoelectric materials and devices," *Proc. XI Int. Conf. on Thermoelectrics*, Oct. 1992.

[32] P. J. Talor, W. A. Jesser, F. D. Rosi, Z. Derzko, "A model for the non-steady-state temperature behavior of thermoelectric cooling of thermoelectric cooling semiconductor devices," *Semicon. Sci. Technol.*, vol. 12, 1997, pp. 443-447.

[33] D. Kondratiev, L. Yershova, "TE Coolers Computer Simulation: Incremental Upgrading of Rate Equations Approach, " *Proc. 6th of the European Thermoelectric Society*, Sept. 2001.

[34] G. K. Ottarsson, "A Ladder Thermoelectric Parallelepiped Generator," *Proc. 21st Int. Conf. on Thermoelectrics*, May 2002.

[35] P. G. Lau, R. J. Buist, "Temperature and Time Dependent Finite Difference Model of a Thermoelectric Pellet and Couple," Proc. XV Conf. on Thermoelectrics, Pasadena, California, USA, 1996.

[36] V. Milanovic, M. Hopcroft, C. Zincke, M. Zaghloul, K. Pister, "Modeling of Thermoelectric Effects in Planar Micromachined Structures Using SPICE," Proceedings of Therminic Int. Workshop, 2000.

[37] P. Turkes, "Thermal Network Calculation for Level-3 Compact Models," Infineon Technologies AG, Application Note AN-PSM-12, Aug. 2001.

[38] H. Sasaki, K. Takahashi, B. Inglis, M. Klonz, "A Numerical Simulation of Thermoelectric Effects in Single-Junction Thermal Converters," *IEEE Trans. Instrumentation and Measurement*, vol. 48, no. 2, April 1999.

[39] K. Takahashi, M. Sasaki, B. Inglis, M. Klonz, "AC-DC Voltage Transfer Difference Due to Seebeck Effect in Thermal Converters," *IEEE Trans. Instrumentation and Measurement*, vol. 48, no. 2, April 1999.

[40] G. Snyder, J. Fleurial, T. Caillat, "Supercooling of Peltier cooler using a current pulse," *J. Appl. Phys.*, vol. 92, no. 3, 2002.

[41] B. Lwo, K. Tseng, C. Kao, L. Lu, "Over-Temperature Forecasts on Electronic Packages Through a Transient R-C Model," *J. Elec. Packaging*, vol. 122, 2000, pp. 42-47.

[42] R. J. Buist, P. G. Lau, "Theoretical analysis of thermoelectric cooling performance enhancement via thermal and electrical pulsing," Proc. of 15th Int. Conf. on Thermoelectrics, Pasadena, California, March 1996.

[43] T. A. Al-Obaidi, H. J. Goldsmid, "Determination of the Thermoelectric Figure of Merit from Thermal Conductivity Measurements," Energy Conversion, vol. 9, 1969, pp. 131-132.

[44] P. E. Gray, *The Dynamic Behavior of Thermoelectric Devices*. New York: The Technology Press of The Massachusetts Institute of Technology and John Wiley & Sons, 1960.

[45] J. A. Chavez, J. A. Ortega, J. Salazar, A. Turo, M. J. Garcia, "SPICE model of thermoelectric elements including thermal effects", *Proceedings of the 17th IEEE Instrumentation and Measurement Technology Conference 2000*, vol. 2, May 2000, pp. 1019-1023.

[46] S. Dilhaire, "Determination of ZT of PN thermoelectric couples by AC electrical measurement," *Proceedings of the 21st International Conference on Thermoelectronics*, 2002.

[47] H. Iwasaki, S. Yokoyama, T. Tsukui, M. Koyano, H. Hori, S. Sano, "Evaluation of the Figure of Merit of Thermoelectric Modules by Harman Method," *Jpn. J. Appl. Phys.*, vol 42, 2003, pp. 3703-3708.

[48] B.P. Lathi, *Signal Processing & Linear Systems*. Berkeley Cambridge Press, 1998.

[49] Tellurex Corporation (2006, April). Available: http://www.tellurex.com/

[50] G. M. Wierzba. (2002). ECE 831 Class Notes. Michigan State University. East Lansing, MI. [CD-ROM].

[51] W. Chen, *Passive and Active Filters Theory and Implementations*, John Wiley & Sons, 1986.

[52] M. Lenz, G. Striedl, U. Frohler, *Thermal Resistance - Theory and Practice*. Infineon Technologies AG. 1999.

[53] D. Maillet, *Thermal Quadrupoles: Solving the Heat Equation through Integral Transforms*, John Wiley & Sons, Nov. 2000.

[54] J.A. Nelder, R. Mead, "A Simplex Method for Function Minimization", *Computer Journal*, vol. 7, 1965, p. 308.

[55] P. M. Mayer, R. J. Ram, "Cross-plane Thermoreflectance Imaging of Thermoelectric Elements," *Materials Research Society Symposium Proceedings*, vol. 886, 2005.

[56] K&K Associates, Thermal Connection. (2006, April). [Online]. Available: http://www.tak2000.com/data2.htm#surffin

[57] C. Vining, "Thermoelectric properties of pressure-sintered Si0.8Ge0.2 thermoelectric alloys," *J. Appl. Phys.*, vol. 69, no. 8, April 1991.

[58] P.J. Timans, "Emissivity of silicon at elevated temperatures," *J. Appl. Phys.*, vol. 74, no. 10, Nov. 1993.

[59] R. B. Roberts, F. Righini, R. C. Compton, *Phil. Mag.,* vol. 52, 1985, p. 1147.

[60] B. Sundqvist, "Thermal diffusivity and thermal conductivity of Chromel, Alumel and Constantan in the range 100-450 K," *J. Appl. Phys.,* vol. 72, no. 2, 1992.

[61] S. Sasaki, H. Masuda, H. Kou, and H. Takahashi, "A Transient Heating Technique for Measuring the Thermal Diffusivity of Metals," *International Journal of Thermophysics,* vol. 19, no. 1, 1998.

[62] V.Volodin, G. Gromov, D. Kondratiev, A. Ogryzko, A. Rogov, L. Yershova, "Z-metering Development", *Proceedings of 2002 X anniversary Forum on Thermoelectricity*, 2002.

[63] H. Iwasaki, M. Koyano, H. Hori, "Evaluation of the Figure of Merit on Thermoelectric Materials by Harman Method," *J. Appl. Phys.*, vol. 41, 2002, pp. 6606-6609.

[64] A. D. Downey, T.P. Hogan, "Circuit model of a thermoelectric module for ac electrical measurements," *Proceedings of the 24th International Conference on Thermoelectrics*, Clemson, South Carolina, June 2005, pp.79-82.

[65] A. D. Downey, E. Timm, P. Poudeu, M. G. Kanatzidis, H. Shock, T. P. Hogan, "Application of Transmission Line Theory for Modeling of a Thermoelectric Module in Multiple Configurations for AC Electrical Measurements," *Materials Research Society Symposium Proceedings,* vol. 886, 2005, pp. 425-430.

[66] P. F. Poudeu, J. D'Angelo, A. D. Downey, R. Pcionek, J. Sootsman, Z. Zhou, O. Palchik, T. P. Hogan, C. Uher, M. G. Kanatzidis,"Effects of Antimony on the Thermoelectric Properties of the Cubic Pb9.6SbyTe10-xSex", *Materials Research Society Symposium Proceedings*, vol. 886, 2005, pp. 195-200.

[67] J. L. Short, J. D'Angelo, A. D. Downey, M. A. Pajor, M. G. Kanatzidis, E. Timm, H. Schock, T. P. Hogan, "Characterization of Thermoelectric Power Generation Modules Made from New Materials," *Materials Research Society Symposium Proceedings*, vol. 886, 2005, pp. 309-315.

[68] J. D'Angelo, J. L. Short, A. D. Downey, M. A. Pajor, E. Timm, H. Schock, M. G. Kanatzidis, T. P. Hogan, "Investigation of Low Resistance Contacts to Pb-Sb-Ag-Te (LAST) Materials for Module Fabrication," *Materials Research Society Symposium Proceedings*, vol. 886, 2005, pp. 317-322.

[69] T. P. Hogan, A. D. Downey, J. Short, J. D'Angelo, E. Quarez, J. Androulakis, P. Poudeu, M. G. Kanatzidis, E. Timm, K. Sarbo, H. Schock, "Progress on the Fabrication and Characterization of High Efficiency Thermoelectric Generators," *Materials Research Society Symposium Proceedings*, vol. 886, 2005, pp. 487-492.

[70] J. Androulakis, K. F. Hsu, R. Pcionek, H. Kong, C. Uher, J. D'Angelo, A. Downey, T. Hogan, M. G. Kanatzidis, "Nanostructuring and High Thermoelectric Efficiency in p-Type $Ag(Pb_{1-y}Sn_y)_mSbTe_{2+m}$," *Adv. Mater,* 2006, in press.

[71] P. Poudeu, J. D'Angelo, A. D. Downey, J. L. Short, T. P. Hogan, M. G. Kanatzidis, "High Thermoelectric Figure of Merit and Nanostructuring in Bulk p-type $Na_{1-x}Pb_mSb_yTe_{m+2}$," *Angew. Chem. Int. Ed.*, 2006, in press.